INVESTIGATION OF THE ROLE OF HYDRIDES IN ZIRCONOCENE CATALYZED OLEFIN POLYMERIZATION

Thesis by

Steven M. Baldwin

In Partial Fulfillment of the Requirements for the

Degree of

Doctor of Philosophy

CALIFORNIA INSTITUTE OF TECHNOLOGY

Pasadena, California

2011

(Defended November 22, 2010)

ACKNOWLEDGEMENTS

I first must thank my collaborator and essentially co-advisor Professor Hans Brintzinger without whom none of this would have happened. Hans has been like a second advisor to me throughout the last four years. Hans has been available for me constantly and has provided the insight and push which were essential to this work. Professor John Bercaw provided me with a wonderful environment in which to develop as a chemist and a person. John's willingness to accept people of vastly different styles has created a unique environment in the Bercaw group which I will miss greatly. Caltech has been a wonderful place to study with fantastic interactions between groups. In particular, I've had wonderful interactions with the Peters, Gray, Grubbs and now Agapie groups. Jonas, Harry and Bob have

Over the years, many members of the Bercaw group have been there for me, providing the chemistry and life knowledge I needed. Dr. Cliff Barr got me started with my first experiments at Caltech. The members of the group when I joined, Professor Jon Owen, Dr. Susan Schofer, Professor Parisa Mehrkhodavandi and Dr. Endy Min provided a strong basis for me to develop. Dr. Jeff Byers was invaluable in teaching me how to think about polymer microstructure and, although none of that ended up appearing in this thesis, these discussions formed the basis for the development of my understanding of polymerization mechanism. Dr. Sara Klamo taught me how to rigorously study mechanism and the importance of good technique. Professor Theo Agapie did more to show me how to operate in lab than any other person. Theo's dedication and talent were a tremendous example to

try to emulate. We've had a string of fantastic post-docs in the Bercaw group who have shared a wealth of knowledge and a diverse set of skills over the years. Professors Tom Driver and Travis Williams brought an encyclopedic knowledge of organic chemistry and different ways of looking at organometallic chemistry. Professor Nilay Hazari brought an extensive knowledge of computational chemistry.

We've had quite a few visitors to the Bercaw group in my time. Recently, we've had two visiting scholars, Drs. Melanie Zimmerman-Meerman and Emmanuelle Despagnet-Ayoub, who've shared lab space with me and been fantastic people. Professors Adam Johnson, Andy Caffyn and John Moss spent significant time with the group and shared their very different backgrounds teaching me how many different roads there are to being a chemist.

Although this thesis is exclusively dedicated to my work while at Caltech, if it wasn't for my interactions outside of the lab, I wouldn't have been able to survive. Firstly, I must thank my baseball buddies, Drs. Jeff Byers and Crystal Shih. Jeff, Crystal and I spent many an evening or afternoon at Dodger Stadium enjoying the highs and lows of Dodger baseball. In the same vein, I must thank Rachel Klet for sharing my only postseason game as we watched the Dodgers whoop up on the Cardinals in 2009. Sports have been a big part of my life at Caltech, and I have had a great time having people over to my house to watch Pittsburgh Steelers games. It started with playoff games with Jeff, Crystal, Dr. Dave Weinberg and Professor Yen Nguyen, but over the last few years it has expanded to weekly games with Gretchen Keller, Dr. Suzanne Golisz and her husband Shane Arney. Suz and

Shane are great hosts who welcomed me into their home and shared many a rousing win or humbling loss. I was glad to be able to attend their wedding and am saddened that they now live so far away.

Outside of sports, I've had a progression of close friends who've kept me sane. Professor Yen Nguyen has been a confidant and close friend for seemingly as long as I've been at Caltech. Along with the other members of the FRESH group, Professor Cora MacBeth, Dr. Libby Mayo and Dr. Wendy Belliston-Bitner, they helped me get settled in at Caltech and learn to balance my life and science. Dr. Crystal Shih, in addition to attending Dodgers games with me, was the guinea pig for my explorations of stir frying and many, many trips to the bookstore store where we both spent way too much money. Over the last few years, Ian Tonks, Dr. Alex Miller and Professor Ned West have shared many an afternoon soda break with me as well as more than a couple late evening breaks. Alex and his fiancée Dr. Jillian Dempsey have welcomed me into their home for numerous wine tasting/drinking events as well as one awesome Thanksgiving feast this year. Over my years at Caltech, Yen Nguyen has been a close friend who may think that I spend too much time listening to her problems, but it is through helping her that I achieve peace. Dr. Anna Folinsky has been a dear friend who has provided a valuable alternate view and makes great vegie lasagna.

I will be leaving my chemistry in good hands in Taylor Lenton, who has been an eager and extremely capable disciple at the altar of zirconocene hydrides. There have been quite a few people at Caltech who I've interacted with much less than I would have liked. Dr.

Morgan Cable would have to lead that list. Morgan is a spark plug and whether playing soccer or attending a Gray group event; it has always been my distinct pleasure and privilege to spend time with Morgan. Even with sitting next to her for the last few years, it still feels like Val Scott falls into this category. Val's humor and vitality have made coming into the office in the mornings a pleasure, and seeing her meet her husband Kent has been a wonderful experience.

My family has been a constant source of support for me. My parents, Paul and Beth, have always been supportive of me, and their encouragement was essential to me getting to where I am today. Having my Uncle Melvin and Aunt Silvia in Los Angeles was a great comfort over the years it took me to complete this work. Finally, I'd like to thank my grandmother, Nan. She always had confidence in me even when I didn't. I'm sorry that she didn't live to see me finish and I will miss her always.

ABSTRACT

The structure and reactivity of zirconocene hydrides in the presence of aluminum alkyls is investigated for both neutral species and cationic species. Unbridged zirconocene dichlorides react with HAl^iBu_2 to yield trihydride dialuminum clusters of the general formula $(R_nC_5H_{5-n})_2Zr(\mu\text{-}H)_3(Al^iBu_2)_3(\mu\text{-}Cl)_2$. Bridged zirconocenes instead predominantly yield a dihydride monoaluminum cluster of the general form $Me_2E(R_nC_5H_{4-n})_2Zr(Cl)(\mu\text{-}H)_2Al^iBu_2$ where E = Si or C. For *tert*-butyl substituted zirconocenes the terminal Cl is replaced by a H. It is shown that steric factors dictate which hydride is formed.

A single type of cationic trihydride dialuminum cluster of general formula $[(R_nC_5H_{4-n})_2Zr(\mu\text{-}H)_3(Al^iBu_2)_2]^+$ is formed for all zirconocene hydrides upon addition of $[Ph_3C][B(C_6F_5)_4]$ regardless of which class of neutral hydride was formed. For {(SBI)Zr} and $\{(Me_2Si)_2(C_5H_3)_2Zr\}$ the resulting cations were crystallographically characterized where SBI stands for $Me_2Si(indenyl)_2$. $[(SBI)Zr(\mu\text{-}H)_3(Al^iBu_2)_2]^+$ reacts with propene to make isotactic polypropene while the Me-substituted analogue $[(SBI)Zr(\mu\text{-}H)_3(AlMe_2)_2]^+$ is a catalyst for hydroalumination. These trihydride cations are shown to be dormant species in polymerization reactions. $[(SBI)Zr(\mu\text{-}H)_3(Al^iBu_2)_2]^+$ is identified as the hydride observed by Babushkin and Brintzinger (Babushkin, D. E.; Brintzinger, H. H. *Chem. Eur. J.* **2007**, *13*, 5294) upon addition of Al^iBu_3 or HAl^iBu_2 to a mixture of $(SBI)ZrCl_2$ and methylaluminoxane.

TABLE OF CONTENTS

LIST OF FIGURES

Chapter 1

Chapter 2

Chapter 3

Chapter 4

Appendix B

LIST OF TABLES

CHAPTER 1

Introduction to Ziegler-Natta Polymerization

1.1 Polymerization Overview

In the simplest sense Ziegler-Natta polymerization is the polymerization of α-olefins using homogeneous or heterogeneous catalysts by group 4 metals (Scheme 1.1) yielding polyolefins which are produced on the order of 10^8 metric tons per year. As would be expected for any process of that great a commercial interest, the field of Ziegler-Natta polymerization is very broad and has been extensively reviewed.[1-10] As such the present introduction will be limited to a general outline of what is known about homogeneous polymerization and where knowledge is still limited.

Scheme 1.1

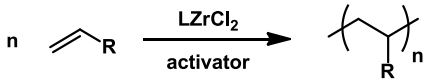

Homogeneous Ziegler-Natta polymerization began with the discovery that $(C_5H_5)_2TiCl_2$ when reacted with trialkylaluminum species catalyzed the polymerization of ethylene with low activities.[11-13] It wasn't until the discovery that addition of water or better yet premixing $AlMe_3$ with water resulted in a highly active polymerization catalyst that propene and higher olefins were also polymerized with homogeneous catalysts.[14-16] Since then a wide range of metallocene precatalysts have been explored yielding polymers of varying degrees of stereospecificity to generate high molecular weight polymers when activated with methylaluminoxane (MAO), the partial hydrolysis product of $AlMe_3$. The

field of metallocene catalyzed homogeneous olefin polymerization has seen renewed industrial interest in recent years due to advances in processing of these traditionally hard to work with products as well as the development of new variants of MAO which enable metallocene catalysts to become economically on par with traditional Ziegler-Natta heterogeneous catalysts for linear low-density polyethene (LLDPE) production.[17] Despite decades of research there remain numerous questions as to how these versatile and valuable catalysts perform which have the promise to allow for increased activity and more versatile catalysts.

1.2 Stereocontrol of Olefin Insertion

The general features of the transition state for olefin enchainment have been established through years of careful experimentation.[8-9] Figure 1.1 outlines the more important features of the insertion transition state as modeled by the chiral metallocene framework derived from $C_2H_4(indenyl)_2ZrCl_2$, $(EBI)ZrCl_2$. The means by which stereospecificity is imparted on the polymerization begins with an α-agostic interaction of the zirconium bound polymeryl chain which locks the polymeryl chain into a specific orientation, the direction of which is dictated by steric interactions with the metallocene framework. The α-agostic interaction is manifest as a secondary KIE of ~1.3 for the terminal olefinic protons of aliphatic olefins when polymerized by a variety of zirconocene catalysts.[18-21]

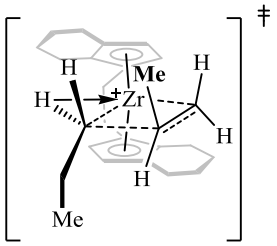

Figure 1.1: Transition state model for insertion of propene into zirconocene alkyl

The incoming monomer is directed so that interaction between the polymeryl chain and the methyl of the incoming olefin are minimized. Pino was able to show this by determining the absolute stereochemistry of propene hydrooligomers formed by the enantiopure zirconocene (*R*,*R*)-C_2H_4(4,5,6,7-tetrahydroindenyl)$ZrCl_2$, (*R*,*R*)-(EBTHI)$ZrCl_2$, ruling out direct steric interaction between the incoming olefin and ligand framework.[22] This relay mechanism of stereocontrol allows for the rational control of polymer microstructure via variation of the geometry of metallocene precatalysts (Figure 1.2).

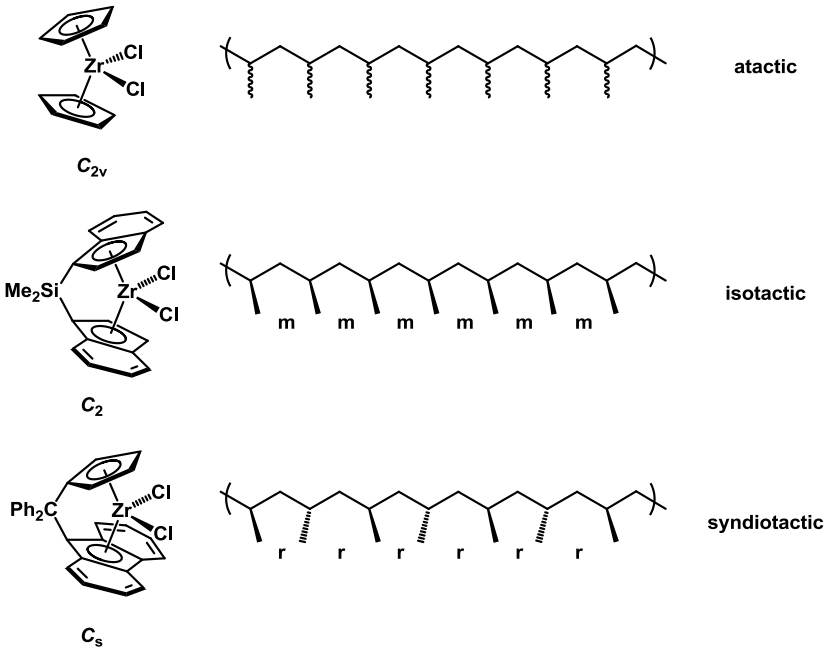

Figure 1.2: Types of polypropene and an example of a catalyst that produces them

For C_2-symmetric precatalysts the two conformations of the insertion transition state with the polymeryl group on either side of the wedge are identical (Figure 1.3), resulting in insertion of the same enantioface of the olefin. On the other hand for C_s-symmetric precatalysts the two transition states with the polymeryl group on opposite sides of the wedge are mirror images of each other, resulting in insertions of opposite enantiofaces of the olefin from the two sides of the wedge. Insertion of olefin results in the movement of the polymeryl chain from one side of the wedge to the other; hence C_s-symmetric precatalysts give syndiotactic polypropene while C_2-symmetric catalysts yield isotactic polypropene. Similar reasoning can be used to extrapolate the specificity of other metallocene architectures with less symmetry than those described in Figure 1.2.[9]

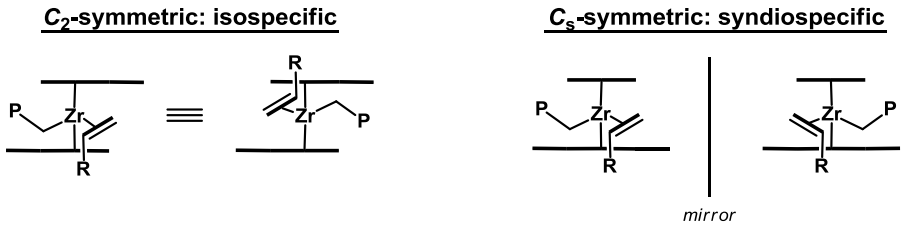

Figure 1.3: Stereocontrol via ligand geometry aka enantiomorphic site control

1.3 Activation and Initiation

As mentioned above, zirconocene dichlorides are not by themselves catalysts for polymerizations nor are their dimethyl analogues. In order to make them into catalysts, an activator is necessary which will convert the neutral zirconocene dialkyl into a cationic monoalkyl species.[1, 10, 23] Typical activators are trityl (Ph_3C^+) or dimethylanilinium ($PhNMe_2H^+$) salts with weakly coordinating anions, most commonly polyfluorinated borates. Strong Lewis acids such as trispentafluorophenylborane ($B(C_6F_5)_3$) also form active catalysts. These activators generate cations through either methide abstraction or protonolysis and so require a metallocene dialkyl species as their precatalyst. In contrast MAO, the activator most commonly used industrially, serves both as an activator as well as an alkylating reagent. MAO is a dynamically complex mixture of $–CH_3–Al–O–$ chains, rings and cages, the speciation of which remains an active area of research.[10] The complexity of MAO and the requirement of large excesses of Al relative to Zr have hampered the direct study of MAO-activated metallocene polymerizations while the borate based activators have been much more easily studied.

Activation with strongly Lewis-acidic boranes or alanes results almost exclusively in a zirconocene methyl cation with a closely associated methylborate anion[24-25] (Figure 1.4), while with low borane to Zr ratios a second species is formed which results from the incomplete activation of the zirconocene to yield a methyl bridged dinuclear monocation similar to the type **II** complex. With trityl activators the Me-bridged species **II** predominates as further activation to ion pairs of type **IV** is slow.[26] However, in the presence of $AlMe_3$ an adduct of type **III** is formed[27-28].

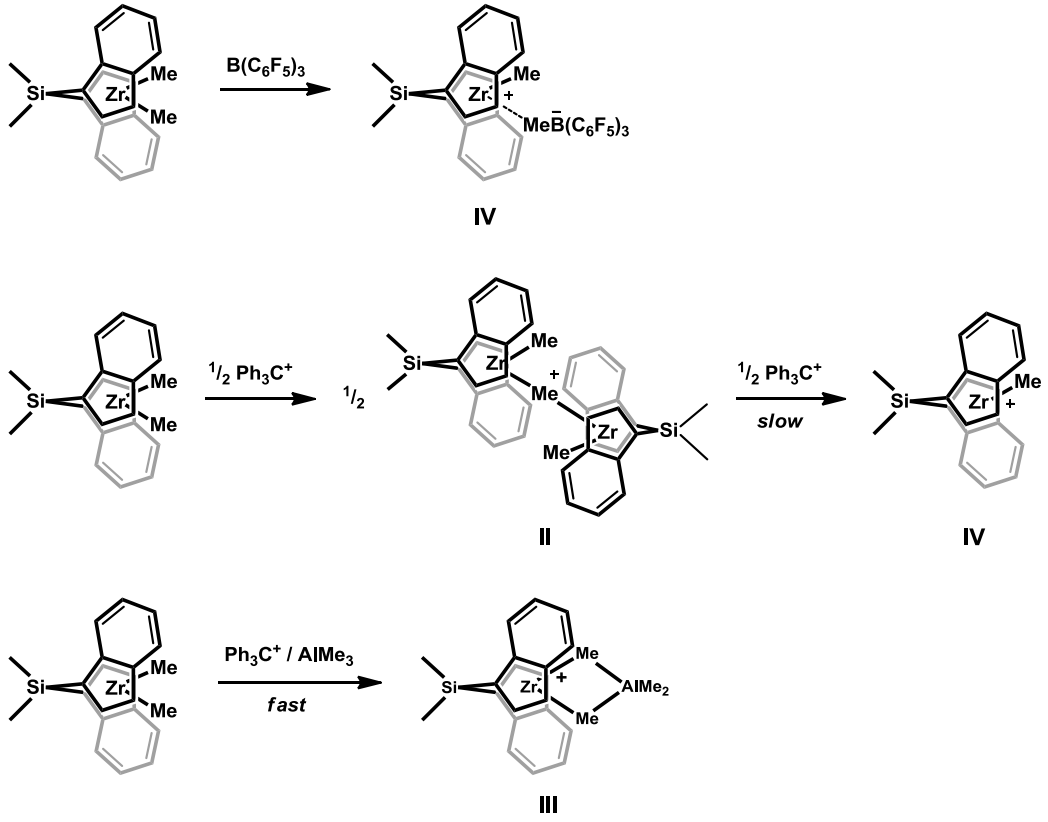

Figure 1.4: Cations formed with boron based activators as modeled by {(SBI)Zr}

MAO is more complicated both in structure and reactivity and hence has proven more difficult to study, but in recent years the initial species formed from zirconocenes by MAO have been identified (Figure 1.5).[29-37] Initially MAO acts as an alkylating agent[38] converting the dichloride to the dimethyl with a weakly associated MAO Lewis acid of type **I** (Figure 1.5). Further equivalents of MAO result in cationization of the zirconocene. Initially a {Zr-Me^+} species of type **II** is formed which is stabilized by coordination of another equiv of the neutral zirconocene through a Me-bridge. Additional MAO and the $AlMe_3$ it contains transforms the Zr to the $AlMe_3$ adduct **III** with its two Me-bridges. Finally, the last product formed is an unstabilized zirconocene methyl cation **IV** with an extremely weakly coordinated [Me-MAO^-] anion. The relative abundances of the four species depends on the Al to Zr ratio as discussed above but is also dependent on the formulation of the MAO[34-35] and the identity of the zirconocene[30-31]. The predominant species under conditions which lead to the highest activity is the $AlMe_3$ adduct **III**.

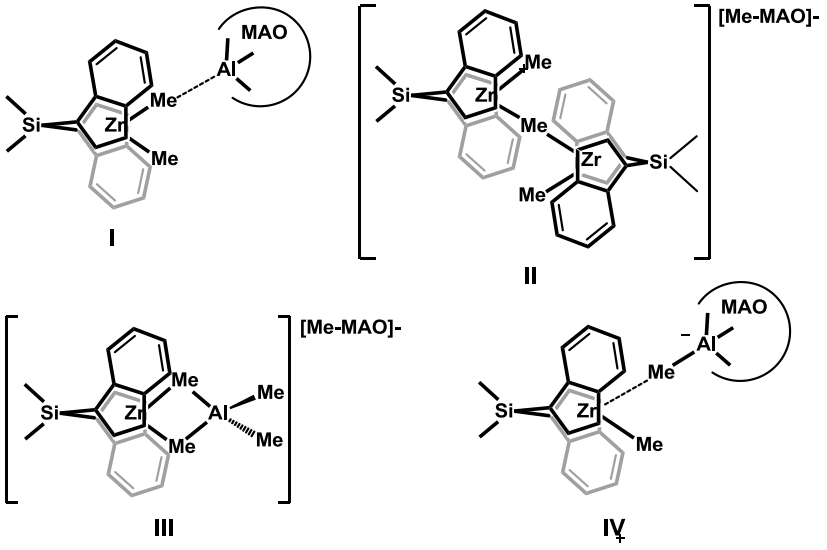

Figure 1.5: Cations formed with MAO as modeled by {(SBI)Zr}

As prealkylation of a zirconocene dichloride requires an extra step and yields a less stable precatalyst many recipes have been developed for the in situ alkylation of zirconocene dichlorides with Al^iBu_3[39-41] or HAl^iBu_2[42-43]. $Al^iBu_3/[Ph_3C][B(C_6F_5)_4]$ systems in general yield a mixture of products, however a few components have been identified by NMR spectroscopy (Figure 1.6). Götz has shown that $Ph_2C(C_5H_5)$(fluorenyl)$ZrCl_2$ yields a complex of type **V** upon reaction with $Al^iBu_3/[PhNMe_2H][B(C_6F_5)_4]$.[44] Bryliakov and Bochmann have seen a similar product formed from Me_2Si(indenyl)$ZrCl_2$ ((SBI)$ZrCl_2$) and $Al^iBu_3/[Ph_3C][B(C_6F_5)_4]$ along with a chloride-bridged dication dimer of type **VI** depending on the ratio of Al to Zr.[45] Bryliakov and Bochmann have also found an additional cationic species which they assigned as **VII** when subjecting (SBI)$HfCl_2$ to the $Al^iBu_3/[Ph_3C][B(C_6F_5)_4]$ conditions.[28]

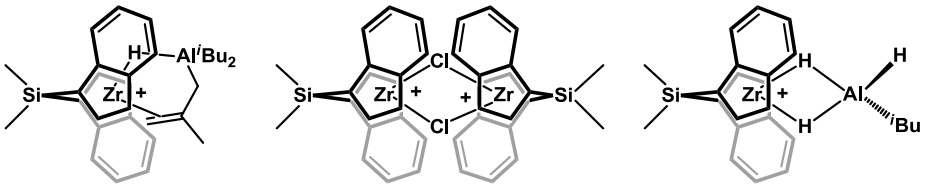

Figure 1.6: Cationic species formed from Al^iBu_3 mixtures with $[Ph_3C^+]$ or $[PhNMe_2H^+]$

Addition of Al^iBu_3 to MAO activated systems predominantly results in species similar to the $AlMe_3$-adduct **III**, with terminal aluminum alkyl groups which are either methyl or isobutyl groups in a statistical distribution.[46] Alternatively, similar results are obtained by activation with modified MAO (MMAO) which is made from Al^iBu_3 in addition to

$AlMe_3$.[36] Further addition of Al^iBu_3 or smaller amounts of HAl^iBu_2 to (SBI)$ZrCl_2$/MAO systems results in a new peak at –1.95 ppm which was believed to be due to a hydride species, however its identity could not be determined at the time.[47] Concurrent UV-vis spectroscopy revealed a decrease of the absorbance of the $AlMe_3$ adduct (490 nm) and the growth of a shoulder at 380 nm. More interestingly a similar absorbance appears when propene is added to the (SBI)$ZrCl_2$/MAO mixture at room temperature suggesting that hydrides are formed during the course of active polymerizations.[48]

1.4 Direct Observation of Catalytic Species

The direct observation of catalytic species during the course of ongoing polymerizations has proven a challenging feat. Actual observation of the propagating species by NMR spectroscopy has only been achieved by a few researchers over the last 10 years (Figure 1.7).[49-54] The monomer of choice for these studies has been 1-hexene, due mainly to the higher solubility of the polymer and greater ease of experimental setup. Only in the case Landis[50] and of Klamo[52] were other olefins examined, with both being able to follow of propene consumption. Klamo also investigated other olefins although ethene was still polymerized too quickly even at –100 ºC for monitoring by NMR. Only in Klamo's system,[52] which used $(C_5Me_5)(C_5H_5)ZrMe(CH_2CMe_3)$ as the precatalyst, was initiation fast relative to propagation such that in the remainder of cases unreacted $[L_2ZrMe][MeB(C_6F_5)_3]$ persisted throughout the course of the reaction[49-51, 53]. Only in the case of Babushkin and Brintzinger was a propagating species from polymerization with

MAO as the activator successfully observed by NMR.[54] They were able to monitor polymerization of 1-hexene with a mixture of (SBI)$ZrMe_2$ and MAO via ^1H NMR and observe species similar to the $AlMe_3$-adduct discussed above, which they assigned to a $AlMe_3$-adduct of a Zr-polymeryl cation (Figure 1.7). Troublingly Babushkin and Brintzinger were unable to account for all the Zr in solution. Up to 60% of the {(SBI)Zr} was present in a form which was not observable by ^1H NMR. In contrast Landis[49, 53] and Klamo[52] do not report any decrease of the total Zr concentration from the expected values. It should finally be noted that Tritto has observed $[Cp_2Zr(polymeryl]^+$ from in situ polymerizations of ethene with the Cp_2ZrCl_2/MAO or $Cp_2ZrMe_2/B(C_6F_5)_3$ systems, however only spectra after all the ethene had been consumed were reported.[25]

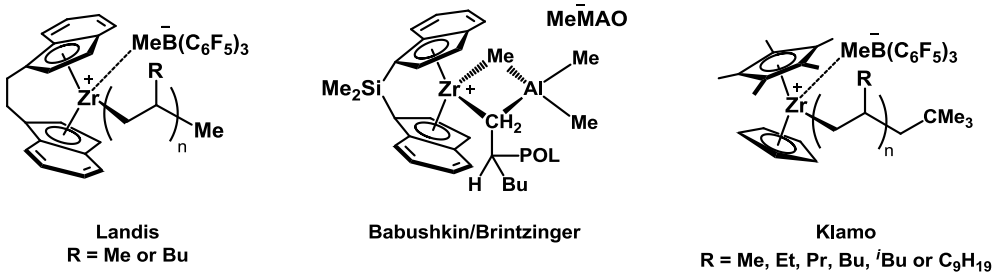

Figure 1.7: Directly observed propagating species

1.5 Kinetics of Polymerization

Predominantly the study of polymerization kinetics has been conducted from a macroscopic viewpoint based primarily on the correlation of polymer yield with reaction time. However since initiation is often much slower than polymerization as noted above, the activity estimated from polymer yield vastly underestimates the microscopic rate constant of polymerization, k_p. For this reason experiments which attempt to measure the

fraction of zirconocenes which are active during the course of the polymerization are vital to determining microscopic rate constants of polymerizations. Landis has utilized a variety of techniques including active site counting to develop a detailed kinetic model of polymerization by the (EBI)$ZrMe_2$/$B(C_6F_5)_3$ catalytic system.[49, 51, 55-58] Analysis of all of this data led to a kinetic model depicted in Scheme 1.2 along with a set of rate constants consistent with the data demonstrating that propagation (k_p) was faster than initiation (k_i) by almost 2 orders of magnitude.[58] Further analysis of the data by Abu-Omar and Caruthers lead to the rather suprising conclusion that inclusion of the full molecular weight distribution of the polymer resulted in a good fit only if a dormant Zr species was included in the kinetic model.[59] Full treatment of the data resulted in a much better fit of the data when only 57% of the catalyst was considered to be active for polymerization (Table 1.1). The identity of the inactive/dormant species could not be ascertained from the data present but a few possibilities could be ruled out.

Scheme 1.2

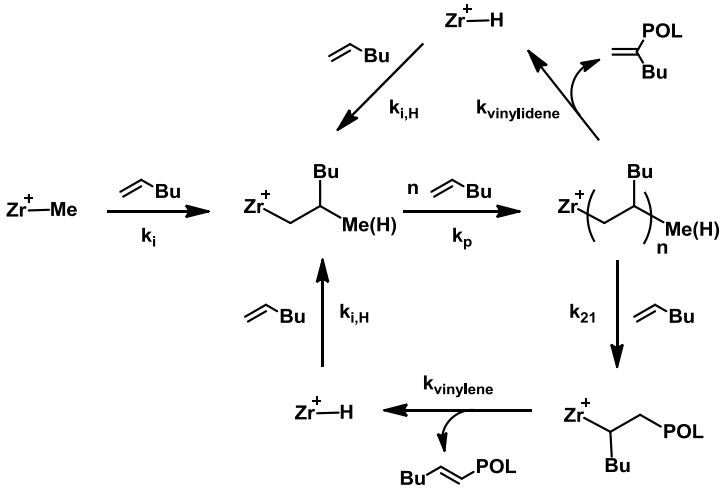

Table 1.1: Kinetic parameters of 1-hexene polymerization by (EBI)$ZrMe_2$ / $B(C_6F_5)_3$

	units	Landis[a]	Abu-Omar & Caruthers[b]
k_i	$M^{-1}\ s^{-1}$	0.033	0.031
k_p	$M^{-1}\ s^{-1}$	2.2	3.7
$k_{vinylidene}$	s^{-1}	0.00066	0.0024
$k_{vinylene}$	$M^{-1}\ s^{-1}$	0.0016	0.014
X_{active}	%	100	57
total SSE[c]	--	43	1.9

[a] from ref 58. [b] from ref 59. [c] SSE = sum of squared error.

1.6 Dormant Species

There are a few proposals for possible dormant Zr species. Among these are secondary Zr-alkyls as would result from 2,1-misinsertions of α-olefins, Zr-allyls which form from C—H bond activation, tight ion pairs which would need to dissociate prior to olefin insertion and Zr-hydrides as would form from chain transfer via β-hydride elimination (Figure 1.8). Evidence for and against each possibility has been accumulated over the years.

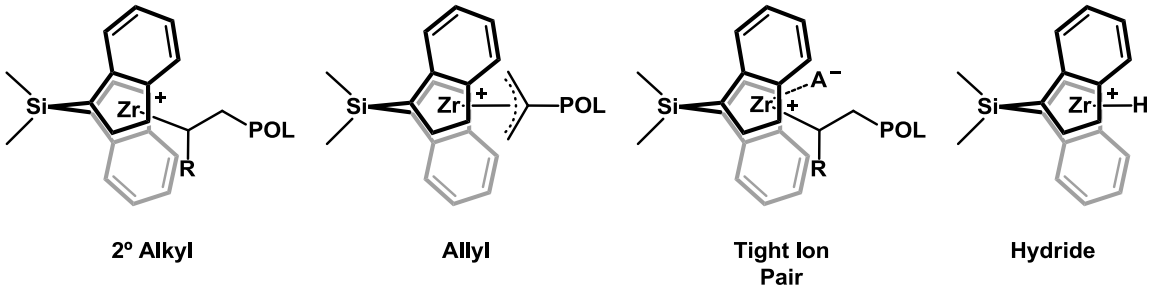

Figure 1.8: Possible dormant states of zirconocene catalysts as modeled by {(SBI)Zr} with A^- standing for a generic anion.

Landis and coworkers have shown that insertion of ethene into secondary Zr-alkyl species as would be formed after a 2,1-misinsertion of propene or 1-hexene are at least as fast as

those into a primary Zr-alkyl ruling out secondary Zr-alkyl species as the dormant state.[51] Prior experiments which had shown large concentrations of secondary Zr-alkyls via hydrogenolysis of active polymerizations[60-61] were shown to be a result of the faster rate of hydrogenolysis of secondary Zr-alkyls relative to primary analogues and not due to a higher concentration of secondary species[51]. On the other hand Busico has performed microstructural analysis of polypropene produced by a nonmetallocene catalyst with different pressures of ethene or hydrogen leading to the conclusion that insertion of propene into a secondary Zr-alkyl is ~ 33 times slower than insertion into a primary Zr-alkyl.[62] The difference in temperature between the two studies (–80 ºC and 25 ºC respectively) as well as in precatalysts does not allow for ease of comparison although a steric argument could be made that as the size of the inserting group increases (H_2 to ethene to propene) the rate of reaction of the secondary alkyl relative to the primary alkyl will decrease due to greater congestion around Zr.

Another candidate for the dormant species is a tight ion pair, resulting in what is known as the intermittent model of polymerization. Namely an anion dissociation event is followed by a series of rapid olefin insertions which are then halted by anion recoordination.[63] Landis was however able to show that addition of 10 equiv propene or ethene to a solution containing [(EBI)Zr(poly-1-hexene)$^+$] resulted in complete conversion of the poly-1-hexenyl species to a poly-propenyl or poly-ethenyl species whereas an intermittent

polymerization model would be expected to only result in partial conversion of the poly-1-hexenyl.[49]

The possibility of a Zr-allyl species as intermediate has been put forward by Landis.[55] Landis has found that polymerization of 1-hexene by the catalyst system of (SBI)ZrMe(CH_2TMS)/[Ph_3C][$B(C_6F_5)_4$] results in rapid consumption of 1-hexene yielding an allylic species as the sole observed Zr-containing product in contrast to the reactions with (EBI)$ZrMe_2$/$B(C_6F_5)_3$ described above which yielded a hydride species as the final Zr-containing product.[53] Allyls are formed following β-hydride elimination through a σ-bond metathesis reaction (Scheme 1.3). Further insertion into Zr-allyls results in incorporation of internal vinylidene groups into the polymer chain. The [(EBI)Zr(allyl)$^+$] was found to be a dormant species as addition of 50 equiv of unlabeled 1-hexene to a sample of the allyl made from 1-^{13}C-1-hexene resulted in rapid consumption of the unlabeled 1-hexene without significant decrease in signals due to the labeled allyl.[53] The caveat to all of this is that Landis was only able to observe the end of the reaction and was not able to say whether the allylic species formed during the course of the polymerization or after all monomer had been consumed.

Scheme 1.3

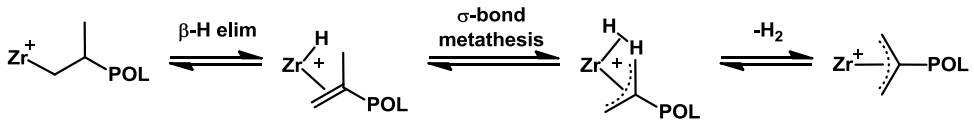

A final possibility for a dormant species is a hydride formed upon β-hydride elimination of a Zr-polymeryl species as first proposed by Collins[64]. Landis has seen a hydride as the final Zr-containing product from polymerization of 1-hexene with (EBI)$ZrMe_2$/$B(C_6F_5)_3$.[53] Fitting of concentration data revealed that the hydride product [(EBI)ZrMe][$HB(C_6F_5)_3$] reacted much more slowly with 1-hexene than did [(EBI)ZrMe][$MeB(C_6F_5)_3$] suggesting that the hydride could indeed be an elusive dormant species. While insertion into the hydride ($k_{i,H}$ = 2.06(2) M^{-1}/s^{-1}) was an order of magnitude faster than insertion into the initial methyl (k_i = 0.2353(6) M^{-1}/s^{-1}), insertion into the hydride was still an order of magnitude slower than insertion into a polymeryl group (k_p = 16.83(6) M^{-1}/s^{-1}) agreeing with the observation of buildup of Zr-hydrides over the course of the reaction. In the kinetic models used previously by Landis[58] and Abu-Omar/Caruthers[59] the reinitiation through insertion into the hydride was assumed to be extremely rapid in comparison to all other processes (Scheme 1.2) which has now been shown to be false. Two problems persist with the dormancy of the hydride species: (1) the identity of such a hydride in the presence of alkylaluminum species would certainly be different than that in Landis' system with only $B(C_6F_5)_3$ as the initiator and (2) the hydride is only observed in some cases while being absent in others.

1.7 Aims of this Thesis

The goals of this thesis are to determine the identity of the hydride observed by Babushkin and Brintzinger in (SBI)$ZrCl_2$ / MAO systems upon addition of Al^iBu_3 or HAl^iBu_2 [47] and to

determine the extent to which these species are possibly related to active polymerizations as implicated by UV-vis spectroscopy[48] and Landis' observations[53]. The identity of the putative hydride has been investigated through a study of the reactivity of zirconocene dichlorides with $HAl^{i}Bu_2$ (Chapter 2). Further work examined the effect of cationization reagents on the hydrides to identify cationic zirconocene hydrides which might form under conditions closer to those of MAO-activated homogeneous polymerization (Chapter 3). Finally these cations have been studied under polymerization conditions to determine whether they are in fact catalysts for olefin polymerization.

1.8 References

1. Bochmann, M. *Organometallics*, **2010**, *29*, 4711.
2. Poater, A.; Cavallo, L. *Dalton Trans.*, **2009**, 8878.
3. Kaminsky, W.; Funck, A.; Hahnsen, H. *Dalton Trans.*, **2009**, 8803.
4. Busico, V. *Dalton Trans.*, **2009**, 8794.
5. Möhring, P. C.; Coville, N. J. *Coordin. Chem. Rev.*, **2006**, *250*, 18.
6. Severn, J. R.; Chadwick, J. C.; Duchateau, R.; Friederichs, N. *Chem. Rev.*, **2005**, *105*, 4073.
7. Bochmann, M. *J. Organomet. Chem.*, **2004**, *689*, 3982.
8. Resconi, L.; Cavallo, L.; Fait, A.; Piemontesi, F. *Chem. Rev.*, **2000**, *100*, 1253.
9. Coates, G. W. *Chem. Rev.*, **2000**, *100*, 1223.
10. Chen, E. Y. X.; Marks, T. J. *Chem. Rev.*, **2000**, *100*, 1391.
11. Breslow, D. S.; Newburg, N. R. *J. Am. Chem. Soc.*, **1957**, *79*, 5072.
12. Natta, G.; Pino, P.; Mazzanti, G.; Giannini, U. *J. Am. Chem. Soc.*, **1957**, *79*, 2975.
13. Natta, G.; Pino, P.; Mazzanti, G.; Giannini, U.; Mantica, E.; Peraldo, M. *J. Polym. Sci.*, **1957**, *26*, 120.

14. Reichert, K. H.; Meyer, K. R. *Makromol. Chem.*, **1973**, *169*, 163.
15. Long, W. P.; Breslow, D. S. *Liebigs Ann. Chem.*, **1975**, 463.
16. Andresen, A.; Cordes, H. G.; Herwig, J.; Kaminsky, W.; Merck, A.; Mottweiler, R.; Pein, J.; Sinn, H.; Vollmer, H. J. *Angew. Chem.-Int. Edit. Engl.*, **1976**, *15*, 630.
17. Tullo, A. H., Metallocenes Rise Again. *C&E News* October 18, 2010, pp 10.
18. Grubbs, R. H.; Coates, G. W. *Acc. Chem. Res.*, **1996**, *29*, 85.
19. Krauledat, H.; Brintzinger, H. H. *Angew. Chem.-Int. Edit. Engl.*, **1990**, *29*, 1412.
20. Piers, W. E.; Bercaw, J. E. *J. Am. Chem. Soc.*, **1990**, *112*, 9406.
21. Leclerc, M. K.; Brintzinger, H. H. *J. Am. Chem. Soc.*, **1995**, *117*, 1651.
22. Pino, P.; Cioni, P.; Wei, J. *J. Am. Chem. Soc.*, **1987**, *109*, 6189.
23. Pédeutour, J. N.; Radhakrishnan, K.; Cramail, H.; Deffieux, A. *Macromol. Rapid. Comm.*, **2001**, *22*, 1095.
24. Yang, X. M.; Stern, C. L.; Marks, T. J. *J. Am. Chem. Soc.*, **1994**, *116*, 10015.
25. Tritto, I.; Donetti, R.; Sacchi, M. C.; Locatelli, P.; Zannoni, G. *Macromolecules*, **1999**, *32*, 264.
26. Bochmann, M.; Lancaster, S. J. *Angew. Chem.-Int. Edit. Engl.*, **1994**, *33*, 1634.
27. Talsi, E. P.; Eilertsen, J. L.; Ystenes, M.; Rytter, E. *J. Organomet. Chem.*, **2003**, *677*, 10.
28. Bryliakov, K. P.; Talsi, E. P.; Voskoboynikov, A. Z.; Lancaster, S. J.; Bochmann, M. *Organometallics*, **2008**, *27*, 6333.
29. Babushkin, D. E.; Semikolenova, N. V.; Zakharov, V. A.; Talsi, E. P. *Macromol. Chem. Phys.*, **2000**, *201*, 558.
30. Bryliakov, K. P.; Semikolenova, N. V.; Yudaev, D. V.; Ystenes, M.; Rytter, E.; Zakharov, V. A.; Talsi, E. P. *Macromol. Chem. Phys.*, **2003**, *204*, 1110.
31. Bryliakov, K. P.; Semikolenova, N. V.; Yudaev, D. V.; Zakharov, V. A.; Brintzinger, H. H.; Ystenes, M.; Rytter, E.; Talsi, E. P. *J. Organomet. Chem.*, **2003**, *683*, 92.
32. Talsi, E. P.; Bryliakov, K. P.; Semikolenova, N. V.; Zakharova, V. A.; Ystenes, M.; Rytter, E. *Mendeleev Commun.*, **2003**, 46.

33. Babushkin, D. E.; Naundorf, C.; Brintzinger, H. H. *Dalton Trans.*, **2006**, 4539.
34. Bryliakov, K. P.; Semikolenova, N. V.; Panchenko, V. N.; Zakharov, V. A.; Brintzinger, H. H.; Talsi, E. P. *Macromol. Chem. Phys.*, **2006**, *207*, 327.
35. Wieser, U.; Schaper, F.; Brintzinger, H. H. *Macromol. Symp.*, **2006**, *236*, 63.
36. Lyakin, O. Y.; Bryliakov, K. P.; Semikolenova, N. V.; Lebedev, A. Y.; Voskoboynikov, A. Z.; Zakharov, V. A.; Talsi, E. P. *Organometallics*, **2007**, *26*, 1536.
37. Talsi, E. P.; Bryliakov, K. P.; Semikolenova, N. V.; Zakharov, V. A.; Bochmann, M. *Kinet. Catal.*, **2007**, *48*, 490.
38. Tritto, I.; Li, S. X.; Sacchi, M. C.; Zannoni, G. *Macromolecules*, **1993**, *26*, 7111.
39. Kleinschmidt, R.; van der Leek, Y.; Reffke, M.; Fink, G. *J. Mol. Catal. A-Chem.*, **1999**, *148*, 29.
40. Kaminaka, M.; Matsuoka, H. Patent JP11240912, 1999.
41. Wang, S. Patent US2005070675, 2005.
42. Gregorius, H.; Fraaije, V.; Lutringhauser, M. Patent DE10258968, 1994.
43. Ohno, R.; Tsutsui, T. Patent EP0582480, 1994.
44. Götz, C.; Rau, A.; Luft, G. *J. Mol. Catal. A-Chem.*, **2002**, *184*, 95.
45. Bryliakov, K. P.; Talsi, E. P.; Semikolenova, N. V.; Zakharov, V. A.; Brand, J.; Alonso-Moreno, C.; Bochmann, M. *J. Organomet. Chem.*, **2007**, *692*, 859.
46. Babushkin, D. E.; Brintzinger, H. H. *Chem.-Eur. J.*, **2007**, *13*, 5294.
47. Babushkin, D. E.; Panchenko, V. N.; Timofeeva, M. N.; Zakharov, V. A.; Brintzinger, H. H. *Macromol. Chem. Phys.*, **2008**, *209*, 1210.
48. Panchenko, V. N.; Brintzinger, H. H. Personal Communication 2008
49. Landis, C. R.; Rosaaen, K. A.; Sillars, D. R. *J. Am. Chem. Soc.*, **2003**, *125*, 1710.
50. Sillars, D. R.; Landis, C. R. *J. Am. Chem. Soc.*, **2003**, *125*, 9894.
51. Landis, C. R.; Sillars, D. R.; Batterton, J. M. *J. Am. Chem. Soc.*, **2004**, *126*, 8890.
52. Klamo, S. B. PhD Thesis, California Institute of Technology, Pasadena, CA, 2005.
53. Christianson, M. D.; Tan, E. H. P.; Landis, C. R. *J. Am. Chem. Soc.*, **2010**, *132*, 11461.
54. Babushkin, D. E.; Brintzinger, H. H. *J. Am. Chem. Soc.*, **2010**, *132*, 452.

55. Landis, C. R.; Christianson, M. D. *P. Natl. Acad. Sci. USA*, **2006**, *103*, 15349.
56. Landis, C. R.; Rosaaen, K. A.; Uddin, J. *J. Am. Chem. Soc.*, **2002**, *124*, 12062.
57. Liu, Z. X.; Somsook, E.; Landis, C. R. *J. Am. Chem. Soc.*, **2001**, *123*, 2915.
58. Liu, Z. X.; Somsook, E.; White, C. B.; Rosaaen, K. A.; Landis, C. R. *J. Am. Chem. Soc.*, **2001**, *123*, 11193.
59. Novstrup, K. A.; Travia, N. E.; Medvedev, G. A.; Stanciu, C.; Switzer, J. M.; Thomson, K. T.; Delgass, W. N.; Abu-Omar, M. M.; Caruthers, J. M. *J. Am. Chem. Soc.*, **2010**, *132*, 558.
60. Busico, V.; Cipullo, R.; Corradini, P. *Makromol. Chem., Rapid. Commun.*, **1993**, *14*, 97.
61. Tsutsui, T.; Kashiwa, N.; Mizuno, A. *Makromol. Chem., Rapid. Commun.*, **1990**, *11*, 565.
62. Busico, V.; Cipullo, R.; Romanelli, V.; Ronca, S.; Togrou, M. *J. Am. Chem. Soc.*, **2005**, *127*, 1608.
63. Schaper, F.; Geyer, A.; Brintzinger, H. H. *Organometallics*, **2002**, *21*, 473.
64. Al-Humydi, A.; Garrison, J. C.; Mohammed, M.; Youngs, W. J.; Collins, S. *Polyhedron*, **2005**, *24*, 1234.

CHAPTER 2

Neutral Alkylaluminum-Complexed Zirconocene Hydrides

2.1 Abstract

Reactions of unbridged zirconocene dichlorides, $(R_nC_5H_{5-n})_2ZrCl_2$ (n = 0, 1 or 2), with diisobutylaluminum hydride, HAl^iBu_2, result in the formation of tetranuclear trihydride clusters of the type $(R_nC_5H_{5-n})_2Zr(\mu\text{-}H)_3(Al^iBu_2)_3(\mu\text{-}Cl)_2$, which contain three $\{Al^iBu_2\}$ units. Ring-bridged *ansa*-zirconocene dichlorides, $Me_2E(R_nC_5H_{4-n})_2ZrCl_2$ with E = C or Si, on the other hand, are found to form binuclear dihydride complexes of the type $Me_2E(R_nC_5H_{4-n})_2Zr(Cl)(\mu\text{-}H)_2Al^iBu_2$ with only one $\{Al^iBu_2\}$ unit. The dichotomy between unbridged and bridged zirconocene derivatives, with regard to tetranuclear *vs*. binuclear product formation, is proposed to be connected to different degrees of rotational freedom of their C_5-ring ligands.

This Chapter is published in part as:
Baldwin, S. M.; Bercaw, J. E.; Brintzinger, H. H. *J. Am. Chem. Soc.*, **2008**, *130*, 17423.
(DOI: 10.1021/ja8054723)

2.2 Introduction

In view of their manifold catalytic properties, a great variety of zirconocene hydride complexes as well as adducts of some of these entities, with organoaluminum or other organometal hydrides, have been isolated and characterized by spectroscopic and/or crystallographic methods.[1-2] From some reaction systems, mononuclear or binuclear zirconocene hydride cations have been isolated.[3-6] Most abundant, however, appear to be neutral—binuclear or oligonuclear—zirconocene hydride complexes, the Zr(IV) centers of which are incorporated in a $\{ZrH_3\}$ core structure.

$\{ZrH_3\}$ coordination patterns have been crystallographically characterized, e.g., in many dimeric zirconocene dihydrides,[7-14] in adducts of a zirconocene hydride moiety with another neutral metal hydride species,[15-16] e.g., with AlH_3 [17-18] or in an anionic $[(C_5Me_5)_2ZrH_3]^-$ entity in contact with suitable cations such as Li^+ or K^+.[19-20] Systems resulting from reaction of zirconocene dichloride or dihydride complexes with organoaluminum hydrides catalyze alkene hydrometallations or polymerizations, and have been reported—based mainly on spectroscopic evidence—to contain oligonuclear species with hydride-bridged $\{ZrAl_2\}$ or $\{Zr_2Al_2\}$ cores. These Zr centers adopt, again, a $\{ZrH_3\}$ coordination geometry (Figure 2.1, structures **A** and **B**, respectively).[21-27]

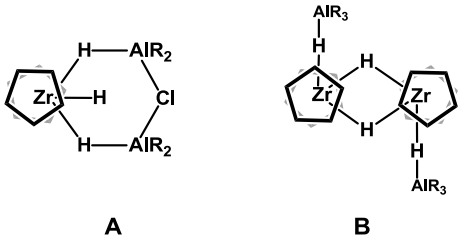

Figure 2.1: $\{ZrH_3\}$ coordination geometries proposed for alkylaluminum-complexed zirconocene hydride complexes in references 21-27.

Recently, however, zirconocene hydride complexes which deviate from the commonly observed $\{ZrH_3\}$ coordination pattern have been encountered in MAO-activated zirconocene precatalyst systems upon addition of HAl^iBu_2 or Al^iBu_3.[28-29] The ^1H NMR spectra of these species show only a single hydride resonance with an integral corresponding to two hydride units per Zr center, which indicates the presence of a $\{ZrH_2\}$ unit with two equivalent H ligands.[29] In order to characterize the species responsible for this NMR signal and the factors which govern the formation of $\{ZrH_2\}$-type, as opposed to $\{ZrH_3\}$-type zirconocene hydride complexes, a reevaluation of some previously described reactions of unbridged zirconocene complexes with diisobutylaluminum hydride and subsequent study of corresponding reactions of several *ansa*-zirconocene dichlorides was undertaken.

For simplicity, diisobutylaluminum hydride is written here, and in the following, as a monomer, even though it is undoubtedly preponderantly present as a trimer in solution under our experimental conditions.[30-32] Similarly, diisobutylaluminum chloride is written as a monomer although it is dimeric in solution.[33]

2.3 Results and Discussion

2.3.1 Unbridged Zirconocene Complexes

In accord with earlier reports, excess $HAl^{i}Bu_2$ reacts with $(C_5H_5)_2ZrCl_2$ (**1**) in benzene-d_6 at 25 ºC to give a species with two characteristic hydride NMR signals: a triplet at –0.89 ppm with an intensity of 1H and a doublet at –2.06 ppm with an intensity of 2H per zirconocene unit (Figure 2.2, **A** and **B**). This signal pattern has previously been ascribed to a trinuclear cluster, $(C_5H_5)_2ZrH_3(Al^{i}Bu_2)_2Cl$, containing a $[(C_5H_5)_2ZrH_3]$ moiety in contact with a chloride-bridged bis(diisobutylaluminum) unit (structure **A** in Figure 2.1).[22] This species has recently been proposed to be an (inactive) component in zirconocene-based reaction systems, which catalyze the hydroalumination of α-olefins.[23-24]

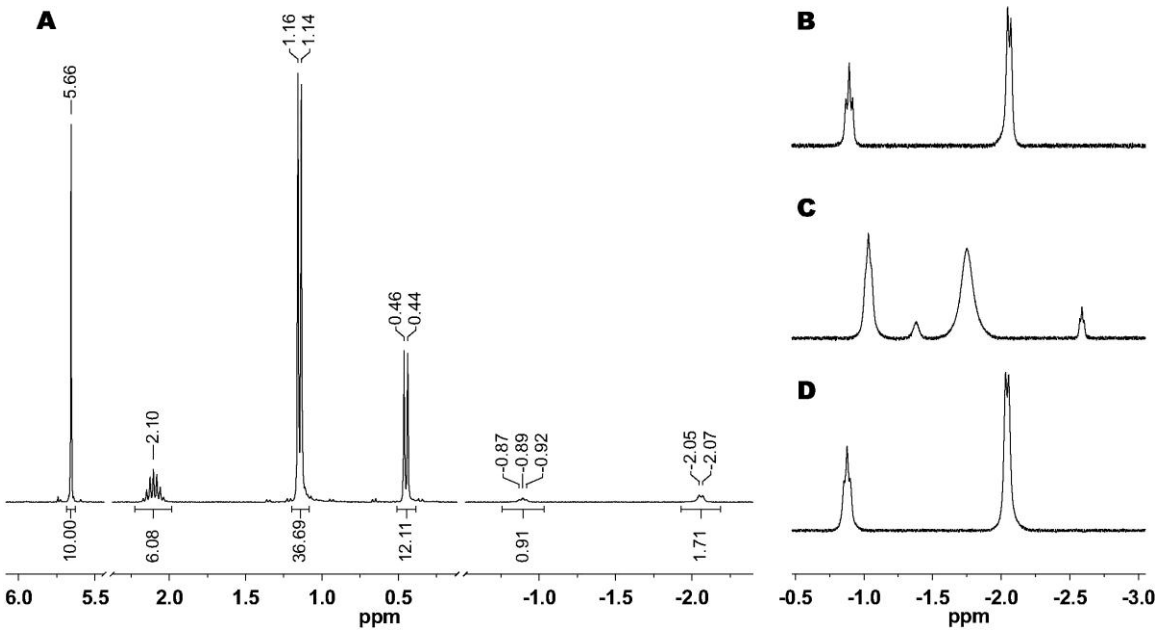

Figure 2.2: ^{1}H NMR spectrum of a 50 mM solution of $(C_5H_5)_2ZrCl_2$ (**1**) in benzene-d_6 at 25 °C after addition of 3 equiv of HAl^iBu_2 (**A**) and blowups of the hydride regions of the same (**B**) as well as a 71 mM solution of $(C_5H_5)_2ZrH_2$ (**3**) in benzene-d_6 at 25 °C after addition of 1 equiv of HAl^iBu_2 and 1 equiv of $ClAl^iBu_2$ (**C**) and a 51 mM solution of $(C_5H_5)_2ZrH_2$ (**3**) in benzene-d_6 at 25 ºC after addition of 1 equiv of HAl^iBu_2 and 1 equiv of $ClAl^iBu_2$ (**D**).

The assignment of structure **A**, to the product formed from $(C_5H_5)_2ZrCl_2$ and HAl^iBu_2, does not appear to be correct. An earlier formulation of this complex, as a $\{ZrH_3Al_2Cl\}$ cluster, was based mainly on cryoscopy data which gave a molar mass close to that expected for **A**.[22] These cryoscopy measurements are likely to be complicated, however, by the low solubility of the dichloride starting compound and by the presence of some free $(HAl^iBu_2)_3$ in equilibrium with it. Careful integration of the isobutyl signals, versus the C_5H_5 signal, in reaction systems containing complex **1** and HAl^iBu_2 consistently yields a $\{Al^iBu_2\}$ to Zr ratio of (3.02 ± 0.03):1. Even when **1** is used in excess, only the product with three

{Al^{i}Bu$_2$} units per zirconocene unit is observed, with an NMR spectrum identical to that described above, while unreacted **1** remains behind as a solid. The reaction of **1** with HAl^{i}Bu$_2$ thus appears to lead to the immediate and complete formation of a tetranuclear cluster of composition $(C_5H_5)_2ZrH_3(Al^iBu_2)_3Cl_2$ (**2**, Scheme 2.1).

Scheme 2.1

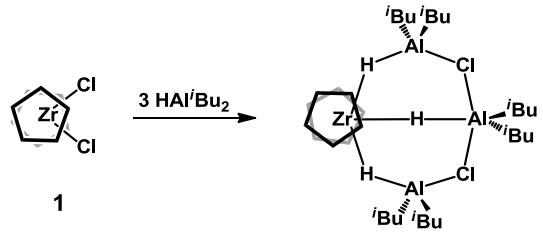

1 **2**

In order to verify that three {Al^{i}Bu$_2$} units and two Cl bridges are indeed present in the reaction product, we have designed the experiment outlined in Scheme 2.2. The zirconocene dihydride, **3**,[34-35] reacts with 1 equiv of HAl^{i}Bu$_2$ per zirconocene unit to form species **4**, characterized by a 1:1 pair of hydride signals at –2.12 and –3.06 ppm in toluene-d_8 solution at –75 ºC (Table 2.1), which had been seen also for adducts of the dimeric zirconocene dihydride complex, **3**, with various aluminum trialkyl compounds (structure **B** in Figure 2.1).[21-24, 26] Addition of 1 equiv of ClAl^{i}Bu$_2$ per zirconocene to such a reaction system—which would be required to form species **A**—gives instead four broad signals between –1 and –3 ppm, which indicate the presence of several mutually interconverting hydride products (Figure 2.2 **C**). Clean formation of the trihydride species **2** with sharp hydride signals at –0.89 ppm (t, 1H) and –2.06 ppm (d, 2H) is observed, however, when exactly 2 equiv of ClAl^{i}Bu$_2$ are added to the reaction system containing 1 equiv each of

$(C_5H_5)_2ZrH_2$ and of HAl^iBu_2 (Figure 2.2 **D**). The exclusive and complete formation of species **2** via this alternative route (Scheme 2.2) corroborates its composition $(C_5H_5)_2ZrH_3(Al^iBu_2)_3Cl_2$.

Scheme 2.2

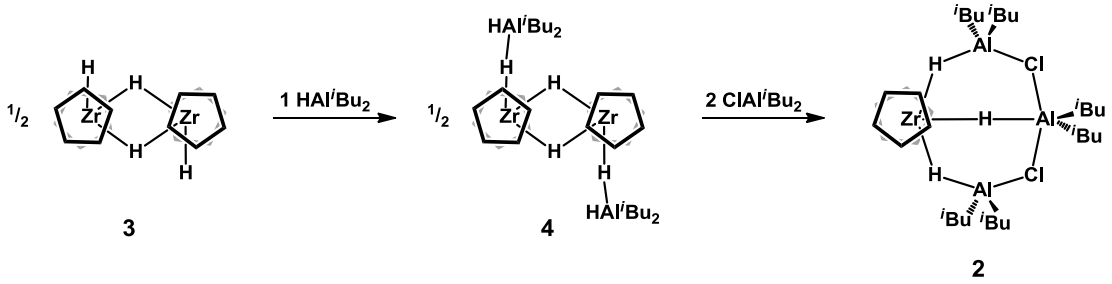

Table 2.1: ^{1}H NMR Signals of Unbridged Zirconocene Complexes and of Their Reaction Products with HAl^{i}Bu$_2$ [a]

	Zr-H	Al^{i}Bu$_2$	ligand
$(C_5H_5)_2ZrCl_2$ (**1**)			5.89 (s, 10H)
$(C_5H_5)_2Zr(\mu\text{-}H)_3(Al^{i}Bu_2)_3(\mu\text{-}Cl)_2$ (**2**)	−0.89 (t, 1H, 7 Hz) −2.03 (d, 2H, 7 Hz)	0.45 (d, 12H, 7 Hz) 1.15 (d, 36H, 6 Hz) 2.10 (m, 6H, 7 Hz)	5.66 (s, 10H)
$((C_5H_5)_2ZrH)_2(\mu\text{-}H)_2$ (**3**)[b]	−3.45 (t, 2H, 7 Hz) 3.85 (t, 2H, 7 Hz)		5.75 (s, 20H)
$((C_5H_5)_2ZrH\cdots HAl^{i}Bu_2)_2(\mu\text{-}H)_2$ (**4**)[c]	−2.11 (br, 2H) −3.05 (br, 2H)	0.39 (d, 8H, 7Hz) 1.18 (d, 24H, 5Hz) 2.36 (br, 4H)	5.40 (s, 20H)
$(C_5H_5)_2Zr(\mu\text{-}H)_3(Al^{i}Bu_2)_3(\mu\text{-}H)_2$ (**5**)[c]	−1.46 (t, 1H, 16 Hz) −2.33 (d, 2H, 17 Hz)	0.44 (br, 12 H) 1.25 (br, 36 H) 2.16 (br, 6 H)	5.34 (s, 10H)
$(^{n}Bu\text{-}C_5H_4)_2ZrCl_2$ (**6**)			0.84 (t, 6H, 8 Hz) 1.22 (s, 4H, 7 Hz) 1.43 (p, 4H, 7 Hz) 2.64 (t, 4H, 7 Hz) 5.74 (pt, 4H, 3 Hz) 5.92 (pt, 4H, 3 Hz)
$(^{n}Bu\text{-}C_5H_4)_2Zr(\mu\text{-}H)_3(Al^{i}Bu_2)_3(\mu\text{-}Cl)_2$ (**7**)	−0.58 (t, 1H, 7 Hz) −1.54 (d, 2H,7 Hz)	0.51 (d, 12H, 7 Hz) 1.18 (d, 36H, 7 Hz) 2.15 (m, 6H, 7 Hz)	0.86 (t, 6H, 8 Hz) 2.24 (t, 4H, 7 Hz)[d] 5.65 (br, 4H) 5.94 (br, 4H)
$(1,2\text{-}Me_2\text{-}C_5H_3)_2ZrCl_2$ (**8**)			5.47 (t, 2H, 3 Hz) 5.62 (d, 4H, 3 Hz)
$(1,2\text{-}Me_2\text{-}C_5H_3)_2Zr(\mu\text{-}H)_3(Al^{i}Bu_2)_3(\mu\text{-}Cl)_2$ (**9**)	−0.20 (t, 1H, 7 Hz) −1.13 (d, 2H, 6 Hz)	0.52 (d, 12H, 7 Hz) 1.19 (d, 36H, 6 Hz) 2.18 (br, 6H)	5.58 (t, 2H, 3 Hz) 5.65 (d, 4H, 3 Hz)
$(Me_3Si\text{-}C_5H_4)_2ZrCl_2$ (**10**)			0.33 (s, 18H) 5.93 (pt, 4H, 3 Hz) 6.39 (pt, 4H, 3 Hz)
$(Me_3Si\text{-}C_5H_4)_2Zr(\mu\text{-}H)_3(Al^{i}Bu_2)_3(\mu\text{-}Cl)_2$ (**11**)[c]	−1.31 (br, 1H) −2.09 (br, 2H)	all broad	0.00 (s,18H) 5.96 (br, 4H) 6.11 (br, 4H)
$(C_5Me_5)_2ZrCl_2$ (**12**)			1.85 (s, 30H)
$(C_5Me_5)_2ZrH_2$ (**13**)	7.50 (s, 2H)		2.02 (s, 30H)
$(C_5Me_5)_2ZrH^{i}Bu$ (**14**)	6.13 (s, 1H)	– 0.03 (d, 2H, 7 Hz) 1.02 (d, 6H, 7 Hz) 2.39 (m, 1H, 7 Hz)	1.91 (s, 30H)
$(C_5Me_5)_2Zr^{i}Bu_2$ (**15**)		0.69 (d, 4H, 7 Hz) 1.25 (d, 12H, 7 Hz) 2.22 (m, 2H, 7 Hz)	1.85 (s, 30H)
$(C_5H_5)_2HfCl_2$			5.81 (s, 10H)
$(C_5H_5)_2Hf(\mu\text{-}H)_3(Al^{i}Bu_2)_3(\mu\text{-}Cl)_2$	−0.26 (br, 2H) −1.13 (br, 1H)	0.44 (d, 7 Hz) 1.10 (d, 6 Hz) 2.04 (m)	5.54 (s, 10H)

[a] In benzene-d_6 at 25 °C. [b] From ref [35]. [c] In toluene-d_8 at -75 °C. [d] Two resonances overlap with ^{i}Bu signals

Further support for this assignment comes from the observation that reaction of the dimeric dihydride **3** with 2 equiv of $ClAl^{i}Bu_2$ yields a 2:1 mixture of the hydride cluster **2** and the dichloride **1**, in accord with the stoichiometry expected from Equation **2.1**.

$$1/2\ ((C_5H_5)_2ZrH_2)_2 + ClAl^{i}Bu_2 \longrightarrow 2/3\ (C_5H_5)_2ZrH_3(Al^{i}Bu_2)_3Cl_2 + 1/3\ (C_5H_5)_2ZrCl_2 \qquad 2.1$$

Although attempts to isolate complex **2** and obtain crystals suitable for x-ray diffraction were unsuccessful, we propose the structure shown in Scheme 2.1 and Scheme 2.2, as a representation of its—presumably time-averaged—C_2-symmetric NMR characteristics. Whether the central Al center of this complex is indeed five-coordinate, as represented in Scheme 2.1, cannot be established on the basis of the evidence reported above. Recent DFT calculations have been reported[36] which include complexes **2**. A five-coordinate central aluminum was found with a 1.72 Å Al-H bond.

When the dimeric zirconocene dihydride **3** is reacted, rather than with $ClAl^{i}Bu_2$, with 3 equiv of $HAl^{i}Bu_2$ per zirconocene unit in toluene-d_8, one observes, at –75 ºC, two hydride NMR signals with an intensity ratio of 2 to 1: a doublet at –2.32 ppm and a triplet at –1.46 ppm (Figure 2.3). These signals closely resemble those assigned to the $\{ZrH_3\}$ core of species **2** (Table 2.1). On the basis of this similarity and on the observation of an additional signal at 3.18 ppm with an integral of 2H, which we assign to two bridging {Al-H-Al} units, the product of this reaction is likely to be the cluster **5**, i.e., an analogue to complex **2** with hydride instead of chloride bridges (Scheme 2.3). Recently reported DFT calculations[36] also found an Al-H bond for the central hydride in this complex.

Scheme 2.3

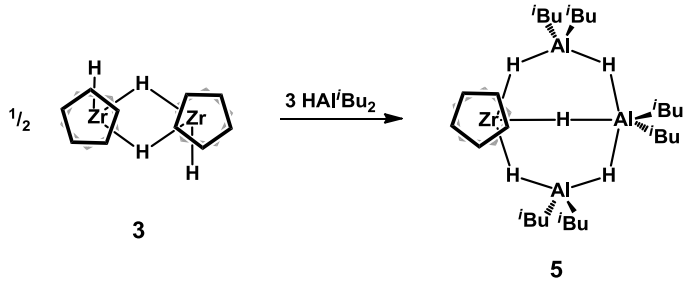

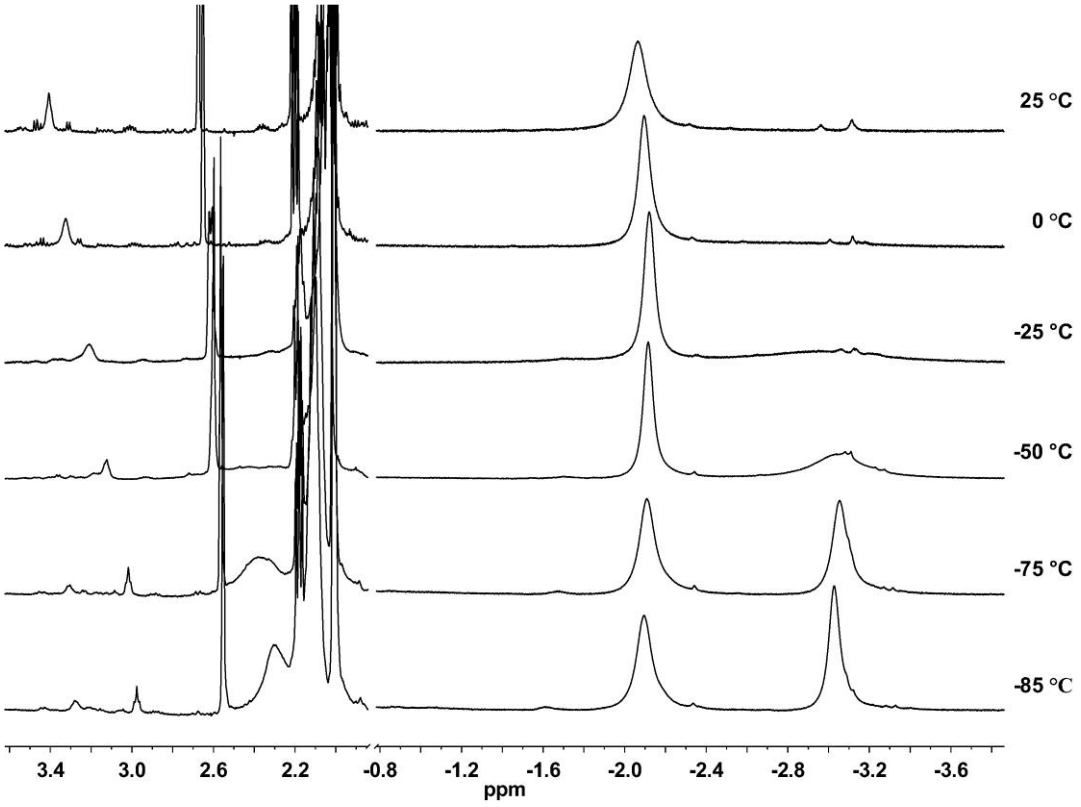

Figure 2.3: ^{1}H NMR spectra of an 11mM solution of Cp_2ZrH_2 in toluene-d_8 at variable temperatures after addition of 1 equiv HAl^{i}Bu$_2$.

When the temperature of this reaction system is increased from –75 to 0 ºC, the Zr-H signals of complex **5** at –2.32 and –1.46 ppm coalesce with each other and with the {Al-*H*-Al} signal at 3.18 ppm. At 25 ºC, finally, all of these signals become so broad as to be

hardly detectable. Facile exchange between lateral and central Zr-H positions, and of both of these with the peripheral Al-H-Al units, is indicated by this observation. The entirely H-bridged species **5** thus appears much more prone to undergo exchange reactions than its congener **2**, which contains two Al-Cl-Al bridges. At above-ambient temperatures, the appearance of violet colorations indicates that decomposition occurs in this system.

Similar spectra as for the system **1**/HAl^{i}Bu$_2$ are observed when unbridged zirconocene dichlorides with substituted C_5-rings are reacted with HAl^{i}Bu$_2$ in benzene or toluene solution (Table 2.1). Reactions of (^{n}Bu-C_5H_4)$_2$ZrCl$_2$ (**6**), (1,2-Me$_2$-C_5H_3)$_2$ZrCl$_2$ (**8**) or (Me$_3$Si-C_5H_4)$_2$ZrCl$_2$ (**10**) with 2 equiv of HAl^{i}Bu$_2$ each give a species with a doublet and a triplet Zr-*H* signal at ca. –1 ppm and –0.2 ppm, respectively (Figure 2.4). Integrals of these and the respective ^{i}Bu and ring ligand signals are in accord with the presence of tetranuclear trihydride clusters, **7**, **9** and **11** (Table 2.1), respectively. In comparison to their unsubstituted analogue **2**, the Zr-H signals of all these complexes appear shifted to lower fields by ca. 0.5 – 1 ppm, presumably due to changes in the electron density of their substituted ring ligands.

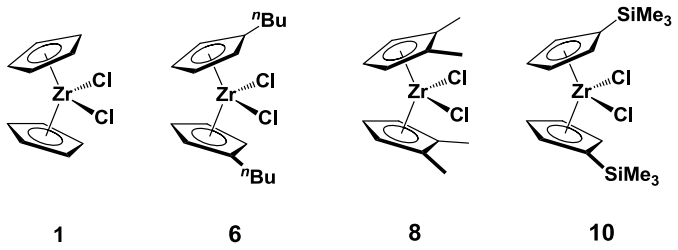

Figure 2.4: Unbridged zirconocenes studied with HAl^{i}Bu$_2$

In distinction to the reaction systems discussed so far, permethylzirconocene dichloride, $(C_5Me_5)_2ZrCl_2$ (**12**), does not give a hydride complex when reacted with 2 equiv of HAl^iBu_2 in benzene-d_6 solution at 25 ºC. Instead, a slight shift of its ^1H NMR signal indicates that its Cl ligands might form an adduct with HAl^iBu_2. The dihydride complex $(C_5Me_5)_2ZrH_2$ (**13**), on the other hand, reacts with 1 – 2 equiv of Al^iBu_3 to give mixtures of the monohydride monoisobutyl complex $(C_5Me_5)_2ZrH^iBu$ (**14**) and the diisobutyl complex $(C_5Me_5)_2Zr^iBu_2$ (**15**). A 10-fold excess of either Al^iBu_3 or HAl^iBu_2 in benzene-d_6 solution at 25 ºC converts the dihydride **13** practically completely to the diisobutyl complex $(C_5Me_5)_2Zr^iBu_2$ (**15**). Remarkably enough, bulky ^{i}Bu groups, rather than hydride units, are thus preferentially transferred from Al to the sterically shielded Zr center of $(Me_5C_5)_2ZrCl_2$.

Apparently, formation of a trihydridic $\{ZrH_3\}$ unit in combination with an array of spatially demanding $\{Al^iBu_2\}$ units is disfavored by steric factors in this case. If formation of the otherwise preferred {Zr-H-Al} bridges is precluded by steric factors, hydride units present in these reaction systems appear to be more favorably accommodated in hydride-bridged alkylaluminum clusters rather than in a Zr-H moiety.

2.3.2 Bridged Zirconocene Complexes.

Alkylaluminum-complexed zirconocene dihydride complexes have been observed, by a ZrH_2 signal at ca. –2.0 ppm, to form in catalyst systems containing *rac*-$Me_2Si(1\text{-indenyl})_2ZrCl_2$, ((SBI)$ZrCl_2$, **16**), and MAO upon addition of excess Al^iBu_3 or HAl^iBu_2.[29]

In the following, we seek to ascertain structural assignments for alkylaluminum-complexed *ansa*-zirconocene hydrides, which differ from their unbridged congeners discussed above by the presence of only two, instead of three, hydride ligands at their Zr centers.

(SBI)$ZrCl_2$ was found to react with a 2- to 5-fold excess of HAl^iBu_2 in benzene or toluene solutions at room temperature to form a hydride product, which obviously contains a $\{ZrH_2\}$ group, as indicated by a broad singlet at –1.29 ppm with an integral corresponding to two protons per zirconocene unit.[29] The (SBI) ligand resonances of this product are shifted only slightly from their positions in the dichloride complex **16** (Figure 2.5, Table 2.2), thus indicating the presence of a neutral zirconocene species with an intact (SBI) ligand framework. Integration of the isobutyl signals indicates that approximately four $\{Al^iBu_2\}$ units are present in solution per zirconocene unit. Use of lower ratios of Al to Zr results in a portion of the (SBI)$ZrCl_2$ remaining unreacted. A finite concentration of free HAl^iBu_2 thus has to be present in these solutions to bring the conversion of the *ansa*-zirconocene dichloride to completion. Ligand and hydride signals for the SBI complex, shown in Figure 2.5, were found to remain essentially unchanged down to –75 ºC by variable-temperature ^1H NMR and no fluxional behavior could be frozen out.

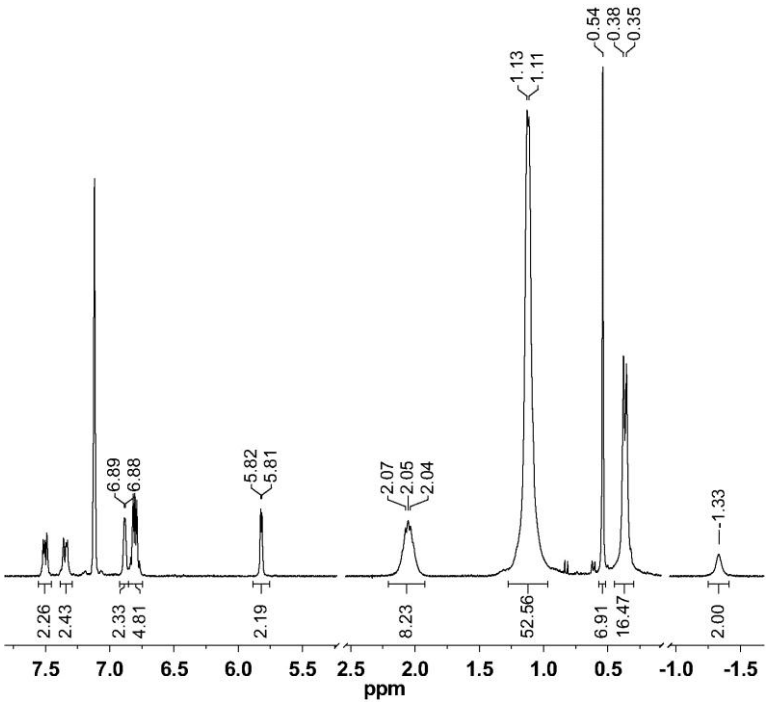

Figure 2.5: ^{1}H NMR spectrum of a 50 mM solution of (SBI)$ZrCl_2$ (**16**) in benzene-d_6 at 25 °C after addition of 3 equiv of HAl^iBu_2.

Table 2.2: ^{1}H NMR Signals of Bridged Zirconocene Complexes and Their Reaction Products with HAl^iBu_2 and/or $ClAl^iBu_2$ [a]

	Zr-H	Al^iBu_2[b]	ligand C_5-H[c]
rac-(SBI)$ZrCl_2$ (**16**)			5.76 (d, 2H, 3 Hz) 6.81 (d, 2H, 3 Hz)
rac-(SBI)$ZrCl(\mu\text{-}H)_2Al^iBu_2$	−1.29 (br, 2H)	0.41 1.16 2.10	5.86 (d, 2H, 3 Hz) 6.92 (d, 2H, 3 Hz)
rac-(SBI)$ZrCl(\mu\text{-}H)_2AlMe_2$	–1.58 (br, 2H)	–0.38	5.73 (br, 2H) 6.69 (br, 2H)
rac-(EBI)$ZrCl_2$ (**17**)			5.75 (d, 2H, 3 Hz) 6.47 (d, 2H, 3 Hz)
rac-(EBI)$ZrCl(\mu\text{-}H)_2Al^iBu_2$	−0.80 (br, 2H)	0.42 1.17 2.10	5.88 (br, 2H) 6.32 (br, 2H)
$Me_2C(C_5H_4)_2ZrCl_2$ (**19**)			5.19 (pt, 4H, 3 Hz) 6.42 (pt, 4H, 3 Hz)
$Me_2C(C_5H_4)_2ZrCl(\mu\text{-}H)_2Al^iBu_2$	−1.36 (br, 2H)	0.47 1.09 2.04	5.23 (br, 4H) 6.13 (br, 4H)
$Me_2Si(C_5H_4)_2ZrCl_2$ (**20**)			5.52 (pt, 4H, 3 Hz) 6.81 (pt, 4H, 3 Hz)
$Me_2Si(C_5H_4)_2ZrCl(\mu\text{-}H)_2Al^iBu_2$	−1.75 (br, 2H)	0.47	5.52 (br, 4H)

		1.13 2.08	6.40 (br, 4H)
$Me_2Si(2,4\text{-}Me_2\text{-}C_5H_2)_2ZrCl_2$ (**21**)			5.05 (d, 2H, 2 Hz) 6.39 (d, 2H, 2 Hz)
$Me_2Si(2,4\text{-}Me_2\text{-}C_5H_2)_2ZrCl(\mu\text{-}H)_2Al^iBu_2$	−0.77 (br, 2H)	0.48 1.08 2.02	5.03 (br, 2H) 6.34 (br, 2H)
$(Me_2Si)_2(C_5H_3)_2ZrCl_2$ (**22**)[d]			6.14 (t, 2H, 3 Hz) 6.72 (d. 4H, 3 Hz)
$(Me_2Si)_2(C_5H_3)_2ZrCl(\mu\text{-}H)_2Al^iBu_2$ [d,e]	−1.72 (s, 2H)	0.42 1.12 2.08	5.98 (br, 2H) 6.76 (br, 4H)
$(Me_2Si)_2(2,4\text{-}^iPr_2\text{-}C_5H)(C_5H_3)ZrCl_2$ (ThpZrCl$_2$, **23**)			6.36 (t, 1H, 3 Hz) 6.46 (s, 1H)
$ThpZrCl(\mu\text{-}H)_2Al^iBu_2$ [d,f]	−1.27 (s, 2H)	0.3-0.5[g] 1.0-1.3 2.0-2.25	6.06 (br, 1H) 6.42 (br, 1H) 6.71 (br, 2H)
rac-(EBTHI)ZrCl$_2$ (**18**)			5.27 (d, 2H, 3 Hz) 6.36 (d, 2H, 3 Hz)
rac-((EBTHI)ZrH)$_2$(μ-H)$_2$ (**24**)	−1.29 (t, 2H, 8 Hz) 5.18 (t, 2H, 7 Hz)		5.07 (br, 2H) 5.27 (d, 2H, 2 Hz) 6.37 (d, 2H, 3 Hz) 6.57 (br, 2H)
rac-(EBTHI)ZrH(μ-H)$_2$Al^{i}Bu$_2$ (**25**)[d,f]	−1.17 (br, 1H) −0.53 (br, 1H) 4.57 (br, 1H)	0.4-0.7[g] 1.1-1.4 2.0-2.4	4.94 (br, 1H) 5.15 (br, 1H) 5.73 (br, 1H) 6.34 (br, 1H)
rac-(EBTHI)ZrCl(μ-H)$_2$Al^{i}Bu$_2$ (**26**)	−0.09 (br, 2H)	0.53 1.20 2.18	5.49 (br, 2H) 6.16 (d, 2H, 3 Hz)
rac-(EBTHI)ZrCl(μ-H)$_2$AlMe$_2$	–0.35 (br)	–0.27	5.31 (br, 2H) 6.00 (br, 2H)
rac-Me$_2$C(indenyl)$_2$ZrCl$_2$ (**27**)			5.67 (d, 2H, 4 Hz) 6.50 (d, 2H, 4 Hz)
rac-Me$_2$C(indenyl)$_2$ZrCl(μ-H)$_2$Al^{i}Bu$_2$ (**29**)	−1.35 (br, 2H)	0.40 1.16 2.08	5.67 (d, 2H, 3 Hz) 6.76[g]
meso-Me$_2$C(indenyl)$_2$ZrCl$_2$ (**28**)			5.53 (d, 2H, 4 Hz) 6.54 (d, 2H, 3 Hz)
meso-Me$_2$C(indenyl)$_2$ZrCl(μ-H)$_2$Al^{i}Bu$_2$ (**30**)	−1.89 (br, 1H) −0.87 (br, 1H)	0.46 1.09 2.01	6.11 (br, 2H) 6.23 (br, 2H)
rac-Me$_2$Si(2-Me$_3$Si-4-Me$_3$C-C$_5$H$_2$)$_2$ZrCl$_2$ (*rac*-BpZrCl$_2$, **31**)			6.17 (d, 2H, 2 Hz) 7.23 (d, 2H, 2 Hz)
rac-BpZrH(μ-H)$_2$Al^{i}Bu$_2$ (**32**)	−1.56 (br, 1H) −0.60 (d, 1H, 8 Hz) 2.68 (dd, 1H, 6, 10 Hz)	0.3-0.5 1.0-1.3 1.9-2.3	5.75 (d, 1H, 2 Hz) 5.93 (d, 2H, 2 Hz) 6.36 (d, 1H, 2 Hz)
meso-Me$_2$Si(3-Me$_3$C-C$_5$H$_3$)$_2$ZrCl$_2$ (*meso*-DpZrCl$_2$, **33**)			5.56 (t, 2H, 3 Hz) 5.89 (t, 2H, 2 Hz)
meso-DpZrH(μ-H)$_2$Al^{i}Bu$_2$ (**34**)	−2.17 (d, 1H, 5 Hz) −0.21 (d, 1H, 10 Hz) 3.31 (dd, 1H, 5, 10 Hz)	0.54 (d, 4H, 7 Hz) 1.21 (m, 12H) 2.19 (m, 2H, 7 Hz)	5.12 (br, 2H) 5.79 (br, 2H) 5.94 (br, 2H)
H$_4$C$_2$(C$_5$H$_4$)$_2$ZrCl$_2$ (**35**)			5.46 (pt, 4H, 3 Hz) 6.50 (pt, 4H, 3 Hz)
H$_4$C$_2$(C$_5$H$_4$)$_2$Zr(μ-H)$_3$(Al^{i}Bu$_2$)$_3$(μ-Cl)$_2$ (**37**)	−1.11 (br, 2H) −0.32 (br, 1H)	0.47 1.13 2.1	5.72 (br, 4H) 6.07 (br, 4H)

$Me_4C_2(C_5H_4)_2ZrCl_2$ (**36**)			5.65 (pt, 4H, 3 Hz) 6.51 (pt, 4H, 3 Hz)
$Me_4C_2(C_5H_4)_2Zr(\mu\text{-}H)_3(Al^iBu_2)_3(\mu\text{-}Cl)_2$ (**38**)	−1.14 (br, 2H) −0.15 (br, 1H)	0.49 1.17 2.12	5.84 (br, 4H) 6.16 (br, 4H)

[a] In benzene-d_6 at 25 °C. [b] Complex-bound and free XAl^iBu_2 exchange-averaged. [c] Remaining resonances omitted because of overlap with XAl^iBu_2. [d] In toluene-d_8. [e] At -75 °C. [f] At -50 °C. [g] Complex-bound and free XAl^iBu_2 partly decoalesce.

Products with a single high-field signal due to a ZrH_2 group are also observed upon reaction of HAl^iBu_2 with several other singly or doubly bridged zirconocene dichlorides, shown in Figure 2.6, such as *rac*-C_2H_4(indenyl)$_2ZrCl_2$ ((EBI)$ZrCl_2$, **17**), *rac*-C_2H_4(4,5,6,7-tetrahydroindenyl)$_2ZrCl_2$ ((EBTHI)$ZrCl_2$, **18**), $Me_2C(C_5H_4)_2ZrCl_2$ (**19**), $Me_2Si(C_5H_4)_2ZrCl_2$ (**20**), *rac*-Me_2Si(2,4-Me_2-$C_5H_2)_2ZrCl_2$ (**21**), $(Me_2Si)_2(C_5H_3)_2ZrCl_2$ (**22**) or $(Me_2Si)_2$(3,5-$^iPr_2$-$C_5H)(C_5H_3)ZrCl_2$ (**23**). The observation of a reaction of HAl^iBu_2 with **18** contradicts a report[7] claiming no reaction between the two species.

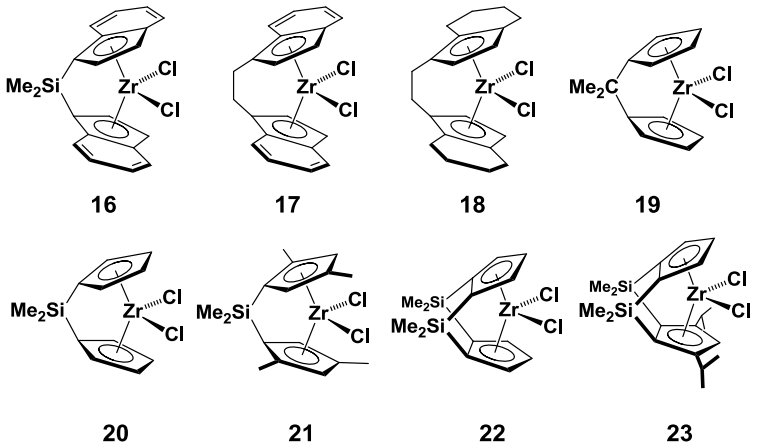

Figure 2.6: Bridged zirconocenes studied with HAl^iBu_2

Formation of a dihydride complex from each of these *ansa*-zirconocene dichlorides by reaction with $HAl^{i}Bu_2$ (Table 2.2) requires the concurrent formation of 2 equiv of the chloroaluminum species $ClAl^{i}Bu_2$. This Lewis acidic byproduct is likely to remain in association with the comparatively Lewis basic zirconocene dihydride. In order to decide whether one or both of the resulting $ClAl^{i}Bu_2$ entities are complexed to the *ansa*-zirconocene dihydride species, related, Cl-free reaction systems were investigated using an *ansa*-zirconocene dihydride as a starting material.

Particularly useful in this regard proved the easily accessible and well-characterized dimeric dihydride, $((EBTHI)ZrH)_2(\mu\text{-}H)_2$ (**24**).[7, 11] The Zr-H signals of this compound, a triplet at 5.17 ppm for its terminal Zr-*H* groups and another triplet at –1.29 ppm for its Zr-H-Zr bridges, disappear when 1 equiv of $HAl^{i}Bu_2$ is added to a solution of **24**. A new species is formed, which gives rise, in toluene-d_8 solution at –75 ºC, to two bridging Zr-H signals, at –1.17 ppm and –0.53 ppm, a terminal Zr-*H* signal at 4.57 ppm and four separate ligand C_5-*H* signals (Figure 2.7A, Table 2.2). Gradient correlation spectroscopy (gCOSY) shows coupling between the terminal and each of the two bridging Zr-H units, but not between the latter two (Figure 2.7B). On the basis of the similarity of this Zr-H NMR pattern to that reported by Wehmschulte and Power[16] for the structurally characterized species $(C_5H_5)_2Zr(H)(\mu\text{-}H)_2Al(H)C_6H_2{}^{t}Bu_3$, we assign the signals shown in Figure 2.7 to the trihydride $(EBTHI)ZrH(\mu\text{-}H)_2Al^{i}Bu_2$ (**25**, Scheme 2.4).

Scheme 2.4

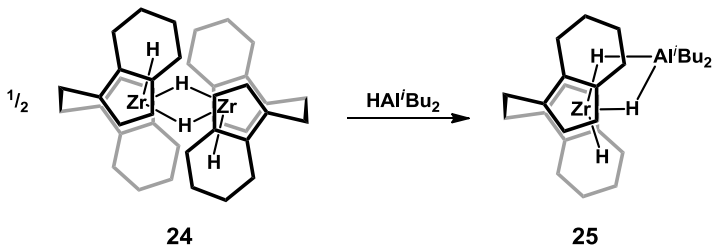

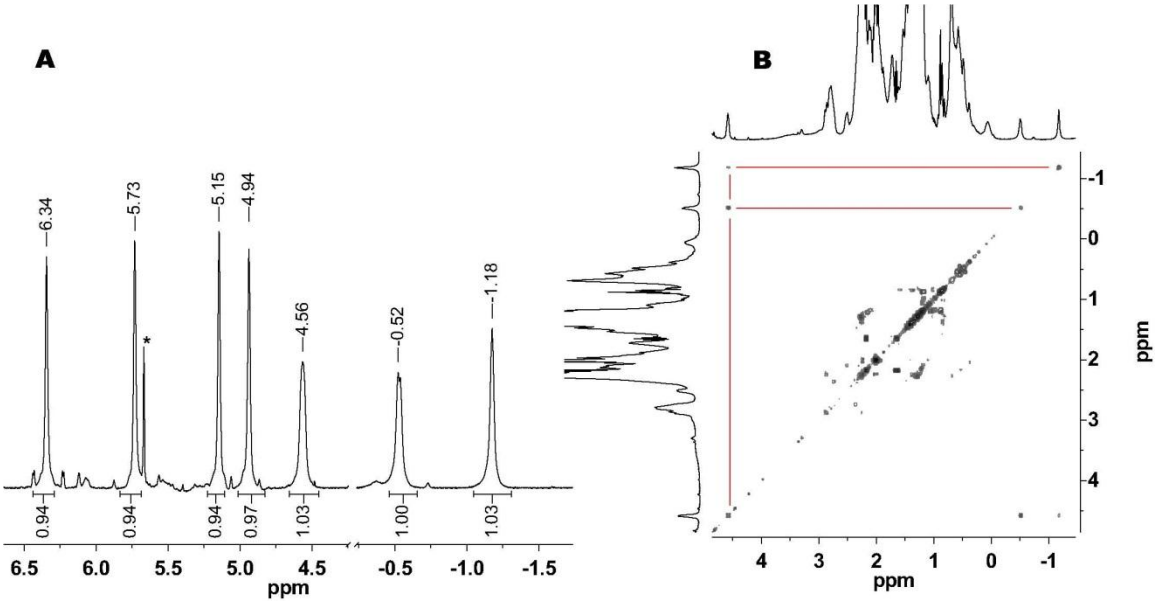

Figure 2.7: ^{1}H NMR spectrum of a 13 mM solution of ((EBTHI)ZrH)$_2$(μ-H)$_2$ (**24**) in toluene-d_8 at -75 °C after addition of 1 equiv of HAl^{i}Bu$_2$ per Zr (* solvent impurity) (**A**) and a gCOSY of a 11 mM solution of ((EBTHI)ZrH)$_2$(μ-H)$_2$ (**24**) in toluene-d_8 at -90 °C after addition of 2 equiv of HAl^{i}Bu$_2$ per Zr (**B**).

Table 2.3: Approximate Coalescence Temperature of (EBTHI)ZrH(μ-H)$_2$Al^{i}Bu$_2$ with different ratios of Zr to HAl^{i}Bu$_2$

[Zr] : [Al]	T_{coal} (°C)
1 : 4	< –90
1 : 2	–90 < T < –75
1 : 1	–75 < T < –50
2 : 1	> 25

The signals shown in Figure 2.7 are strongly broadened at higher temperatures, with the onset of this coalescence being critically dependent on the [HAl^iBu_2]/[Zr] ratio used (Table 2.3). The signals of (EBTHI)ZrH(μ-H)$_2Al^iBu_2$ are not observable at any temperature in the presence of 4 equiv of HAl^iBu_2, whereas in the presence of 2 equiv of HAl^iBu_2, the observation of sharp signals requires cooling to –90 ºC. Sharp signals as in Figure 2.7 can be observed even at room temperature, however, together with those of the initial ((EBTHI)ZrH)$_2$(μ-H)$_2$, when only 0.5 equiv of HAl^iBu_2 is added per zirconocene, so as to minimize the presence of any free HAl^iBu_2 in the reaction system. This acceleration of exchange processes by excess HAl^iBu_2 indicates that an associative exchange reaction with free HAl^iBu_2 induces a dynamic side exchange in complex **25** (cf., Scheme 2.5).

Scheme 2.5

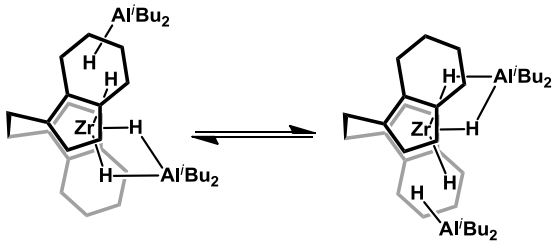

25 **25'**

On the basis of the proceeding, it was concluded that the dihydride complex formed upon addition of HAl^iBu_2 to the dichloride (EBTHI)$ZrCl_2$ (**18**) is the cluster **26**, i.e., an analogue of the trihydride complex **25** in which the terminal hydride is replaced by a chloride, while both hydride ligands are bridging to an {Al^iBu_2} unit, as indicated by their high-field chemical shift. When this view is tested by adding, instead of HAl^iBu_2, 1 equiv of $ClAl^iBu_2$

per Zr to a toluene-d_8 solution of ((EBTHI)ZrH)$_2$(μ-H)$_2$, we observe, together with the expected dihydride cluster **26**, a mixture of the dichloride **18**, the trihydride cluster **25** and free HAl^{i}Bu$_2$, i.e., a decay of **26** under release of HAl^{i}Bu$_2$. When this decay of **26** is suppressed, however, by addition of 2 equiv of HAl^{i}Bu$_2$ per Zr (Figure 2.8C), one observes indeed exactly the same signals as in the reaction system containing the dichloride **18** and excess HAl^{i}Bu$_2$ (Figure 2.8A). This reaction sequences shows unequivocally that of the 2 equiv of chloride originally contained in the zirconocene dichloride complex, only one is retained in the reaction product, whereas 1 equiv of ClAl^{i}Bu$_2$ is apparently released into solution (Scheme 2.6). Accordingly, addition of a second equiv of ClAl^{i}Bu$_2$ to the reaction system made up of the dihydride **24** and 2 equiv of HAl^{i}Bu$_2$ and 1 equiv of ClAl^{i}Bu$_2$ per Zr leaves the positions and integrals of the previous signals unchanged (Figure 2.8 **D**). It causes, however, a sharpening of the signals assigned to the dihydride cluster **26**, quite obviously by accelerating an associative side exchange of this species analogous to that described in Scheme 2.5.

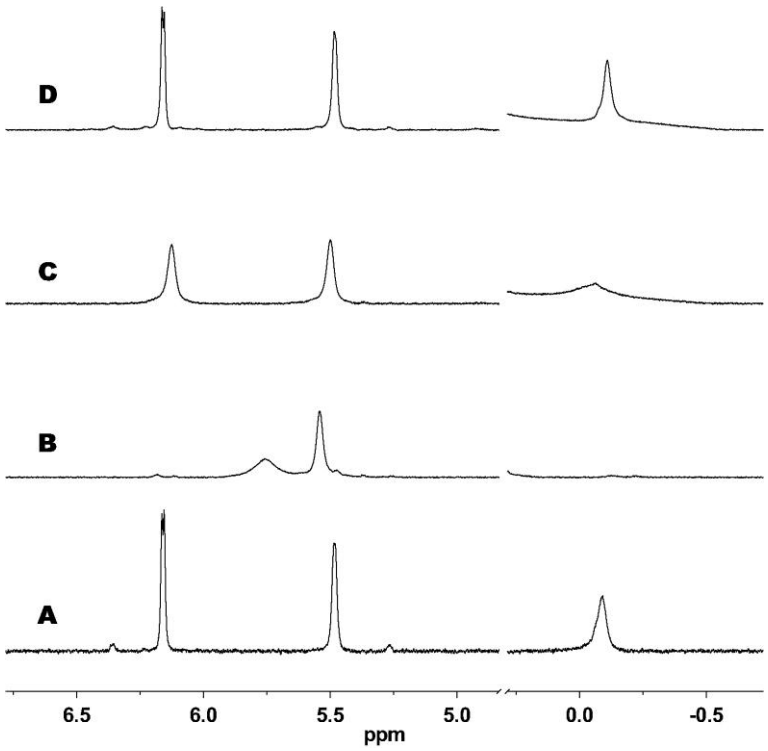

Figure 2.8: ^{1}H NMR spectra of a 47 mM solution of (EBTHI)$ZrCl_2$ (**18**) in benzene-d_6 following addition of HAl^iBu_2 (**A**) and a 14 mM solution of $((EBTHI)ZrH)_2(\mu\text{-}H)_2$ (**24**) following addition of 2 equiv of HAl^iBu_2 per Zr (**B**) and addition of 1 equiv of $ClAl^iBu_2$ (**C**) and a second 1 equiv of $ClAl^iBu_2$ (**D**).

Scheme 2.6

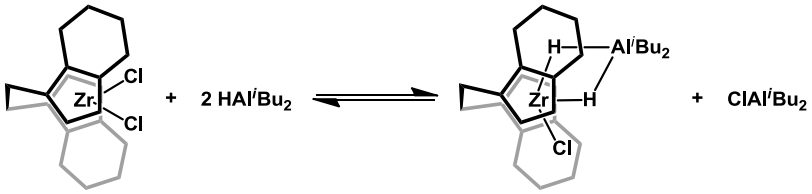

18 **26**

The view that addition of HAl^iBu_2 to one of the *ansa*-zirconocene dichlorides shown in Figure 2.6 gives the corresponding zirconocene monochloride dihydride clusters containing one Al^iBu_2 unit is supported by experiments with a pair of racemic and meso-configured $Me_2C(indenyl)_2ZrCl_2$ complexes, *rac*-**27** and *meso*-**28** (Scheme 2.7). The racemic

dihydride cluster **29** gives, as expected, a single ZrH_2 signal at –1.35 ppm. Its meso counterpart **30**, on the other hand, in which the $\{(\mu\text{-H})_2Al^iBu_2\}$ moiety is likely to stay on the open side of the complex, yields two separate ZrH signals at –1.89 and –0.87 ppm (Figure 2.9). The close coincidence of the average of these two values with the chemical shift of the $\{ZrH_2\}$ group in the racemic isomer supports the notion that the latter has a similarly unsymmetric structure as the meso isomer and that the appearance of a single ZrH_2 resonance in this—and by implication also in the other—racemic complexes arises from a rapid side exchange of the type shown in Scheme 2.7.

Scheme 2.7

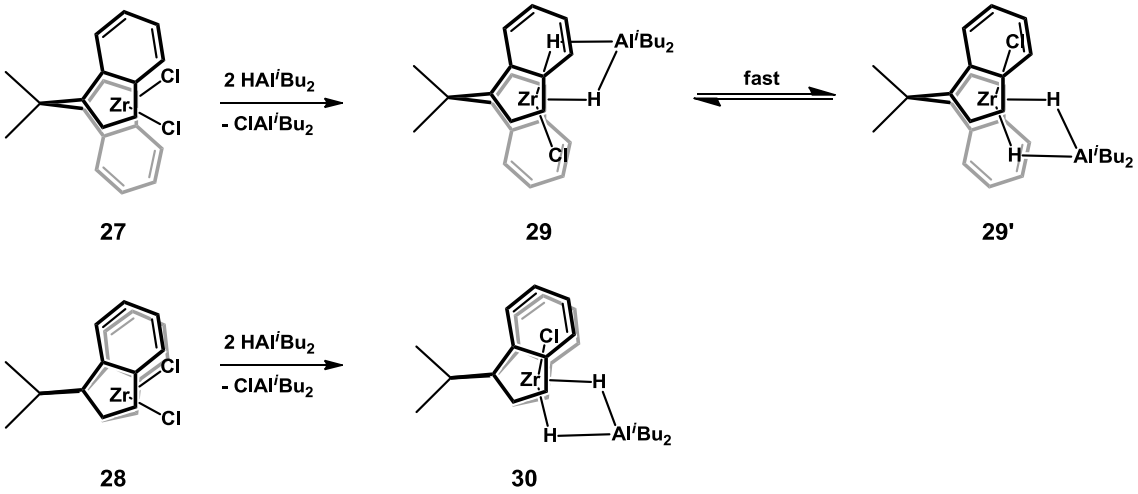

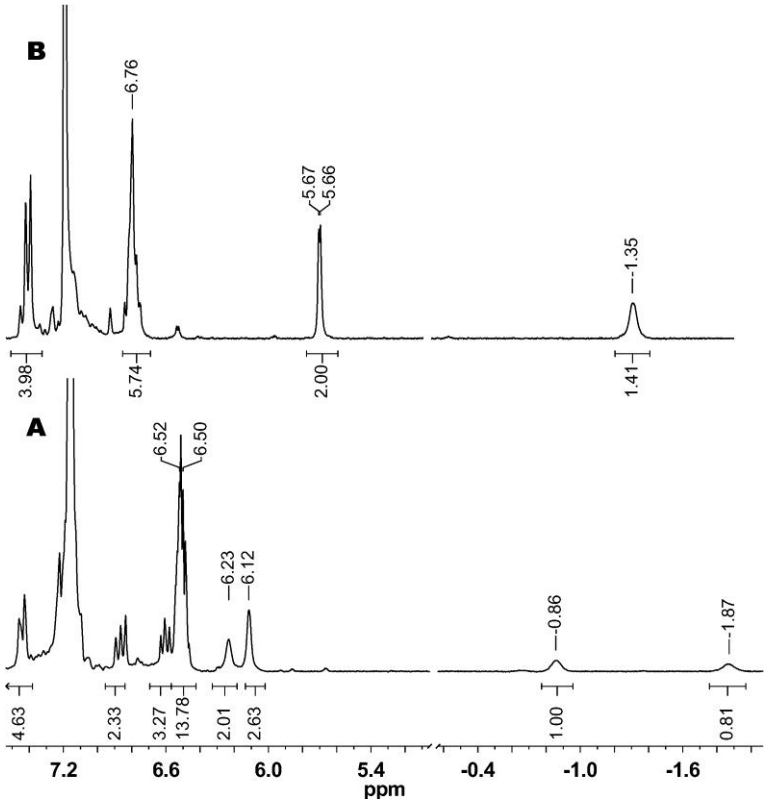

Figure 2.9: ^{1}H NMR spectra of a 17 mM solution of *meso*-$Me_2C(indenyl)_2ZrCl_2$ (**27**) in benzene-d_6 upon addition of 2 equiv $HAl^{i}Bu_2$ (**A**) and a 12 mM solution of *rac*-$Me_2C(indenyl)_2ZrCl_2$ in (**28**) benzene-d_6 upon addition of 2 equiv $HAl^{i}Bu_2$ (**B**).

A remarkable mode of reaction with $HAl^{i}Bu_2$, which differs from that described above for the bridged dichloride complexes **17-24**, is observed for the ^{t}Bu-substituted complexes **31** and **33** (Scheme 2.7). When complex **31**, *rac*-$Me_2Si(2\text{-}Me_3Si\text{-}4\text{-}Me_3C\text{-}C_5H_2)_2ZrCl_2$ ($BpZrCl_2$), in which both C_5-ring ligands are shielded by a Me_3Si and a Me_3C group, is reacted with 2 equiv of $HAl^{i}Bu_2$ in toluene-d_8 at –50 ºC, about half of it is converted to a new species with three Zr-H signals at –1.67, –0.62 and 2.65 ppm. A gCOSY analysis (Figure 2.10 **B**), which shows coupling of the signal at 2.65 ppm with both of the high-field

Zr-H signals but no coupling between these high-field signals and the observation of duplicate sets of C_5-H, Me_3C and Me_3Si ligand signals are closely analogous to the NMR pattern described above for the trihydride complex (EBTHI)ZrH(μ-H)$_2$Al^{i}Bu$_2$ (**25**). We can thus conclude that a trihydride complex carrying one {Al^{i}Bu$_2$} unit, *rac*-BpZrH(μ-H)$_2$Al^{i}Bu$_2$ (**32**), is formed by reaction of HAl^{i}Bu$_2$ with the dichloride **31** (Scheme 2.8). In this reaction system, 2 equiv of ClAl^{i}Bu$_2$ are apparently displaced by HAl^{i}Bu$_2$ from the Zr center and released into solution. This Cl/H displacement appears to be an equilibrium reaction, as shown by an almost complete (ca. 90%) conversion of **31** to **32** in the presence of a 10-fold excess of HAl^{i}Bu$_2$ (Figure 2.10). In distinction to the (EBTHI)Zr trihydride complex **25**, the hydride signals of complex **32** do not coalesce or broaden even at room temperature in the presence of excess HAl^{i}Bu$_2$. Side exchange, while still observable here in polarization transfer experiments (Figure 2.11), is undoubtedly greatly hindered by the α-positioned Me3Si groups, which block the approach of HAl^{i}Bu$_2$ required for the associative exchange outlined in Scheme 2.5.

Scheme 2.8

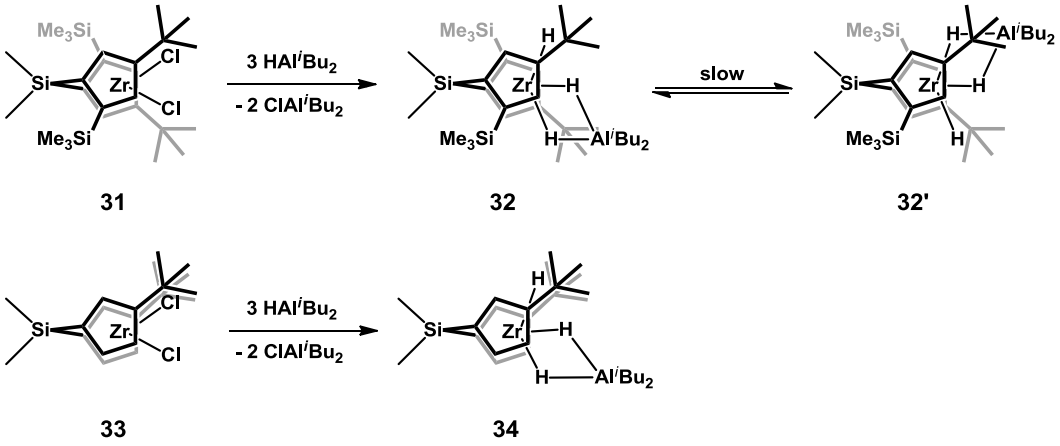

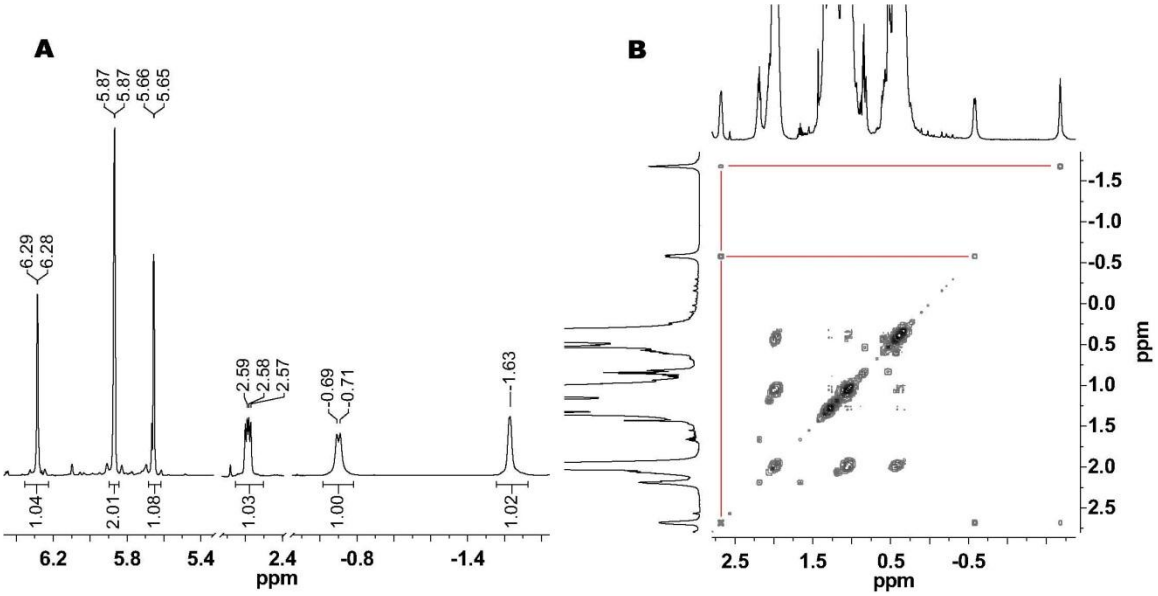

Figure 2.10: ^{1}H NMR spectrum of a 48 mM solution of *rac*-$Me_2Si(2\text{-}Me_3Si\text{-}4\text{-}Me_3C\text{-}C_5H_2)_2ZrCl_2$ (**31**) in toluene-d_8 at 25 ºC after addition of 10 equiv of HAl^{i}Bu$_2$ (**A**) and a gCOSY of a 48 mM solution of **31** in toluene-d_8 at –90 ºC after addition of 5 equiv of HAl^{i}Bu$_2$

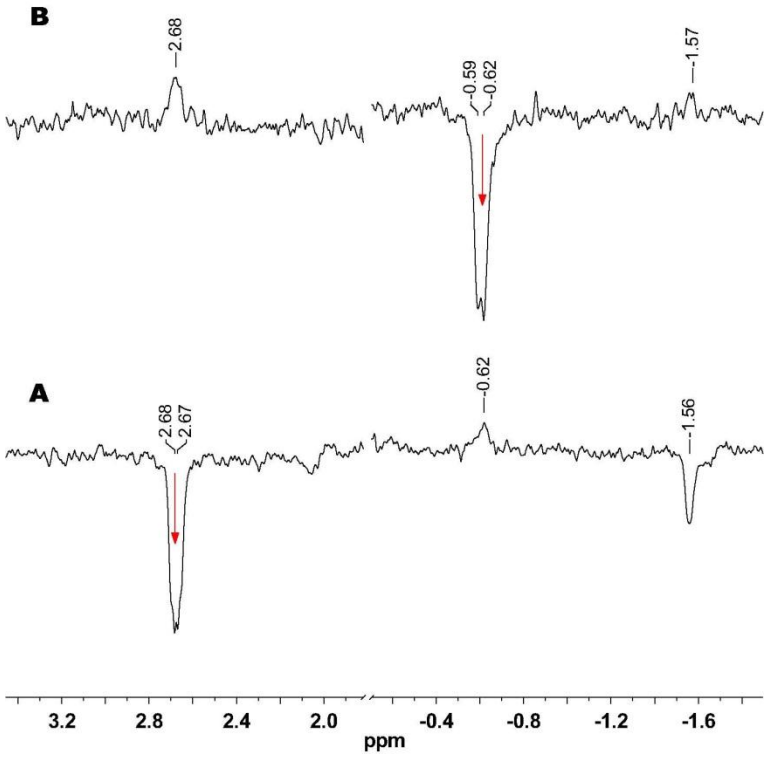

Figure 2.11: NOEDIF spectra of a 43 mM solution of *rac*-$Me_2Si(2\text{-}Me_3Si\text{-}4\text{-}Me_3C\text{-}C_5H_2)_2ZrCl_2$ (**31**) in benzene-d_6 at 25 ºC after addition of 2 equiv of HAl^iBu_2 irradiating the terminal hydride (**A**) and central hydride (**B**) resonances (marked with red arrow).

A related case concerns a reaction system which contains, together with 2 equiv of HAl^iBu_2, the dichloride *meso*-$Me_2Si(3\text{-}Me_3C\text{-}C_5H_3)_2ZrCl_2$ (**33**). This complex differs from the previous representative **31** by the absence of the α-positioned Me_3Si groups and by the placement of both *tert*-butyl substituents on the same side of the complex. The reaction product, *meso*-$Me_2Si(3\text{-}Me_3C\text{-}C_5H_3)_2ZrH(\mu\text{-}H)_2Al^iBu_2$ (**34**), is characterized, in toluene-d_8 at –50 ºC, by three sharp Zr-H signals at –2.25, –0.28 and 3.22 ppm and by a single set of three C_5-ring CH and one *tert*-butyl signal, in accord with its C_s symmetry. The NMR spectrum observed for complex **34** at –50 ºC persists essentially unchanged at temperatures

up to 25 ºC. Here, as in the *meso*-configured bisindenyl complex **30** discussed above, we see no signs for any side exchange of the {Zr(μ-H)$_2$Al^{i}Bu$_2$} moiety (Figure 2.12). Apparently, the Al^{i}Bu$_2$ group is locked into one side of the complex molecule by the *tert*-butyl groups, which make the other side of the complex inaccessible. A significant nuclear Overhauser effect (NOE) enhancement of the signals of the *tert*-butyl and the terminal Zr-H groups in complex **34**, indicates that these groups are in close proximity. In contrast to all other cases discussed so far, we observe here, even at room temperature, separate isobutyl signals for 2 equiv of free ClAl^{i}Bu$_2$ (0.48 (d, 8H, 7 Hz), 1.05 (d, 24 H, 7 Hz) and 2.03 ppm (m, 4H, 7 Hz)) and for 1 equiv of a complex bound {Al^{i}Bu$_2$} unit (0.54 (d, 4H, 7 Hz), 1.21 (m, 12H) and 2.19 ppm (m, 2H, 7 Hz)). This attests to the efficient shielding of complex **34** against associative exchange reactions and confirms the stoichiometry of the reaction shown in Scheme 2.8.

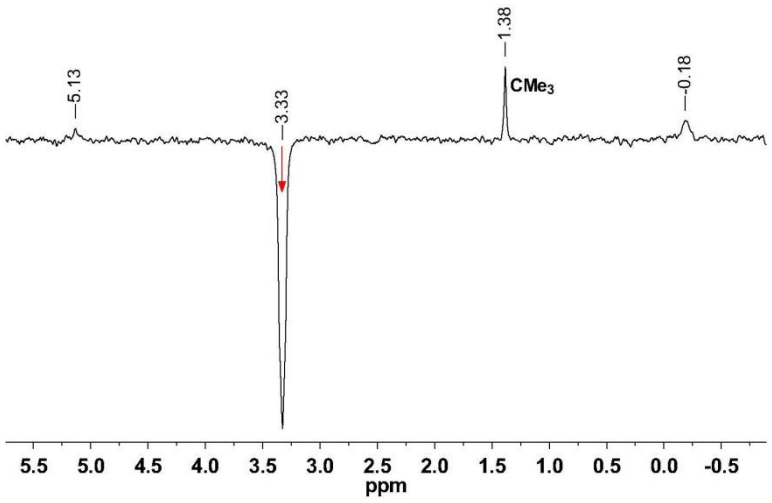

Figure 2.12: NOEDIF spectrum of an 11 mM solution of *meso*-Me$_2$Si(3-Me$_3$C-C$_5$H$_3$)$_2$ ZrCl$_2$ (**33**) in benzene-d_6 after addition of 3 equiv HAl^{i}Bu$_2$ irradiating the terminal hydride marked by the red arrow.

The observation that bridged zirconocene dichloride complexes with bulky substituents in a β-position of each C_5-ring react with HAl^iBu_2 to give the trihydride clusters $Cp^x_2ZrH(\mu\text{-}H)_2Al^iBu_2$, instead of the otherwise prevailing chlorodihydride clusters $Cp^x_2ZrCl(\mu\text{-}H)_2Al^iBu_2$, can be explained by the serious mutual repulsion, which Cl ligands and β-^{t}Bu substituents in *ansa*-zirconocenes are known to suffer.[37-38] Much of this repulsion is likely to be released when a Zr-Cl bond with a length of ca. 2.45 Å is replaced by a much shorter Zr-H bond (ca. 1.95 Å), which allows the hydride ligand to escape from repulsive contacts by staying on the "inside" of the β-^{t}Bu substituent. This steric shielding appears to favor the formation of the trihydride cluster over its chlorodihydride congener; at the same time, it will largely suppress an associative approach of HAl^iBu_2 or $ClAl^iBu_2$ from the side of the terminal hydride.

2.3.3 Bridged versus Unbridged Zirconocene Complexes.

All the results presented so far thus indicate a clear dichotomy between unbridged and bridged zirconocene complexes: all unbridged representatives discussed in Section 2.3.1 react with HAl^iBu_2 to form clusters containing three $\{Al^iBu_2\}$ units and a $\{ZrH_3\}$ coordination core. An exception to this rule is the complex $(C_5H_5)_2Zr(H)(\mu\text{-}H)_2Al(H)(1,3,5\text{-}^tBu_3C_6H_3)$ described by Power[16], where the exceptional steric demand of the supermesityl group appears to preclude the approach of further AlR_2X units. All the bridged complexes shown in Figure 2.6, on the other hand, react with HAl^iBu_2 to give an adduct with only one $\{Al^iBu_2\}$ unit. The vast majority of these contain a $\{ZrClH_2\}$ coordination core; only the

most heavily congested *ansa*-zirconocenes with β-^{t}Bu substituents are found to contain a {ZrH_3} core in contact with a single Al^{i}Bu$_2$ unit. In the following, possible causes for this dichotomy between unbridged and bridged zirconocene complexes are explored.

With regard to steric factors, bridged zirconocenes should be at least as accessible for contacts with further {Al^{i}Bu$_2$} units as their unbridged counterparts. Especially the totally unsubstituted *ansa*-zirconocenes **19** and **20** would appear to be more open than their unbridged congeners **1**, **6**, **8** or **10**, yet even they differ from the latter by an apparent incapability to expand their binuclear {Zr(Cl)(μ-H)$_2$Al^{i}Bu$_2$} coordination geometry to the tetranuclear {Zr(μ-H)$_3$(Al^{i}Bu$_2$)$_3$(μ-Cl)$_2$} alternative. The preference of unbridged complexes for the latter coordination mode does not appear to be based on electronic factors either: Several observables, such as reduction potentials of dichloride complexes or CO stretching frequencies in the corresponding Zr(II) dicarbonyl derivatives, as well as single-electron affinities determined by DFT-based calculations, all point toward a net electron-withdrawing effect of a Me_2C or Me_2Si bridge[39] and, hence, toward a greater tendency of bridged than of unbridged zirconocenes to accept an electron-rich hydride in exchange for a less donating chloride ligand. Neither do hydride affinities, calculated by DFT-based methods as enthalpy differences for the hypothetical reaction $(C_5H_5)_2ZrH_2 + H^- \rightarrow (C_5H_5)_2ZrH_3^-$, indicate any preferred hydride uptake when the interanullar wedge angle is increased to values characteristic for *ansa*-zirconocenes complexes such as **19** or **20**.[40]

The only remaining explanation would thus appear to be that the dichotomy between unbridged and bridged zirconocenes with regard to their reactions with $HAl^{i}Bu_2$ is connected to different degrees of rotational freedom of the C_5-ring ligands in these two classes of complexes. In order to test this hypothesis, we have studied reactions of $HAl^{i}Bu_2$ with two ethanediyl-bridged zirconocenes, **35** and **36** (Figure 2.13). In distinction to their congeners with Me_2C- and Me_2Si-bridges, which enforce a strictly eclipsed conformation of their C_5-ring ligands, ethanediylbridged titanocene and zirconocene complexes are known to deviate significantly from an eclipsed C_5-ring conformation. Crystal structures reported for complexes **35** and **36** [39, 41] reveal dihedral bridgehead-centroid-centroid-bridgehead angles of 21º and 15º, respectively. This and the observation of ^{1}H NMR spectra with time-averaged C_{2V} symmetry in solutions of **35** and **36** indicate an essentially unobstructed fluctuation between right and left-handed deviations from C_{2V} symmetry, i.e., a significant measure of torsional freedom of the C_5-rings in these ethanediylbridged complexes.

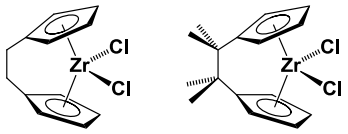

35 **36**

Figure 2.13: C_2-bridged simple metallocenes studied with $HAl^{i}Bu_2$

Reactions of complexes **35** and **36** with 4 equiv of $HAl^{i}Bu_2$ do indeed give the trialuminum trihydrides $H_4C_2(C_5H_4)_2Zr(\mu\text{-}H)_3(Al^{i}Bu_2)_3(\mu\text{-}Cl)_2$ (**37**) and $Me_4C_2(C_5H_4)_2Zr(\mu\text{-}H)_3(Al^{i}Bu_2)_3(\mu\text{-}Cl)_2$ (**38**), respectively, as judged by their typical NMR doublet and triplet signals between –0.5 and –2 ppm with integral ratios of 2:1, which are characteristic for complexes of this type (Figure 2.14, Table 2.2). The outcome of this test reaction, which sets complexes **35** and **36** clearly apart from their single-atom bridged congeners **19**, **20** and **22**, strongly indicates that the accessibility of a staggered C_5-ring conformation is the decisive criterion for the dichotomy between unbridged zirconocene complexes vis-à-vis those with a single-atom bridge with regard to their respective reactions with $HAl^{i}Bu_2$. Possible steric interactions of the $\{Al^{i}Bu\}$ groups directly with the interannular bridging units would be expected to be stronger with a $\{Me_4C_2\}$ bridge, due to its greater spatial extension, than with a $\{C_2H_4\}$ bridges probably more comparable to that with a $\{Me_2C\}$ bridge. The observation that the reactions of **35** and **36** with $HAl^{i}Bu_2$ result in hydride complexes of the same type would thus rule out direct steric interactions between $\{Al^{i}Bu_2\}$ groups and bridging units as a decisive criterion for the relative stabilities of $\{ZrCl(\mu\text{-}H)_2Al^{i}Bu_2\}$ vs. $\{Zr(\mu\text{-}H)_3(Al^{i}Bu_2)_3(\mu\text{-}Cl)_2\}$ species.

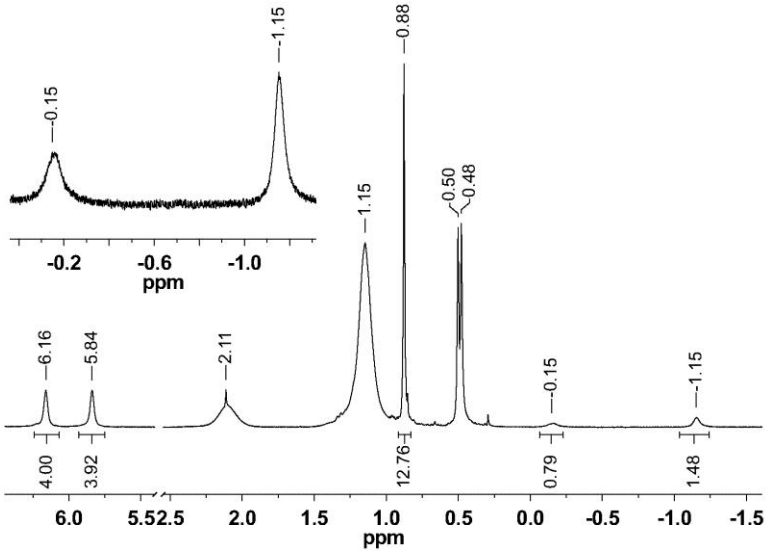

Figure 2.14: ^{1}H NMR spectrum of a 30 mM solution of $Me_4C_2(C_5H_4)_2ZrCl_2$ (**36**) in benzene-d_6 at 25 ºC after addition of 4 equiv of HAl^iBu_2.

Formation of a trialuminum cluster $\{Zr(\mu\text{-}H)_3(Al^iBu_2)_3(\mu\text{-}Cl)_2\}$ apparently requires that the Al-bound CH_2 groups of its $\{Al^iBu_2\}$ units fit snugly into spatial niches in the C-H periphery of the C_5-ring ligands. This appears to be achieved more favorably with staggered than with eclipsed C_5-rings. The view that the $\{Al\text{-}CH_2\}$ groups of these complexes are in close contact with C_5-ring H atoms, is supported by the observation of a significant NOE signal for complex **38**, which connects these $\{Al\text{-}CH_2\}$ groups with the β-H atoms of the C_5-ring ligands (Figure 2.15). A significant NOE signal connects the signal at 0.88 ppm due to the CH_3 groups of the interanullar bridge of complex **38** with the C_5-H signal at 5.84 ppm and identifies the latter as being due to the α-positioned H atoms and that at 6.16 ppm as the resonance of the β-H atoms. This order of the chemical shifts of α- and β-positioned C_5-H atoms, which we find also for the dimeric dihydride **24** and for the

dihydride cluster **26**, groups these five-coordinate hydride-bridged zirconocene complexes together with typical four-coordinate, 16-electron dichloride complexes.[42] This indicates that the Zr centers of these hydride-bridged complexes do not reach a full 18-electron complement and might explain why pentacoordination, rather than an even more electron-deficient tetracoordination, is prevalent in these hydride-bridged complexes. In ethanediyl-bridged complexes with bisindenyl and bis(tetrahydroindenyl) ligands, such as **17** and **18**, however, the increased steric bulk of the annulated/substituted ring ligands appears to be sufficient to restrict reactions with HAl^iBu_2 again to the formation of $\{ZrCl(\mu\text{-}H)_2Al^iBu_2\}$ rather than $\{Zr(\mu\text{-}H)_3(Al^iBu_2)_3(\mu\text{-}Cl)_2\}$ clusters.

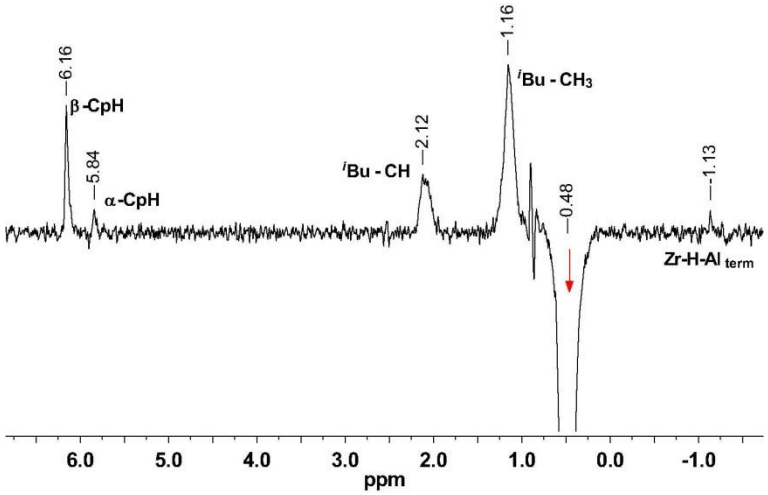

Figure 2.15: NOESY1D spectrum of a 30 mM solution of $Me_4C_2(C_5H_4)ZrCl_2$ (**36**) in benzene-d_6 at 25 ºC after addition of 4 equiv HAl^iBu_2 with irradiation of the Al-CH_2 resonance marked with the red arrow.

These results show that either a chloride or a hydride can occupy the terminal position in hydride-bridged monoaluminum clusters formed by typical *ansa*-zirconocenes, depending on the ligand framework of the zirconocene complex studied. In order to assess the scope

of related hydride-complex formation reactions, other representatives of the general class of heterobinuclear {ZrX(μ-H)$_2$Al^{i}Bu$_2$} clusters were sought. Reaction of the fluoride analogue of complex **18**, (EBTHI)ZrF$_2$, with 1 or 2 equiv of HAl^{i}Bu$_2$ is found to yield, in accord with previous studies,[7] the dihydride **24** as the only zirconocene product, with no indication for an intermediate of the kind (EBTHI)ZrF(μ-H)$_2$Al^{i}Bu$_2$. This might, thus, be a case where the coexistence of "hard" fluoride and "soft" hydride coligands is unfavorable, such that the reaction leads to the disjoined products, i.e., to ((EBTHI)ZrH$_2$)$_2$ and (FAl^{i}Bu$_2$)$_n$.

With a view toward "softer" coligands, we have tried to find evidence for the existence of clusters of the type {ZrMe(μ-H)$_2$AlR$_2$} containing a methyl group as a terminal ligand. When the chloride-containing complex (SBI)ZrCl(μ-H)$_2$Al^{i}Bu$_2$ is treated with AlMe$_3$, a shift of its Zr-H signal from –1.22 ppm to a limiting value of –1.65 ppm, reached at high excess of AlMe$_3$ ([AlMe$_3$]/[Zr] = 128), indicates the occurrence of some reaction. Product formation, as measured by the change in chemical shift, $\Delta\delta$(Zr-H), is found to be a function of the absolute concentration of AlMe$_3$ (Figure 2.17), however, rather than of the ratio [AlMe$_3$]/[Zr] (Figure 2.17). Experiments conducted at two different total concentrations of Zr ([Zr]$_{TOT}$) were found to give chemical shifts for the Zr-*H* resonance which fit to Equation 2.2 whereas for an exchange reaction the chemical shifts should be modeled by Equation 2.3 (see Appendix 1 for derivation). Based on the fit of the data to Equation 2.2 an equilibrium constant (K) for the adduct formation in Scheme 2.9 can be obtained of 6.3 ± 0.4 mM^{-1}. The product thus appears to be an adduct, most likely with AlMe$_3$ attached to

the terminal Cl ligand of (SBI)ZrCl(μ-H)$_2$Al^{i}Bu$_2$, rather than the sought-for Me-versus-Cl exchange product (Scheme 2.9). Either Me or ^{i}Bu can occupy terminal Zr(μ-H)$_2$Al-alkyl positions in such a complex. A closely related exchange of terminal ^{i}Bu and Me groups between the cation (SBI)Zr(μ-Me)$_2$AlMe$_{2-x}$^{i}Bu$_x^+$ and mixed alkylaluminum dimers, Al$_2$(μ-Me)$_2$Me$_{4-x}$^{i}Bu$_x$, has been shown to occur to an extent which is close to statistical expectations.[28]

Scheme 2.9

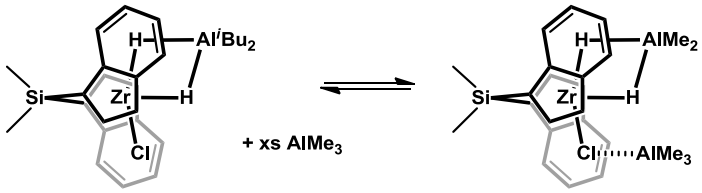

$$\frac{1}{\Delta\delta} = \frac{1}{\Delta\delta_{\max}} + \frac{1}{\Delta\delta_{\max} K\sqrt{[Al_2Me_6]}} \qquad \textbf{2.2}$$

$$\left(\frac{\Delta\delta_{max}}{\Delta\delta} - 1\right)\frac{\Delta\delta_{\max}}{\Delta\delta} = \frac{[Zr]_{TOT}}{K[Al_2Me_6]} \qquad \textbf{2.3}$$

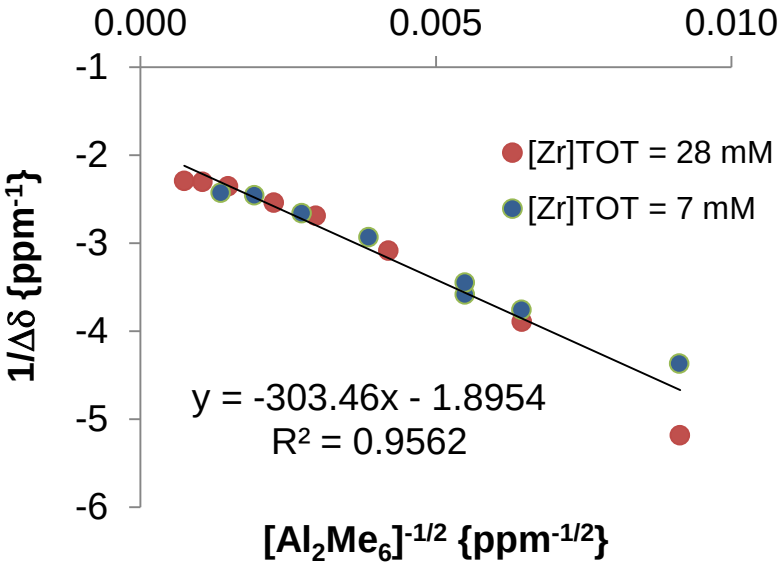

Figure 2.16: Bernesi-Hilldebrand-type plot of Zr-*H* chemical shift of (SBI)ZrCl(μ-H)$_2$Al^{i}Bu$_2$ upon addition of increasing amounts of AlMe$_3$ with two different initial concentrations of (SBI)ZrCl(μ-H)$_2$Al^{i}Bu$_2$ modeling Equation 2.2.

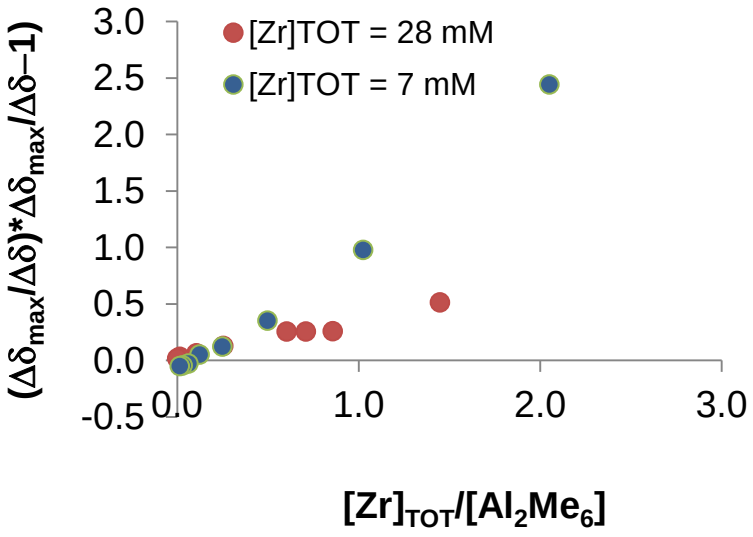

Figure 2.17: Plot of Zr-*H* chemical shift of (SBI)ZrCl(μ-H)$_2$Al^{i}Bu$_2$ upon addition of increasing amounts of AlMe$_3$ with two different initial concentrations of (SBI)ZrCl(μ-H)$_2$Al^{i}Bu$_2$ modeling Equation 2.3.

When the dimethyl complex (SBI)$ZrMe_2$ is reacted with slightly more than 2 equiv of HAl^iBu_2 in benzene or toluene solution, at room temperature or at –75 ºC, several Zr-H signals appear between ca. –0.5 and –2 ppm. This observation and an intense darkening of the reaction mixture in the course of 1-2 h, indicate that any (SBI)$ZrMe(\mu\text{-}H)_2Al^iBu_2$ formed in this reaction decays to other species, possibly to complexes which contain their Zr center in a reduced oxidation state. Similar decay reactions appear to proceed upon addition of HAl^iBu_2 to mixtures of (SBI)$ZrMe_2$ and $AlMe_3$ in various ratios. Addition of HAl^iBu_2 to 1:1 mixtures of (SBI)$ZrMe_2$ and $B(C_6F_5)_3$, in the absence or presence of excess $AlMe_3$, appears to lead to partial transfer of $\{C_6F_5\}$ groups from boron to aluminum, as indicated by signals at –124.8, –155.2 and –163.7 ppm in the ^{19}F NMR spectra of the reaction.[43] The sought-for species, (SBI)$ZrMe(\mu\text{-}H)_2Al^iBu_2$, might be in equilibrium with HAl^iBu_2 and (SBI)Zr(Me)H; the latter is likely to form, by reductive elimination of methane,[44-46] the Zr(II) species (SBI)Zr. This would then most probably lead to further decay reactions under the prevailing reaction conditions. $((EBTHI)ZrH_2)_2$ in benzene-d_6 reacts with excess $AlMe_3$—in the absence or presence of MAO—to give mainly the dimethyl complex (EBTHI)$ZrMe_2$, together with some hydride species with a resonance at –1.54 ppm; several C_5-H signals between 5 and 6 ppm indicate the formation of additional products. In these cases, evolution of CH_4 is evident by the appearance of its characteristic sharp signal at 0.16 ppm, while this spectral region is obscured by the Me_2Si resonances in reactions systems involving (SBI)Zr derivatives. Thus the sought after (SBI)$ZrMe(\mu\text{-}H)_2Al^iBu_2$ appears to be unstable under typical reaction conditions.

2.4 Conclusions

Our results show that reactions with $HAl^{i}Bu_2$ give different reaction products—tetranuclear trihydrides $\{Zr(\mu\text{-}H)_3(Al^{i}Bu_2)_3(\mu\text{-}Cl)_2\}$ versus binuclear dihydrides $\{ZrCl(\mu\text{-}H)_2Al^{i}Bu_2\}$—from unbridged zirconocenes and from zirconocene dichlorides with a single-atom bridge, respectively. Binuclear complexes $\{ZrH(\mu\text{-}H)_2Al^{i}Bu_2\}$, which contain a Zr-H instead of a Zr-Cl unit, are formed when $HAl^{i}Bu_2$ is reacted with a zirconocene dihydride or with a zirconocene dichloride carrying particularly congested ring ligands. A terminal Zr-Me group instead of a Zr-Cl or Zr-H unit, however, appears to render otherwise analogous binuclear dihydrides prone to decay, possibly due to reductive CH_4 elimination.[44-46]

2.5 Experimental

General Considerations. All operations were carried out under a protective dinitrogen atmosphere, either in a glovebox or on a vacuum manifold. Benzene-d_6, toluene-d_8 and other solvents used were dried by vacuum transfer either from sodium benzophenone or from "titanocene".[47] Zirconocene complexes used as starting materials were either purchased from Strem Chemicals, Newburyport (**1**, **6**, **12**, **17** and $(C_5H_5)_2HfCl_2$); obtained as gifts from Dr. M. Ringwald, MCAT, Konstanz ((EBTHI)ZrF_2,[48] **27**, **28** [49] and **36** [50]) and from BASELL Polyolefins, Frankfurt/Main (**16** [51]); or prepared in our laboratories according to published procedures (**3**,[52] **8**,[53] **10**,[54] **13**,[55-56] **18**,[57] **19**,[58] **20**,[59] **21**,[60] **22**,[61] **23**,[62] **24**,[7, 11] **31**[63] and **33**[38, 64]. Trimethylaluminum, triisobutylaluminum, diisobutylaluminum

hydride and diisobutylaluminum chloride were used as obtained from Aldrich Chemical Co., Milwaukee. **CAUTION**: *alkylaluminum compounds are pyrophoric and must be handled with special precautions* (see, e.g., Shriver, D.F. *The Manipulation of Air-sensitive Compounds*; Robert E. Krieger Publishing Company; Malabar, Florida, 1982). NMR spectra were obtained using Varian Inova 400, 500 or Mercury 300 spectrometers. Chemical shifts are referenced to residual solvents peaks, 7.16 ppm for benzene and 7.00 ppm for the central aromatic proton resonance of toluene.

Synthesis of $H_4C_2(C_5H_4)ZrCl_2$, 35. In a modification of literature methods[39] a 100 mL round-bottom flask was charged with 0.5057 g (3.273 mmol) of $Mg(C_5H_4)_2$ and 1.2125 g (3.2731 mmol) 1,2-ditosylethane. A swivel frit was affixed and ~50 mL of thf was vacuum transferred onto the solids at –78 ºC. The mixture was allowed to warm to room temperature during which time a hot pink color evolved. After allowing the reaction to stir overnight the reaction was filtered and washed 3x to afford an orange solution. Thf was pumped off to yield a yellowish-orange oil. Approximately 40 mL pentane was vacuum transferred onto the oil to yield a yellow suspension. 10.5 mL of a 1.45 M solution of BuLi (15.2 mmol, 4.7 equiv) in hexanes was added dropwise at –78 ºC under an Ar atmosphere. The reaction was allowed to slowly warm to room temperature yielding a white precipitate. After stirring at room temperature for 3 hours the reaction was filtered and washed 3x with pentane to yield 350.6 mg of $Li_2[C_2H_4(C_5H_4)_2]$ (63.0% yield). The ligand was metallated with $ZrCl_4$ following reference[39].

NMR Scale Syntheses of Neutral Zirconocene Hydrides. Reaction mixtures for NMR measurements were prepared by dissolving a weighed amount of solid zirconocene starting compound, in an oven-dried J Young NMR tube, in benzene-d_6 or toluene-d_8 under inert atmosphere. Aluminum reagents were added as neat liquids via microliter syringes.

$(C_5H_5)_2Zr(\mu\text{-}H)_3(Al^iBu_2)_3(\mu\text{-}Cl)_2$ (2). 36.1 mg (0.123 mmol) Cp_2ZrCl_2 and 21.9 μL (0.123 mmol, 1 equiv) HAl^iBu_2. ^{1}H NMR (300 MHz, benzene-d_6) δ 5.66 (s, 10H, C_5-H), 2.10 (n, 6H, $^1J_{HH}$ = 7 Hz, ^{i}Bu-CH), 1.15 (d, $^3J_{HH}$ = 6 Hz, 36H, ^{i}Bu-CH_3), 0.45 (d, $^3J_{HH}$ = 7 Hz, 12H, ^{i}Bu-CH_2), -0.89 (t, $^2J_{HH}$ = 7.0 Hz, 1H, Zr-H-$Al_{central}$), -2.06 (d, $^2J_{HH}$ = 6.8 Hz, 2H, Zr-H-$Al_{lateral}$).

$((C_5H_5)_2ZrH\cdots HAl^iBu_2)_2(\mu\text{-}H)_2$ (4). 20.0 mg (0.0762 mmol) Cp_2ZrH_2 and 13.6 μL (0.0763 mmol, 1 equiv) HAl^iBu_2. ^{1}H NMR (500 MHz, toluene-d_8, -75 ºC) δ 5.40 (s, 20H, C_5-H), 2.10 (m, 4H, ^{i}Bu-CH), 1.18 (d, $^3J_{HH}$ = 5 Hz, 22H, ^{i}Bu-CH_3), 0.39 (d, $^3J_{HH}$ = 7 Hz, 8H, ^{i}Bu-CH_2), -2.11 (s, 2H, Zr-H-Zr), -3.05 (s, 2H Zr-H-Al).

$(C_5H_5)_2Zr(\mu\text{-}H)_3(Al^iBu_2)_3(\mu\text{-}H)_2$ (5). 21.5 mg (0.0820 mmol) Cp_2ZrCl_2 and 43.8 μL (0.246 mmol, 3 equiv) HAl^iBu_2. ^{1}H NMR (500 MHz, toluene-d_8, -75 ºC) δ 5.34 (s, 10H, C_5-H), 3.17 (s, 2H, Al-H-Al), 2.16 (br, 6H, ^{i}Bu-CH), 1.25 (br, 36H, ^{i}Bu-CH_3), 0.46 (d, $^3J_{HH}$ = 19.5 Hz, 10H, ^{i}Bu-CH_2), -1.46 (t, $^2J_{HH}$ = 15 Hz, 1H, Zr-H-$Al_{central}$), -2.33 (d, $^2J_{HH}$ = 15 Hz, 2H, Zr-H-$Al_{lateral}$).

(^{n}Bu-C$_5$H$_4$)$_2$Zr(μ-H)$_3$(Al^{i}Bu$_2$)$_3$(μ-Cl)$_2$ (7). 15.9 mg (0.0393 mmol) (^{n}Bu-C$_5$H$_4$)$_2$ZrCl$_2$ and 21 μL (0.12 mmol, 3 equiv) HAl^{i}Bu$_2$. ^{1}H NMR (300 MHz, benzene-d_6, 25 ºC) δ 5.94 (br, 4H, C$_5$-H), 5.65 (t, $^3J_{HH}$ = 3 Hz, 4H, C$_5$-H), 2.25 (m, J = 7 Hz, 5H, C$_5$-CH_2CH$_2$CH$_2$CH$_3$), 2.14 (m, $^3J_{HH}$ = 7 Hz, 6H, ^{i}Bu-CH), 1.31 (m, 8H, C$_5$-CH$_2$CH_2CH_2CH$_3$), 1.18 (d, $^3J_{HH}$ = 7 Hz, 37H, ^{i}Bu-CH$_3$), 0.88 (m, 7H, C$_5$-CH$_2$CH$_2$CH$_2$CH_3), 0.51 (d, $^3J_{HH}$ = 7 Hz, 12H, ^{i}Bu-CH$_2$), -0.58 (t, $^2J_{HH}$ = 7 Hz, 1H, Zr-H-Al$_{central}$), -1.53 (d, $^2J_{HH}$ = 7 Hz, 2H, Zr-H-Al$_{lateral}$).

(1,2-Me$_2$-C$_5$H$_3$)$_2$Zr(μ-H)$_3$(Al^{i}Bu$_2$)$_3$(μ-Cl)$_2$ (9). 3.9 mg (0.011 mmol) (1,2-Me$_2$-C$_5$H$_3$)$_2$ZrCl$_2$ and 4.0 μL (0.022 mmol, 2 equiv) HAl^{i}Bu$_2$. ^{1}H NMR (300 MHz, benzene-d_6, 25 ºC) δ 5.65 (d, $^3J_{HH}$ = 3 Hz, 2H, C$_5$-H), 5.58 (t, $^3J_{HH}$ = 3 Hz, 1H, C$_5$-H), 2.18 (m, 4H, ^{i}Bu-CH), 1.79 (s, 6H, C$_5$-CH3), 1.19 (d, $^3J_{HH}$ = 6 Hz, 25H, ^{i}Bu-CH$_3$), 0.52 (d, $^3J_{HH}$ = 7 Hz, 8H, ^{i}Bu-CH$_2$), -0.20 (t, $^2J_{HH}$ = 6 Hz, 1H, Zr-H-Al$_{central}$), -1.13 (d, $^2J_{HH}$ = 5 Hz, 2H, Zr-H-Al$_{lateral}$).

(Me$_3$Si-C$_5$H$_4$)$_2$Zr(μ-H)$_3$(Al^{i}Bu$_2$)$_3$(μ-Cl)$_2$ (11). 3.9 mg (0.011 mmol) (Me$_3$Si-C$_5$H$_4$)$_2$ZrCl$_2$ and 4.0 μL (0.022 mmol, 2 equiv) HAl^{i}Bu$_2$. ^{1}H NMR (500 MHz, toluene-d_8, -75 ºC) δ 6.11 (br, 4H, C$_5$-H), 5.96 (br, 4H, C$_5$-H), 0.00 (s, 20H, C$_5$-Si(CH_3)$_3$), -1.31 (br, 1H, Zr-H-Al$_{central}$), -2.10 (br, 2H, Zr-H-Al$_{lateral}$).

(C$_5$Me$_5$)$_2$ZrH^{i}Bu (14). 20.0 mg (0.0550 mmol) (C$_5$Me$_5$)$_2$ZrH$_2$ and 14.0 μL (0.0555 mmol, 1 equiv) Al^{i}Bu$_3$. 1:5 mix of **14**:**15**. ^{1}H NMR (300 MHz, benzene-d_6, 25 ºC) δ 5.68 (s, 1H, Zr-H), 1.91 (s, 30 H, C$_5$-CH$_3$), 1.02 (d, $^3J_{HH}$ = 7 Hz, 6H, ^{i}Bu-CH$_3$), -0.03 (d, $^3J_{HH}$ = 7 Hz, 2H, ^{i}Bu-CH$_2$).

(C$_5$Me$_5$)$_2$Zr^{i}Bu$_2$ (15). 6.5 mg (0.018 mmol) (C$_5$Me$_5$)$_2$ZrH$_2$ and 32.0 μL (0.180 mmol, 10 equiv) HAl^{i}Bu$_2$. ^{1}H NMR (300 MHz, benzene-d_6, 25 ºC) 1.85 (s, 30 H, C$_5$-CH$_3$), 2.22 (m,

$^3J_{HH}$ = 7 Hz, 2H, ^{i}Bu-CH), 1.25 (d, $^3J_{HH}$ = 7 Hz, 12H, ^{i}Bu-CH_3), 0.69 (d, $^3J_{HH}$ = 7 Hz, 4H, ^{i}Bu-CH_2).

***rac*-(SBI)ZrCl(μ-H)$_2$Al^{i}Bu$_2$.** 16.4 mg (0.0366 mmol) *rac*-(SBI)$ZrCl_2$ and 13.0 μL (0.0729 mmol, 2 equiv) HAl^iBu_2. ^{1}H NMR (300 MHz, benzene-d_6, 25 ºC) δ 7.51 (dd, $^3J_{HH}$ = 5, 4 Hz, 2H, Ar-H), 7.34 (m, 2H, Ar-H), 6.88 (d, $^3J_{HH}$ = 3 Hz, 2H, C_5-H), 6.80 (p, *J* = 6 Hz, 4H, Ar-H), 5.82 (d, $^3J_{HH}$ = 3 Hz, 2H, C_5-H), 2.05 (m, 7H, ^{i}Bu-CH), 1.12 (d, $^3J_{HH}$ = 4 Hz, 47H, ^{i}Bu-CH_3), 0.54 (s, 6H, Si$(CH_3)_2$), 0.37 (d, $^3J_{HH}$ = 7 Hz, 15H, ^{i}Bu-CH_2), -1.33 (br, 2H, Zr-H-Al).

***rac*-(SBI)ZrCl(μ-H)$_2$AlMe$_2$.** 2.4 mg (0.0054 mmol) *rac*-(SBI)$ZrCl_2$ and 0.6 mg (0.01 mmol, 2 equiv) $HAlMe_2$. ^{1}H NMR (300 MHz, benzene-d_6, 25 ºC) δ 7.35 (dd, $^3J_{HH}$ = 20, 9 Hz, 4H, Ar-H), 6.79 (m, 4H, Ar-H), 6.69 (br, 2H, C_5-H), 5.73 (br, 2H, C_5-H), 0.53 (s, 6H, Si$(CH_3)_2$), -1.58 (br, 2H, Zr-H-Al).

***rac*-(EBI)ZrCl(μ-H)$_2$Al^{i}Bu$_2$.** 6.4 mg (0.0366 mmol) *rac*-(EBI)$ZrCl_2$ and 13.0 μL (0.0729 mmol, 2 equiv) HAl^iBu_2. ^{1}H NMR (300 MHz, benzene-d_6, 25 ºC) δ 7.44 (d, $^3J_{HH}$ = 9 Hz, 2H, Ar-H), 7.37 (d, $^3J_{HH}$ = 9 Hz, 2H, Ar-H), 6.94 (m, 2H, Ar-H), 6.86 (m, 2H, Ar-H), 6.32 (br, 2H, C_5-H), 5.86 (br, 2H, C_5-H), 3.14 (m, 2H, C_2H_4), 2.80 (m, 2H, C_2H_4), 2.10 (br, 7H, ^{i}Bu-CH), 1.17 (s, 40H, ^{i}Bu-CH_3), 0.42 (d, $^3J_{HH}$ = 5 Hz, 10H, ^{i}Bu-CH_2), -0.80 (s, 2H, Zr-H-Al).

Me$_2$C(C$_5$H$_4$)$_2$ZrCl(μ-H)$_2$Al^{i}Bu$_2$. Me$_2$C(C$_5$H$_4$)$_2$$ZrCl_2$ and excess HAl^iBu_2. ^{1}H NMR (400 MHz, benzene-d_6, 25 ºC) δ 6.12 (br, 4H, C_5-H), 5.23 (br, 4H, C_5-H), 2.04 (br, 17H, ^{i}Bu-

CH), 1.09 (br, 101H, ^{i}Bu-CH_3), 1.02 (s, 12H, $C(CH_3)_2$), 0.47 (d, J = 7 Hz, 31H, ^{i}Bu-CH_2), -1.36 (s, 1H, Zr-H-Al).

$Me_2Si(C_5H_4)_2ZrCl(\mu\text{-}H)_2Al^{i}Bu_2$. 6.7 mg (0.019 mmol) $Me_2Si(C_5H_4)_2ZrCl_2$ and 20.6 μL (0.116 mmol, 6 equiv) $HAl^{i}Bu_2$. ^{1}H NMR (300 MHz, benzene-d_6, 25 ºC) δ 6.40 (br, 4H, C_5-H), 5.52 (br, 4H, C_5-H), 2.08 (s, 27H, ^{i}Bu-CH), 1.13 (d, $^3J_{HH}$ = 4.9 Hz, 168H, ^{i}Bu-CH_3), 0.47 (d, $^3J_{HH}$ = 7.0 Hz, 56H, ^{i}Bu-CH_2), 0.16 (s, 8H, $Si(CH_3)_2$), -1.75 (s, 2H, Zr-H-Al).

$Me_2Si(2,4\text{-}Me_2\text{-}C_5H_2)_2ZrCl(\mu\text{-}H)_2Al^{i}Bu_2$. $Me_2Si(2,4\text{-}Me_2\text{-}C_5H_2)_2ZrCl_2$ and excess $HAl^{i}Bu_2$. ^{1}H NMR (250 MHz, benzene-d_6, 25 ºC) δ 6.34 (s, 2H, C_5-H), 5.00 (s, 2H, C_5-H), 2.20 (s, 6H, C_5-CH_3), 1.94 (s, 6H, C_5-CH_3), 1.21 (d, $^3J_{HH}$ = 5 Hz, 57H, ^{i}Bu-CH_3), 0.53 (d, $^3J_{HH}$ = 7 Hz, 16H, ^{i}Bu-CH_2), 0.24 (s, 6H, $Si(CH_3)_2$), -0.76 (s, Zr-H-Al).

$(Me_2Si)_2(C_5H_3)_2ZrCl(\mu\text{-}H)_2Al^{i}Bu_2$. 4.5 mg (0.011 mmol) $(Me_2Si)_2(C_5H_3)_2ZrCl_2$ and 4.0 μL (0.022 mmol, 2 equiv) $HAl^{i}Bu_2$. ^{1}H NMR (500 MHz, toluene-d_8, 25 ºC) δ 6.76 (d, $^3J_{HH}$ = 3 Hz, 4H, C_5-H), 5.99 (t, $^3J_{HH}$ = 3 Hz, 2H, C_5-H), 1.11 (d, $^3J_{HH}$ = 5 Hz, 49H, ^{i}Bu-CH_3), 0.42 (d, $^3J_{HH}$ = 7 Hz, 16H, ^{i}Bu-CH_2), 0.37 (s, 6H, $Si(CH_3)_2$), 0.23 (s, 6H, $Si(CH_3)_2$), -1.71 (s, 2H, Zr-H-Al).

$(Me_2Si)_2(2,4\text{-}^{i}Pr_2\text{-}C_5H)(C_5H_3)ZrCl(\mu\text{-}H)_2Al^{i}Bu_2$. 4.5 mg (0.011 mmol) $(Me_2Si)_2(2,4\text{-}^{i}Pr_2\text{-}C_5H)(C_5H_3)ZrCl_2$ and 4.0 μL (0.022 mmol, 2 equiv) $HAl^{i}Bu_2$. ^{1}H NMR (500 MHz, toluene-d_8, -50 ºC) δ 6.70 (s, 2H, C_5-H), 6.41 (s, 1H, C_5-H), 6.05 (s, 1H, C_5-H), 3.14 (m, 2H, C_5-C*H*$(CH_3)_2$), -1.28 (s, 2H, Zr-H-Al).

***rac*-(EBTHI)$ZrH(\mu\text{-}H)_2Al^{i}Bu_2$ (25).** 6.5 mg (0.0091 mmol) *rac*-$((EBTHI)ZrH)_2(\mu\text{-}H)_2$ and 4.0 μL (0.018 mmol, 2 equiv) $HAl^{i}Bu_2$. ^{1}H NMR (500 MHz, toluene-d_8, -75 ºC) δ 6.34

(s, 1H, C_5-H), 5.73 (s, 1H, C_5-H), 5.15 (s, 1H, C_5-H), 4.94 (s, 1H, C_5-H), 4.56 (s, 1H, Zr-H), 1.20 (s, 23H, ^{i}Bu-CH_3), 0.54 (s, 8H, ^{i}Bu-CH_2), -0.53 (d, $^2J_{HH}$ = 8 Hz, 1H, Zr-H-Al), -1.18 (s, 1H, Zr-H-Al).

***rac*-(EBTHI)ZrCl(μ-H)$_2$Al^{i}Bu$_2$ (26).** 14.1 mg (0.0331 mmol) *rac*-(EBTHI)$ZrCl_2$ and excess HAl^iBu_2. ^{1}H NMR (300 MHz, benzene-d_6, 25 ºC) δ 6.16 (d, $^3J_{HH}$ = 3 Hz, 2H, C_5-H), 5.48 (s, 2H, C_5-H), 2.94 (dt, $^3J_{HH}$ = 12, 6 Hz, 2H, C_2H_4), 2.41 (dd, $^3J_{HH}$ = 12, 9 Hz, 5H, C_6-H_2), 2.17 (m, $^3J_{HH}$ = 8 Hz, 14H, ^{i}Bu-CH), 1.86 (d, $^3J_{HH}$ = 7 Hz, 6H, C_6-H_2), 1.37 (d, $^3J_{HH}$ = 7 Hz, 7H, C_6-H_2), 1.20 (br, 46H, ^{i}Bu-CH_3), 0.53 (d, $^3J_{HH}$ = 5.9 Hz, 16H, ^{i}Bu-CH_2), -0.09 (s, 2H, Zr-H-Al).

***rac*-(EBTHI)ZrCl(μ-H)$_2$AlMe$_2$.** 2.4 mg (0.0056 mmol) *rac*-(EBTHI)$ZrCl_2$ and 1.3 mg (0.022 mmol, 2 equiv) $HAlMe_2$. ^{1}H NMR (300 MHz, benzene-d_6, 25 ºC) δ 6.00 (br, 2H, C_5-H), 5.31 (br, 2H, C_5-H), 2.78 (dt, $^3J_{HH}$ = 17, 6 Hz, 2H, C_2H_4), 2.22 (m, 12H, H_4indenyl), 1.80 (s, 4H, H_4indenyl), 1.33 (dd, $^3J_{HH}$ = 13, 7 Hz, 4H, H_4indenyl), -0.35 (br, Zr-H-Al).

***rac*-Me$_2$C(indenyl)$_2$ZrCl(μ-H)$_2$Al^{i}Bu$_2$ (29).** 3.6 mg (0.0083 mmol) *rac*-$Me_2C(indenyl)_2$-$ZrCl_2$ and excess HAl^iBu_2. ^{1}H NMR (300 MHz, benzene-d_6, 25 ºC) δ 7.38 (d, $^3J_{HH}$ = 10 Hz, 4H Ar-H), 6.77 (m, 8H, Ar-H & C_5-H), 5.66 (d, $^3J_{HH}$ = 3 Hz, 2H, C_5-H), 2.08 (br, 12H, ^{i}Bu-CH), 1.57 (s, 6H, $C(CH_3)_2$), 1.16 (s, 78H, ^{i}Bu-CH_3), 0.40 (s, 23H, ^{i}Bu-CH_2), -1.35 (s, 2H, Zr-H-Al).

***meso*-Me$_2$C(indenyl)$_2$ZrCl(μ-H)$_2$Al^{i}Bu$_2$ (30).** 5.0 mg (0.012 mmol) *meso*-Me_2C-$(indenyl)_2ZrCl_2$ and 4.1 μL (0.023 mmol, 2 equiv) HAl^iBu_2. ^{1}H NMR (300 MHz, benzene-d_6, 25 ºC) δ 7.44 (d, $^3J_{HH}$ = 9 Hz, 4H, Ar-H), 6.86 (m, 2H, Ar-H), 6.61 (m, 2H, Ar-H), 6.50

(m, 14H, Ar-H & C_5-H), 6.23 (s, 2H, C_5-H), 6.12 (s, 2H, C_5-H), 2.03 (s, 21H, ^{i}Bu-CH), 1.94 (s, 8H, $C(CH_3)_2$), 1.86 (s, 5H, $C(CH_3)_2$), 1.65 (s, 4H, $C(CH_3)_2$), 1.59 (s, 7H, $C(CH_3)_2$), 1.10 (s, 167H, ^{i}Bu-CH_3), 0.47 (s, 46H, ^{i}Bu-CH_2), -0.86 (s, 1H, Zr-H-Al), -1.88 (m, 1H, Zr-H-Al).

***rac*-$Me_2Si(2\text{-}Me_3Si\text{-}4\text{-}Me_3C\text{-}C_5H_2)_2ZrH(\mu\text{-}H)_2Al^iBu_2$ (32).** 17.7 mg (0.0303 mmol) *rac*-$Me_2Si(2\text{-}Me_3Si\text{-}4\text{-}Me_3C\text{-}C_5H_2)_2ZrCl_2$ and excess HAl^iBu_2. ^{1}H NMR (300 MHz, benzene-d_6, 25 ºC) δ 6.36 (d, $^4J_{HH}$ = 2 Hz, 1H, C_5-H), 5.92 (d, $^4J_{HH}$ = 2 Hz, 2H, C_5-H), 5.75 (d, $^4J_{HH}$ = 2 Hz, 1H, C_5-H), 2.68 (dd, $^2J_{HH}$ = 10, 5 Hz, 1H, Zr-H), 2.02 (m, $^3J_{HH}$ = 7 Hz, 13H, ^{i}Bu-CH_2), 1.35 (s, 9H), 1.30 (s, 9H), 1.05 (d, $^3J_{HH}$ = 7 Hz, 68H, ^{i}Bu-CH_3), 0.65 (m, 9H), 0.47 (m, 41H, ^{i}Bu-CH_2), 0.39 (s, 23H, $Si(CH_3)_3$), -0.60 (s, $^2J_{HH}$ = 10 Hz 1H, Zr-H), -1.56 (d, $^2J_{HH}$ = 3 Hz, 1H, Zr-H).

***meso*-$Me_2Si(3\text{-}Me_3C\text{-}C_5H_3)_2ZrH(\mu\text{-}H)_2Al^iBu_2$ (34).** 3.5 mg (0.0076 mmol) *meso*-$Me_2Si(3\text{-}Me_3C\text{-}C_5H_3)_2ZrCl_2$ and 4.1 μL (0.023 mmol, 3 equiv) HAl^iBu_2. ^{1}H NMR (500 MHz, toluene-d_8, 25 ºC) δ 6.29 (d, $^3J_{HH}$ = 2 Hz, 1H, C_5-H), 5.87 (d, $^4J_{HH}$ = 1 Hz, 2H, C_5-H), 5.65 (d, $^3J_{HH}$ = 2 Hz, 1H, C_5-H), 2.59 (dd, $^3J_{HH}$ = 10, 5 Hz, 1H, Zr-H), 2.00 (m, 27H, ^{i}Bu-CH), 1.31 (s, 9H, C_5-$(CH_3)_3$), 1.25 (s, 9H, C_5-$(CH_3)_3$), 1.06 (m, 150H, ^{i}Bu-CH_3), 0.43 (m, 37H, ^{i}Bu-CH_2), 0.39 (s, 9H, $Si(CH_3)_3$), 0.35 (s, 9H, $Si(CH_3)_3$), -0.70 (d, $^3J_{HH}$ = 9 Hz, 1H, Zr-H-Al), -1.63 (s, 1H, Zr-H-Al).

$H_4C_2(C_5H_4)_2Zr(\mu\text{-}H)_3(Al^iBu_2)_3(\mu\text{-}Cl)_2$ (37). 6.0 mg (0.019 mmol) $H_4C_2(C_5H_4)_2ZrCl_2$ and 6.7 μL (0.038 mmol, 2 equiv) HAl^iBu_2. ^{1}H NMR (300 MHz, benzene-d_6, 25 ºC) δ 6.07 (s,

4H, C_5-H), 5.72 (s, 4H, C_5-H), 2.08 (s, 16H, ^{i}Bu-CH_3), 1.13 (br, 75H, ^{i}Bu-CH_2), 0.47 (d, $^3J_{HH}$ = 6.9 Hz, 22H, ^{i}Bu-CH_2), -0.31 (br, 1H, Zr-H-Al), -1.11 (br, 2H, Zr-H-Al).

$Me_4C_2(C_5H_4)_2Zr(\mu\text{-}H)_3(Al^iBu_2)_3(\mu\text{-}Cl)_2$ (38). 8.0 mg (0.021 mmol) $Me_4C_2(C_5H_4)_2ZrCl_2$ and excess HAl^iBu_2.^{1}H NMR (300 MHz, benzene-d_6, 25 ºC) δ 6.16 (s, 4H, C_5-H), 5.84 (s, 4H, C_5-H), 2.11 (br, 8H, ^{i}Bu-CH), 1.15 (br, 37H, ^{i}Bu-CH_3), 0.88 (s, 12H, C_2Me_4), 0.49 (d, $^3J_{HH}$ = 7 Hz, 12H, ^{i}Bu-CH_2), -0.15 (br, 1H, Zr-H-Al), -1.15 (br, 2H, Zr-H-Al).

$(C_5H_5)_2Hf(\mu\text{-}H)_3(Al^iBu_2)_3(\mu\text{-}Cl)_2$ (2). 4.3 mg (0.011 mmol) Cp_2HfCl_2 and 20.2 μL (0.113 mmol, 10 equiv) HAl^iBu_2. ^{1}H NMR (300 MHz, benzene-d_6) δ 5.54 (s, 10H, C_5-H), 2.04 (m, ^{i}Bu-CH), 1.10 (d, J = 6 Hz, ^{i}Bu-CH_3), 0.46 (d, J = 7 Hz, ^{i}Bu-CH_2), -0.26 (br, 2H, Zr-H-Al), -1.13 (br, 1H, Zr-H-Al).

2.6 References

1. Chen, E. Y.-X.; Rodriguez-Delgado, A., In *Comprehensive Organometallic Chemistry III*, Mingos, D. M. P.; Crabtree, R. H.; Bochmann, M., Eds. Elsevier: Amsterdam, The Netherlands, 2007; Vol. 4, p 878.
2. Lancaster, S. J., In *Comprehensive Organometallic Chemistry III*, Mingos, D. M. P.; Crabtree, R. H.; Bochmann, M., Eds. Elsevier: Amsterdam, The Netherlands, 2007; Vol. 4, p 753.
3. Yang, X. M.; Stern, C. L.; Marks, T. J. *Angew. Chem.-Int. Edit. Engl.*, **1992**, *31*, 1375.
4. Jordan, R. F., Chemistry of Cationic Dicyclopentadienyl Group 4 Metal-Alky I Complexes. In *Adv. Organomet. Chem.*, Stone, F. G. A.; Robert, W., Eds. Academic Press: 1991; Vol. 32, pp 325.
5. Bryliakov, K. P.; Talsi, E. P.; Semikolenova, N. V.; Zakharov, V. A.; Brand, J.; Alonso-Moreno, C.; Bochmann, M. *J. Organomet. Chem.*, **2007**, *692*, 859.

6. Carr, A. G.; Dawson, D. M.; Thornton-Pett, M.; Bochmann, M. *Organometallics*, **1999**, *18*, 2933.
7. Arndt, P.; Spannenberg, A.; Baumann, W.; Burlakov, V. V.; Rosenthal, U.; Becke, S.; Weiss, T. *Organometallics*, **2004**, *23*, 4792.
8. Bai, G. C.; Müller, P.; Roesky, H. W.; Uson, I. *Organometallics*, **2000**, *19*, 4675.
9. Chirik, P. J.; Henling, L. M.; Bercaw, J. E. *Organometallics*, **2001**, *20*, 534.
10. Choukroun, R.; Dahan, F.; Larsonneur, A. M.; Samuel, E.; Petersen, J.; Meunier, P. *Organometallics*, **1991**, *10*, 374.
11. Grossman, R. B.; Doyle, R. A.; Buchwald, S. L. *Organometallics*, **1991**, *10*, 1501.
12. Jones, S. B.; Petersen, J. L. *Inorg. Chem.*, **1981**, *20*, 2889.
13. Larsonneur, A. M.; Choukroun, R.; Jaud, J. *Organometallics*, **1993**, *12*, 3216.
14. Lee, H.; Desrosiers, P. J.; Guzei, I.; Rheingold, A. L.; Parkin, G. *J. Am. Chem. Soc.*, **1998**, *120*, 3255.
15. Khan, K.; Raston, C. L.; McGrady, J. E.; Skelton, B. W.; White, A. H. *Organometallics*, **1997**, *16*, 3252.
16. Wehmschulte, R. J.; Power, P. P. *Polyhedron*, **1999**, *18*, 1885.
17. Etkin, N.; Stephan, D. W. *Organometallics*, **1998**, *17*, 763.
18. Sizov, A. I.; Zvukova, T. M.; Belsky, V. K.; Bulychev, B. M. *J. Organomet. Chem.*, **2001**, *619*, 36.
19. Etkin, N.; Hoskin, A. J.; Stephan, D. W. *J. Am. Chem. Soc.*, **1997**, *119*, 11420.
20. Fermin, M. C.; Ho, J. W.; Stephan, D. W. *Organometallics*, **1995**, *14*, 4247.
21. Wailes, P. C.; Weigold, H.; Bell, A. P. *J. Organomet. Chem.*, **1972**, *43*, C29.
22. Shoer, L. I.; Gell, K. I.; Schwartz, J. *J. Organomet. Chem.*, **1977**, *136*, C19.
23. Parfenova, L. V.; Pechatkina, S. V.; Khalilov, L. M.; Dzhemilev, U. M. *Russ. Chem. Bull.*, **2005**, *54*, 316.
24. Parfenova, L. V.; Vil'danova, R. F.; Pechatkina, S. V.; Khalilov, L. M.; Dzhemilev, U. M. *J. Organomet. Chem.*, **2007**, *692*, 3424.

25. Tritto, I.; Zucchi, D.; Destro, M.; Sacchi, M. C.; Dall'Occo, T.; Galimberti, M. *J. Mol. Catal. A-Chem.*, **2000**, *160*, 107.
26. Götz, C.; Rau, A.; Luft, G. *J. Mol. Catal. A-Chem.*, **2002**, *184*, 95.
27. González-Hernández, R.; Chai, J. F.; Charles, R.; Pérez-Camacho, O.; Kniajanski, S.; Collins, S. *Organometallics*, **2006**, *25*, 5366.
28. Babushkin, D. E.; Brintzinger, H. H. *Chem.-Eur. J.*, **2007**, *13*, 5294.
29. Babushkin, D. E.; Panchenko, V. N.; Timofeeva, M. N.; Zakharov, V. A.; Brintzinger, H. H. *Macromol. Chem. Phys.*, **2008**, *209*, 1210.
30. Ziegler, K.; Kroll, W. R.; Larbig, W.; Steudel, O. W. *Liebigs Ann. Chem.*, **1960**, *629*, 53.
31. Hoffmann, E. G. *Liebigs Ann. Chem.*, **1960**, *629*, 104.
32. Vestin, R.; Vestin, U.; Kowalewski, J. *Acta Chem. Scand. A, Phys. Inorg. Chem.*, **1985**, *39*, 767.
33. Hoffmann, E. G. *Z. Elektrochem.*, **1960**, *64*, 616.
34. Wailes, P. C.; Weigold, H. *J. Organomet. Chem.*, **1970**, *24*, 405.
35. Bickley, D. G.; Hao, N.; Bougeard, P.; Sayer, B. G.; Burns, R. C.; McGlinchey, M. J. *J. Organomet. Chem.*, **1983**, *246*, 257.
36. Pankratyev, E. Y.; Tyumkina, T. V.; Parfenova, L. V.; Khalilov, L. M.; Khursan, S. L.; Dzhemilev, U. M. *Organometallics*, **2009**, *28*, 968.
37. Brintzinger, H. H.; Prosenc, M. H.; Schaper, F.; Weeber, A.; Wieser, U. *J. Mol. Struct.*, **1999**, *485*, 409.
38. Wiesenfeldt, H.; Reinmuth, A.; Barsties, E.; Evertz, K.; Brintzinger, H. H. *J. Organomet. Chem.*, **1989**, *369*, 359.
39. Zachmanoglou, C. E.; Docrat, A.; Bridgewater, B. M.; Parkin, G.; Brandow, C. G.; Bercaw, J. E.; Jardine, C. N.; Lyall, M.; Green, J. C.; Keister, J. B. *J. Am. Chem. Soc.*, **2002**, *124*, 9525.
40. Burger, P. Personal Communication 2007

41. Bühl, M.; Hopp, G.; von Philipsborn, W.; Beck, S.; Prosenc, M. H.; Rief, U.; Brintzinger, H. H. *Organometallics*, **1996**, *15*, 778.
42. Gutmann, S.; Burger, P.; Prosenc, M. H.; Brintzinger, H. H. *J. Organomet. Chem.*, **1990**, *397*, 21.
43. Bochmann, M.; Sarsfield, M. J. *Organometallics*, **1998**, *17*, 5908.
44. Chirik, P. J.; Bercaw, J. E. In *Polym. Prepr.*, 2000; Am. Chem. Soc., Div. Polym. Chem: 2000; p 393.
45. McAlister, D. R.; Erwin, D. K.; Bercaw, J. E. *J. Am. Chem. Soc.*, **1978**, *100*, 5966.
46. Pool, J. A.; Lobkovsky, E.; Chirik, P. J. *J. Am. Chem. Soc.*, **2003**, *125*, 2241.
47. Marvich, R. H.; Brintzinger, H. H. *J. Am. Chem. Soc.*, **1971**, *93*, 2046.
48. Spannenberg, A.; Arndt, P.; Baumann, W.; Burlakov, V. V.; Rosenthal, U.; Becke, S.; Weiss, T. *Organometallics*, **2004**, *23*, 3819.
49. Voskoboynikov, A. Z.; Agarkov, A. Y.; Chernyshev, E. A.; Beletskaya, I. P.; Churakov, A. V.; Kuz'mina, L. G. *J. Organomet. Chem.*, **1997**, *530*, 75.
50. Schwemlein, H.; Brintzinger, H. H. *J. Organomet. Chem.*, **1983**, *254*, 69.
51. Herrmann, W. A.; Rohrmann, J.; Herdtweck, E.; Spaleck, W.; Winter, A. *Angew. Chem.-Int. Edit. Engl.*, **1989**, *28*, 1511.
52. Wailes, P. C.; Weigold, H. *Inorg. Synth.*, **1979**, *19*, 223.
53. Deck, P. A.; Beswick, C. L.; Marks, T. J. *J. Am. Chem. Soc.*, **1998**, *120*, 1772.
54. Lappert, M. F.; Riley, P. I.; Yarrow, P. I. W.; Atwood, J. L.; Hunter, W. E.; Zaworotko, M. J. *J. Chem. Soc. Dalton*, **1981**, 814.
55. Manriquez, J. M.; McAlister, D. R.; Sanner, R. D.; Bercaw, J. E. *J. Am. Chem. Soc.*, **1976**, *98*, 6733.
56. Schock, L. E.; Marks, T. J. *J. Am. Chem. Soc.*, **1988**, *110*, 7701.
57. Wild, F.; Wasiucionek, M.; Huttner, G.; Brintzinger, H. H. *J. Organomet. Chem.*, **1985**, *288*, 63.
58. Nifant'ev, I. E.; Churakov, A. V.; Urazowski, I. F.; Mkoyan, S. G.; Atovmyan, L. O. *J. Organomet. Chem.*, **1992**, *435*, 37.

59. Köpf, H.; Klouras, N. *Z. Naturforsch., B: Chem. Sci.*, **1983**, *38*, 321.
60. Hüttenhofer, M.; Prosenc, M.-H.; Rief, U.; Schaper, F.; Brintzinger, H. H. *Organometallics*, **1996**, *15*, 4816.
61. Cano, A.; Cuenca, T.; Gomezsal, P.; Royo, B.; Royo, P. *Organometallics*, **1994**, *13*, 1688.
62. Herzog, T. A.; Zubris, D. L.; Bercaw, J. E. *J. Am. Chem. Soc.*, **1996**, *118*, 11988.
63. Chacon, S. T.; Coughlin, E. B.; Henling, L. M.; Bercaw, J. E. *J. Organomet. Chem.*, **1995**, *497*, 171.
64. Yoder, J. C.; Day, M. W.; Bercaw, J. E. *Organometallics*, **1998**, *17*, 4946.

CHAPTER 3

Cationic Alkylaluminum-Complexed Zirconocene Hydrides

3.1 Abstract

The *ansa*-zirconocene complex *rac*-$Me_2Si(1\text{-indenyl})_2ZrCl_2$ ((SBI)$ZrCl_2$) reacts with diisobutylaluminum hydride and trityl tetrakis(perfluorophenyl)borate in hydrocarbon solutions to give the cation $[(SBI)Zr(\mu\text{-}H)_3(Al^iBu_2)_2]^+$, the identity of which is derived from NMR data and supported by a crystallographic structure determination. Analogous reactions proceed with many other zirconocene dichloride complexes. $[(SBI)Zr(\mu\text{-}H)_3(Al^iBu_2)_2]^+$ reacts reversibly with $ClAl^iBu_2$ to give the dichloro-bridged cation $[(SBI)Zr(\mu\text{-}Cl)_2Al^iBu_2]^+$. Reaction with $AlMe_3$ first leads at to mixed-alkyl species $[(SBI)Zr(\mu\text{-}H)_3(AlMe_x{}^iBu_{2-x})_2]^+$ via exchange of alkyl groups between aluminum centers. At higher $AlMe_3$/Zr ratios, $[(SBI)Zr(\mu\text{-}Me)_2AlMe_2]^+$, a constituent of methylalumoxane-activated catalyst systems, is formed in an equilibrium with the trihydride cation $[(SBI)Zr(\mu\text{-}H)_3(AlR_2)_2]^+$, which strongly predominates at comparable HAl^iBu_2 and $AlMe_3$ concentrations, implicating the latter's presence in olefin polymerization catalyst systems.

This Chapter in part has been submitted for publication:
Baldwin, S. M.; Bercaw, J. E.; Brintzinger, H. H.; Henling, L. M.; Day, M. W. *J. Am. Chem. Soc.*, submitted.
(DOI: 10.1021/ja1050428)

3.2 Introduction

Alkylaluminum-complexed zirconocene hydride complexes have been shown to be present in a variety of catalytic systems, e.g., for hydro- and carboalumination reactions of unsaturated substrates, including their asymmetric variants.[1-2] While there is still some uncertainty concerning the compositions and structures of the complexes occurring in these reaction systems,[3] Chapter 1 shows the two types of neutral complexes that arise in such reaction systems containing diisobutylaluminum hydride, $HAl^{i}Bu_2$, depending on the type of zirconocene used: trihydride complexes containing three $\{Al^{i}Bu_2\}$ units connected by two Cl-bridges are formed from most unbridged zirconocene dichlorides (Scheme 3.1). Ring-bridged *ansa*-zirconocene precursors, on the other hand, react with $HAl^{i}Bu_2$ to yield, in most cases, chloro dihydride complexes containing only one $\{Al^{i}Bu_2\}$ unit (Scheme 3.1). This dichotomy appears to be caused by steric interference due to the eclipsed ring conformation, which is enforced by a single-atom interannular bridge.

Scheme 3.1

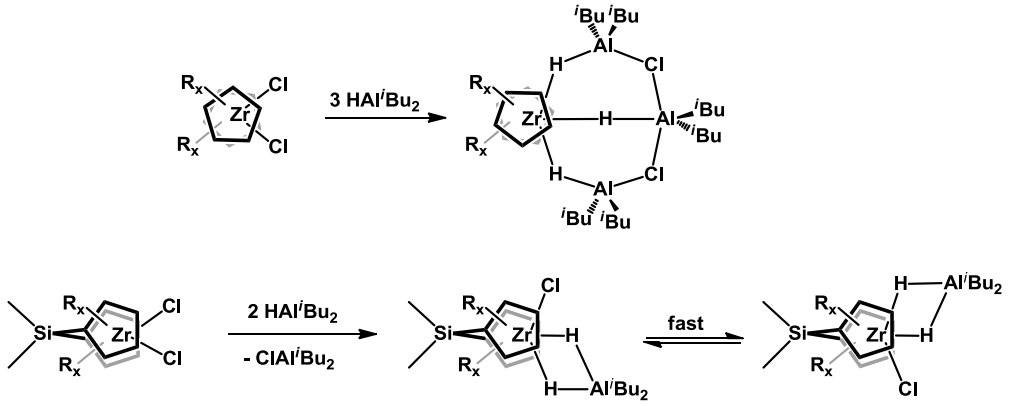

Apart from such neutral species, alkylaluminum-complexed zirconocene hydrides might also give rise to cationic species, particularly in zirconocene-based reaction systems containing methylalumoxane (MAO) or other "cationization" reagents typically employed for olefin polymerization catalysis.[4] Cationic zirconocene hydride species have been crystallographically characterized either as discrete ion pairs[5-8] or with stabilizing Lewis bases[9-15]. Numerous other examples of cationic zirconocene hydrides, in ion pairs[16-21] and with stabilizing Lewis bases,[17, 22-25] have been identified by NMR. In many polymerization systems the presence of alkylaluminum species would likely preclude these types of hydride species. Three alkylaluminium-complexed hydrides have recently been observed by NMR[26-28] and three borane-complexed zirconocene hydrides have been structurally characterized[29-32] (Figure 3.1). The identity of the species formed from (SBI)$ZrCl_2$ (*rac*-$Me_2Si(1\text{-indenyl})_2ZrCl_2$) with MAO and Al^iBu_3 remained elusive. In this chapter, an exploration of cationic species produced in reaction systems containing a zirconocene dichloride, in the presence of an alkylaluminum hydride and a cationization reagent, will be investigated focusing mainly on the often-studied *ansa*-zirconocene (SBI)$ZrCl_2$.

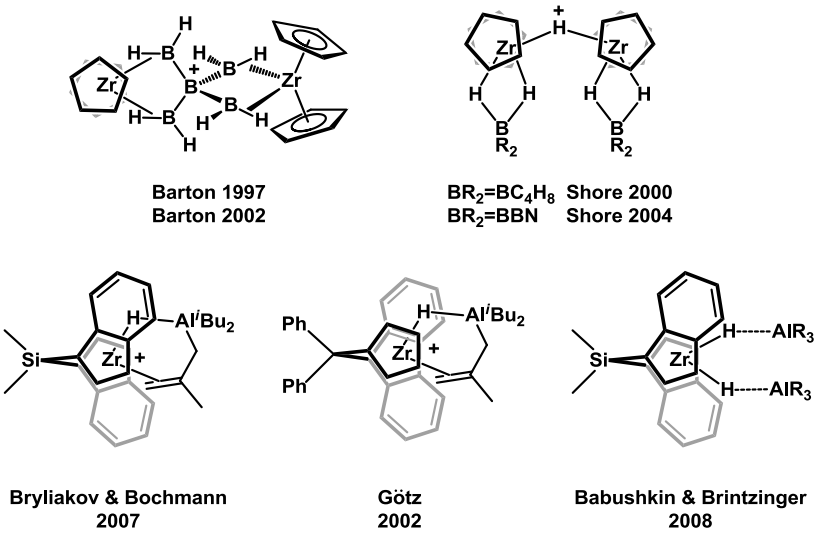

Figure 3.1: Known cationic zirconocene hydrides without Lewis base stabilization

3.3 Results and Discussion

3.3.1 The reaction system (SBI)ZrCl$_2$/HAl^{i}Bu$_2$/[Ph$_3$C][B(C$_6$F$_5$)$_4$].

In a typical experiment, a 4 mM benzene-d_6 solution of the neutral complex (SBI)Zr(Cl)(μ-H)$_2$Al^{i}Bu$_2$, is obtained by reaction of (SBI)ZrCl$_2$ with 5 equiv of HAl^{i}Bu$_2$. Attempts to make more concentrated solutions result in formation of a zirconocene-containing oil. When the neutral hydride species is then treated at room temperature with one equiv of trityl tetrakis(perfluorophenyl)borate, [Ph$_3$C][B(C$_6$F$_5$)$_4$], the reaction mixture immediately assumes a bluish-green tint. ^{1}H NMR of the solution reveals a single product characterized by a doublet at –2.25 ppm with $^2J_{HH} \approx 8$ Hz and an integration of 2 H per zirconocene unit (Figure 3.2), which is indicative of a ZrH$_2$ group. A gCOSY reveals that this doublet is coupled to a triplet at 0.30 ppm, which is partly obscured by Al-C*H$_2$* signals (Figure 3.3). This triplet must then be due to a third Zr-bound hydride ligand, such that this set of

hydride signals is to be assigned to a zirconocene complex with three Zr-bound hydride ligands, one in central position and two in lateral positions. The complete conversion of 1 equiv of the trityl salt to triphenyl methane (δ 5.42 pm) implies the formation of a zirconocene monocation. For a proper balancing of charges, this cation would have to contain two $\{Al^{i}Bu_2^{+}\}$ units, presumably in contact with the Zr-bound hydride ligands.

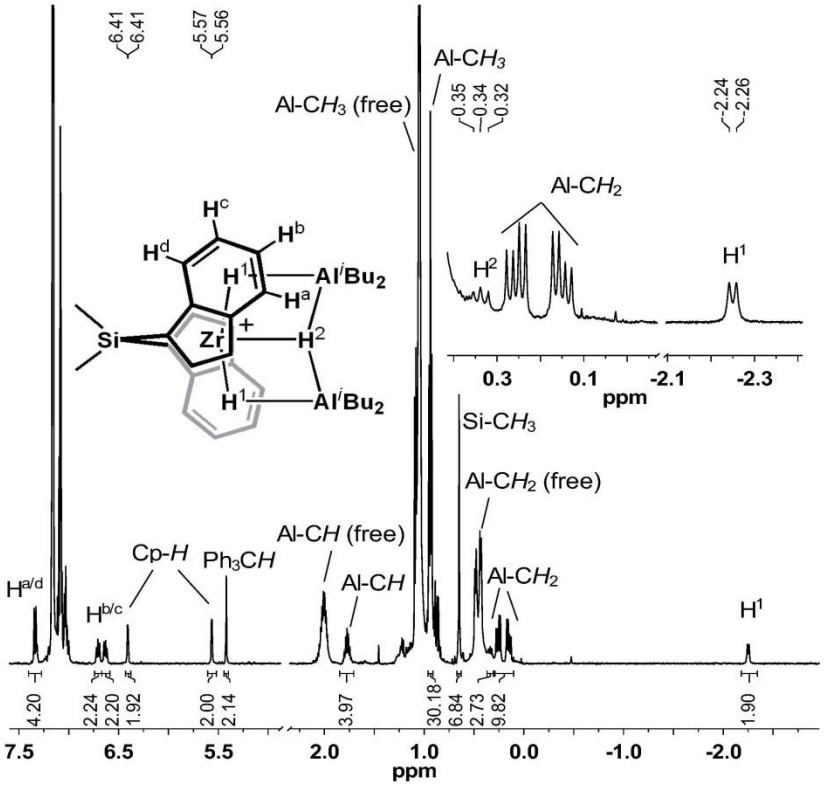

Figure 3.2: ^{1}H NMR spectrum of the cationic hydride $[(SBI)Zr(\mu\text{-}H)_3(Al^{i}Bu_2)_2]^{+}$ in benzene-d_6 solution, obtained by treating a 4 mM solution of $(SBI)ZrCl_2$ first with 5 equiv of $HAl^{i}Bu_2$ and then with 1 equiv of $[Ph_3C][B(C_6F_5)_4]$ (25 ºC, 500 MHz).

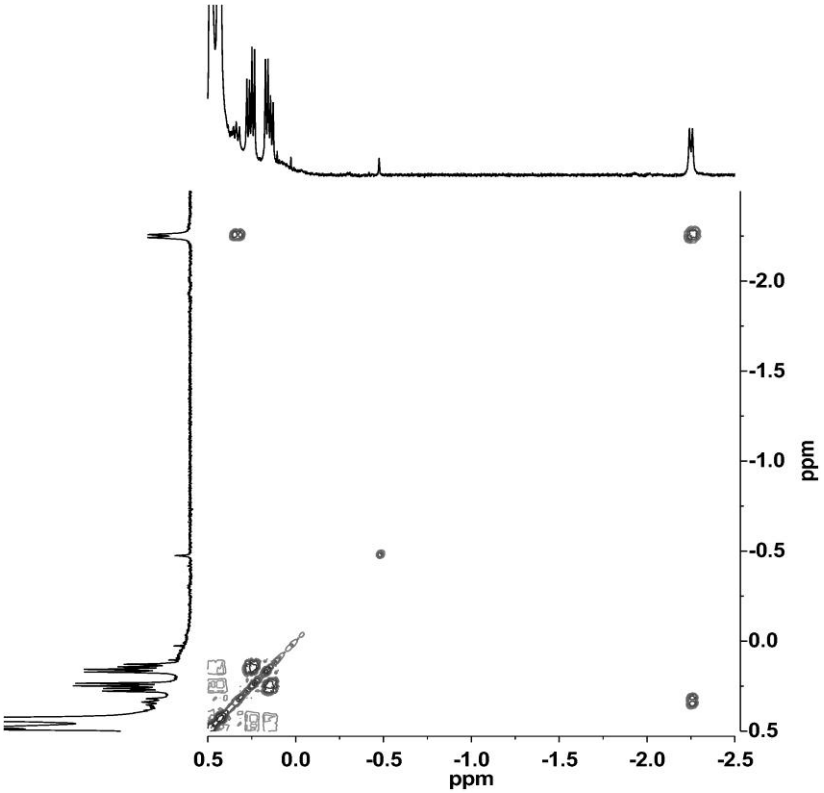

Figure 3.3: High-field region of gCOSY of the cation $[(SBI)Zr(\mu\text{-}H)_3(Al^iBu_2)_2]^+$ (reaction conditions as in Figure 3.2).

The $\{Al^iBu_2^+\}$ units of the resulting cationic complex, $[(SBI)Zr(\mu\text{-}H)_3(Al^iBu_2)_2]^+$, give rise to C*H* and CH_3 signals centered at 1.77 and 0.94 ppm, respectively, and to a CH_2 signal with a well-resolved diastereotopic splitting of 0.11 ppm, centered at 0.20 ppm. Integration of these signals, which are well-separated from those of the free $\{^i$BuAl$\}$ species present, clearly support the presence of two $\{Al^iBu_2^+\}$ moieties per zirconocene unit. Formation of $ClAl^iBu_2$ can be deduced from a characteristic splitting of the Al-H resonance into three separate resonances due to formation of mixed $HAl^iBu_2/ClAl^iBu_2$ clusters,[33] and from the observation of the isobutyl ^{1}H resonances of $ClAl^iBu_2$ at temperatures below –25 ºC.

Conversion of (SBI)$ZrCl_2$ to the trihydride cation, $[(SBI)Zr(\mu\text{-}H)_3(Al^iBu_2)_2]^+$, can thus be described as outlined in Scheme 3.2.

Scheme 3.2

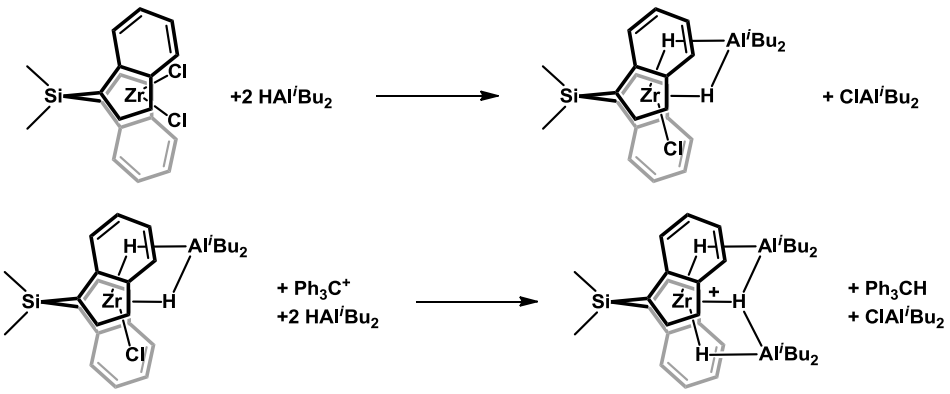

The observation of separate signals for complex-bound and free {Al^{i}Bu} groups implies that exchange between these units is slow on the NMR time scale. Coalescence of these signals did not occur upon heating such a reaction system before the cation decomposed at 75 ºC, but an EXSY study performed at room temperature revealed substantial exchange between complex-bound and free {Al^{i}Bu} groups. At mixing times of 300 ms, sizeable EXSY crosspeaks (Figure 3.4) are observed between the respective isobutyl signals of the trihydride cluster and those of {Al^{i}Bu} units in solution, but no such crosspeaks are observed between the hydride signals of these species. Crosspeaks are observed, however, between the hydride signals of the HAl^{i}Bu$_2$ / ClAl^{i}Bu$_2$ clusters showing that increased relaxation due to the quadrupolar nature of Al is not responsible for the absence of these peaks. This indicates that a rather fast exchange involves primarily the isobutyl residues of

free and complex bound {Al^{i}Bu} units, while the {Zr(μ-H)$_3$Al$_2$} core of the trihydride cation remains intact on this time scale.

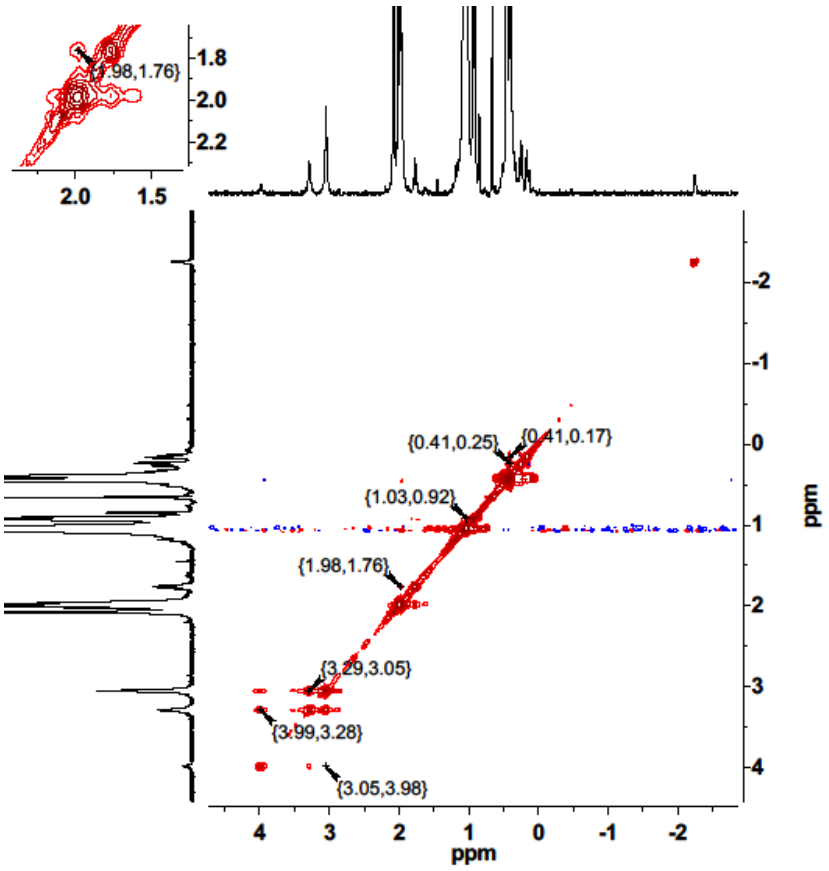

Figure 3.4: EXSY spectrum of 3 mM toluene-d_8 solution of [(SBI)Zr(μ-H)$_3$(Al^{i}Bu$_2$)$_2$]$^+$ collected with a mixing time of 300 ms. (25 ºC, 500 MHz). Inset shows close up of methyne signals of isobutyl groups. Red peaks indicate exchange, blue would indicate NOE interaction.

Yellow crystals of [(SBI)Zr(μ-H)$_3$(Al^{i}Bu$_2$)$_2$][B(C$_6$F$_5$)$_4$] were obtained by reaction of 21.7 mg of (SBI)ZrCl$_2$ with 10 equiv of HAl^{i}Bu$_2$ and 1 equiv of [Ph$_3$C][(F$_6$C$_5$)B] in 1.25 g of toluene, separating the green oil formed from the toluene layer, redissolving the oil in a

minimal volume of fresh toluene, and storing this solution for several weeks at −40 ºC. An X-ray crystallographic structure determination revealed a structure in the non-centrosymmetric space group $P2_12_12_1$, with two $[(SBI)Zr(\mu\text{-}H)_3(Al^iBu_2)_2]^+$ cations of opposite chirality and two $[B(C_6F_5)_4]^-$ anions per asymmetric unit along with a molecule of toluene. Structural refinement resulted in closely similar geometries for both of the cations, one of which is shown in Figure 3.5.

While the quality of the structure suffers from considerable disorder with regard to the orientation of the Al-bound isobutyl groups, the geometry of the $\{(SBI)Zr(\mu\text{-}H)_3Al_2\}$ core, with hydride positions located in the difference Fourier map, clearly supports the structural assignments derived from the NMR data discussed above. Zr-H and Al-H bond distances are in the ranges of 1.88(3)-1.99(4) Å and 1.58(3)-2.07(4) Å, respectively (Table 3.1). Zr-H and Al-H bond distances in similarly wide ranges of 1.845-2.012 Å and 1.604-1.980 Å, respectively, have previously been reported for Zr-(μ-H)-Al bridges in neutral zirconocene hydride complexes with a ZrH_3 core geometry.[34-38]

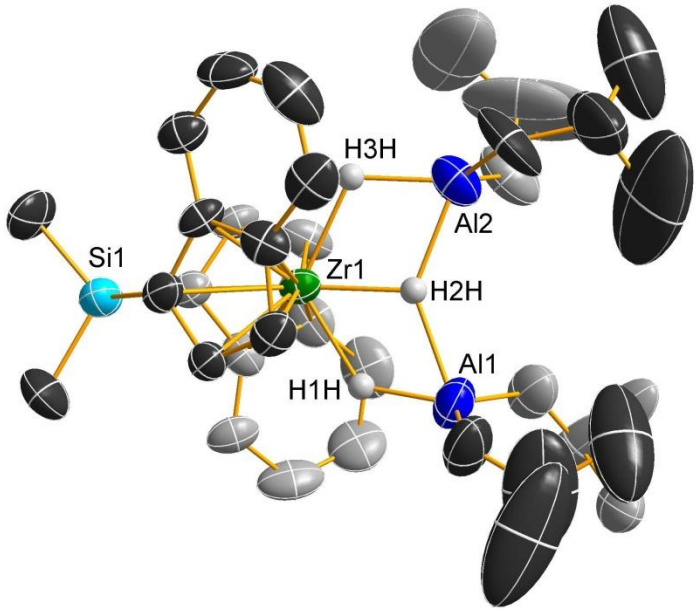

Figure 3.5: Structure of one of the two unique $[(SBI)Zr(\mu\text{-}H)_3(Al^iBu_2)_2]^+$ cations in the asymmetric unit of crystals of $[(SBI)Zr(\mu\text{-}H)_3(Al^iBu_2)_2][B(C_6F_5)_4] \cdot$ ½ toluene (thermal ellipsoids at 50% probability, hydride positions taken from the difference Fourier map; other H atoms omitted).

Table 3.1: Selected distances and angles for the cation $[(SBI)Zr(\mu\text{-}H)_3(Al^iBu_2)_2]^+$

Bond distances (Å)		**nonbonding distances (Å)**		**bond angles (°)**	
Zr1-H1H	1.92(4)	Zr1-Al1	3.1779(20)	H1H-Zr1-H3H	123.1(14)
Zr1-H2H	1.88(3)	Zr1-Al2	3.0945(19)	H1H-Zr1-H2H	56.7(13)
Zr1-H3H	1.99(4)			H2H-Zr1-H3H	66.4(14)
Al1-H1H	1.58(3)			H1H-Al2-H2H	60.4(16)
Al1-H2H	1.95(4)			H2H-Al1-H3H	70.7(15)
Al2-H2H	1.92(3)			ctr1-Zr1-ctr2[a]	126.514(24)
Al2-H3H	1.73(3)				
Zr1-ctr1	2.1897(5)				
Zr1-ctr2	2.1913(5)				
Zr2-H4H	1.99(4)	Zr2-Al3	3.1015(20)	H4H-Zr2-H6H	129.4(14)
Zr2-H5H	1.92(3)	Zr2-Al4	3.1917(18)	H4H-Zr2-H5H	64.9(14)
Zr2-H6H	1.94(4)			H5H-Zr2-H6H	65.0(14)
Al3-H6H	1.75(3)			H5H-Al3-H6H	70.3(16)
Al3-H5H	1.85(4)			H4H-Al4-H5H	66.0(15)
Al4-H5H	2.07(4)			ctr3-Zr2-ctr4[b]	126.868(24)
Al4-H4H	1.78(3)				
Zr2-ctr3	2.1883(5)				
Zr2-ctr4	2.2055(5)				

[a] (ctr1: C1A-C5A, ctr2: C10A-C14A) [b] (ctr3: C1B-C5B, ctr4: C10B-C14B)

3.3.2 Alkylaluminum-complexed trihydride cations derived from other metallocene complexes.

In addition to (SBI)$ZrCl_2$, we have studied several other zirconocene dichlorides (Figure 3.6) with regard to their reactions with excess HAl^iBu_2 and one equivalent of $[Ph_3C][B(C_6F_5)_4]$. As with (SBI)$ZrCl_2$, we observe in each case mutually coupled doublet and triplet high-field signals with intensities of 2H and 1H per zirconocene unit, respectively (Table 2.2). More sterically hindered metallocenes, such as $(C_5Me_5)_2ZrCl_2$ or $(C_5Me_4H)_2ZrCl_2$, did not react under these conditions, while *tert*-butyl substituted metallocenes, such as *rac*-$Me_2Si(3\text{-}SiMe_3\text{-}5\text{-}CMe_3C_5H_2)_2ZrCl_2$ and *meso*-$Me_2C(4\text{-}CMe_3C_5H_3)_2ZrCl_2$, decompose to unidentified products. In some cases, the signals of complex-bound isobutyl C*H*, CH_2 and/or CH_3 groups are sufficiently separate from their uncomplexed counterparts to allow their individual integration, which supports the presence of two $\{Al^iBu_2\}$ moieties per zirconocene unit. There is no reasonable doubt, therefore, that each of the zirconocene dichlorides shown in Figure 3.6 forms a cationic trihydride complex containing two $\{Al^iBu_2\}$ units, in complete analogy to $[(SBI)Zr(\mu\text{-}H)_3(Al^iBu_2)_2]^+$.

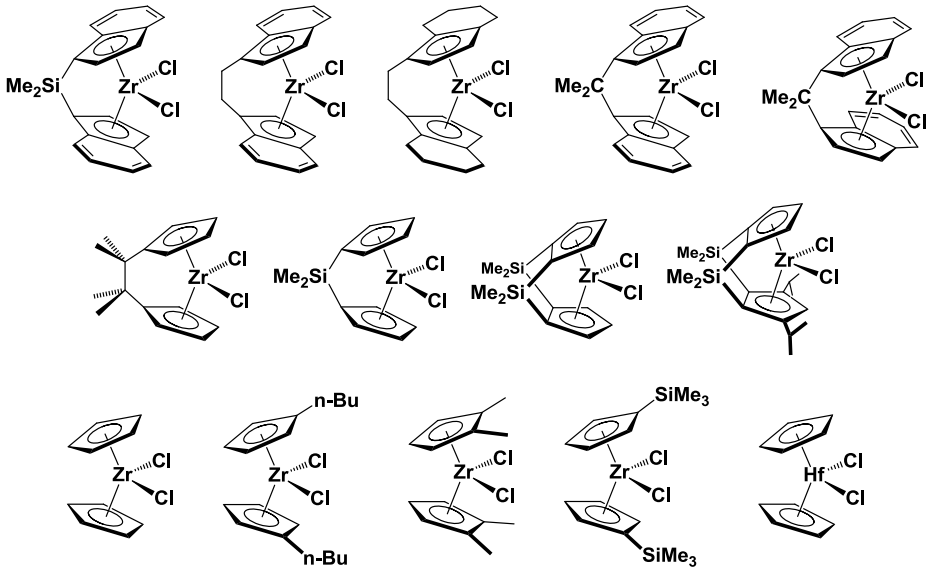

Figure 3.6: Zirconocenes studied with $HAl^{i}Bu_2/[Ph_3C][B(C_6F_5)_4]$

Table 3.2: ^{1}H NMR data of {^{i}Bu$_2$Al}-complexed zirconocene trihydride cations ($[B(C_6F_5)_4]^-$ salts in benzene-d_6 solution, 25 ºC, δ in ppm, 300 MHz).

	Zr-H	Al^{i}Bu$_2$	ligand[a]
rac-(SBI)Zr	–2.25 (d, 2H, 8 Hz) 0.34 (t, 1H, 8 Hz)	0.26(dd, 4H, 14, 7 Hz)[b] 0.15(dd, 4H, 14, 7 Hz)[b] 0.94(t, 24H, 7 Hz)[c] 1.77(n, 4H, 7 Hz)	5.57 (d, 2H, 3 Hz) 6.41 (d, 2H, 3 Hz) 0.65 (s, (C*H*$_3$)$_2$Si)
rac-C_2H_4(indenyl)$_2$Zr	–1.72 (d, 2H, 8 Hz) –0.29 (t, 1H, 8 Hz)	0.19 (dd, 7, 3 Hz)[d] 0.93[c,d] 1.74 (n, 4H, 7 Hz)	5.56 (d, 2H, 3Hz) 5.74 (d, 2H, 3 Hz)
rac-(EBTHI)Zr	–1.08 (t, 1H, 7 Hz) –0.46 (d, 2H, 6 Hz)	0.35 (m)[d] 0.96 (dt, 9, 5 Hz)[d] 1.88 (n, 7 Hz)[d]	5.26 (d, 2H, 3 Hz) 5.81 (d, 2H, 3 Hz)
rac-Me_2C(indenyl)$_2$Zr	–1.72 (d, 2H, 7 Hz) –0.82[e]	0.25 (qd, 8H, 15, 7, 7 Hz) 0.91 (dd, 24H, 6, 4 Hz) 1.76 (m, 4H)	5.33 (t, 2H, 3 Hz) 6.49 (d, 2H, 3 Hz) 1.69 (s, (C*H*$_3$)$_2$C)
meso-Me_2C(indenyl)$_2$Zr	–3.47 (d, 1H, 7 Hz) –0.91 (d, 1H, 6 Hz) 1.53(m)[e]	0.47 (m)[e] 0.88 (m)[e] 2.00 (m)[e]	4.84 (d, 1H, 3 Hz) 6.40 (d, 1H, 3 Hz)
$Me_4C_2(C_5H_4)_2Zr$	–1.60 (t, 1H, 7 Hz) –1.37 (d, 2H, 7 Hz)	0.36 (d, 8H 7 Hz) 0.95 (d, 24H, 7 Hz) 1.86 (m, 4H, 7 Hz)	5.73 (pt, 4H, 3 Hz) 5.95 (pt, 4H, 3 Hz) 0.88 (s, (C*H*$_3$)$_4$C$_2$)
$Me_2Si(C_5H_4)_2Zr$	–2.04 (d, 2H, 9 Hz) –1.27 (t, 1H, 8 Hz)	0.34 (d, 7 Hz) 0.86 (m) 1.82 (m)	5.24 (br, 4H) 6.22 (br, 4H) 0.17 (s, (C*H*$_3$)$_2$Si)
$(Me_2Si)_2(C_5H_3)_2Zr$	–2.03 (d, 2H, 7 Hz) –1.04 (t, 1H, 7 Hz)	0.34 (dd, 8H, 28, 7 Hz) 0.92 (m, 24H) 1.82 (m, 4H)	6.10 (br, 1H) 6.41 (br, 1H) 6.53 (br, 2H) 0.17 (s, (C*H*$_3$)$_2$Si)
$(Me_2Si)_2(C_5H_3)(^iPr_2C_5H)Zr$	–1.47 (d, 2H, 6 Hz) –0.50 (br, 1H)	0.43 (d, 7 Hz)[d] 0.96 (m)[d] 1.89 (m)[d]	5.94 (t, 2H, 2.7 Hz) 6.49 (d, 4H, 2.7 Hz) –0.08 (s, (C*H*$_3$)$_2$Si)
$(C_5H_5)_2Zr$	–2.39 (t, 1H, 8 Hz) –2.27 (d, 2H, 8 Hz)	0.28 (d, 8H, 7 Hz) 0.92 (d, 24H, 7Hz) 1.81 (n, 4H, 7 Hz)	5.59 (s, 10H)
$(^nBuC_5H_4)_2Zr$	–1.97 (t, 1H, 8 Hz) –1.61 (d, 2H, 8 Hz)	0.40 (d, 7 Hz)[d] 0.96 (d, 7 Hz)[d] 1.87 (m)[d]	5.67 (d, 4H, 2 Hz) 5.73 (d, 4H, 3Hz)
$(Me_3SiC_5H_4)_2Zr$	–2.30 (br, 1H) –1.84 (d, 2H, 9 Hz)	0.46[d] 0.95 (d, 6 Hz)[d] 1.86 (m, 4H)	6.01 (br, 4H) 6.11 (br, 4H)
$(1,2\text{-}Me_2C_5H_3)_2Zr$	–1.79 (br, 1H) –1.42 (d, 7 Hz, 2H)	0.43 (d, 7 Hz)[d] 0.97 (d, 6 Hz)[d] 1.88 (m, 7 Hz)[d]	5.29 (d, 4H, 3 Hz) 5.86 (t, 2H, 3 Hz) 1.74 (s, 4Cp-Me)
$(C_5H_5)_2Hf$	–2.27 (t, 6 Hz, 1H) –1.40 (d, 6 Hz, 2H)	0.26 (d, 12H, 7 Hz) 0.92 (d, 7 Hz)[d] 1.80 (m, 4H, 7Hz)	5.48 (s, 10H)

[a] C_5-*H* unless otherwise noted; [b] resolved diastereotopic splitting by 0.11 ppm; [c] diasterotopic splitting not resolved; [d] not sufficiently resolved for integration; [e] peak obscured by other signals, shift determined from gCOSY.

All the zirconocene complexes studied here—ring-bridged and unbridged alike—uniformly give the previously unreported type of alkylaluminum-complexed zirconocene trihydride cation described above. The relative positions of the two Zr-hydride signals, however, differ among the trihydride cations listed in Table 2.2. For all of the complexes with a single-atom bridge, the doublet of the lateral Zr-H_2 group appears at higher fields than the central Zr-*H* triplet, whereas all of the trihydride cations without interannular bridge give rise to a Zr-H_2 doublet at lower field than their Zr-*H* triplet. Complexes with an ethanediyl linker on the other hand exhibit no uniform ordering of their two hydride resonances (Table 2.2) calling into question whether one simple explanation for the order of the hydride signals exists. These observations set the unbridged trihydride cations apart from their neutral trihydride precursors, for all of which the Zr-H_2 doublet had been found at higher fields than the Zr-*H* triplet. This signal cross-over upon conversion of each of the unbridged neutral trihydride precursors to its cationic counterpart appears to be connected with the net loss of the centrally positioned $[Cl_2Al^iBu_2]^-$ unit in the course of this reaction (Scheme 3.3).

Scheme 3.3

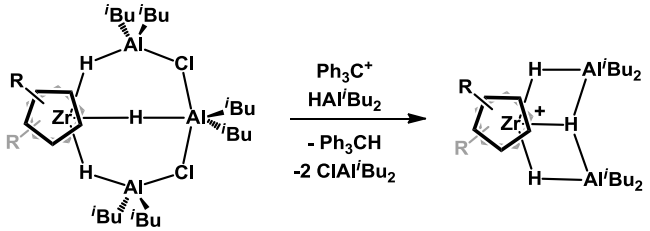

A $[B(C_6F_5)_4]^-$ salt of the doubly Cp-bridged cation $[(Me_2Si)_2(C_5H_3)_2Zr(\mu\text{-}H)_3(Al^iBu_2)_2]^+$ was obtained from benzene-d_6 solution in form of colorless crystals. An X-ray crystallographic structure determination yielded the structure shown in Figure 3.7. Once again, the positions of the hydrides were obtained from the difference map and are entirely in accord with the NMR assignments given above. This structure is of better quality than that of $[(SBI)Zr(\mu\text{-}H)_3(Al^iBu_2)_2]^+$ shown in Figure 3.5. The heavy-atom geometry of its $Zr(\mu\text{-}H)_3(Al^iBu_2)_2$ core, with Zr-H and Al-H distances in the range of 1.9495(1)-2.0850(1) Å and 1.6449(1)-1.8871(1) Å, respectively, is closely similar to that of $[(SBI)Zr(\mu\text{-}H)_3(Al^iBu_2)_2]^+$, thus attesting to the unexpectedly pervasive tendency of zirconocene-based reaction systems to form alkylaluminum-complexed trihydride cations of this kind. The mean Zr-Al distance (Table 3.3) in $[(Me_2Si)_2(C_5H_3)_2Zr(\mu\text{-}H)_3(Al^iBu_2)_2]^+$ (3.086 Å) is somewhat shorter than that in $[(SBI)Zr(\mu\text{-}H)_3(Al^iBu_2)_2]^+$ (3.289 Å), thus indicating a closer approach of the H-Al^iBu_2 units to the Zr center in the more open, doubly ring-bridged complex.

Table 3.3: Selected distances and angles for the cation $[(Me_2Si)_2(C_5H_3)_2Zr(\mu\text{-}H)_3(Al^iBu_2)_2]^+$

Bond distances (Å)		**nonbonding distances (Å)**		**bond angles (°)**	
Zr1-H1H	1.9786(1)	Al1-Zr1	3.0893(1)	H1H-Zr1-H2H	64.795(2)
Zr1-H2H	2.0850(1)	Al2-Zr1	3.0831(1)	H1H-Zr1-H3H	128.616(3)
Zr1-H3H	1.9495(1)			H2H-Zr1-H3H	63.840(2)
Al1-H1H	1.6449(1)			H1H-Al1-H2H	75.844(2)
Al1-H2H	1.8871(1)			H1H-Al2-H3H	74.995(2)
Al2-H2H	1.8290(1)			ctr1-Zr1-ctr2	122.646(2)
Al2-H3H	1.6747(1)				
Zr1-ctr1	2.1568(1)				
Zr1-ctr2	2.1543(1)				

(ct1: C1-C5, ctr2: C6-C10)

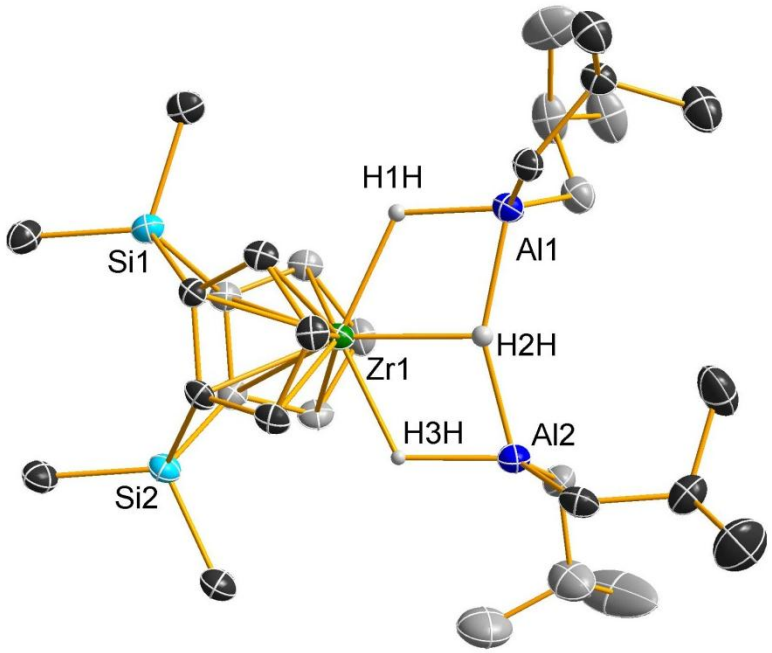

Figure 3.7: Structure of the cation $[(Me_2Si)_2(C_5H_3)_2Zr(\mu\text{-}H)_3(Al^iBu_2)_2]^+$ in crystals of its $[B(C_6F_5)_4]^-$ salt (thermal ellipsoids drawn at 50% probability, hydride positions taken from the difference Fourier map; other H atoms omitted).

There are six structurally characterized cationic aluminum hydrides of which all are terminal hydrides and only one of which contains an organic Al ligand (Figure 3.8).[39-42] The average Al-H bond in these complexes is 1.53(12) Å with all examples shorter than any single Al-H observed in the two cations reported here. This observation is most likely due to the bridging nature of these hydrides when compared to the known terminal {Al-H^+}. The Al-H bond lengths are more in line with those seen in neutral Zr-H-Al species which average 1.72(10) Å.[43] Similarly the Zr-H distances are not abnormal, as bond lengths of around 2 Å are observed for both cationic (1.99(8) Å) and neutral (2.02(18) Å) Zr-H's.[43]

The limited variability of these values suggest neither steric nor electronics have a large effect on structural parameters in these hydrides.

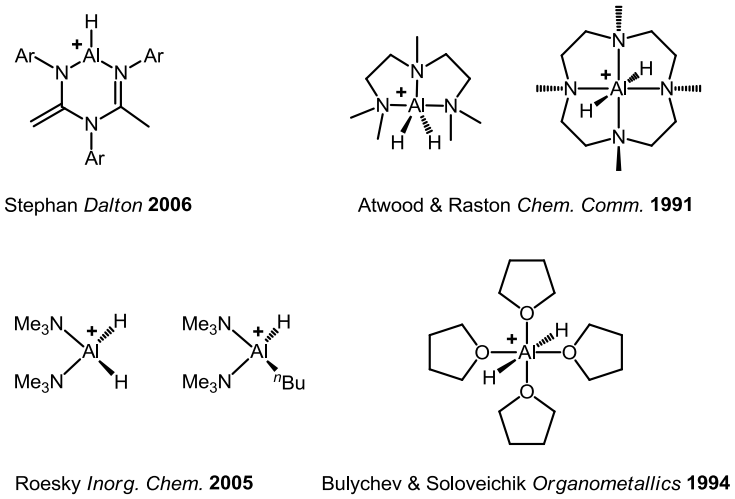

Figure 3.8: Known crystallographically characterized cationic Al hydrides

Attempts to make the related titanocene derivative failed, as addition of $HAl^{i}Bu_2$ to Cp_2TiCl_2 results in evolution of H_2 gas and the formation of a lavender solution which does not exhibit any Cp-H resonances by ^1H NMR, making it highly likely to be a Ti(III) species. The analogous Hf complex is readily formed from Cp_2HfCl_2 following the same procedure as discussed above for zirconocenes. Very similar spectral features have been described[44] for the product of a reaction of (SBI)$HfCl_2$ with $Al^{i}Bu_3$ and $[Ph_3C][B(C_6F_5)_4]$ and might thus be due to a cation of the type described here.

3.3.3 Interconversion reactions of [(SBI)Zr(μ-H)$_3$(Al^{i}Bu$_2$)$_2$]$^+$ with other cationic complexes.

The cationic complex, [(SBI)Zr(μ-H)$_3$(Al^{i}Bu$_2$)$_2$]$^+$, described above, reversibly interconverts with other zirconocene cations, some of which have been observed in zirconocene-based pre-catalyst systems. A first case, in point, concerns the blue-green coloration observed when [(SBI)Zr(μ-H)$_3$(Al^{i}Bu$_2$)$_2$]$^+$ is formed according to Scheme 3.2. That this coloration might be due to some side or sequential reaction product, rather than to the trihydride cation itself, is suggested by the observation that the intensity of this coloration depends on the reaction conditions.

When [(SBI)Zr(μ-H)$_3$(Al^{i}Bu$_2$)$_2$]$^+$ is prepared, as described above, in the presence of 5 equiv of HAl^{i}Bu$_2$, the reaction mixture gives rise to an absorption band at 614 nm. Absorbance at this wavelength increases when only a stoichiometric 4 equiv of HAl^{i}Bu$_2$ are used and is increased even more by use of substoichiometric amounts of HAl^{i}Bu$_2$ (Figure 3.9). In the presence of 10 equiv of HAl^{i}Bu$_2$, on the other hand, any absorption at 614 nm is minimal. When ClAl^{i}Bu$_2$ is added to such a solution, absorption at 614 nm increases (Figure 3.10).

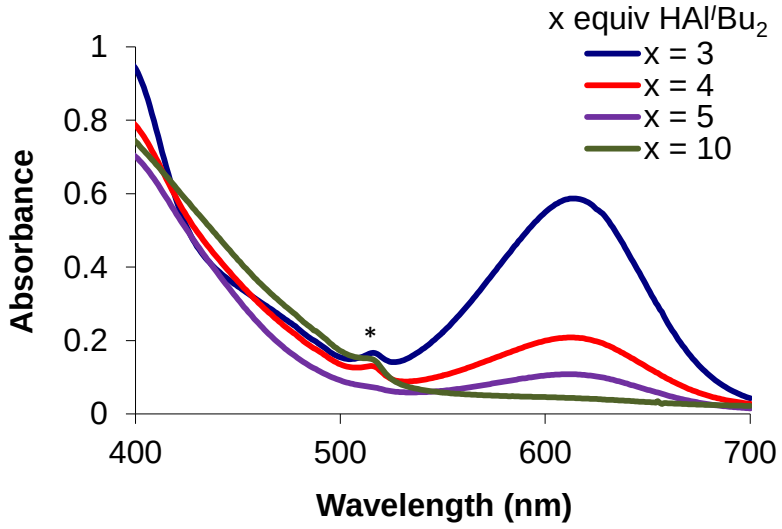

Figure 3.9: UV/vis absorption spectra of toluene solutions containing 0.56 mM (SBI)$ZrCl_2$ in the presence of 3, 4, 5 or 10 equiv of HAl^{i}Bu$_2$, after addition of 1 equiv of [Ph_3C][$B(C_6F_5)_4$] (path length 1 cm; * artifact due to change of gratings).

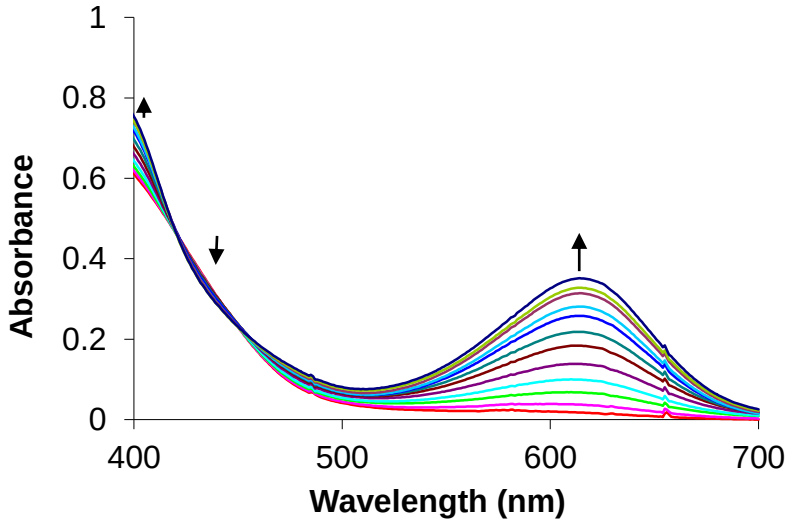

Figure 3.10: UV-vis spectra of a 2.79 mM solution of [(SBI)Zr(μ-H)$_3$(Al^{i}Bu$_2$)$_2$]$^+$ made with 10 equiv HAl^{i}Bu$_2$ upon successive additions of 2 equiv ClAl^{i}Bu$_2$.

Upon addition of $ClAl^iBu_2$ to a solution of $[(SBI)Zr(\mu\text{-}H)_3(Al^iBu_2)_2]^+$ we observe a new set of signals by ^1H NMR. These signals are particularly clear-cut when only 1 equiv of HAl^iBu_2 and 2 equiv $ClAl^iBu_2$ are used in the generation of the cation. In these spectra, signals due to complex-bound Al-^{i}Bu groups, at 1.88 ppm (m, $^3J_{HH}$ = 7 Hz, C*H*) and at 0.27 ppm (d, $^3J_{HH}$ = 7 Hz, CH_3), are cleanly separated from signals due to other $\{Al^iBu\}$ species in solution. Comparison of their integrals with those of the zirconocene ligand signals, at 6.26 and 5.18 ppm (d, $^3J_{HH}$ = 3 Hz, C_5H), clearly indicates the presence of only one $\{Al^iBu_2\}$ group per zirconocene unit (Figure 3.11). This stoichiometry and the reversible appearance and disappearance of these signals upon addition of $ClAl^iBu_2$ or HAl^iBu_2, respectively, lead us to attribute this set of signals to a $ClAl^iBu_2$-complexed zirconocene chloride cation, $[(SBI)Zr(\mu\text{-}Cl)_2Al^iBu_2]^+$, formed from $[(SBI)Zr(\mu\text{-}H)_3(Al^iBu_2)_2]^+$ in an equilibrium according to Scheme 3.4. The same species, $[(SBI)Zr(\mu\text{-}Cl)_2Al^iBu_2]^+$, was formed when $(SBI)ZrCl_2$ was reacted with Et_3SiH, $[Ph_3C][B(C_6F_5)_4]$ and $ClAl^iBu_2$ in ratios of 1:150:1:1. Reaction of $(SBI)ZrCl_2$ with Et_3SiH and $[Ph_3C][B(C_6F_5)_4]$, without any added chloroaluminum reagent, gave an insoluble green solid, presumably the $[B(C_6F_5)_4]^-$ salt of the dimeric dication $[\{(SBI)Zr\}_2(\mu\text{-}Cl)_2]^{2+}$, structurally characterized by Bryliakov et al.[27] Reaction of this solid with 5 equiv of $ClAl^iBu_2$ in benzene-d_6 gave a dark blue solution, which displayed the ^{1}HNMR signals of $[(SBI)Zr(\mu\text{-}Cl)_2Al^iBu_2]^+$, thus providing further support for the identity of this species. A reaction of $(SBI)ZrMe_2$ with $[Ph_3C][B(C_6F_5)_4]$, $AlMe_3$ and $AlCl_3$ in ratios of 1:1:6:1 gave the related cation $[(SBI)Zr(\mu\text{-}Cl)_2AlMe_2]^+$ the ligand C_5H signals of which appear at 6.35 and 5.29 ppm, i.e. at somewhat lower fields

than those of $[(SBI)Zr(\mu\text{-}Cl)_2Al^iBu_2]^+$ (6.26 and 5.18 ppm). Apparently, two Zr-Cl-Al bridges are sufficient to satisfy the coordination requirements of the Zr center in such a complex, in distinction to Zr-H-Al bridges, three of which appear to be required to complete the coordination of the Zr center, most likely due to the more electron-deficient nature of Zr-H-Al compared to Zr-Cl-Al bridges.

Scheme 3.4

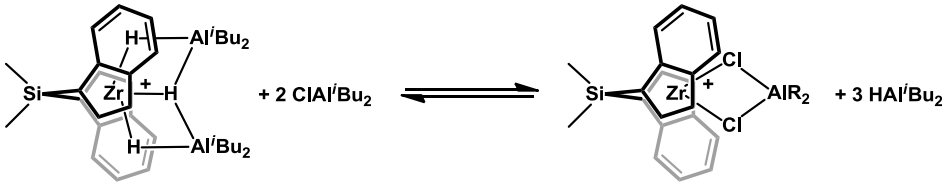

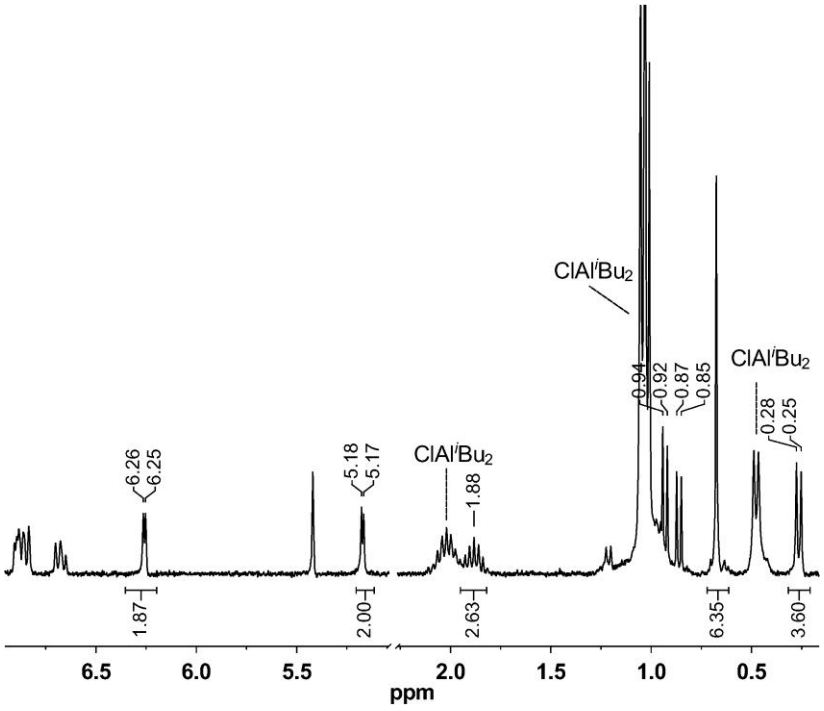

Figure 3.11: ^{1}H NMR spectrum of $[(SBI)Zr(\mu\text{-}Cl)_2(Al^iBu_2)]^+$ formed from reaction with 1 equiv HAl^iBu_2 and 1 equiv $ClAl^iBu_2$.

A related question would concern the degree to which CH_3Al instead of ClAl species could participate in similar equilibria. Addition of relatively small amounts of $AlMe_3$ to a solution of the cation $[(SBI)Zr(\mu\text{-}H)_3(Al^iBu_2)_2]^+$ in benzene-d_6 causes the appearance of additional signals in the vicinity of those of $[(SBI)Zr(\mu\text{-}H)_3(Al^iBu_2)_2]^+$. When only 1/3 equiv of $AlMe_3$ per Zr is added (i.e. [AlMe]/[Zr] = 1), we observe, next to the doublet at –2.25 ppm, two doublets centered at –2.05 ppm (Figure 3.12 **B**). This signal can be assigned to a cation similar to $[(SBI)Zr(\mu\text{-}H)_3(Al^iBu_2)_2]^+$, in which one of the Al-bound isobutyl groups is replaced by a methyl group (Scheme 3.4), such that the complex's lateral hydride positions are rendered inequivalent. The same signal can be obtained starting from the dimethyl zirconocene, $(SBI)ZrMe_2$, by reaction with 1 equiv of $[Ph_3C][B(C_6F_5)_4]$ and 4 equiv of HAl^iBu_2 indicating the presence of one methyl group.

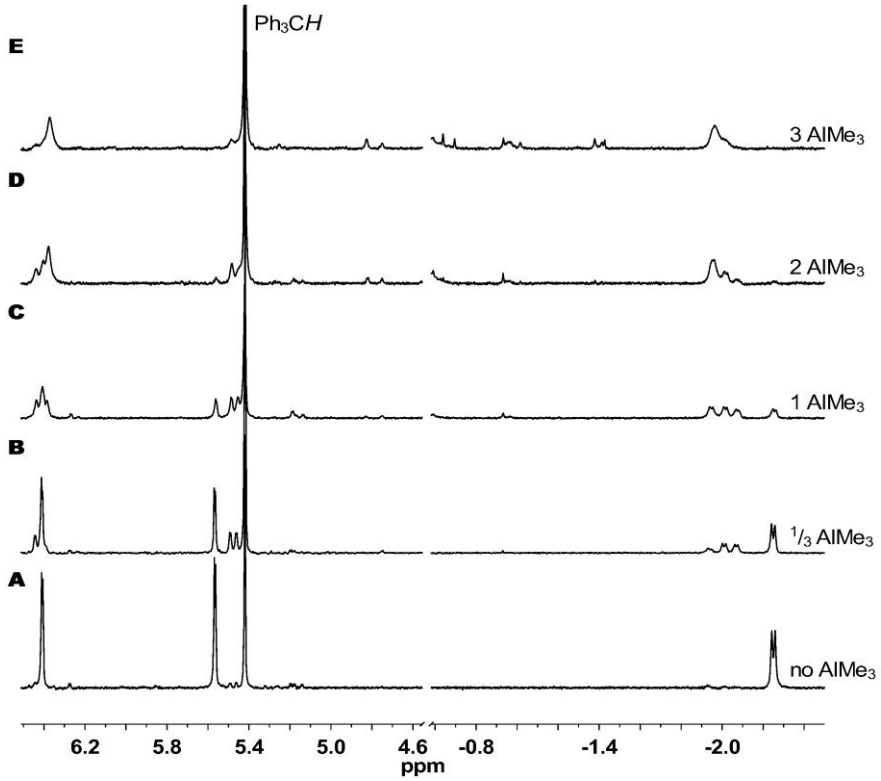

Figure 3.12: ^{1}H NMR spectra of a 3 mM solution of $[(SBI)Zr(\mu\text{-}H)_3(Al^{i}Bu_2)_2]^+$ in benzene-d_6, obtained by reaction of $(SBI)ZrCl_2$ with 5 equiv of $HAl^{i}Bu_2$ and 1 equiv of $[Ph_3C][B(C_6F_5)_4]$, before (A) and after addition of $^1/_3$ (B), 1 (C), 2 (D) or 3 (E) equiv of $AlMe_3$ relative to Zr.

Addition of $AlMe_3$ at somewhat higher $[AlMe_3]/[Zr]$ ratios causes a coalescence of these signals, first to two broad features centered at –1.95 ppm and then to one very broad signal ($\nu_{½}$ = 29 Hz), likewise centered at –1.95 ppm (Figure 3.12 **C**-**E**)) . These observations are undoubtedly due to the formation of increasing fractions of related cations, in which isobutyl residues at both Al centers are exchanged for methyl groups (Scheme 3.5). The broadening of the Zr-hydride signals of these mixed-alkyl aluminum species, henceforth referred to as $[(SBI)Zr(\mu\text{-}H)_3(AlR_2)_2]^+$, is probably due to the statistical nature of this

exchange. A statistical mixture of alkyl groups in the terminal aluminum positions of $[(SBI)Zr(\mu\text{-}Me)_2AlMe_2]^+$, when isobutyl aluminum species are introduced, has been previously shown by Babushkin and Brintzinger[45] and is consistent with the observations here.

Scheme 3.5

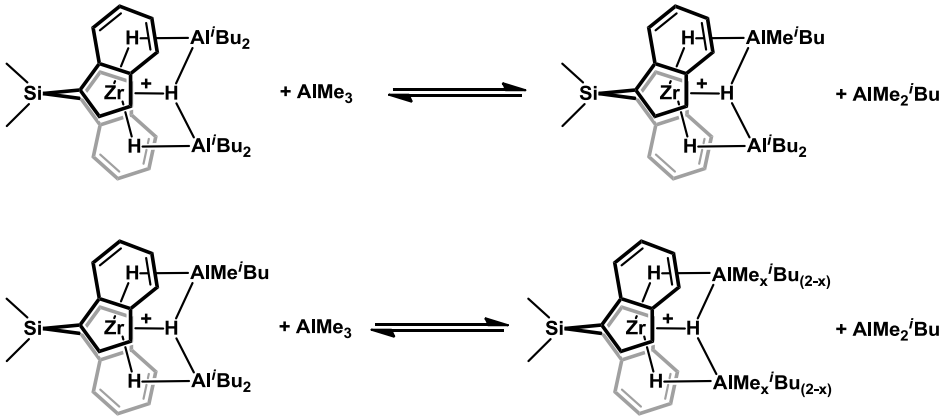

A purely $\{Me_2Al\}$-complexed cation, $[(SBI)Zr(\mu\text{-}H)_3(AlMe_2)_2]^+$, is accessible by reaction of $(SBI)ZrCl_2$ with 1 equiv of $[Ph_3C][B(C_6F_5)_4]$ in the presence of excess $HAlMe_2$. Its hydride signals (–0.17 and –2.10 ppm) are found close to those seen in Figure 3.12 **E** and are sharper than these, in accord with the assignment of the latter to methyl-rich mixed-alkyl aluminum complexed cations $[(SBI)Zr(\mu\text{-}H)_3(AlR_2)_2]^+$. ^1H NMR data for several other $\{Me_2Al\}$-complexed zirconocene hydride cations (Table 3.4) reveal shifts of the respective hydride signals, which vary greatly, without apparent rationale, when compared to those of the respective $\{{}^iBu_2Al\}$-complexed cations. Sensitivity of the Zr-H signals to the nature of the Al-bound R groups in cations of the type $[(SBI)Zr(\mu\text{-}H)_3(AlR_2)_2]^+$ is apparent

from the observation that addition of an aluminum alkyl with longer alkyl chains, such as trioctylaluminum, causes a strong broadening of the hydride signal and its shift, in this case, to higher fields (–2.4 ppm). Addition of $AlMe_3$ to the system results in $\{Al(octyl)_2\}$- and $\{AlMe_2\}$-complexed hydride cations with comparable intensities. $(SBI)ZrCl_2$-based pre-catalysts activated by excess methylalumoxane (MAO), to which HAl^iBu_2 has been added, have been reported to give rise to a set of signals, including a broad Zr-H_2 resonance at ca. –2 ppm, which were assigned at that time to species of the generic type $(SBI)ZrH_2{\cdot}2AlR_2X$.[28] These signals are now seen to be identical to those assigned above to mostly dimethylaluminum-complexed trihydride cations, $[(SBI)Zr(\mu\text{-}H)_3(AlR_2)_2]^+$ (cf. Figure 3.12 **E**). We can thus conclude that the zirconocene hydride species produced in MAO-activated reaction systems upon addition of HAl^iBu_2 are likewise cations of the type $[(SBI)Zr(\mu\text{-}H)_3(AlR_2)_2]^+$. This assignment is further supported by the observation of a gCOSY cross-peak in MAO-activated $(SBI)ZrCl_2$ solution containing HAl^iBu_2, connecting the broad ZrH_2 signal at –2.01 ppm to another Zr*H* resonance at 0.60 ppm, largely hidden under the low-field tail of the MAO signal.

Table 3.4: ^{1}H NMR data of {Me_2Al}-complexed zirconocene trihydride cations ($[B(C_6F_5)_4]^-$ salts in benzene-d_6 solution, 25 ºC, δ in ppm, 300 MHz).[a]

	Zr-H	ligand[b]
rac-(SBI)Zr	–2.06 (d, 2H, 4 Hz) –0.17 (br, 1H)	5.40 (d, 2H, 2.7 Hz) 6.29 (d, 2H, 2 Hz) 0.62 (s, $(CH_3)_2Si$)
rac-(EBI)Zr	–1.45 (d, 2H, 9 Hz) –1.00 (br, 1H)	5.49 (d, 2H, 3 Hz) 5.60 (d, 2H, 2 Hz)
rac-(EBTHI)Zr	–0.94 (br, 2H)[c]	5.70 (d, 2H, 3 Hz) 5.15 (d, 2H, 3 Hz)
$Me_2Si(C_5H_4)_2Zr$	–2.93 (d, 2H, 7 Hz) –1.61 (t, 1H, 10 Hz)	5.13 (pt, 4H, 2 Hz) 5.91 (pt, 4H, 2 Hz) 0.21 (s, $(CH_3)_2Si$)

[a] Signals of complex-bound {$Al(CH_3)_2$} groups not resolved from those of free $HAl(CH_3)_2$; [b] C_5-*H* unless otherwise noted; [c] Central hydride resonance not resolved, probably due to overlap with $Al(CH_3)_2$ signals.

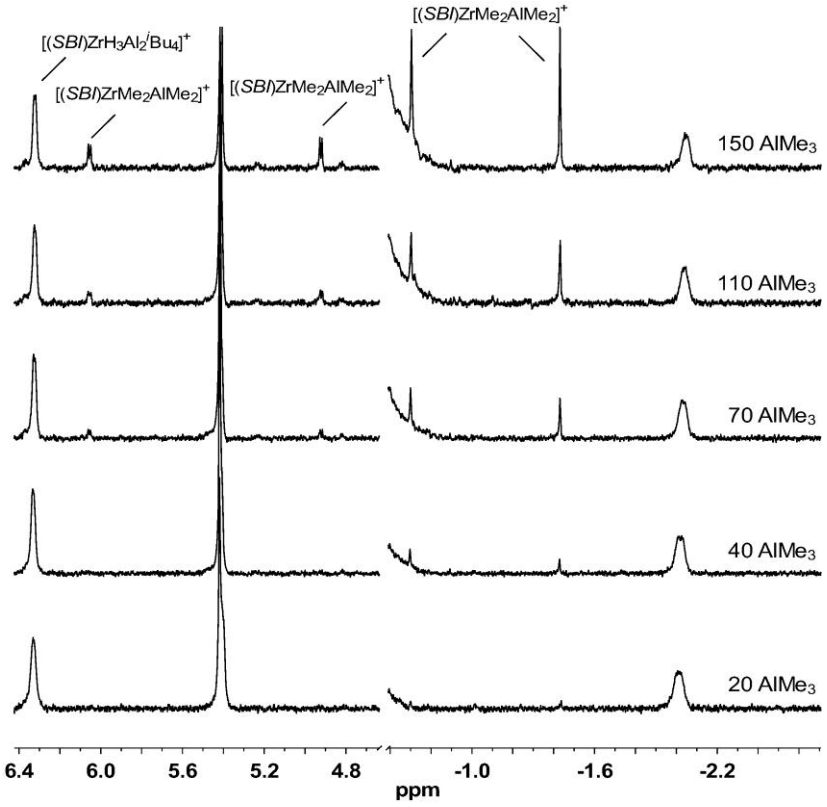

Figure 3.13: ^{1}H NMR spectra of a 3 mM solution of $[(SBI)Zr(\mu\text{-}H)_3(Al^iBu_2)_2]^+$ with 3.5 equiv of free HAl^iBu_2 upon addition of 20-150 equiv of $AlMe_3$ relative to Zr.

Upon addition of $AlMe_3$ in yet higher concentrations to solutions containing cations of the type $[(SBI)Zr(\mu\text{-}H)_3(AlR_2)_2]^+$, we observe, in addition to the signals due to these cations, another set of signals comprising characteristic $\{Zr(\mu\text{-}Me)_2Al\}$ and $\{AlMe_2\}$ signals at –1.43 and –0.71 ppm (Figure 3.13), which indicate formation of cations of the type $[(SBI)Zr(\mu\text{-}Me)_2AlR_2]^+$.[45-47] These cations, thus, appear to arise from the alkylaluminum-complexed zirconocene trihydride cations, $[(SBI)Zr(\mu\text{-}H)_3(AlR_2)_2]^+$, by an equilibrium reaction of the type represented in Scheme 3.6.

Scheme 3.6

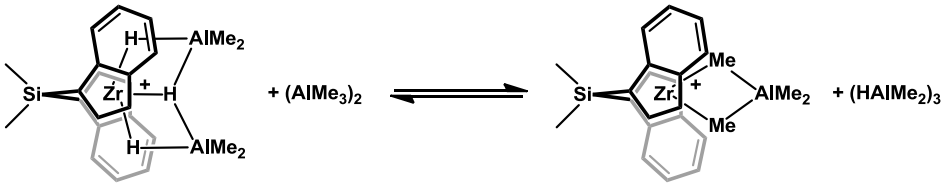

Based on the ^1H NMR spectra of reaction systems containing HAl^iBu_2 in an initial ratio of $[HAl^iBu_2]/[Zr]_{tot}$ of 7.5:1 and $AlMe_3$ at variable ratios of $AlMe_3$ to Zr_{tot} of 40:1 to 110:1, we estimate an equilibrium constant for the reaction shown in Scheme 3.6. The concentration of $(AlMe_3)_2$ and $(HAlMe_2)_3$ were determined from the integration of Al-H and Al-CH_3 while the concentration of the two zirconocenes was determined from the integrations of the Si-CH_3 groups. In order to accurately establish the equilibrium constant, it is necessary in this case to treat $(HAlMe_2)_3$ and $(AlMe_3)_2$ as trimers and dimers respectively.[48-49] Fitting the concentrations to Equation 3.1 yielded an equilibrium constant

of $K_{eq} = 0.97(15)\cdot10^{-2}$ indicating that at comparable concentrations of $HAl^{i}Bu_2$ and $AlMe_3$ they trihydride cation would be by far the dominant species.

$$K_{eq} = \frac{[(SBI)Zr(\mu\text{-}Me)_2AlMe_2]^+ \cdot [(HAlMe_2)_3]}{[(SBI)Zr(\mu\text{-}H)_3(AlMe_2)_2]^+ \cdot [(AlMe_3)_2]} \qquad 3.1$$

3.4 Conclusions

The studies described above have brought to light a hitherto unreported family of zirconocene hydride cations stabilized by adduct formation with two $HAlR_2$ units, so as to attain the $\{ZrH_3\}$ coordination geometry observed before for related neutral zirconocene hydride species. These cationic hydride complexes are subject to ligand exchange equilibria in the presence of chloroaluminum or methylaluminum compounds. In the first instance, the $\{Zr(\mu\text{-}H)_3(AlR_2)_2^+\}$ arrangement is replaced by the previously unreported doubly Cl-bridged entity $\{Zr(\mu\text{-}Cl)_2AlR_2^+\}$, while exposure to excess $MeAlR_2$ gives rise to species containing a $\{Zr(\mu\text{-}Me)_2AlR_2^+\}$ geometry, which have previously been observed in zirconocene-based olefin-polymerization catalysts.[45-47] In equilibria of this kind, trihydride-bridged cations are strongly preferred over dimethyl-bridged zirconocene cations. This indicates that the former are likely to arise in typical MAO-activated, zirconocene-based, olefin-polymerization catalysts, whenever these acquire any hydride units.

3.5 Experimental

General Considerations. All operations were carried out under a protective dinitrogen atmosphere, either in a glovebox or on a vacuum manifold. Benzene-d_6, toluene-d_8 and

other solvents used were dried by vacuum transfer either from sodium/benzophenone or from "titanocene".[50] Zirconocene complexes used as starting materials were either purchased from Strem Chemicals, Newburyport ($(C_5H_5)_2ZrCl_2$, $(C_5H_5)_2HfCl_2$, $(^nBuC_5H_4)_2ZrCl_2$, $(C_5Me_5)_2ZrCl_2$, Me_2Si(1-indenyl)$_2ZrCl_2$ and C_2H_4(1-indenyl)$_2ZrCl_2$), obtained as gifts from Dr. M. Ringwald, MCAT, Konstanz (*rac*-Me_2C(1-indenyl)$_2ZrCl_2$, *meso*-Me_2C(1-indenyl)$_2ZrCl_2$ [51] and $Me_4C_2(C_5H_4)_2ZrCl_2$ [52]), or prepared in our laboratories according to published procedures ((1,2-$Me_2C_5H_3)_2ZrCl_2$,[53] $(Me_3SiC_5H_4)_2ZrCl_2$,[54] C_2H_4(4,5,6,7-tetrahydro-1-indenyl)$_2ZrCl_2$,[55] $Me_2Si(C_5H_4)_2ZrCl_2$,[56] $(Me_2Si)_2$(3,5-$^iPr_2C_5H$) $(C_5H_3)ZrCl_2$,[57] $(Me_2Si)_2(C_5H_3)_2ZrCl_2$,[58] *rac*-$Me_2Si$(2-$SiMe_3$-4-$CMe_3C_5H_2)_2ZrCl_2$ [59] and *meso*-Me_2C(3-$CMe_3C_5H_3)_2ZrCl_2$ [60-61]. Trimethylaluminum, triisobutylaluminum, diisobutylaluminum hydride, diisobutylaluminum chloride and trioctylaluminum were used as obtained from Aldrich Chemical Company, Milwaukee. Lithium aluminum hydride was obtained from Aldrich Chemical Company and purified prior to use. MAO was obtained as a 30% toluene solution from Albermarle and dried at 50°C for 3 hours under vacuum to yield a free flowing white powder.

NMR spectra were obtained using Varian Inova 500 or Mercury 300 spectrometers. Chemical shifts are referenced to residual solvents peaks, 7.16 ppm for benzene and 7.00 ppm for the central aromatic proton resonance of toluene. UV-vis spectra were recorded on an Agilent 8453 spectrometer. X-ray diffraction data were collected on a Bruker KAPPA APEXII X-ray diffractometer.

Synthesis of $HAlMe_2$. $HAlMe_2$ was synthesized in analogy to previous literature.[62-66] Commercial $LiAlH_4$ was purified by extraction of the gray commercial solid with Et_2O in a swivel frit on the high-vacuum line. The clear solution was filtered and then the Et_2O was removed *in vacuo* to yield pure $LiAlH_4$ as a white powder. In a glove box a 50 mL pear-shaped flask was charged with 1.2 g (32 mmol) of purified $LiAlH_4$ and 2.7 mL (28 mmol) of $AlMe_3$. A swivel frit was attached and the apparatus was taken to the high-vacuum line, where 15 mL benzene was vacuum-transferred in from a storage flask containing sodium/benzophenone. The mixture was heated to 75 ºC under argon with stirring for 2 hours, filtered hot and then cooled in an ice bath. Benzene was removed *in vacuo* to yield $HAlMe_2$ as a viscous oil which was stored in the glove box. (***CAUTION***: all alkyl aluminum reagents used in this synthesis are pyrophoric and the $LiAlH_4$ residue, if it still contains any Et_2O, is also extremely pyrophoric)

NMR Scale Syntheses of Cationic Metallocene Hydrides. Each zirconocene dichloride was weighed in a glove box into a 1-dram vial and 0.7 mL of benzene-d_6 was added. Then 5 or 10 equivalents of neat HAl^iBu_2 were syringed in via microliter syringe or in the case of $HAlMe_2$, the neat $HAlMe_2$ gel was smeared onto the side of the vial with a spatula. The vial was capped and shaken to dissolve the zirconocene dichloride and form the respective neutral hydride species. One equivalent of $[Ph_3C][B(C_6F_5)_4]$ was weighed into a second vial. The neutral zirconocene solution was added and the solution was mixed to generate

the cationic hydride species. The solution was then transferred to a J-Young NMR tube for NMR analysis. ^{19}F NMR spectra were identical for all species studied, showing three characteristic signals for the uncomplexed $[B(C_6F_5)_4]^-$ anion at -126.68 (br, 8F), -157.32 (t, 4F 21 Hz) and -161.19 ppm (br, 8F). Therefore, only ^{1}H NMR spectra are reported. For each zirconocene only a single product was observed by NMR.

[*rac*-(SBI)Zr(μ-H)$_3$(Al^{i}Bu$_2$)$_2$][B(C$_6$F$_5$)$_4$]. 2.0 mg (0.0045 mmol) *rac*-$Me_2Si(1\text{-indenyl})_2ZrCl_2$, 4.0 μL (0.022 mmol, 5 equiv) HAl^iBu_2 and 4.1 mg (0.0044 mmol, 1 equiv) of $[Ph_3C][B(C_6F_5)_4]$. ^{1}H NMR (500 MHz, benzene-d_6) δ 7.34 (d, $^3J_{HH}$ = 9 Hz, 4H, Ar-H), 6.71 (m, 2H, Ar-H), 6.63 (m, 2H, Ar-H), 6.41 (d, $^3J_{HH}$ = 3 Hz, 2H, C_5-H), 5.57 (d, $^3J_{HH}$ = 3 Hz, 2H, C_5-H), 1.77 (n, $^3J_{HH}$ = 7 Hz, 4H, ^{i}Bu-CH), 0.94 (t, $^3J_{HH}$ = 7 Hz, 24H, ^{i}Bu-CH_3), 0.65 (s, 4H, $Si(CH_3)_2$), 0.34 (m, 1H, Zr-H_2), 0.26 (dd, $^3J_{HH}$ = 14, 7 Hz, 4H, ^{i}Bu-CH_2), 0.15 (dd, $^3J_{HH}$ = 14, 7 Hz, 4H, ^{i}Bu-CH_2), -2.25 (d, $^2J_{HH}$ = 8 Hz, 2H, Zr-H_2).

[*rac*-(EBI)Zr(μ-H)$_3$(Al^{i}Bu$_2$)$_2$][B(C$_6$F$_5$)$_4$]. 1.3 mg (0.0031 mmol) *rac*-$C_2H_4(1\text{-indenyl})_2ZrCl_2$, 3.0 μL (0.016 mmol, 5 equiv) HAl^iBu_2 and 3.0 mg (0.0033 mmol, 1 equiv) of $[Ph_3C][B(C_6F_5)_4]$. ^{1}H NMR (300 MHz, benzene-d_6) δ 7.45 (m, 2H, Ar-H), 6.81 (m, 4H, Ar-H), 6.55 (s, 2H, Ar-H), 5.73 (d, $^3J_{HH}$ = 3 Hz, 2H, C_5-H), 5.55 (d, $^3J_{HH}$ = 3 Hz, 2H, C_5-H), 3.32 (m, 4H, C_2H_4), 3.04 (m, 3H, C_2H_4), 1.75 (m, $^3J_{HH}$ = 7 Hz, ^{i}Bu-CH), 0.93 (m, ^{i}Bu-CH_3), 0.19 (dd, $^3J_{HH}$ = 7, 3 Hz, 13H, ^{i}Bu-CH_2), -0.29 (t, $^2J_{HH}$ = 8 Hz, 1H, Zr-H), -1.73 (d, $^2J_{HH}$ = 8 Hz, 2H, Zr-H_2).

[*rac*-(EBTHI)Zr(μ-H)$_3$(Al^{i}Bu$_2$)$_2$][B(C$_6$F$_5$)$_4$]. 1.4 mg (0.0033 mmol) *rac*-$C_2H_4(4,5,6,7\text{-tetrahydro-1-indenyl})_2ZrCl_2$, 3.0 μL (0.016 mmol, 5 equiv) HAl^iBu_2 and 3.1 mg (0.0034

mmol, 1 equiv) of $[Ph_3C][B(C_6F_5)_4]$. ^{1}H NMR (300 MHz, benzene-d_6) δ 5.80 (d, $^3J_{HH}$ = 3 Hz, 2H, Ar-H), 5.26 (d, $^3J_{HH}$ = 3 Hz, 2H, Ar-H), 3.97 (m, 1H), 3.33 (m, 1H), 2.70 (m, 2H), 2.47 (m, 4H), 2.18 (m, 6H), 1.88 (n, 7 Hz, ^{i}Bu-CH), 1.55 (m, 2H), 1.30 (m, 7H), 0.97 (dt, $^3J_{HH}$ = 9, 5 Hz, ^{i}Bu-CH_3), 0.35 (m, ^{i}Bu-CH_2), -0.47 (d, $^2J_{HH}$ = 6 Hz, 2H, Zr-H_2), -1.09 (t, $^2J_{HH}$ = 6 Hz, 1H, Zr-H).

[*rac*-Me_2C(1-indenyl)$_2$Zr(μ-H)$_3$(Al^{i}Bu$_2$)$_2$][B(C_6F_5)$_4$]. 1.7 mg (0.0039 mmol) *rac*-Me_2C(1-indenyl)$_2ZrCl_2$, 3.5 μL (0.020 mmol, 5 equiv) HAl^iBu_2 and 3.5 mg (0.0038 mmol, 1 equiv) of $[Ph_3C][B(C_6F_5)_4]$. ^{1}H NMR (300 MHz, benzene-d_6) δ 7.29 (d, $^3J_{HH}$ = 9 Hz, 2H, Ar-H), 6.62 (m, 4H, Ar-H), 6.35 (d, $^3J_{HH}$ = 3 Hz, 2H, C_5-H), 5.33 (d, $^3J_{HH}$ = 3 Hz, 2H, C_5-H), 1.76 (m, 4H, ^{i}Bu-CH), 1.69 (s, 3H, $C(CH_3)_2$), 0.91 (dd, $^3J_{HH}$ = 6, 4 Hz, 24H, ^{i}Bu-CH_3), 0.80 (m, Zr-H), 0.25 (qd, $^3J_{HH}$ = 15, 7, 7 Hz, 8H, ^{i}Bu-CH_2), -1.72 (d, $^2J_{HH}$ = 7 Hz, 2H, Zr-H_2).

[*meso*-Me_2C(1-indenyl)$_2$Zr(μ-H)$_3$(Al^{i}Bu$_2$)$_2$][B(C_6F_5)$_4$]. 2.2 mg (0.0051 mmol) *meso*-Me_2C(1-indenyl)$_2ZrCl_2$, 4.5 μL (0.024 mmol, 5 equiv) HAl^iBu_2 and 4.7 mg (0.0051 mmol, 1 equiv) of $[Ph_3C][B(C_6F_5)_4]$. ^{1}H NMR (300 MHz, benzene-d_6) δ 7.39 (m, 2H, Ar-H), 6.94 (m, 2H, Ar-H), 6.50 (m, 1H, Ar-H), 6.40 (d, $^3J_{HH}$ = 3 Hz, 1H, C_5-H), 6.29 (m, 1H, Ar-H), 4.84 (d, $^3J_{HH}$ = 3 Hz, 1H, C_5-H), 2.00 (m, ^{i}Bu-CH), 1.53 (m, Zr-$H_{central}$), 1.33 (s, 2H), 1.22 (s, 4H), 0.88 (m, ^{i}Bu-CH_3), 0.47 (m, ^{i}Bu-CH_2), -0.91 (d, $^2J_{HH}$ = 6 Hz, 1H, Zr-$H_{lateral}$), -3.47 (d, $^2J_{HH}$ = 7 Hz, 1H, Zr-$H_{lateral}$).

[Me_4C_2(C_5H_4)$_2$Zr(μ-H)$_3$(Al^{i}Bu$_2$)$_2$][B(C_6F_5)$_4$]. 1.2 mg (0.0032 mmol) $Me_4C_2(C_5H_4)_2ZrCl_2$, 3.0 μL (0.016 mmol, 5 equiv) HAl^iBu_2 and 3.0 mg (0.0033 mmol, 1 equiv) of $[Ph_3C][B(C_6F_5)_4]$. ^{1}H NMR (300 MHz, benzene-d_6) δ 5.95 (pt, $^3J_{HH}$ = 2 Hz, 4H, C_5-H),

5.73 (t, $^3J_{HH}$ = 2 Hz, 4H, C_5-H), 1.86 (m, $^3J_{HH}$ = 7 Hz, 4H, ^{i}Bu-CH), 0.94 (t, $^3J_{HH}$ = 9 Hz, 24H, ^{i}Bu-CH_3), 0.88 (s, 16H, $C_2(CH_3)_4$), 0.36 (d, $^3J_{HH}$ = 7 Hz, 12H, ^{i}Bu-CH_2), -1.37 (d, $^2J_{HH}$ = 7.3 Hz, 2H, Zr-H_2), -1.60 (t, $^2J_{HH}$ = 7.5 Hz, 1H, Zr-H).

$[Me_2Si(C_5H_4)_2Zr(\mu\text{-}H)_3(Al^iBu_2)_2][B(C_6F_5)_4]$. 12.6 mg (0.0362 mmol) $Me_2Si(C_5H_4)_2ZrCl_2$, 32.2 μL (0.181 mmol, 5 equiv) HAl^iBu_2 and 33.4 mg (0.0362 mmol, 1 equiv) of $[Ph_3C][B(C_6F_5)_4]$. ^{1}H NMR (300 MHz, benzene-d_6) δ 6.22 (s, 4H, C_5-H), 5.24 (s, 4H, C_5-H), 1.83 (m, ^{i}Bu-CH), 0.94 (m, ^{i}Bu-CH_3), 0.35 (d, $^3J_{HH}$ = 7 Hz, ^{i}Bu-CH_2), 0.17 (s, 6H, $Si(CH_3)_2$), -1.22 (t, $^2J_{HH}$ = 8 Hz, 1H, Zr-H), -2.02 (d, $^2J_{HH}$ = 8 Hz, 2H, Zr-H_2).

$[(Me_2Si)_2(C_5H_3)_2Zr(\mu\text{-}H)_3(Al^iBu_2)_2][B(C_6F_5)_4]$. 1.0 mg (0.0025 mmol) $(Me_2Si)_2(C_5H_3)_2$ $ZrCl_2$, 4.4 μL (0.025 mmol, 10 equiv) HAl^iBu_2 and 2.3 mg (0.0025 mmol, 1 equiv) of $[Ph_3C][B(C_6F_5)_4]$. ^{1}H NMR (300 MHz, benzene-d_6) δ 6.49 (d, $^3J_{HH}$ = 3 Hz, 4H, C_5-H), 5.94 (t, $^3J_{HH}$ = 3 Hz, 2H, C_5-H), 1.82 (m, ^{i}Bu-CH), 0.92 (m, ^{i}Bu-CH_3), 0.34 (d, $^3J_{HH}$ = 7 Hz, ^{i}Bu-CH_2), -0.08 (s, 6H, $Si(CH_3)_2$), -1.04 (t, $^2J_{HH}$ = 7 Hz, 1H, Zr-H), -2.03 (d, $^2J_{HH}$ = 7 Hz, 2H, Zr-H_2).

$[(Me_2Si)_2(3,5\text{-}^iPr_2C_5H)(C_5H_3)Zr(\mu\text{-}H)_3(Al^iBu_2)_2][B(C_6F_5)_4]$. 1.5 mg (0.0033 mmol) $[(Me_2Si)_2(3,5\text{-}^iPr_2C_5H)(C_5H_3)ZrCl_2$, 6.0 μL (0.033 mmol, 10 equiv) HAl^iBu_2 and 3.1 mg (0.0034 mmol, 1 equiv) of $[Ph_3C][B(C_6F_5)_4]$. ^{1}H NMR (300 MHz, benzene-d_6) δ 6.53 (s, 2H, C_5-H), 6.41 (s, 1H, C_5-H), 6.10 (s, 1H, C_5-H), 2.63 (m, 2H, ^{i}Pr-CH), 1.89 (m, ^{i}Bu-CH), 0.96 (m, ^{i}Bu-CH_3), 0.80 (d, $^3J_{HH}$ = 7 Hz, ^{i}Pr-CH_3), 0.43 (d, $^3J_{HH}$ = 7 Hz, ^{i}Bu-CH_2), 0.17 (s, 12H, Si-CH_3), -0.50 (br, 1H, Zr-H), -1.47 (d, $^2J_{HH}$ = 6 Hz, 2H, Zr-H_2).

[$(C_5H_5)_2Zr(\mu\text{-}H)_3(Al^iBu_2)_2$][$B(C_6F_5)_4$]. 2.3 mg (0.0079 mmol) $(C_5H_5)_2ZrCl_2$, 7.0 μL (0.039 mmol, 5 equiv) HAl^iBu_2 and 7.3 mg (0.0079 mmol, 1 equiv) of $[Ph_3C][B(C_6F_5)_4]$. ^{1}H NMR (300 MHz, benzene-d_6) δ 5.59 (s, 10H, C_5-H), 1.81 (n, $^3J_{HH}$ = 7 Hz, 4H, ^{i}Bu-CH), 0.92 (d, $^3J_{HH}$ = 7 Hz, 24H, ^{i}Bu-CH_3), 0.28 (d, $^3J_{HH}$ = 7 Hz, 8H, ^{i}Bu-CH_2), -2.27 (d, $^2J_{HH}$ = 8 Hz, 2H, Zr-H_2), -2.39 (t, $^2J_{HH}$ = 8 Hz, 1H, Zr-H_2).

[(^{n}BuC$_5$H$_4$)$_2$Zr(μ-H)$_3$(Al^{i}Bu$_2$)$_2$][B(C$_6$F$_5$)$_4$]. 2.9 mg (0.0072 mmol) $(^nBuC_5H_4)_2ZrCl_2$, 6.4 μL (0.036 mmol, 5 equiv) HAl^iBu_2 and 6.5 mg (0.0070 mmol, 1 equiv) of $[Ph_3C][B(C_6F_5)_4]$. ^{1}H NMR (300 MHz, benzene-d_6) δ 5.73 (m, 4H, C_5-H), 5.67 (m, 4H, C_5-H), 2.16 (t, $^3J_{HH}$ = 7 Hz, 5H, C_5-^{n}Bu), 1.86 (m, $^3J_{HH}$ = 7 Hz, ^{i}Bu-CH), 1.20 (m, 16H, C_5-^{n}Bu), 0.96 (d, $^3J_{HH}$ = 7 Hz, ^{i}Bu-CH_3), 0.88 (t, $^3J_{HH}$ = 7 Hz, 15H, C_5-^{n}Bu), 0.40 (d, $^3J_{HH}$ = 7 Hz, ^{i}Bu-CH_2), -1.61 (d, $^2J_{HH}$ = 8 Hz, 2H, Zr-H_2), -1.96 (t, $^2J_{HH}$ = 8 Hz, 1H, Zr-H).

[($Me_3SiC_5H_4$)$_2$Zr(μ-H)$_3$(Al^{i}Bu$_2$)$_2$][B(C$_6$F$_5$)$_4$]. 1.6 mg (0.0037 mmol) $(TMSC_5H_4)_2ZrCl_2$, 3.3 μL (0.019 mmol, 5 equiv) HAl^iBu_2 and 3.5 mg (0.0038 mmol, 1 equiv) of $[Ph_3C][B(C_6F_5)_4]$. ^{1}H NMR (300 MHz, benzene-d_6) δ 6.11 (s, 4H, C_5-H), 6.01 (s, 4H, C_5-H), 1.87 (m, 4H, ^{i}Bu-CH), 0.95 (d, J = 6 Hz, ^{i}Bu-CH_3), 0.46 (m, ^{i}Bu-CH_2), 0.03 (s, 18H, C_5-$SiMe_3$), -1.84 (d, $^2J_{HH}$ = 9 Hz, 2H, Zr-H_2), -2.30 (br, 1H, Zr-H).

[(1,2-$Me_2C_5H_3$)$_2$Zr(μ-H)$_3$(Al^{i}Bu$_2$)$_2$][B(C$_6$F$_5$)$_4$]. 1.0 mg (0.0029 mmol) (1,2-$Me_2C_5H_4)_2$ $ZrCl_2$, 5.1 μL (0.029 mmol, 10 equiv) HAl^iBu_2 and 2.6 mg (0.0028 mmol, 1 equiv) of $[Ph_3C][B(C_6F_5)_4]$. ^{1}H NMR (300 MHz, benzene-d_6) δ 5.86 (m, 2H, C_5-H), 5.29 (d, $^3J_{HH}$ = 3 Hz, 4H, C_5-H), 1.88 (m, $^3J_{HH}$ = 7 Hz, ^{i}Bu-CH), 1.74 (s, 12H, C_5-CH_3), 0.97 (d, $^3J_{HH}$ = 6 Hz,

^{i}Bu-CH_3), 0.43 (d, $^3J_{HH}$ = 7 Hz, ^{i}Bu-CH_2), -1.42 (d, $^2J_{HH}$ = 7 Hz, 2H, Zr-H_2), -1.79 (br, 1H, Zr-H).

[$(C_5H_5)_2Hf(\mu\text{-}H)_3(Al^{i}Bu_2)_2$][$B(C_6F_5)_4$]. 4.3 mg (0.0113 mmol) $(C_5H_5)_2HfCl_2$, 20.2 μL (0.113 mmol, 10 equiv) $HAl^{i}Bu_2$ and 10.4 mg (0.0113 mmol, 1 equiv) of [Ph_3C][$B(C_6F_5)_4$]. ^{1}H NMR (300 MHz, benzene-d_6) δ 5.48 (s, 10H, C_5-H), 1.80 (m, $^3J_{HH}$ = 7 Hz, 4H, ^{i}Bu-CH), 0.92 (d, $^3J_{HH}$ = 7 Hz, ^{i}Bu-CH_3), 0.26 (d, $^3J_{HH}$ = 7 Hz, 12H, ^{i}Bu-CH_2), -1.40 (d, $^2J_{HH}$ = 6 Hz, 2H, Zr-H_2), -2.27 (t, $^2J_{HH}$ = 6 Hz, 1H, Zr-H).

[*rac*-(SBI)Zr(μ-H)$_3$($AlMe_2$)$_2$][$B(C_6F_5)_4$]. 1.0 mg (0.0022 mmol) *rac*-Me_2Si(1-indenyl)$_2$ $ZrCl_2$, 1.4 mg (0.024 mmol, 11 equiv) $HAlMe_2$ and 2.1 mg (0.0023 mmol, 1 equiv) of [Ph_3C][$B(C_6F_5)_4$]. ^{1}H NMR (300 MHz, benzene-d_6) δ 6.70 (dd, $^3J_{HH}$ = 20, 8 Hz, 6H, Ar-H), 6.29 (d, $^3J_{HH}$ = 2 Hz, 2H, C_5-H), 5.40 (d, $^3J_{HH}$ = 3 Hz, 2H, C_5-H), 0.62 (s, 6H, Si(CH_3)$_2$), -0.15 (m, Zr-H), -2.06 (d, $^2J_{HH}$ = 4 Hz, 2H, Zr-H_2).

[*rac*-(EBI)Zr(μ-H)$_3$($AlMe_2$)$_2$][$B(C_6F_5)_4$]. 1.8 mg (0.0043 mmol) *rac*-C_2H_4(1-indenyl)$_2$ $ZrCl_2$, 2.1 mg (0.036 mmol, 8 equiv) $HAlMe_2$ and 4.0 mg (0.0043 mmol, 1 equiv) of [Ph_3C][$B(C_6F_5)_4$]. ^{1}H NMR (300 MHz, benzene-d_6) δ 7.42 (d, $^3J_{HH}$ = 9 Hz, 3H, Ar-H), 6.88 (dd, $^3J_{HH}$ = 21, 9 Hz, 7H, Ar-H), 6.64 (m, 2H, Ar-H), 5.60 (d, $^3J_{HH}$ = 3 Hz, 2H, C_5-H), 5.49 (d, $^3J_{HH}$ = 3 Hz, 2H, C_5-H), 1.36 (s, 4H, C_2H_4), -1.00 (br, 1H, Zr-H), -1.45 (d, $^3J_{HH}$ = 9 Hz, 2H, Zr-H_2).

[*rac*-(EBTHI)Zr(μ-H)$_3$($AlMe_2$)$_2$][$B(C_6F_5)_4$]. 2.0 mg (0.0046 mmol) *rac*-C_2H_4(4,5,6,7-tetrahydro-1-indenyl)$_2$$ZrCl_2$, 2.2 mg (0.038 mmol, 8 equiv) $HAlMe_2$ and 4.2 mg (0.0046 mmol, 1 equiv) of [Ph_3C][$B(C_6F_5)_4$]. ^{1}H NMR (300 MHz, benzene-d_6) δ 5.70 (d, $^3J_{HH}$ = 3

Hz, 2H, C_5-H), 5.15 (d, $^3J_{HH}$ = 3 Hz, 2H, C_5-H), 2.50 (m, 3H), 2.17 (m, 6H), 1.41 (m, 6H), -0.94 (s, 2H, Zr-H_2).

$[Me_2Si(C_5H_4)_2Zr(\mu\text{-}H)_3(AlMe_2)_2][B(C_6F_5)_4]$. 1.8 mg (0.0052 mmol) *rac*-$Me_2Si(C_5H_4)_2$ $ZrCl_2$, 2.4 mg (0.041 mmol, 8 equiv) $HAlMe_2$ and 4.8 mg (0.0052 mmol, 1 equiv) of $[Ph_3C][B(C_6F_5)_4]$. ^{1}H NMR (300 MHz, benzene-d_6) δ 5.91 (pt, $^3J_{HH}$ = 2 Hz, 4H, C_5-H), 5.13 (pt, $^3J_{HH}$ = 2 Hz, 4H, C_5-H), 0.21 (s, 6H, $Si(CH_3)_2$), -1.61 (t, $^2J_{HH}$ = 9 Hz, 1H, Zr-H), -2.93 (d, $^2J_{HH}$ = 7 Hz, 2H, Zr-H_2).

Synthesis of $[(SBI)Zr(\mu\text{-}H)_3(Al^iBu_2)_2][B(C_6F_5)_4]$. In a glovebox 100.3 mg (0.2236 mmol) $(SBI)ZrCl_2$ and 205.8 mg (0.2231 mmol, 1 equiv) of $[Ph_3C][B(C_6F_5)_4]$ were weighed into a 25 mL round bottom flask. Approximately 15 mL of toluene which had been vacuum transferred from titanocene was added resulting in an orange-red solution. 1.2 mL (6.7 mmol, 30 equiv) of HAl^iBu_2 was syringed into the solution resulting in a green solution which faded to yellow upon stirring. A swivel frit with another 25 mL round bottom was attached and the reaction vessel was taken to a high vacuum line. The reaction was allowed to stir at room temperature for 30 minutes following which toluene was removed *in vacuo* until no more liquid would come off leaving 2-3 mL of a red solution. Approximately 10 mL of pentane was vacuum transferred onto the reaction from titanocene. After stirring for one hour at room temperature a yellow precipitate was collected by filtration and washed twice with pentane. 128.0 mg (47% yield) of $[(SBI)Zr(\mu\text{-}H)_3(Al^iBu_2)_2][B(C_6F_5)_4]$ was collected. ^{1}H NMR of the solid was indistinguishable with that formed in situ with the exception of the absence of peaks due to free HAl^iBu_2 or $ClAl^iBu_2$. Attempts to obtain

elemental analysis of the compound were unsuccessful as the pale yellow solid was found to darken overnight at room temperature in a vacuum sealed ampoule. The solid could be stored for over one month at –40 ºC in a glovebox freezer suggesting that the low yield obtained in this reaction was due at least in part to the prolonged stirring at room temperature.

^{1}H NMR of [(SBI)Zr(μ-H)$_3$(AlMe$_x$^{i}Bu$_{2-x}$)$_2$][B(C$_6$F$_5$)$_4$]. Mixed alkyl hydrides were prepared from a 3 mM solution of [(SBI)Zr(μ-H)$_3$)(Al^{i}Bu$_2$)$_2$]$^+$ prepared in situ with 5 equiv of HAl^{i}Bu$_2$ and then adding $^1/_3$, 1, 2 or 3 equiv of AlMe$_3$ to the NMR tube via microliter syringe. Shaking the sealed tube and collecting ^{1}H NMR spectra yielded the spectra shown in Figure 3.12.

To test the reversibility of this reaction, 1.2 mg (SBI)ZrMe$_2$ (2.9 μmol) was dissolved in 0.7 mL benzene-d_6 and added to 2.5 mg [Ph$_3$C][B(C$_6$F$_5$)$_4$] to give an orange cloudy solution of [(SBI)ZrMe]$^+$. 2.6 μL HAl^{i}Bu$_2$ (15 μmol, 5 equiv) was then added. Immediate ^{1}H NMR showed the presence of [(SBI)Zr(μ-H)$_3$)(Al^{i}Bu$_2$)$_2$]$^+$ which after stirring for 2 hours became the dominant species (Figure 3.14).

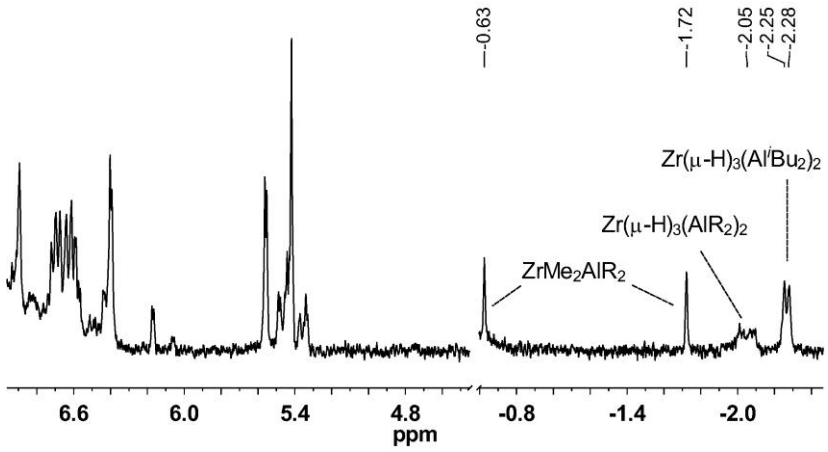

Figure 3.14: ^{1}H NMR of 4.1 mM solution of [(SBI)Zr(μ-H)$_3$(AlMe$_x$^{i}Bu$_{2-x}$)$_2$][B(C$_6$F$_5$)$_4$] in benzene-d_6 prepared from [(SBI)ZrMe]$^+$ with 5.0 equiv of HAl^{i}Bu$_2$.

gCOSY of [(SBI)Zr(μ-H)$_3$(AlMe$_x$^{i}Bu$_{2-x}$)$_2$][Me-MAO]$^-$. A 1.9 mM solution of [(SBI)Zr(μ-H)$_3$(AlMe$_x$^{i}Bu$_{2-x}$)$_2$][Me-MAO]$^-$ was prepared by first adding 50.6 mg MAO, which had been dried under vacuum at 50°C for 3 hours, to a 20 mL vial in the glove box. 3.5 mL of benzene-d_6 was then added and the mixture was stirred to dissolve as much MAO as possible. The mixture was allowed to sit undisturbed for 30 minutes after which time 3 mL of MAO solution was pipetted off leaving behind a gel. 2.6 mg of (SBI)ZrCl$_2$ (5.8 μmol) was then added to the solution to give an orange solution containing [(SBI)ZrMe$_2$AlMe$_2$]$^+$ and [(SBI)ZrMe$^{+\cdots}$MeMAO$^-$]. 0.7 mL of this solution was transferred to a J Young tube and 15 μL HAl^{i}Bu$_2$ was added neat via microliter syringe. A gCOSY spectrum (Figure 3.15) was obtained which showed coupling of the {Zr(μ-H)$_2$} peak to a downfield peak at 0.58 ppm consistent with the central {Zr(μ-H)}.

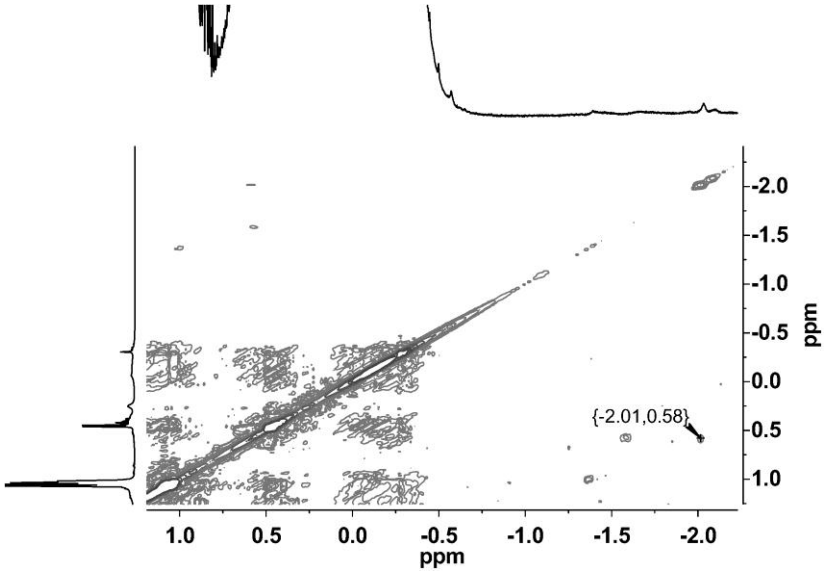

Figure 3.15: gCOSY of a solution of $[(SBI)Zr(\mu\text{-}H)_3(AlMe_x{}^iBu_{2-x})_2][MeMAO]^-$ showing coupling between hydride signals.

^{1}H NMR spectrum of the dichloro-bridged cation $[(SBI)Zr(\mu\text{-}Cl)_2Al{}^iBu_2]^+$. (Method 1A: $HAl{}^iBu_2$ / $ClAl{}^iBu_2$) 1.0 mg $(SBI)ZrCl_2$ (2.2 μmol) and 2.1 mg $[Ph_3C][B(C_6F_5)_4]$ (2.3 μmol) were added to a 1-dram vial in the glove box. 0.7 mL benzene-d_6 was added. 0.4 μL $HAl{}^iBu_2$ (2 μmol) and 0.4 μL $ClAl{}^iBu_2$ (2 μmol) were added neat via miclroliter syringe. The mixture was shaken to yield a blue solution with blue oil. The mixture was transferred to a J-Young NMR tube and spectra were obtained (Figure 3.11). ^{1}H NMR (300 MHz, benzene-d_6) δ 6.86 (m, 4H, Ar-H), 6.68 (m, 2H, Ar-H), 6.26 (d, $^3J_{HH}$ = 3 Hz, 2H, C_5-H), 5.17 (d, $^3J_{HH}$ = 3 Hz, 2H, C_5-H), 1.88 (m, $^3J_{HH}$ = 7 Hz, 2H, ^{i}Bu-CH), 0.93 (d, $^3J_{HH}$ = 7 Hz, 6H, ^{i}Bu-CH_3), 0.86 (d, $^3J_{HH}$ = 7 Hz, 6H, ^{i}Bu-CH_3), 0.68 (s, 6H, $Si(CH_3)_2$), 0.26 (d, $^3J_{HH}$ = 7 Hz, 4H, ^{i}Bu-CH_2).

(Method 1B: HAl^iBu_2 / $ClAl^iBu_2$) The same species can be formed by first making the hydride cation, $[(SBI)Zr(\mu\text{-}H)_3(Al^iBu_2)_2][B(C_6F_5)_4]$, and then adding an excess of $ClAl^iBu_2$. 1.0 mg $(SBI)ZrCl_2$ (2.2 μmol) and 4.0 μL HAl^iBu_2 (22 μmol) along with 0.7 mL benzene-d_6 were added to a 1-dram vial in the glove box. The resulting solution was added to a second vial containing 2.2 mg $[Ph_3C][B(C_6F_5)_4]$ (2.4 μmol) resulting in a solution of the hydride cation. 8.0 μL of neat $ClAl^iBu_2$ (41 μmol) was then added via miclroliter syringe. The mixture was shaken to yield a blue solution. The mixture was transferred to a J-Young NMR tube and spectra identical to Method A were obtained.

(Method 2: Et_3Si^+) In the glove box, a slurry of 2.1 mg $(SBI)ZrCl_2$ (4.7 μmol) was formed in a solution containing 4.3 mg (4.7 μmol) of $[Ph_3C][B(C_6F_5)_4]$ in 0.7 mL benzene-d_6. The slurry was added to a J-Young tube and 0.9 μL $ClAl^iBu_2$ (5 μmol) was added to the side of the tube without mixing. The sample was removed from the box, frozen and the head space was evacuated on the high-vacuum line. 0.04 mL Et_3SiH (300 μmol) was vacuum-transferred in from a storage flask containing CaH_2. Upon thawing and mixing a blue solution and blue oil formed. The sample was pumped down to remove excess Et_3SiH and then redissolved in benzene-d_6. Spectra identical to those from Method A were obtained.

^{1}H NMR spectrum of the dichloro-bridged cation $[(SBI)Zr(\mu\text{-}Cl)_2AlMe_2]^+$. 1.0 mg (2.5 μmol) $(SBI)ZrMe_2$ and 1.0 mg $AlCl_3$ (7.5 μmol, 3 equiv) were weighed into a 1-dram vial. 1.4 μL (15 μmol, 6 equiv) $AlMe_3$ was syringed onto the side of the vial. 2.3 mg

$[Ph_3C][B(C_6F_5)_4]$ (2.5 μmol, 1 equiv) was weighed into a second 1-dram vial and was dissolved in 0.7 ml benzene-d_6. The $[Ph_3C]^+$ solution was added to the vial containing the zirconocene and mixed thoroughly to give a green solution which turned blue over the course of a few minutes. The solution was transferred to a J-Young tube for NMR analysis. ^{1}H NMR (500 MHz, benzene-d_6) δ 6.94 (s, 6H, Ar-H), 6.71 (s, 3H, Ar-H), 6.35 (s, 2H, C_5-H), 5.29 (s, 2H, C_5-H), 0.62 (s, 8H, $Si(CH_3)_2$).

UV-vis spectra of $[(SBI)Zr(\mu\text{-}Cl)_2(Al^iBu_2)]^+$. A 2.79 mM stock solution of (SBI)ZrCl(μ-H)$_2$(Al^iBu_2) was prepared by dissolving 12.5 mg (SBI)$ZrCl_2$ (27.9 μmol) in 10.0 mL toluene, vacuum-transferred from titanocene, to which was added 14.9 μL HAl^iBu_2 (83.6 μmol, 3.00 equiv). A 2.79 mM stock solution of $[Ph_3C][B(C_6F_5)_4]$ was likewise prepared by dissolving 25.7 mg of $[Ph_3C][B(C_6F_5)_4]$ in 10.0 mL toluene. For each UV-vis experiment 2.00 mL of each solution was combined and diluted to a volume of 10.0 mL to afford a 0.558 mM solution of $[(SBI)Zr(\mu\text{-}H)_3(Al^iBu_2)_2][B(C_6F_5)_4]$ to which was then added an additional amount of neat HAl^iBu_2 to afford solutions containing 3, 4, 5 or 10 equivalents of HAl^iBu_2. Following measurement of the UV-vis spectrum of each sample (Figure 3.9) enough HAl^iBu_2 was added to reach 10 equiv relative to Zr. All samples afforded the same final spectrum regardless of how many equivalents of HAl^iBu_2 were initially added. To show the reversible nature of this equilibrium, successive 2.2 μL aliquots of $ClAl^iBu_2$ (11 μmol, 2.0 equiv) were added to one of the final samples

containing 10 equiv $HAl^{i}Bu_2$, collecting UV-vis spectra between each addition (Figure 3.10).

Synthesis of $[\{(SBI)Zr(\mu\text{-}Cl)\}_2][B(C_6F_5)_4]_2$. In a glove box, 103.6 mg (231.0 mmol) $(SBI)ZrCl_2$ and 213 mg (230.9 mmol, 1 equiv) $[Ph_3C][B(C_6F_5)_4]$ were weighed into a 25 mL round bottom flask. A swivel frit and a second 25 mL round bottom were attached and 10 mL of toluene was added. The solution was degassed and 0.35 mL Et_3SiH was vacuum-transferred in at –78 ºC from a storage flask containing CaH_2. The solution was allowed to warm to room temperature giving a green solution and a green oil. After stirring for 30 minutes the solvent was removed *in vacuo* and 10 mL pentane was vacuum-transferred in from a titanocene-containing storage flask. After stirring for 5 minutes the reaction was filtered to give a green powder which was rinsed 3 times with pentane. 243.0 mg green powder was collected from the frit (96% yield). $[\{(SBI)Zr(\mu\text{-}Cl)\}_2][B(C_6F_5)_4]_2$ was found to be completely insoluble in benzene, toluene, bromobenzene or a 1:1 mixture of toluene and 1,2-difluorobenzene. Attempts to dissolve it in dichloromethane resulted in decomposition even at –70 ºC. Upon exposure to air the green solid was found to rapidly change to a bright red color.

Addition of 3.6 μL (18 μmol, 10 equiv) of $ClAl^{i}Bu_2$ to a slurry of 4.0 mg (1.8 μmol) of $[\{(SBI)Zr(\mu\text{-}Cl)\}_2][B(C_6F_5)_4]_2$ in 0.7 ml benzene-d_6 followed by sonication and stirring overnight resulted in the spectra identical to that observed in Figure 3.11. In the absence of

$ClAl^{i}Bu_2$ sonication and stirring $[\{(SBI)Zr(\mu\text{-}Cl)\}_2][B(C_6F_5)_4]_2$ overnight in benzene-d_6 did not yield any C_5-*H* ^{1}H NMR signals.

^{1}H NMR spectrum of the cation $[(SBI)Zr(\mu\text{-}H)_3(AlR_2)_2]^+$ with R = n-octyl. A measured amount of $AlOct_3$ solution in hexanes (25% by weight) was added to a J-Young tube via microliter syringe in the glovebox. The tube was evacuated for a minimum of 30 minutes to remove the hexanes. To this was then added a 3 mM solution of $[(SBI)Zr(\mu\text{-}H)_3(Al^{i}Bu_2)_2][B(C_6F_5)_4]$ prepared as above. ^{1}H NMR spectra were collected with various ratios of $AlOct_3$ to $HAl^{i}Bu_2$ (Figure 3.16).

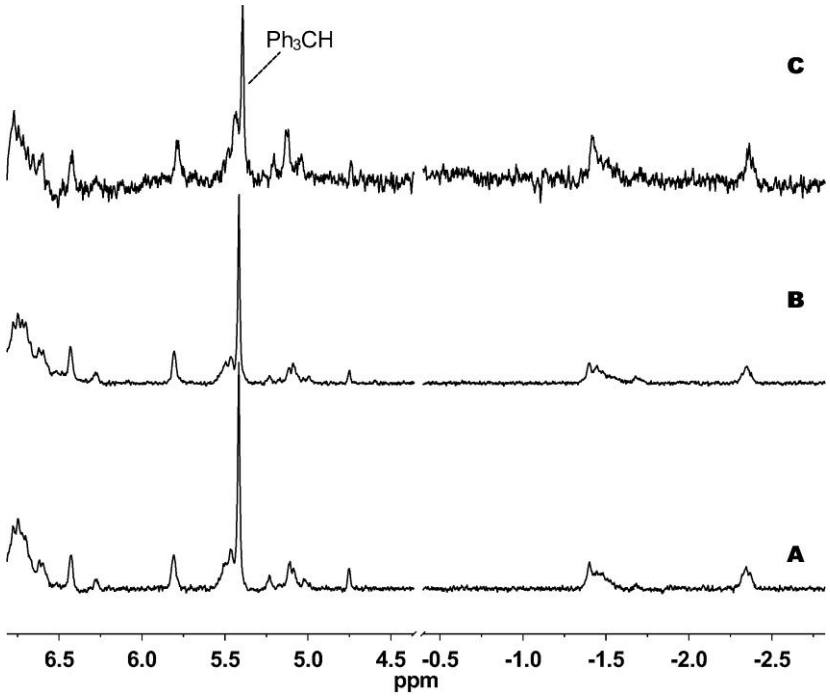

Figure 3.16: ^{1}H NMR of $[(SBI)Zr(\mu\text{-}H)_3(Al^{i}Bu_2)_2]^+$ and $AlOct_3$ with different equivalents of $HAl^{i}Bu_2$ to $AlOct_3$ of 5:10 (**A**), 10:10 (**B**) and 10:100 (**C**).

^{1}H NMR spectrum of $[(SBI)Zr(\mu\text{-}H)_3(AlR_2)_2]^+$ with R = n-octyl, isobutyl, methyl. A solution of $[(SBI)Zr(\mu\text{-}H)_3(AlR_2)_2]^+$ was prepared as above with 10 equiv $AlOct_3$ and 10 equiv HAl^iBu_2 (similar to Figure 3.16A). To this solution was added 2.1 μL $AlMe_3$ (22 μmol, 10 equiv). A ^{1}H NMR spectrum was obtained (Figure 3.17).

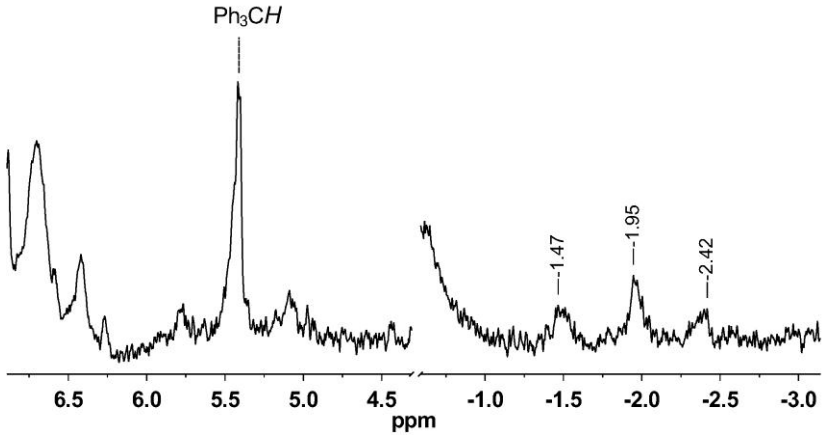

Figure 3.17: ^{1}H NMR of $[(SBI)Zr(\mu\text{-}H)_3(Al^iBu_2)_2]^+$ with 10 equiv of HAl^iBu_2, $AlOct_3$ and $AlMe_3$.

Determination of the Equilibrium Constant for the Reaction $[(SBI)Zr(\mu\text{-}H)_3(AlR_2)_2]^+$ + $(AlMe_3)_2$ ⇆ $[(SBI)ZrMe_2AlMe_2]^+$ + $(HAlMe_2)_2$. A solution containing 3.1 mM $[(SBI)Zr(\mu\text{-}H)_3(Al^iBu_2)_2]^+$ was prepared by reacting 1.0 mg (2.2 μmol) of $(SBI)ZrCl_2$ and 3.0 μL (17 μmol, 7.7 equiv) of $HAl^iBu_2)_2$ with 2.1 mg (2.2 μmol, 1 equiv) of $[Ph_3C][B(C_6F_5)_4]$ in 0.7 mL of toluene-d_8 in a J-Young NMR tube in the glove box. ^{1}H NMR spectra were collected, at room temperature, after stepwise additions of 4.3-μL (45 μmol, 20 equiv) increments of neat $AlMe_3$ via microliter syringe in the glove box. Integrals

of the Si-CH_3 signals for both zirconocene species, as well as of the *H*-Al and CH_3-Al signals at 3.72 and 0.31-0.34 ppm, respectively were monitored (Table 3.5). Values for 70–210 equiv of $AlMe_3$ were used for calculation of the equilibrium constant, since the Si-CH_3 signal of $[(SBI)ZrMe_2AlMe_2]^+$ was first clearly observed at 70 equiv of $AlMe_3$ (Figure 3.18), while at higher $AlMe_3$ concentrations $[(SBI)ZrMe_2AlMe_2]^+$ precipitated in the form of a red oil. The integrals of the CH_3-Al signals were corrected to represent the concentration of $(AlMe_3)_2$ by subtracting 2 times the integrals of the Si-CH_3 signal of $[(SBI)Zr(\mu\text{-}H)_3(AlMe_2)_2]^+$ at 0.58 ppm and six times the integral of the *H*-Al signal of $(HAlMe_2)_3$ and division of the resulting value by 18. From eight such measurements, an average value of $K_{eq} = 0.97(15)*10^{-2}$ was determined.

Table 3.5: Determination of K_{eq} from concentration data for a reaction system containing $[(SBI)Zr(\mu\text{-}H)_3(AlMe_2)_2]^+$ and 70 - 210 equiv of $AlMe_3$.

equiv $AlMe_3$	**Integrals**					**Normalized "Concentration"** [a]				**K_{eq} (10^{-3})**
	Si(CH_3)$_2$			*H*-Al	CH_3-Al (10^2)	ZrH_3^+	$ZrAlMe_4^+$	$(HAlMe_2)_3$	$(AlMe_3)_2$ (10^1)	
	ZrH_3^+	$ZrAlMe_4^+$	Zr_{TOT}							
70	83.4	14.2	97.5	137	153	13.9	2.4	45.5	79.6	9.7
90	83.4	14.1	97.5	144	192	13.9	2.4	48.0	101	8.1
110	80.3	17.2	97.6	149	231	13.4	2.9	49.6	123	8.7
130	77.4	19.9	97.3	161	282	12.9	3.3	53.8	150	9.2
150	74.8	22.6	97.3	167	326	12.5	3.8	55.7	175	9.6
170	75.6	21.1	96.7	186	397	12.6	3.5	62.1	214	8.1
190	67.3	30.5	97.8	162	377	11.2	5.1	54.1	203	12.1
210	65.9	31.3	97.2	185	461	11.0	5.2	61.8	249	11.8
									average **K_{eq}** ±	9.7 ±1.5

[a] "Concentration" refers to normalized integrals, such that tabulated concentrations are accurate relative to each other but are not absolute concentrations. Conversions to absolute concentrations were omitted, since any such factors would cancel out in determining the dimensionless value of K_{eq}. The total absolute concentration of Zr in all solution was 3.1 mM.

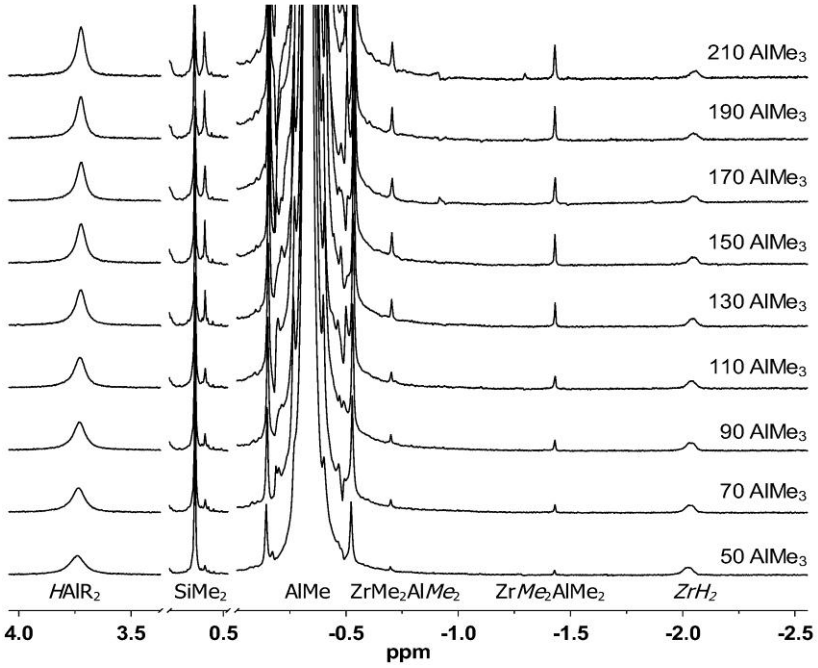

Figure 3.18: ^{1}H NMR spectra of a 3.1 mM solution of $[(SBI)Zr(\mu\text{-}H)_3(Al^iBu_2)_2]^+$ with 3.5 equiv of free HAl^iBu_2 upon addition of 50-210 equiv of $AlMe_3$ relative to Zr.

X-ray Crystallography Details. Data for $[(SBI)Zr(\mu\text{-}H)_3(Al^iBu_2)_2][B(C_6F_5)_4]\cdot\frac{1}{2}(C_7H_8)$ (**1**) and $[(Me_2Si)_2(C_5H_3)Zr(\mu\text{-}H)_3(Al^iBu_2)_2]$ $[B(C_6F_5)_4]$ (**2**) were collected on a Bruker KAPPA APEX II using Mo Kα X-ray source (α = 0.71073 Å). The crystals were mounted on a glass fiber under Paratone-N oil and all data were collected at 100 K. Data was collected using ω scans. Data collection and cell parameter determination were conducted using the APEX2 program. Integration of the data frames and final cell parameter refinement were performed using SAINT software. Absorption correction of the data was carried out semi-empirically based on equivalent reflections for **2,** for **1** no absorption correction was applied. Subsequent calculations were carried out using SHELAXS software. Structure determination was done using direct methods and difference Fourier techniques. All

hydrogen atom positions were idealized, and rode on the atom of attachment with exceptions noted in the subsequent paragraph. A summary of relevant crystallographic data is presented in Table 3.6.

For both complexes, the hydrides were located in the difference maps and their positions were refined. For **2** no restraints were applied while for **1** the thermal factors were restrained to be 1.2 times the U_{eq} of the corresponding metal atoms. Additionally in **1** all six-membered rings were constrained to be regular hexagons. The toluene was constrained to be flat and the anisotropic displacement parameters (ADP's) to simulate isotropic behavior. The eight isobutyl groups were restrained to have the same geometry with no target values for the bond lengths. The ADP's of the isobutyl groups were restrained to simulate isotropic behavior however no restraints were placed on their sizes.

Table 3.6: X-ray Crystallographic Data for all compounds

	[(SBI)Zr(μ-H)$_3$(Al^{i}Bu$_2$)$_2$]$^+$	**[(Me$_2$Si)$_2$(C$_5$H$_3$)Zr(μ-H)$_3$(Al^{i}Bu$_2$)$_2$]$^+$**
Empirical Formula	$[C_{36}H_{57}Al_2SiZr][C_{24}BF_{20}]^-\cdot½(C_7H_8)$	$[C_{30}H_{54}Al_2Si_2ZrH_3]^+ [C_{24}BF_{20}]^-$
Crystal Habit, color	Block, yellow	Blade, colorless
Crystal Size (mm)	0.27 x 0.22 x 0.09	0.28 x 0.20 x 0.04
Crystal System	Orthorhombic	Monoclinic
Space Group	$P2_12_12_1$	$P2_1/n$
Volume (Å^3)	12669.3(9)	5766.9(5)
a (Å)	17.3916(7)	16.2579(8)
b (Å)	26.6355(12)	17.1922(7)
c (Å)	27.3497(12)	21.1975(10)
α (°)	90	90
β (°)	90	103.262(3)
γ (°)	90	90
Z	8	4
Formula weight (g/mol)	1388.20	1298.17
Density (calculated) (Mg/m^3)	1.456	1.495
Absorption coefficient (mm^{-1})	0.318	0.364
F_{000}	5656	2640
Total no. reflections	115139	75246
Unique reflections	23731	12697
Final R indices [$I > 2\sigma(I)$]	$R_1 = 0.0623$, $wR_2 = 0.0749$ 13557 reflections	$R_1 = 0.0422$, $wR_2 = 0.0681$ 8862 reflections
R indices (all data)	$R_1 = 0.1201$, $wR_2 = 0.0779$	$R_1 = 0.0795$, $wR_2 = 0.0719$
Largest diff. peak and hole (e$^-$Å^{-3})	0.703 and -0.470	0.741 and -0.489
GOF	1.804	1.883

3.6 References

1. Negishi, E.; Tan, Z. *Top. Organomet. Chem.*, **2005**, *8*, 139.
2. Dzhemilev, U. M.; Ibragimov, A. G., In *Modern Reduction Methods*, Andersson, P. G.; Munslow, P. J., Eds. Wiley-VCH: Weinheim, 2008; p 447.
3. Pankratyev, E. Y.; Tyumkina, T. V.; Parfenova, L. V.; Khalilov, L. M.; Khursan, S. L.; Dzhemilev, U. M. *Organometallics*, **2009**, *28*, 968.
4. Chen, E. Y. X.; Marks, T. J. *Chem. Rev.*, **2000**, *100*, 1391.
5. Yang, X. M.; Stern, C. L.; Marks, T. J. *Angew. Chem.-Int. Edit. Engl.*, **1992**, *31*, 1375.
6. Yang, X. M.; Stern, C. L.; Marks, T. J. *J. Am. Chem. Soc.*, **1994**, *116*, 10015.
7. Carr, A. G.; Dawson, D. M.; Thornton-Pett, M.; Bochmann, M. *Organometallics*, **1999**, *18*, 2933.
8. Arndt, P.; Jäger-Fiedler, U.; Klahn, M.; Baumann, W.; Spannenberg, A.; Burlakov, V. V.; Rosenthal, U. *Angew. Chem. Int. Edit.*, **2006**, *45*, 4195.
9. Jordan, R. F.; Bajgur, C. S.; Dasher, W. E.; Rheingold, A. L. *Organometallics*, **1987**, *6*, 1041.
10. Choukroun, R.; Douziech, B.; Donnadieu, B. *Organometallics*, **1997**, *16*, 5517.
11. Blaschke, U.; Erker, G.; Nissinen, M.; Wegelius, E.; Frohlich, R. *Organometallics*, **1999**, *18*, 1224.
12. Driess, M.; Aust, J.; Merz, K.; van Wullen, C. *Angew. Chem. Int. Edit.*, **1999**, *38*, 3677.
13. Driess, M.; Ackermann, H.; Aust, J.; Merz, K.; von Wullen, C. *Angew. Chem. Int. Edit.*, **2002**, *41*, 450.
14. Lee, H.; Jordan, R. F. *J. Am. Chem. Soc.*, **2005**, *127*, 9384.
15. Liu, F. C.; Chen, S. C.; Lee, G. H.; Peng, S. M. *J. Organomet. Chem.*, **2007**, *692*, 2375.
16. Jia, L.; Yang, X. M.; Stern, C. L.; Marks, T. J. *Organometallics*, **1997**, *16*, 842.
17. Blaschke, U.; Menges, F.; Erker, G.; Frohlich, R. *Eur. J. Inorg. Chem.*, **1999**, 621.
18. Garratt, S.; Carr, A. G.; Langstein, G.; Bochmann, M. *Macromolecules*, **2003**, *36*, 4276.

19. Al-Humydi, A.; Garrison, J. C.; Mohammed, M.; Youngs, W. J.; Collins, S. *Polyhedron*, **2005**, *24*, 1234.
20. Christianson, M. D.; Tan, E. H. P.; Landis, C. R. *J. Am. Chem. Soc.*, **2010**, *132*, 11461.
21. Chen, C.; Lee, H.; Jordan, R. F. *Organometallics*, **2010**, *29*, 5373.
22. Jordan, R. F.; Lapointe, R. E.; Bradley, P. K.; Baenziger, N. *Organometallics*, **1989**, *8*, 2892.
23. Jordan, R. F.; Bradley, P. K.; Baenziger, N. C.; Lapointe, R. E. *J. Am. Chem. Soc.*, **1990**, *112*, 1289.
24. Grossman, R. B.; Doyle, R. A.; Buchwald, S. L. *Organometallics*, **1991**, *10*, 1501.
25. Casey, C. P.; Carpenetti, D. W. *J. Organomet. Chem.*, **2002**, *642*, 120.
26. Götz, C.; Rau, A.; Luft, G. *J. Mol. Catal. A-Chem.*, **2002**, *184*, 95.
27. Bryliakov, K. P.; Talsi, E. P.; Semikolenova, N. V.; Zakharov, V. A.; Brand, J.; Alonso-Moreno, C.; Bochmann, M. *J. Organomet. Chem.*, **2007**, *692*, 859.
28. Babushkin, D. E.; Panchenko, V. N.; Timofeeva, M. N.; Zakharov, V. A.; Brintzinger, H. H. *Macromol. Chem. Phys.*, **2008**, *209*, 1210.
29. Thomas, R. L.; Rath, N. P.; Barton, L. *J. Am. Chem. Soc.*, **1997**, *119*, 12358.
30. Liu, F. C.; Liu, J. P.; Meyers, E. A.; Shore, S. G. *J. Am. Chem. Soc.*, **2000**, *122*, 6106.
31. Thomas, R. L.; Rath, N. P.; Barton, L. *Inorg. Chem.*, **2002**, *41*, 67.
32. Chen, X. N.; Liu, F. C.; Plecnik, C. E.; Liu, S. M.; Du, B.; Meyers, E. A.; Shore, S. G. *Organometallics*, **2004**, *23*, 2100.
33. Eisch, J. J.; Rhee, S. G. *J. Organomet. Chem.*, **1972**, *38*, C25.
34. Khan, K.; Raston, C. L.; McGrady, J. E.; Skelton, B. W.; White, A. H. *Organometallics*, **1997**, *16*, 3252.
35. Etkin, N.; Hoskin, A. J.; Stephan, D. W. *J. Am. Chem. Soc.*, **1997**, *119*, 11420.
36. Etkin, N.; Stephan, D. W. *Organometallics*, **1998**, *17*, 763.
37. Wehmschulte, R. J.; Power, P. P. *Polyhedron*, **1999**, *18*, 1885.
38. Sizov, A. I.; Zvukova, T. M.; Belsky, V. K.; Bulychev, B. M. *J. Organomet. Chem.*, **2001**, *619*, 36.

39. Atwood, J. L.; Robinson, K. D.; Jones, C.; Raston, C. L. *J. Chem. Soc. Chem. Comm.*, **1991**, 1697.
40. Knjazhansky, S. Y.; Nomerotsky, I. Y.; Bulychev, B. M.; Belsky, V. K.; Soloveichik, G. L. *Organometallics*, **1994**, *13*, 2075.
41. Stasch, A.; Roesky, H. W.; Noltemeyer, M.; Schmidt, H. G. *Inorg. Chem.*, **2005**, *44*, 5854.
42. Masuda, J. D.; Stephan, D. W. *Dalton Trans.*, **2006**, 2089.
43. Allen, F. H. *Acta Crystallogr. B*, **2002**, *58*, 380.
44. Bryliakov, K. P.; Talsi, E. P.; Voskoboynikov, A. Z.; Lancaster, S. J.; Bochmann, M. *Organometallics*, **2008**, *27*, 6333.
45. Babushkin, D. E.; Brintzinger, H. H. *Chem.-Eur. J.*, **2007**, *13*, 5294.
46. Bochmann, M.; Lancaster, S. J. *Angew. Chem.-Int. Edit. Engl.*, **1994**, *33*, 1634.
47. Bochmann, M.; Lancaster, S. J. *J. Organomet. Chem.*, **1995**, *497*, 55.
48. Hoffmann, E. G. *Liebigs Ann. Chem.*, **1960**, *629*, 104.
49. Vestin, R.; Vestin, U.; Kowalewski, J. *Acta Chem. Scand. A, Phys. Inorg. Chem.*, **1985**, *39*, 767.
50. Marvich, R. H.; Brintzinger, H. H. *J. Am. Chem. Soc.*, **1971**, *93*, 2046.
51. Voskoboynikov, A. Z.; Agarkov, A. Y.; Chernyshev, E. A.; Beletskaya, I. P.; Churakov, A. V.; Kuz'mina, L. G. *J. Organomet. Chem.*, **1997**, *530*, 75.
52. Schwemlein, H.; Brintzinger, H. H. *J. Organomet. Chem.*, **1983**, *254*, 69.
53. Deck, P. A.; Beswick, C. L.; Marks, T. J. *J. Am. Chem. Soc.*, **1998**, *120*, 1772.
54. Lappert, M. F.; Riley, P. I.; Yarrow, P. I. W.; Atwood, J. L.; Hunter, W. E.; Zaworotko, M. J. *J. Chem. Soc. Dalton*, **1981**, 814.
55. Wild, F.; Wasiucionek, M.; Huttner, G.; Brintzinger, H. H. *J. Organomet. Chem.*, **1985**, *288*, 63.
56. Köpf, H.; Klouras, N. *Z. Naturforsch., B: Chem. Sci.*, **1983**, *38*, 321.
57. Cano, A.; Cuenca, T.; Gomezsal, P.; Royo, B.; Royo, P. *Organometallics*, **1994**, *13*, 1688.

58. Herzog, T. A.; Zubris, D. L.; Bercaw, J. E. *J. Am. Chem. Soc.*, **1996**, *118*, 11988.
59. Chacon, S. T.; Coughlin, E. B.; Henling, L. M.; Bercaw, J. E. *J. Organomet. Chem.*, **1995**, *497*, 171.
60. Wiesenfeldt, H.; Reinmuth, A.; Barsties, E.; Evertz, K.; Brintzinger, H. H. *J. Organomet. Chem.*, **1989**, *369*, 359.
61. Yoder, J. C.; Day, M. W.; Bercaw, J. E. *Organometallics*, **1998**, *17*, 4946.
62. Wartik, T.; Schlesinger, H. I. *J. Am. Chem. Soc.*, **1953**, *75*, 835.
63. Hui, B. C.; Victoriano, D. Patent 4,924,019, 1990.
64. Grady, A. S.; Puntambekar, S. G.; Russell, D. K. *Spectrochim Acta A*, **1991**, *47*, 47.
65. Downs, A. J.; Greene, T. M.; Collin, S. E.; Whitehurst, L. A.; Brain, P. T.; Morrison, C. A.; Pulham, C. R.; Smart, B. A.; Rankin, D. W. H.; Keys, A.; Barron, A. R. *Organometallics*, **2000**, *19*, 527.
66. Vass, G.; Tarczay, G.; Magyarfalvi, G.; Bodi, A.; Szepes, L. *Organometallics*, **2002**, *21*, 2751.

CHAPTER 4

Polymerization and Hydroalumination of Propene by Cationic Alkylaluminum-Complexed Zirconocene Hydrides

4.1 Abstract

Alkylaluminum-complexed zirconocene trihydride cation, $[(SBI)Zr(\mu\text{-}H)_3(Al^iBu_2)_2]^+$, catalyzes the formation of isotactic polypropene when exposed to propene at –30 ºC. This cation remains the sole observable species in catalyst systems free of {AlMe} compounds. In the presence of $AlMe_3$, however, exposure to propene causes the trihydride cation to be completely converted to the doubly Me-bridged cation, $[(SBI)Zr(\mu\text{-}Me)_2AlMe_2]^+$, with concurrent consumption of all hydride species via the hydroalumination of propene. $[(SBI)Zr(\mu\text{-}Me)_2AlMe_2]^+$ then becomes the resting state for further propene polymerization, which produces, by chain transfer to Al, mainly $\{AlMe_2\}$-capped isotactic polypropene.

This Chapter is published in part as:
Baldwin, S. M.; Bercaw, J. E.; Brintzinger, H. H. *J. Am. Chem. Soc.*, **2010**, *132*, 13969. (DOI: 10.1021/ja105040r)

4.2 Introduction

As shown in Chapter 3, Me-bridged heterodinuclear cation $[(SBI)Zr(\mu\text{-}Me)_2AlMe_2]^+$, a known constituent of catalyst systems activated by methylalumoxane (MAO),[1-3] reacts reversibly with alkylaluminum hydrides to form the previously unreported alkylaluminum-complexed zirconocene trihydride cation $[(SBI)Zr(\mu\text{-}H)_3(AlR_2)_2]^+$ (Scheme 4.1).

Scheme 4.1

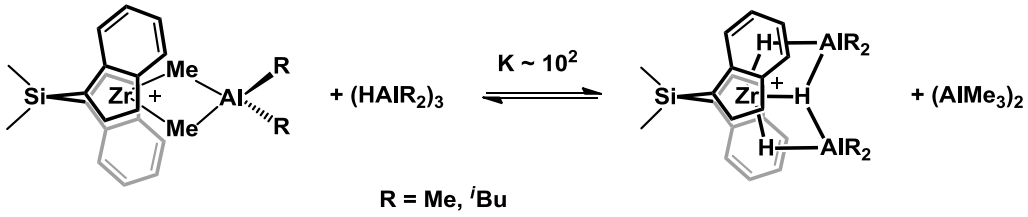

An equilibrium constant of ca. 10^2, determined for the reaction shown in Scheme 4.1, indicates that substantial portions of any MAO-activated zirconocene catalyst will be converted to the trihydride cation whenever such a catalyst system acquires hydride equivalents. Since many recipes seek to increase the activity and/or stability of zirconocene-based catalysts by addition of diisobutylaluminium hydride,[4-5] or of triisobutylaluminium[6-8] (from which hydride equivalents can be derived by elimination of isobutene), alkylaluminum-complexed zirconocene trihydride cations are likely to be abundant in such catalyst systems. This chapter will investigate what role cationic trihydride complexes of this type might play in zirconocene-based catalyst systems for the polymerization of α-olefins.

4.3 Results

4.3.1 Reaction of [(SBI)Zr(μ-H)$_3$(Al^{i}Bu$_2$)$_2$]$^+$ with Propene

A toluene-d_8 solution of [(SBI)Zr(μ-H)$_3$(Al^{i}Bu$_2$)$_2$]$^+$ was generated, as in Chapter 3, via reaction of (SBI)ZrCl$_2$ with 20 equiv of HAl^{i}Bu$_2$ and 1 equiv of [Ph$_3$C][B(C$_6$F$_5$)$_4$]. Reaction of [(SBI)Zr(μ-H)$_3$(Al^{i}Bu$_2$)$_2$]$^+$ with 20 equiv of propene at –30 ºC was monitored by ^{1}H NMR (Figure 4.1). Signals due to propene vanished over the course of the reaction while Al-H signals, due to HAl^{i}Bu$_2$, and the C$_5$-*H* and Zr(μ-*H*)$_2$ signals of [(SBI)Zr(μ-H)$_3$(Al^{i}Bu$_2$)$_2$]$^+$, at 5.45 and –2.47 ppm, respectively, remain constant in size throughout the reaction. No signals for polypropene were observed by NMR due to the low solubility of isotactic polypropene in toluene particularly at low temperatures, however, upon removal from the spectrometer, solid polypropene is observed in the J-Young tube. No signals due to new zirconocene species or alkylaluminum species were detectable in such catalyst systems during the consumption of 20 or 40 equiv of propene.

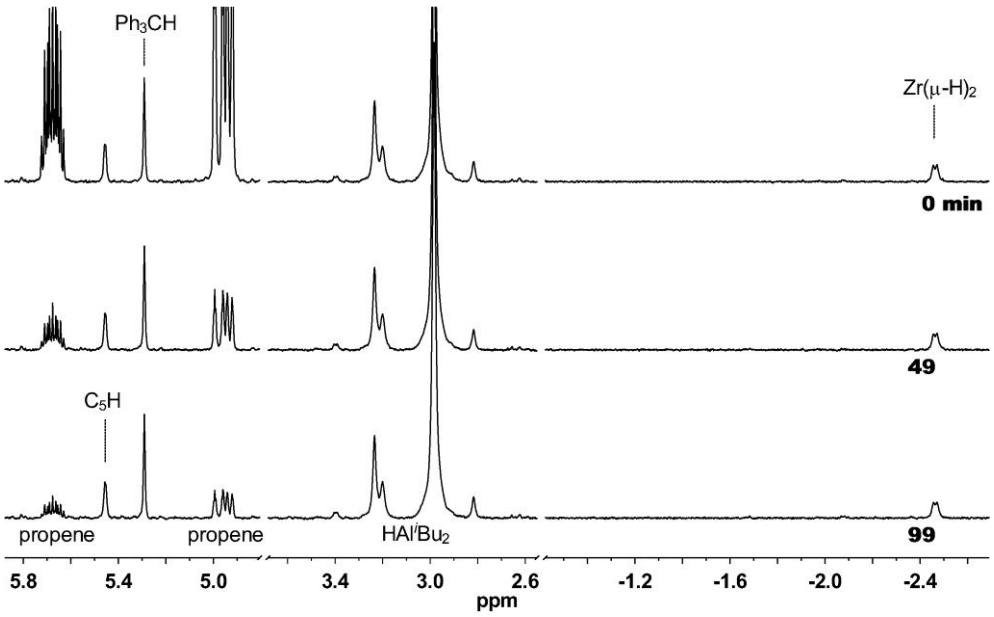

Figure 4.1: ^{1}H NMR spectra of a toluene-d_8 solution of the {Al^{i}Bu$_2$}-complexed trihydride cation [(SBI)Zr(μ-H)$_3$(Al^{i}Bu$_2$)$_2$]$^{+}$ immediately, 49 and 99 min after warming to –30 ºC in the presence of 20 equiv of propene.

The amount of polymer produced in NMR scale reactions was too small for analysis, therefore batch reactions were performed at 10-times scale to provide enough polymer for ^{13}C NMR and gel permeation chromatography (GPC) analysis. ^{13}C NMR spectra of the polymer (Figure 4.2) reveal the formation of highly isotactic polypropene (96% [mmmm]). ^{1}H NMR of the same sample (Figure 4.3) reveal the customary vinylidene end groups even though such resonances are too small to be observed in ^{13}C NMR. Resonances for other end groups are not observable in either ^{1}H or ^{13}C NMR. This is consistent with the observation by GPC of a molecular weight (M_n) of 79000 and a polydispersity index (PDI) of 1.90, consistent with a single site catalyst, was observed (Figure 4.4). The high molecular weight of the polymer yields a mean degree of polymerization (P_n) of

approximately 1880. That P_n is almost 2 orders of magnitude higher than that expected from the initial ratio of propene to Zr (40:1) suggests that the available monomer is incorporated into Zr-bound polymer chains at only a small fraction of the Zr centers present. Such a situation will typically arise if chain growth is faster than chain initiation, which in this case probably occurs by insertion of propene into one of the Zr-H bonds of the hydride cation, $[(SBI)Zr(\mu\text{-}H)_3(Al^iBu_2)_2]^+$, to generate contact ion pairs of the type $[(SBI)ZrCH_2R^{+\cdots}(F_5C_6)_4B^-]$.[9] Such a low percentage of initiation has been previously observed numerous times, as discussed in Section 1.4, and is thus not all that surprising for the current system.

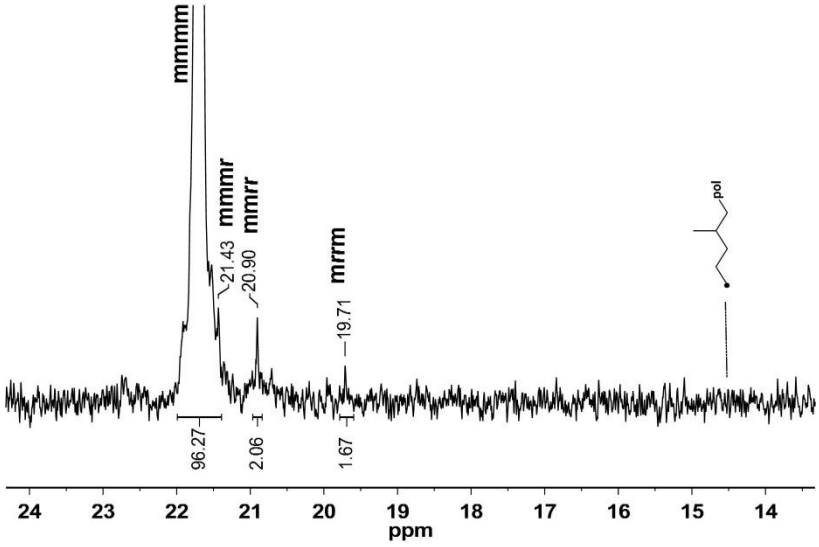

Figure 4.2: ^{13}C NMR spectrum of polypropene produced by $[(SBI)Zr(\mu\text{-}H)_3(Al^iBu_2)_2]^+$ in saturated tetrachloroethane-d_2 solution containing ca. 1 mg/mL of $Cr(acac)_3$ at 120 °C.

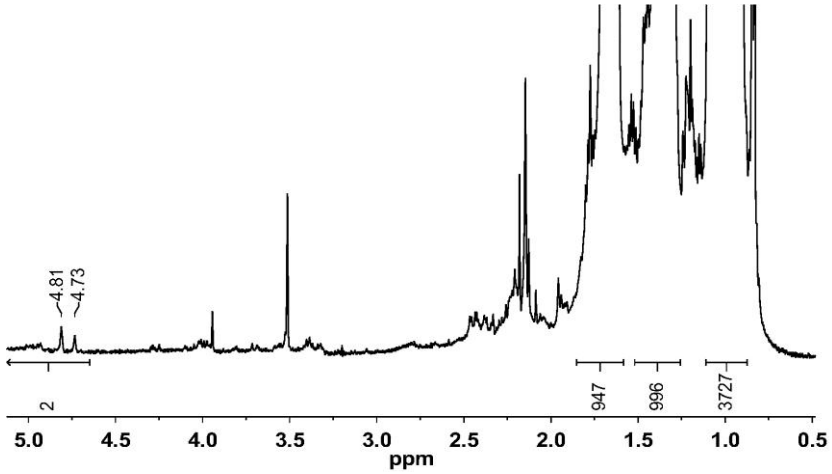

Figure 4.3: ^{1}H NMR spectrum of polypropene, produced by $[(SBI)Zr(\mu\text{-}H)_3(Al^{i}Bu_2)_2]^+$ in saturated tetrachloroethane-d_2 solution at 120 ºC (the signal at 3.5 ppm is due to an impurity in the solvent).

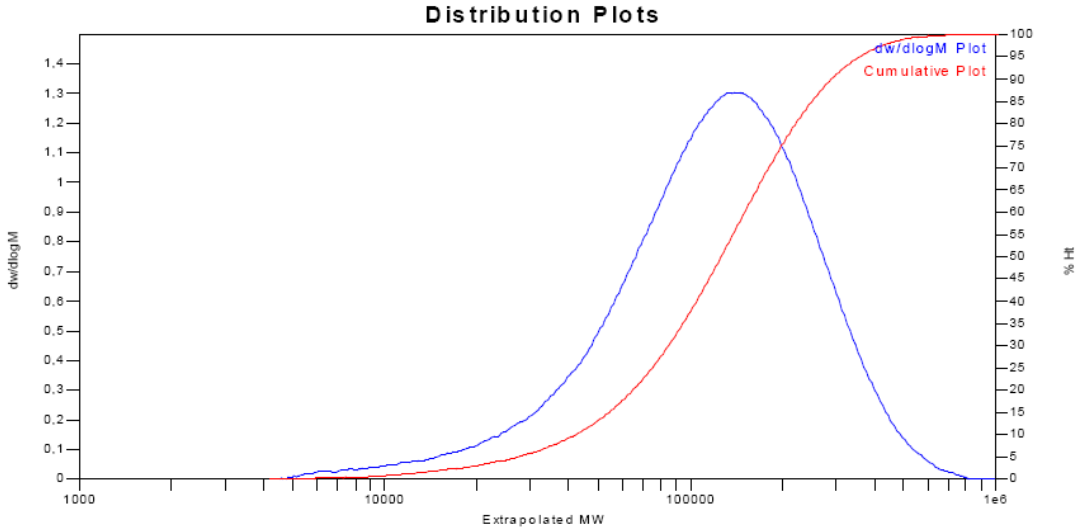

Figure 4.4: GPC of polypropene sample produced by $[(SBI)Zr(\mu\text{-}H)_3(Al^{i}Bu_2)_2]^+$.

The NMR data of the polymer product show that chain growth is terminated mainly by β-hydride transfer from Zr-bound polymer chains either to Zr or propene. Any zirconocene hydride thus generated, e.g., of the type $[(SBI)ZrH^{+\cdots}(F_5C_6)_4B^-]$, would be expected to

rapidly react, either with propene to start a new chain, or with HAl^iBu_2 to regenerate of the trihydride cation, $[(SBI)Zr(\mu\text{-}H)_3(Al^iBu_2)_2]^+$, such that this cation remains the dominant catalyst resting state.

Confirmation that $[(SBI)Zr(\mu\text{-}H)_3(Al^iBu_2)_2]^+$ is capable of polymerization propene provides the final piece of evidence that the hydride species observed by Babushkin and Brintzinger[10] is in fact $[(SBI)Zr(\mu\text{-}H)_3(AlR_2)_2]^+$ where R is a mixture of methyl and isobutyl groups. That the trihydride cation is not consumed during the course of the polymerization is compelling evidence that $[(SBI)Zr(\mu\text{-}H)_3(Al^iBu_2)_2]^+$ is a dormant state for polymerizations and, so, is capable of building up under the right conditions.

4.3.2 Reaction of $[(SBI)Zr(\mu\text{-}H)_3(AlMe_2)_2]^+$ with Propene

Closely related reaction systems containing the $\{AlMe_2\}$-complexed trihydride cation, $[(SBI)Zr(\mu\text{-}H)_3(AlMe_2)_2]^+$, yield markedly different results. A toluene-d_8 solution of $[(SBI)Zr(\mu\text{-}H)_3(AlMe_2)_2]^+$ was prepared by reaction of $(SBI)ZrCl_2$ with 20 equiv of $HAlMe_2$ and 1 equiv of $[Ph_3C][B(C_6F_5)_4]$. Reaction of $[(SBI)Zr(\mu\text{-}H)_3(AlMe_2)_2]^+$ with 40 equiv propene at –30 ºC was monitored by ^1H NMR (Figure 4.5). Over an initial period of ca. 2 h, the *H*$AlMe_2$ signal at 2.72 ppm diminishes together with the signals of propene, while signals at 1.36 and 1.05 ppm are growing in. An additional signal, at 3.59 ppm, grows in during the initial phase of the reaction but then vanishes as all the hydride is consumed. Virtually the same results are obtained with reaction systems containing both

the trihydride cation, $[(SBI)Zr(\mu\text{-}H)_3(AlR_2)_2]^+$, and the dimethyl-bridged cation, $[(SBI)Zr(\mu\text{-}Me)_2AlR_2]^+$, with R = Me or ^{i}Bu obtained by adding 25 equiv $AlMe_3$ to a solution of $[(SBI)Zr(\mu\text{-}H)_3(Al^iBu_2)_2]^+$ generated, as above, with 10 equiv of HAl^iBu_2 and then 1 equiv of $[Ph_3C][B(C_6F_5)_4]$ (Figure 4.6).

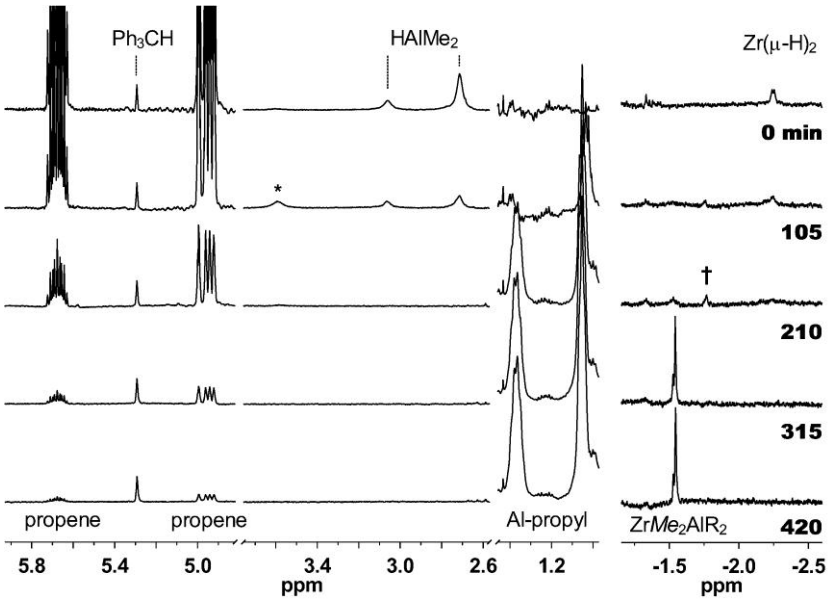

Figure 4.5: ^{1}H NMR spectra of a toluene-d_8 solution of the cation $[(SBI)Zr(\mu\text{-}H)_3(AlMe_2)_2]^+$ taken immediately, 105, 210, 315, and 420 min after warming to –30 ºC in the presence of 40 equiv of propene. †, signal due to intermediate species; *, signal due to AlR_3 adduct of $HAlMe_2$.

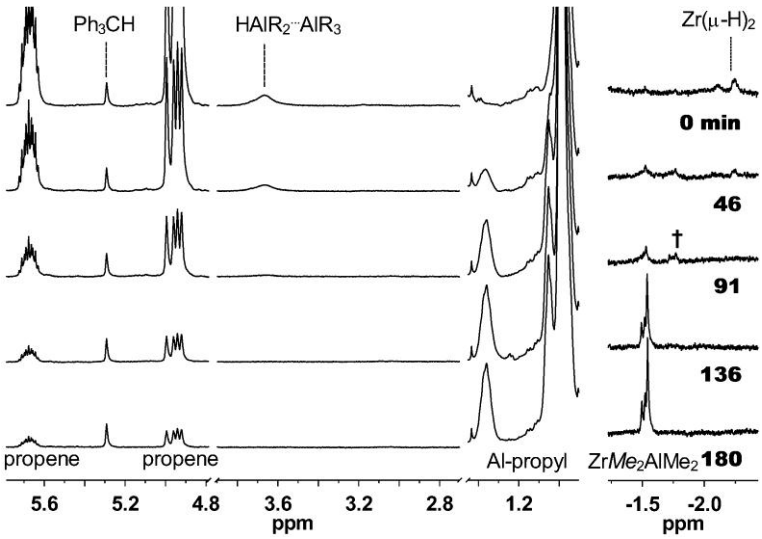

Figure 4.6: ^{1}H NMR spectra of a toluene-d_8 solution of $[(SBI)Zr(\mu\text{-}H)_3(Al^{i}Bu_2)_2]^{+}$ with 25 equiv $AlMe_3$ taken immediately, 46, 91, 136 and 180 minutes after warming to –30 ºC in the presence of 20 equiv propene. †, signal due to intermediate species.

The new peaks at 1.36 and 1.05 ppm were initially speculated to be due to the β-CH_2 and CH_3 groups respectively of Al-^{n}Pr species due to their proximity to the methyne and methyl signals of the Al-^{i}Bu groups. Warming a solution such as that in Figure 4.6 to room temperature resulted in a ^{1}H NMR (Figure 4.7 **A**) spectrum which was unable to unambiguously confirm that these resonances were due to Al-^{n}Pr as there was significant overlap with isobutyl resonances, however a gCOSY (Figure 4.7 **B**) did establish these resonances are in fact coupled to each other, as well as another resonance, which overlapped with the methylene resonance of Al-^{i}Bu, consistent with the α-CH_2 of an Al-^{n}Pr. To confirm this assignment, the solution was quenched with an excess of phenol to protonate any Al-alkyls. The production of propane, in addition to methane, was observed by ^{1}H NMR (Figure 4.8) [11] confirming the formation of $^{n}PrAlR_2$ during the course of the

disappearance of hydride. The peak at 3.59 ppm is also explained by this reaction. Eisch has observed[12-13] the formation of adducts of $HAlR_2$ and AlR_3 with chemical shifts downfield of that of free HAl^iBu_2. Independent confirmation of this was provided by the addition of $AlMe_3$ to a toluene-d_8 solution of $HAlMe_2$ which yielded a new hydride resonance at 3.67 ppm at room temperature. The appearance of such a peak during the initial phase of the reaction when $HAlMe_2$ is used as the aluminum hydride is consistent with the formation of a trialkylaluminum species in Figure 4.5. In the reaction with $HAl^iBu_2/AlMe_3$, this peak is present from the outset of the reaction due to the presence of a large amount of trialkylaluminum species in the initial reaction mixture. In both cases, once all hydride is consumed, this peak is no longer observed. These observations indicate that propene is reacting with $HAlMe_2$ via hydroalumination to yield $^nPrAlMe_2$.

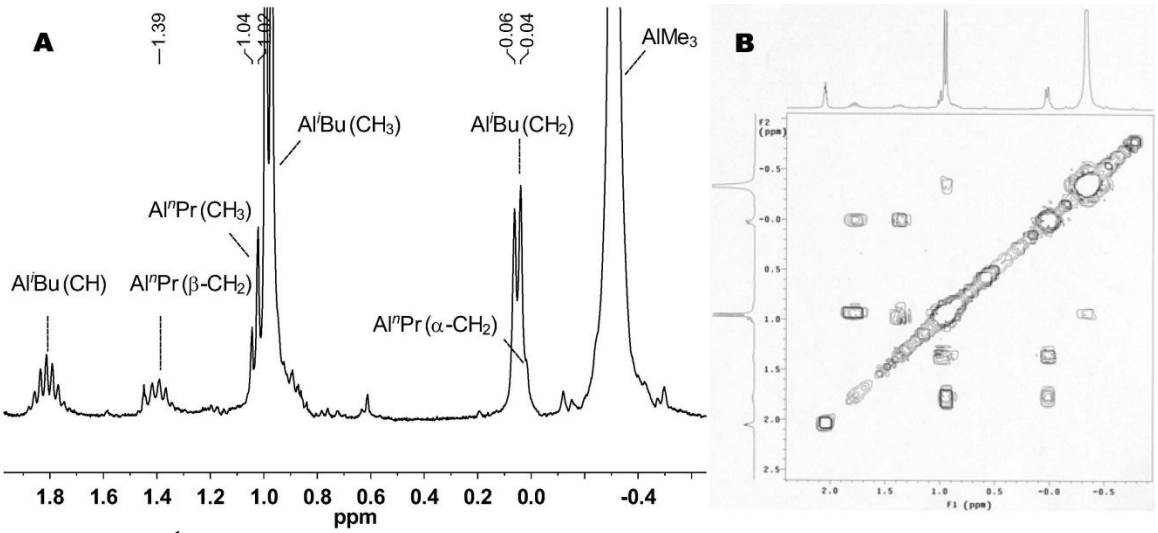

Figure 4.7: ^1H NMR (**A**) and gCOSY (**B**) at 25 ºC of alkyl region of a solution of $^nPrAlR_2$ prepared by reaction of propene with mixture of $[(SBI)Zr(\mu\text{-}H)_3(Al^iBu_2)_2]^+$ and $[(SBI)Zr(\mu\text{-}Me)_2AlMe_2]^+$ at –30 ºC.

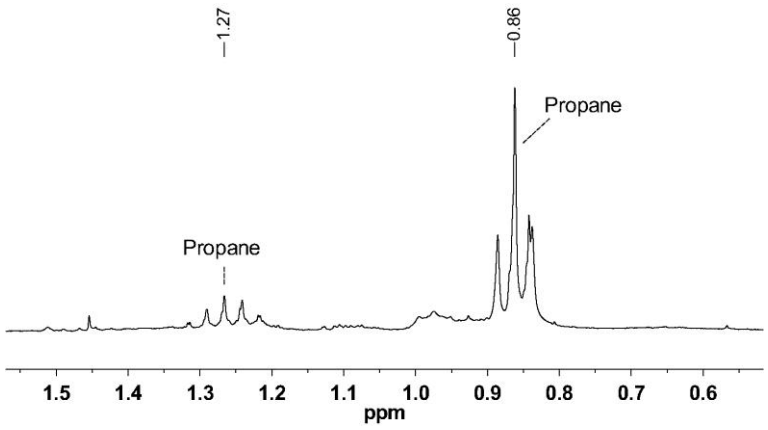

Figure 4.8: ^{1}H NMR of polymer solution produced from $[(SBI)Zr(\mu\text{-}H)_3(Al^{i}Bu_2)_2]^{+}$ and $[(SBI)Zr(\mu\text{-}Me)_2AlMe_2]^{+}$ quenched with phenol.

Olefin hydroaluminations are well known to be catalyzed by zirconocene hydrides;[14-22] they are generally accepted to occur by olefin insertion into Zr-H bonds and subsequent alkyl-hydride exchange between Zr and Al centers. It is surprising that in the present system hydroalumination occurs only if $HAlMe_2$ or $AlMe_3$ is present in the reaction medium and not at all with $HAl^{i}Bu_2$ alone. The divergent reactivity of systems containing $AlMe_3$ and those without is not easily explained.

When using $HAl^{i}Bu_2$ as the source of hydride equivalents, hydroalumination is only observed upon addition of $AlMe_3$. It is observed, however, that a threshold amount of $AlMe_3$ is required before the switch in reactivity occurs. Only after all hydride is converted to the $R_2AlH\cdots AlR_3$ form is hydroalumination observed, while the hydride spectrum shown in Figure 4.9 **D**, in which a ratio of $HAl^{i}Bu_2$ to $AlMe_3$ of 10 to 5 has been employed, results solely in polymerization of propene. The possibility that the AlR_3 adduct of $HAlR_2$ is more

prone to transmetallation than the pure $HAl^{i}Bu_2$ trimer or mixed $ClAlR_2$ clusters can be ruled out though by the observation that $HAlMe_2$, by itself, yields the hydroalumination product, thus the divergent reactivity must be related to the presence of sufficient methyl groups and not to a change in the speciation of the aluminum hydride clusters. From our present results, we cannot determine what thermodynamic and/or kinetic factors are responsible for this difference in reactivity. It is, however, worth mentioning that it has been shown that the degenerative rate of exchange between zirconocene methyls and $MeAlR_2$ species, as expected, decreases as the bulk of R is increased from methyl to 2,6-di-*tert*-butyl-4-Me-phenoxide.[23]

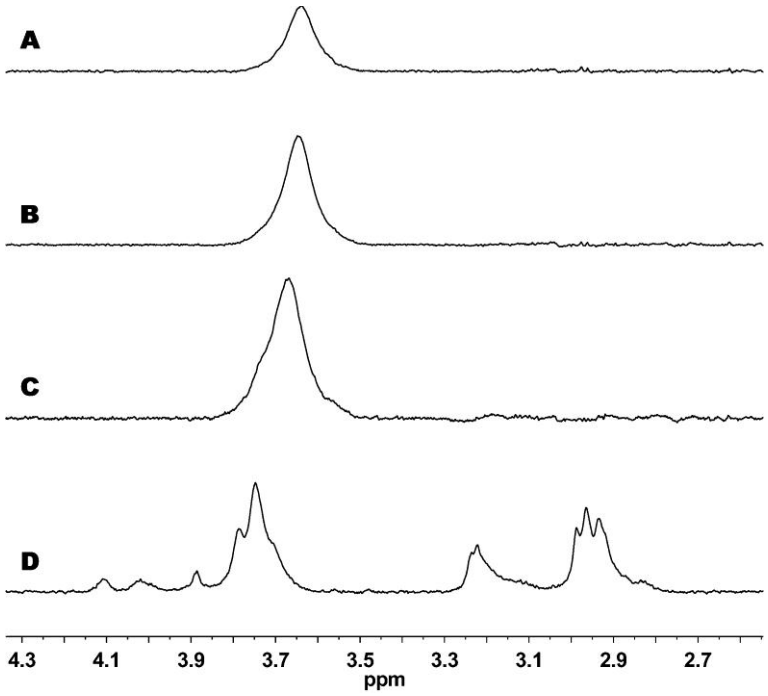

Figure 4.9: Al-hydride region of ^{1}H NMR spectra at –30 ºC of catalyst mixtures of $(SBI)ZrCl_2$, $[Ph_3C][B(C_6F_5)_4]$, x $HAl^{i}Bu_2$ and y $AlMe_3$. **A**: x = 5, y = 50. **B**: x = 10, y = 50. **C**: x = 10, y = 25. **D**: x = 10, y = 5. In all cases except **D** hydroalumination occurred upon exposure to propene.

During the course of the hydroalumination reaction, the signals of the trihydride cation $[(SBI)Zr(\mu\text{-}H)_3(AlR_2)_2]^+$ diminish in size together with the decreasing concentration of Al hydrides while, simultaneously, those of $^n PrAlR_2$ appear (Figure 4.10). The hydroalumination reaction appears to be the exclusive reaction during the initial phase of propene consumption as shown by the equal rates of disappearance of propene and aluminum hydride over this period. Thus the transmetallation reaction must be significantly faster than the second insertion of propene which is not the case in the system with only isobutyl groups. The apparent zero order nature of the hydroalumination reaction suggests that an initial dissociative event of the trihydride cation must occur as the rate limiting step, however the kinetics of this step and further elucidation of the reaction is ongoing.

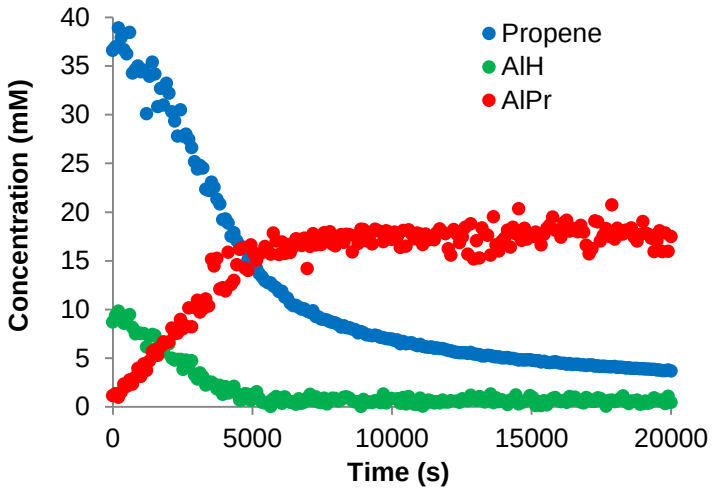

Figure 4.10: Concentration of propylene and Al species over the course of hydroalumination and polymerization reactions from a mixture of $(SBI)ZrCl_2$, $[Ph_3C][B(C_6F_5)_4]$, HAl^iBu_2, $AlMe_3$ and propene in a 1:1:5:50:20 ratio as monitored by ^1H NMR at –30 ºC.

Upon consumption of all the hydride, signals assignable to $[(SBI)Zr(\mu\text{-}Me)_2AlR_2]^+$ grow in. When Al hydride species are no longer detectable, the signals of $[(SBI)Zr(\mu\text{-}H)_3(AlR)_2]^+$ have likewise vanished, due to its conversion to $[(SBI)Zr(\mu\text{-}Me)_2AlR_2]^+$ according to Scheme 4.1. The ensuing catalyst system continues to consume propene, giving rise now to polypropene, which ^{13}C NMR (Figure 4.12) shows to be as isotactic as that obtained with $[(SBI)Zr(\mu\text{-}H)_3(Al^iBu_2)_2]^+$. Isopropyl end groups are the most abundant end groups in this polymer which is to be expected if chain growth is mainly terminated by chain transfer to Al rather than β-hydride transfer. Accordingly, GPC analysis (Figure 4.13) yields a substantially diminished mean degree of polymerization, $P_n \approx 45$. P_n is still significantly higher than would be expected from the ratio of propene to Zr (20:1) and even more so after taking into account the 9 equiv of propene which are consumed through hydroalumination, which gives an 11:1 ration of propene to Zr at the onset of polymerization. After consumption of all Al hydride, the dimethyl-bridged complex, $[(SBI)Zr(\mu\text{-}Me)_2AlR_2]^+$, becomes the sole detectable catalyst species in these reaction systems (Scheme 4.2).

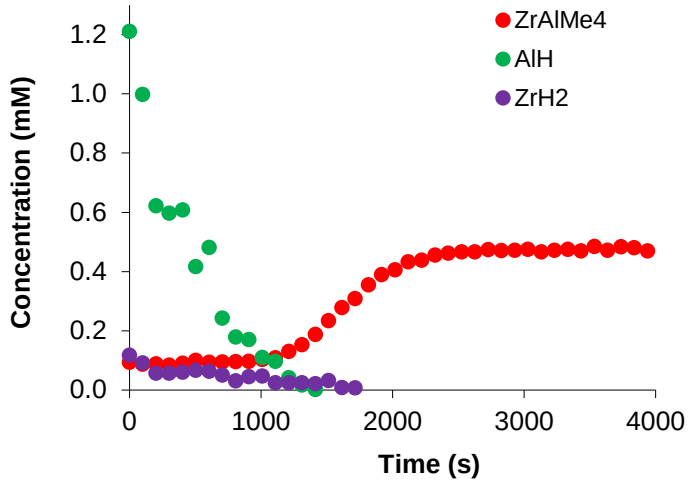

Figure 4.11: Concentration of $[(SBI)Zr(\mu\text{-}Me)_2AlR_2]^+$, $[(SBI)Zr(\mu\text{-}H)_3(AlR)_2]^+$ and $HAlR_2$ over the course of hydroalumination and polymerization reaction from a mixture of $(SBI)ZrCl_2$, $[Ph_3C][B(C_6F_5)_4]$, HAl^iBu_2, $AlMe_3$ and propene in a 1:1:10:50:20 ratio as monitored by ^1H NMR at –30 ºC.

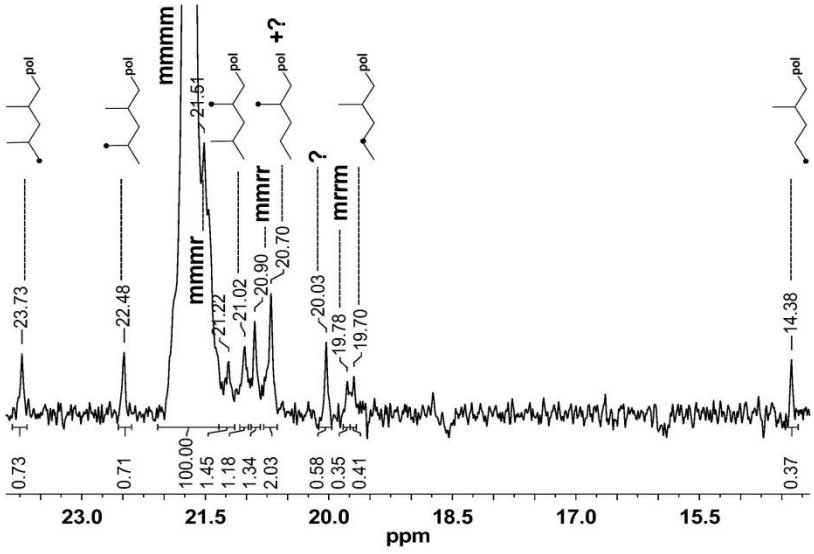

Figure 4.12: ^{13}C NMR spectrum of polypropene produced by $[(SBI)Zr(\mu\text{-}H)_3(Al^iBu_2)_2]^+$ and $AlMe_3$ *(vide supra)* in tetrachloroethane-d_2 solution at 120 ºC.

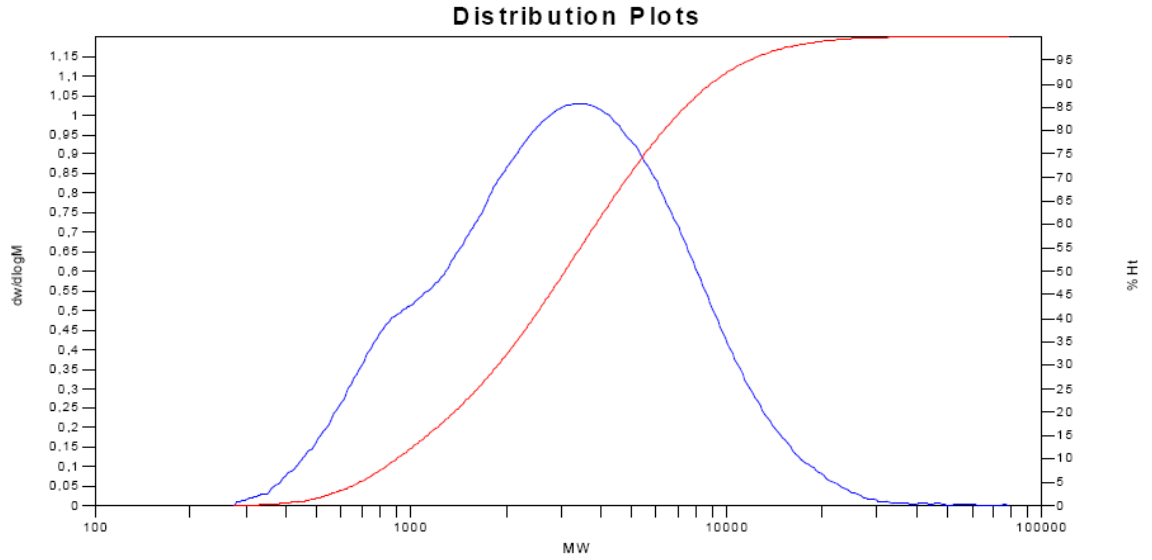

Figure 4.13: GPC trace of polymer sample prepared with a mixture of [(SBI)Zr(μ-H)$_3$(Al^{i}Bu$_2$)$_2$]$^+$ and AlMe$_3$.

Scheme 4.2

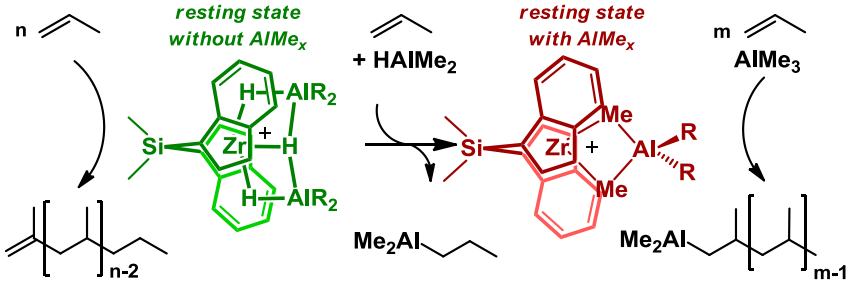

That use of [(SBI)Zr(μ-H)$_3$(AlMe$_2$)$_2$]$^+$ results in consumption of hydride suggests that, in MAO-activated systems, the hydride cation will not become the dominant species in solution, however under different conditions than the quite limited ones studied here it is possible that a steady state concentration of [(SBI)Zr(μ-H)$_3$(AlR$_2$)$_2$]$^+$ might accumulate as hydride equivalents are generated by β-hydride elimination and consumed by insertion of olefin into zirconocene hydrides.

4.4 Conclusions

The results presented above show that the {Al^{i}Bu$_2$}-complexed cation, [(SBI)Zr(μ-H)$_3$(Al^{i}Bu$_2$)$_2$]$^+$, is a catalyst for propene polymerization, while its {AlMe$_2$}-complexed analogue, [(SBI)Zr(μ-H)$_3$(AlMe$_2$)$_2$]$^+$, is primarily a catalyst for the hydroalumination of propene, being converted, in the course of this reaction, to the cation [(SBI)Zr(μ-Me)$_2$AlR$_2$]$^+$, another catalyst for propene polymerization. The confirmation that the trihydride cation is a polymerization catalyst provides the final piece of evidence to confirm its relevance to propene polymerization. Thus it can be confirmed that [(SBI)Zr(μ-H)$_3$(AlR$_2$)$_2$]$^+$ is the species observed by Babushkin and Brintzinger[3] upon addition of HAl^{i}Bu$_2$ or Al^{i}Bu$_3$ to (SBI)ZrCl$_2$/MAO mixtures. The possibility of hydrides as dormant species in polymerization seems to be plausible based on the observation that insertion of propene into [(SBI)Zr(μ-H)$_3$(Al^{i}Bu$_2$)$_2$]$^+$ occurs, but this initial insertion, is significantly slower than further insertions as seen by the significantly higher P_n than would be expected from the ratio of propene to Zr. This is consistent with the recent stopped-flow NMR results of Landis.[24] Further work remains to determine detailed kinetic parameters for the polymerization reactions presented here in order to determine the extent to which hydrides would be expected to accumulate during the course of polymerization and if that could account to for the unobserved Zr of Babushkin and Brintzinger[25] and that which is inferred by the kinetic models of Abu-Omar and Caruthers.[26]

4.5 Experimental

General Experimental Details. All operations were carried out under a protective dinitrogen atmosphere, either in a glovebox or on a vacuum manifold. Phenol was obtained from J. T. Baker and used as obtained. Deuterated solvents were obtained from Cambridge Isotope Laboratories. Tetrachloroethane-d_2 and benzene-d_6 were used as obtained. Toluene was obtained from EMD Chemicals. Toluene (d_8 and d_0) was dried by vacuum transfer from "titanocene".[27] (SBI)$ZrCl_2$ was purchased from Strem Chemicals and used as obtained. $AlMe_3$ and HAl^iBu_2 were used as obtained as neat compounds from Aldrich Chemical Company. $HAlMe_2$ was prepared as reported in Chapter 3. NMR spectra were obtained using Varian Inova 500 or Mercury 300 spectrometers. Chemical shifts are referenced to residual solvents peaks, 7.00 ppm for the central aromatic proton resonance of toluene and 6.00 ppm for the ^1H signal of tetrachloroethane. Polypropene ^{13}C NMR spectra were referenced to 21.69 ppm for the mmmm pentad of the methyl signal. GPC measurements were conducted, at 160 ºC and a flow rate of 1 ml/min in 1,2,4-trichlorobenzene, by means of a Polymer Laboratories instrument with three "PLgel Olexis" columns, using either triple detection (refractory index RI, viscosity DP, and light scattering LS15 + LS90) or linear calibration (RI, polyethylene standards).

NMR scale reaction of propene with $[(SBI)Zr(\mu\text{-}H)_3(Al^iBu_2)_2]^+$. A 3.1 mM solution of $[(SBI)Zr(\mu\text{-}H)_3(Al^iBu_2)_2]^+$ was prepared by adding a solution of 1.0 mg (2.2 μmol) of (SBI)$ZrCl_2$ and 7.9 μL (44 μmol, 20 equiv) of HAl^iBu_2 in 0.7 mL of toluene-d_8 to 2.1 mg

(2.3 μmol, 1 equiv) of $[Ph_3C][B(C_6F_5)_4]$ in a 1 dram vial. The solution was transferred to a J-Young tube and cooled to liquid-nitrogen temperature. From a calibrated gas bulb, 44.3 μmol (20 equiv) of propene were condensed onto the frozen solution. The tube was warmed to −78 ºC in a dry ice/acetone bath and the contents mixed at this temperature. The tube was then inserted into an NMR spectrometer cavity thermostated at –30 ºC. ^{1}H NMR spectra (8 scans, 2.6 s acquisition, 10 s delay) were measured immediately after thermal equilibration and then at intervals of 101 seconds. An identical experiment was set up with 88.1 μmol (40 equiv) of propene. The tube was warmed to −78 ºC in a dry ice/acetone bath and the contents mixed at this temperature. The tube was then placed in an acetone bath maintained at −30 °C for 6 hours after which time the tube was removed and allowed to warm to room temperature. A ^{1}H NMR spectrum was which shows no new alkylaluminum species.

NMR scale reaction of propene with $[(SBI)Zr(\mu\text{-}H)_3(AlMe_2)_2]^+$. A 3.1 mM solution of $[(SBI)Zr(\mu\text{-}H)_3(AlMe_2)_2]^+$ was prepared as above, except 2.5 mg $HAlMe_2$ (43 μmol, 20 equiv) were substituted for the HAl^iBu_2. The solution was transferred to a J-Young tube and cooled to liquid-nitrogen temperature. From a calibrated gas bulb, 88.2 μmol (40 equiv) of propene were condensed onto the frozen solution. The NMR tube was warmed to −78 ºC in a dry ice/acetone bath and the contents mixed at this temperature. The NMR tube was then inserted into an NMR spectrometer cavity thermostated at –30 ºC. ^{1}H NMR spectra (1 scan, 10 s acquisition, 0 s delay) were measured immediately after thermal equilibration and then at intervals of 300s.

NMR scale reaction of propene with a mixture of $[(SBI)Zr(\mu\text{-}H)_3(Al^iBu_2)_2]^+$ and $AlMe_3$. As above, a 3.1 mM solution of $[(SBI)Zr(\mu\text{-}H)_3(Al^iBu_2)_2]^+$ was prepared with 4.0 μL HAl^iBu_2 (22 μmol, 10 equiv). 5.3 μL $AlMe_3$ (55 μmol, 25 equiv) was added to the J-Young NMR tube and the solution was cooled to liquid-nitrogen temperature. From a calibrated gas bulb, 44.3 μmol (20 equiv) of propene were condensed onto the frozen solution. The NMR tube was warmed to −78 ºC in a dry ice/acetone bath and the contents mixed at this temperature. The NMR tube was then inserted into an NMR spectrometer cavity thermostated at –30 ºC. ^1H NMR spectra (8 scans, 2.6 s acquisition, 10 s delay) were measured immediately after thermal equilibration and then at intervals of 300s. Spectra thus obtained are shown in Figure 4.6.

Assignment of ^{n}Pr-AlR_2. A solution prepared similar to above was allowed to warm to room temperature following consumption of all of the propene. One clear new multiplet is observed for the Al-$CH_2CH_2CH_3$ (β-CH_2) at 1.39 ppm while signals for the Al-$CH_2CH_2CH_3$ (α-CH_2) and Al-$CH_2CH_2CH_3$ overlapped with signals from Al-^{i}Bu groups (Figure 4.7). A gCOSY was obtained (Figure 4.7B) which showed that the β-CH_2 signal couples to peaks overlapping with the isobutyl methyl and methylene signals.

Further evidence for the assignment of the signals to an aluminum propyl was obtained by quenching a sample as described in above with phenol. The sample was allowed to warm to room temperature following consumption of all propene. A J-Young to 14/20 adapter was attached to the top of the J-Young tube and connected to a Schlenk line. Under an Ar flow

a solution of 9.2 mg phenol in 0.25 ml benzene-d_6 was added to the top of the J-Young valve. Upon opening the valve the vacuum present in the NMR tube pulled the phenol solution into the NMR tube which was cooled to –78 ºC in a dry ice/acetone bath. The top of the tube was washed with a further 0.1 ml benzene-d_6. The tube was closed and shaken resulting in a loss of color, formation of precipitate (presumably $Al(OPh)_3$) and bubbling. A ^{1}H NMR was obtained (Figure 4.8) which clearly showed signals due to propane at 1.27 (spt, $^3J_{HH}$ = 7 Hz) and 0.86 (t, $^3J_{HH}$ = 7 Hz) in addition to signals for excess phenol and CH_4 (not shown).

Larger scale reaction of propene with [(SBI)Zr(μ-H)$_3$(Al^{i}Bu$_2$)$_2$]$^+$. To obtain sufficient polymer for NMR measurements, reactions were conducted on a somewhat larger scale under the same conditions as described above. In a 25-mL side-arm flask a toluene solution containing 10.0 mg (22.3 μmol) of (SBI)$ZrCl_2$, 79.5 μL (446 μmol, 20 equiv) of HAl^iBu_2 and 20.6 mg (22.3μmol, 1 equiv) of $[Ph_3C][B(C_6F_5)_4]$ was cooled in liquid nitrogen. From a calibrated gas bulb, 103.66 mL of propene at a pressure of 79 mm Hg (440 μmol, 20 equiv), was condensed onto the frozen reaction mixture. The flask was warmed to –30 ºC and stirred at this temperature. After ca. 4 hours, the reaction was quenched by addition of a methanol/HCl mixture and the polymer isolated by filtration and dried overnight at room temperature in a dynamic vacuum. Yield 19.8 mg. Of this polymer, a saturated solution in ca. 0.7 mL of tetrachloroethane-d_2 was prepared at 120 ºC and ^{1}H and ^{13}C spectra were taken at this temperature. The ^{1}H NMR spectrum was recorded after measuring a ^{13}C NMR spectrum at 120 ºC for a period of 13 hours. Some isomerization of H_2C=C(Me)-CH_2-

C(Me)- to H_3C-C(Me)=C*H*-C(Me)- must have occurred during this time, as indicated by a broad signal at 4.9-5.0 ppm. The polymer is found to be highly isotactic with [mmmm] = 0.96. No end group signals are detectable by ^{13}C NMR. Another polypropene sample was prepared, under otherwise identical conditions, using a higher ration of [propene]/[Zr] = 40. Gel permeation chromatography (GPC) of a polypropene sample, analogously prepared as described above at [propene]/[Zr] = 40, yielded a polydisperity index (PDI) of 1.90 and a number-average molar mass M_n = 78,921 (Figure 4.4), equivalent to a mean degree of polymerization P_n = 1880.

Larger scale reaction of propene with a mixture of $[(SBI)Zr(\mu\text{-}H)_3(Al^iBu_2)_2]^+$ and $AlMe_3$. In analogy to the previous case, a 25-mL side-arm flask, containing a toluene solution of 10.0 mg (22.3 μmol) of $(SBI)ZrCl_2$, 20.6 mg (22.3 μmol, 1 equiv) of $[Ph_3C][B(C_6F_5)_4]$, 39.7 μL (223 μmol, 10 equiv) of HAl^iBu_2 and 53.4 μL (557 μmol, 25 equiv) of $AlMe_3$ was cooled in liquid nitrogen and 904 μmol (25 equiv) of propene were condensed onto the frozen reaction mixture. The flask was warmed to –30 ºC and stirred at this temperature for ca. 4 hours. After quenching the reaction with methanol/HCl, the polymer was isolated by filtration and dried overnight at room temperature in a dynamic vacuum to yield 29.2 mg of polypropene. Of this polymer, a saturated tetrachloroethane-d_2 solution was prepared at 120 ºC and ^1H and ^{13}C spectra were taken at this temperature. Comparison of the combined integral of the H_2C=C signals at 4.74 and 4.81 ppm with that of the main-chain signals indicates that one H_2C=C group is present per 1325 main-chain units. The polymer is found to be highly isotactic with [mmmm] = 0.96. Most abundant end

groups are iso-propyl groups, which arise as chain ends from hydrolysis of $AlMe_2$-capped chains, produced by polymer-vs.-Me exchange between Zr and Al centers and, as a consequence, also as chain starts from propene insertion into the Zr-Me bonds formed by such an exchange. The abundance of iso-propyl groups, as measured from the well-resolved signals at 11.48 and 23.73 ppm, is 0.72 per 98 steroregular main-chain units (integrals estimated for an unresolved iso-propyl signal at 21.51 ppm (0.72, vide supra) and for the mmmr pentad at 21.40 ppm (1.34 = [mmrr]) have to be subtracted from the main signal at 21.69 ppm). For *n*-propyl chain starts an abundance of 0.39 per 98 main-chain units is estimated from the signals at 14.38 and 19.70 ppm. Based on this estimate, the n-propyl signal at 20.70 ppm is too large. Apparently, it coincides with another signal close to it. For this signal, as for another signal observed at 20.03 ppm, no obvious assignments are apparent at this time.

The abundance of n-propyl chain starts, which arise either from propene insertion into Zr-H bonds generated by β-H transfer to the metal or from β-H transfer to a monomer, is normally equal to that of unsaturated chain ends, since either one of these processes produces a 2-propenyl end group. In the present polymer, however, unsaturated chain ends are hardly detectable at all from ^{13}C NMR spectra, while the ^{1}H NMR spectrum indicates an abundance of ca. 0.073 H_2C=C groups per 98 main-chain units, i.e. ca. 5 times less than *n*-propyl chain starts. Apparently, a substantial fraction of chains start by propene insertion into Zr-H bonds, which are derived from residual H-Al units still present is the reaction

system, rather than from β-H transfer, while the growth of almost all chains is eventually terminated by transfer from Zr to Al. A mean degree of polymerization, P_n = 45, corresponds to the number-average molar mass M_n = 1,873, obtained together with a value of PDI = 2.10 from a GPC analysis of this polymer sample (Figure 4.13).

4.6 References

1. Bochmann, M.; Lancaster, S. J. *Angew. Chem.-Int. Edit. Engl.*, **1994**, *33*, 1634.
2. Bochmann, M.; Lancaster, S. J. *J. Organomet. Chem.*, **1995**, *497*, 55.
3. Babushkin, D. E.; Brintzinger, H. H. *Chem.-Eur. J.*, **2007**, *13*, 5294.
4. Gregorius, H.; Fraaije, V.; Lutringhauser, M. Patent DE10258968, 1994.
5. Ohno, R.; Tsutsui, T. Patent EP0582480, 1994.
6. Kleinschmidt, R.; van der Leek, Y.; Reffke, M.; Fink, G. *J. Mol. Catal. A-Chem.*, **1999**, *148*, 29.
7. Kaminaka, M.; Matsuoka, H. Patent JP11240912, 1999.
8. Wang, S. Patent US2005070675, 2005.
9. Landis, C. R.; Christianson, M. D. *P. Natl. Acad. Sci. USA*, **2006**, *103*, 15349.
10. Babushkin, D. E.; Panchenko, V. N.; Timofeeva, M. N.; Zakharov, V. A.; Brintzinger, H. H. *Macromol. Chem. Phys.*, **2008**, *209*, 1210.
11. Fulmer, G. R.; Miller, A. J. M.; Sherden, N. H.; Gottlieb, H. E.; Nudelman, A.; Stoltz, B. M.; Bercaw, J. E.; Goldberg, K. I. *Organometallics*, **2010**, *29*, 2176.
12. Eisch, J. J.; Rhee, S. G. *J. Organomet. Chem.*, **1972**, *42*, C73.
13. Eisch, J. J.; Rhee, S. G. *J. Organomet. Chem.*, **1972**, *38*, C25.
14. Negishi, E.; Kondakov, D. Y. *Chem. Soc. Rev.*, **1996**, *25*, 417.
15. Dzhemilev, U. M.; Ibragimov, A. G. *Russ. Chem. Rev.*, **2000**, *29*, 121.
16. Negishi, E.; Tan, Z. *Top. Organomet. Chem.*, **2005**, *8*, 139.

17. Parfenova, L. V.; Pechatkina, S. V.; Khalilov, L. M.; Dzhemilev, U. M. *Russ. Chem. Bull.*, **2005**, *54*, 316.
18. Parfenova, L. V.; Balaev, A. V.; Gubaidullin, I. M.; Abzalilova, L. R.; Pechatkina, S. V.; Khalilov, L. M.; Spivak, S. I.; Dzhemilev, U. M. *Int. J. Chem. Kinet.*, **2007**, *39*, 333.
19. Parfenova, L. V.; Vil'danova, R. F.; Pechatkina, S. V.; Khalilov, L. M.; Dzhemilev, U. M. *J. Organomet. Chem.*, **2007**, *692*, 3424.
20. Dzhemilev, U. M.; Ibragimov, A. G., In *Modern Reduction Methods*, Andersson, P. G.; Munslow, P. J., Eds. Wiley-VCH: Weinheim, 2008; p 447.
21. Pankratyev, E. Y.; Tyumkina, T. V.; Parfenova, L. V.; Khalilov, L. M.; Khursan, S. L.; Dzhemilev, U. M. *Organometallics*, **2009**, *28*, 968.
22. Parfenova, L. V.; Berestova, T. V.; Tyumkina, T. V.; Kovyazin, P. V.; Khalilov, L. M.; Whitby, R. J.; Dzhemilev, U. M. *Tetrahedron: Asymmetry*, **2010**, *21*, 299.
23. Siedle, A. R.; Newmark, R. A.; Lamanna, W. M.; Schroepfer, J. N. *Polyhedron*, **1990**, *9*, 301.
24. Christianson, M. D.; Tan, E. H. P.; Landis, C. R. *J. Am. Chem. Soc.*, **2010**, *132*, 11461.
25. Babushkin, D. E.; Brintzinger, H. H. *J. Am. Chem. Soc.*, **2010**, *132*, 452.
26. Novstrup, K. A.; Travia, N. E.; Medvedev, G. A.; Stanciu, C.; Switzer, J. M.; Thomson, K. T.; Delgass, W. N.; Abu-Omar, M. M.; Caruthers, J. M. *J. Am. Chem. Soc.*, **2010**, *132*, 558.
27. Marvich, R. H.; Brintzinger, H. H. *J. Am. Chem. Soc.*, **1971**, *93*, 2046.

APPENDIX A

Determination of Equilibrium Constants from ^{1}H NMR of Species in Rapid Exchange

A.1 Abstract

The equilibrium constant for two species in rapid chemical exchange on the NMR time scale can be determined from the variation of the averaged chemical shift using a Benesi-Hildebrand type relation.

A.2 Introduction

Benesi and Hildebrand developed a relationship between the UV-vis spectrum of I_2 and benzene mixtures and the equilibrium between I_2 and ($I_2 \cdot C_6H_6$).[1] This relation has since been developed into a powerful tool for the analysis of complexation and host-guest interactions (A.1). In this appendix a similar analysis will be applied to NMR spectroscopic examination of complexation which was developed for a specific case of $AlMe_3$ complexation of a alkylaluminum-complexed zirconocene hydride but is in fact a general relationship.

$$C_6H_6 + I_2 \leftrightarrow C_6H_6 \cdot I_2 \qquad \text{A.1}$$

A.3 Adduct Formation

Adduct formation of (SBI)ZrCl(μ-H)$_2$Al^{i}Bu$_2$ with Al_2Me_6, is represented by Equation A.**2**, with **A** representing the starting complex, $\mathbf{X_2}$ the $AlMe_3$ dimer and **AX** the adduct, simple modification of this equilibrium can be made for any specific complexation.

$$A + \frac{1}{2}X_2 \leftrightarrow AX \quad \text{A.2}$$

Equation A.3 expresses the equilibrium constant, K, for this reaction:

$$K = \frac{[AX]}{[A]\sqrt{[X_2]}} \quad \text{A.3}$$

Under conditions of rapid exchange between **A** and **AX** the chemical shift of the resulting signal, δ, is the weighted average of the chemical shifts of **A**, δ_A, and **AX**, δ_{AX} (Equation A.4).

$$\delta = \frac{[A]}{[A]+[AX]}\delta_A + \frac{[AX]}{[A]+[AX]}\delta_{AX} \quad \text{A.4}$$

The difference in chemical shift, $\Delta\delta$, of the signal at any given concentration of added **X**, δ and that of pure **A** is given by Equation A.5.

$$\Delta\delta = \delta - \delta_A \quad \text{A.5}$$

Combining Equation A.4 and Equation A.5 we get:

$$\Delta\delta = \left(\frac{[A]}{[A]+[AX]} - 1\right)\delta_A + \frac{[AX]}{[A]+[AX]}\delta_{AX} \quad \text{A.6}$$

which simplifies to:

$$\Delta\delta = \frac{[AX]}{[A]+[AX]}(\delta_{AX} - \delta_A) \quad \text{A.7}$$

Expressing the maximum change in chemical shift as $\Delta\delta_{max}$, yields Equation A.8.

$$\Delta\delta_{max} = \delta_{AX} - \delta_A \quad \text{A.8}$$

Taking the reciprocal of Equation A.7 and using Equation A.8 gives Equation A.9:

$$\frac{1}{\Delta\delta} = \frac{1}{\Delta\delta_{max}} + \frac{1}{\Delta\delta_{max}} \cdot \frac{[A]}{[AX]} \quad \text{A.9}$$

Together with the equilibrium constant, Equation A.3, this yields a Benesi-Hildebrand type relation (Equation A.10):

$$\frac{1}{\Delta\delta} = \frac{1}{\Delta\delta_{max}} + \frac{1}{\Delta\delta_{max} K\sqrt{[X_2]}} \qquad \text{A.10}$$

Assuming that K is small, the amount of $\mathbf{X_2}$ added is approximately equal to the amount of $\mathbf{X_2}$ in solution. A plot of the reciprocal of the change in chemical shift against the reciprocal of the square root of the concentration of Al_2Me_6 added should thus be linear, with a slope of $1/(K*\Delta\delta_{max})$ and a y-axis intercept of $1/\Delta\delta_{max}$, neither of which should depend on $[Zr]_{TOT}$.

A.4 Exchange Reaction

The reaction of $(SBI)ZrCl(\mu\text{-}H)_2Al^iBu_2$ to exchange either the Zr-bound Cl or an Al-bound ^{i}Bu with one of the methyl groups of Al_2Me_6, to yield Al_2Me_5X where X = Cl or ^{i}Bu, is represented by Equation A.11, with **A** representing the starting $\{ZrClH_2\}$ complex, $\mathbf{X_2}$ the $AlMe_3$ dimer, **B** the exchange product and **Y** the Al_2Me_5X product:

$$A + X_2 \leftrightarrow B + Y \qquad \text{A.11}$$

Equation A.12 expresses the equilibrium constant, K_2, for the exchange reaction:

$$K_2 = \frac{[B][Y]}{[A][X_2]} \qquad \text{A.12}$$

We can use the same derivation as for Equation A.9, except [**AX**] is now replaced by [**B**].

$$\frac{1}{\Delta\delta} = \frac{1}{\Delta\delta_{max}} + \frac{1}{\Delta\delta_{max}} \cdot \frac{[A]}{[B]} \qquad \text{A.13}$$

Using the equilibrium constant, Equation A.12, this yields a Benesi-Hildebrand type relation (Equation A.14):

$$\frac{1}{\Delta\delta} = \frac{1}{\Delta\delta_{max}} + \frac{1}{\Delta\delta_{max}} \cdot \frac{[Y]}{K[X_2]} \qquad \text{A.14}$$

Since we are adding $\mathbf{X_2}$ to **A**, [**Y**] is equal to [**B**], yielding:

$$\frac{1}{\Delta\delta} = \frac{1}{\Delta\delta_{max}} + \frac{1}{\Delta\delta_{max}} \cdot \frac{[B]}{K[X_2]} \qquad \text{A.15}$$

Alternatively Equation A.15 can be modified by using the following relationship which is derived by combining Equation A.4, A.5 and A.8:

$$\Delta\delta = \Delta\delta_{max} \frac{[B]}{[A] + [B]} \qquad \text{A.16}$$

Solving for [**B**] and substituting into Equation A.15 gives:

$$\frac{1}{\Delta\delta} = \frac{1}{\Delta\delta_{max}} + \frac{\Delta\delta}{\Delta\delta_{max}} \cdot \frac{[A] + [B]}{\Delta\delta_{max} K[X_2]} \qquad \text{A.17}$$

With $[A] + [B] = [Zr]_{TOT}$ and $[X_2] = [Al_2Me_6]$, Equation A.17 can be rearranged to:

$$\left(\frac{\Delta\delta_{max}}{\Delta\delta} - 1\right) \frac{\Delta\delta_{max}}{\Delta\delta} = \frac{[Zr]_{TOT}}{K \cdot [Al_2Me_6]} \qquad \text{A.18}$$

The value of $\Delta\delta_{max}$ can be estimated from the chemical shift at the highest concentrations of Al_2Me_6. Assuming that K_2 is small, the amount of Al_2Me_6 added is approximately equal to the amount of Al_2Me_6 in solution. Therefore, a plot of the left side of Equation A.18 against $[Zr]_{TOT}/[Al_2Me_6]$ should give a straight line going through the origin, with a slope of 1/K, which should thus be independent of $[Zr]_{TOT}$.

A.5 Conclusion

The equilibrium constant for two species in rapid equilibrium can be obtained by monitoring the change in the averaged NMR chemical shift of the mixture as one component is added to solution. Complexation and exchange reactions can be differentiated based on the way the averaged chemical shift varies with concentration.

A.6 References

1. Benesi, H. A.; Hildebrand, J. H. *J. Am. Chem. Soc.*, **1949**, *71*, 2703.

APPENDIX B

Toward Synthesis of Zirconocene Polymerization Catalysts with Tethered Anions

B.1 Abstract

Zirconocene dichlorides with pendant boranes were synthesized via hydroboration of the analogous pendant olefins. These complexes show promise for the synthesis of zirconocenes with pendant anions, which will allow for the careful study of the effect of anions on metallocene catalyzed polymerization.

B.2 Introduction

As discussed in Chapter 1, the mechanism of polymerization of α-olefins by group 4 metallocene catalysts has been extensively studied and the general features of the transition state for propagation including how the metallocene ligand framework directs stereoselectivity have been established.[1-4] One remaining question concerns the extent to which and the manner in which the anion influences polymerization. Numerous experimental[5-17] and computational[18-30] studies have shown a limited influence of the anion on polymerization, mainly observed as an increase in polymerization rate with decreasing coordination ability of the anion. Stereospecificity is a bit more complex with some models suggesting an increase in stereospecificity with coordination ability[6, 11] while others show only a change in the relative rates of insertion to site epimerization which don't seem to correlate with coordination ability[10]. It would be desirable however to create a system in which it is possible to directly probe the influence of anion on the various steps of

polymerization. In furtherance of this goal it was imagined that tethering an anion to one side of a metallocene wedge would enable us to directly probe the nature of the cation-anion interaction by studying the influence of an anion that is in a fixed location relative to the polymerization center.

The tethering of an anion to a zirconocene to form a zwitterionic complex is by no means a new idea.[31-33] Attachment of the anion has been mainly focused on either the cylcopentadienyl rings or the ligands in the metallocene wedge. In the following, a method of tethering an anionic borate to the bridge in an *ansa*-metallocene is attempted such that tethering the anion will result in an observable change in the coordination chemistry of the zirconocene as well as a change in the stereoselectivity of propene polymerization of the metallocenes. Two metallocene frameworks were chosen which would be elaborated to tethered anionic complexes (Figure B.1). $Me_2Si(3\text{-}^tBu\text{-}C_5H_3)(C_5H_4)ZrCl_2$ ($^tBuSpZrCl_2$) produces a moderately isotactic polypropene ([mmmm] = 78%)[34-36] while $Me_2C(C_5H_4)$(fluorenyl) $ZrCl_2$ ((Ewen)$ZrCl_2$) produces syndiotactic polypropene ([rrrr] = 86%)[37] allowing considerable room for the anion to influence stereoselectivity in a positive or negative direction.

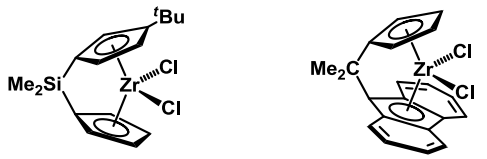

$^tBuSpZrCl_2$ (Ewen)$ZrCl_2$

Figure B.1: Complexes used as inspiration for current work

B.3 Results and Discussion

B.3.1 ^{t}BuSpZrCl$_2$ derived complexes

$Li_2(^{t}BuSp)$ has been synthesized via consecutive salt metathesis reactions from Me_2SiCl_2 and appropriately substituted LiCp reagents.[34] A similar approach was taken here using commercially available Me(vinyl)$SiCl_2$ (Scheme B.1). Reaction of $Li^{t}BuC_5H_4$ with an excess of Me(vinyl)$SiCl_2$ in thf yields the monosubstituted product in 96% yield. Further reaction with $Mg(C_5H_4)_2$ yields Me(vinyl)Si(3-^{t}Bu-C_5H_4)(C_5H_5). For these vinylsilane metathesis reactions it was found that the choice of Mg as the countercation for $[C_5H_5]^-$ was crucial as LiCp tended to give mixtures of products regardless of conditions. Deprotonation of the ligand proved challenging, giving multiple products including ones arising from addition of alkyl lithium reagents across the vinyl silane.

Scheme B.1

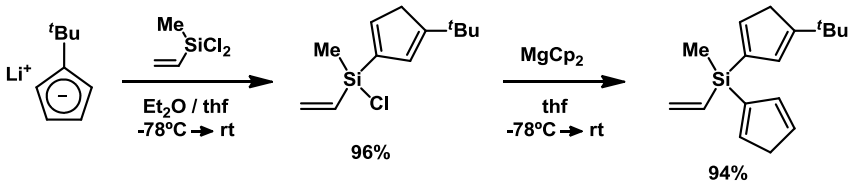

The Zr complex could be formed via amine elimination from $Zr(NMe_2)_4$ in a methodology developed by Jordan (Scheme B.2).[38-42] Thus reaction of Me(vinyl)Si(3-^{t}Bu-C_5H_4)(C_5H_5) with $Zr(NMe_2)_4$ afforded Me(vinyl)Si(3-^{t}Bu-C_5H_3)(C_5H_4)$Zr(NMe_2)_2$ in 86% yield as a 1:1 mixture of diastereomers. Reaction with an excess of Me_3SiCl affords the dichloride in 93% yield still as a 1:1 mixture of diastereomers. Hydroboration of the mixture with $HB(C_6F_5)_2$ resulted in disappearance of the vinyl resonances however at this point it was

decided that a more symmetric system was desirable, so as to allow for simpler NMR analysis and avoidance of the necessity of separation of the diastereomers. ^{19}F NMR revealed a complicated set of signals which seems consistent with diastereotopic complexes.

Scheme B.2

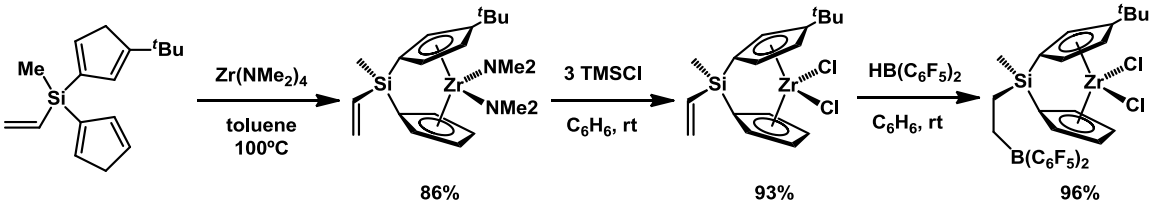

B.3.2 $Me_2C(Cp)(Flu)ZrCl_2$ derived complexes

Me(3-butenyl)C(C_5H_4)(fluorenyl)$ZrCl_2$ is a known precatalyst for olefin polymerization and has been utilized as a self-immobilizing catalyst under the assumption that the tethered olefin will become incorporated into polymeryl chains resulting in a zirconocene catalyst which has been "heterogenized" by covalent attachment to an insoluble polymer.[43-45] While it has since been shown that insertions of this type are in fact rare,[46] Me(3-butenyl)C(C_5H_4)(fluorenyl)$ZrCl_2$ remains a good catalyst for the synthesis of polyethene with low amounts of long chain branching.[47-49]

Hydroboration of Me(3-butenyl)C(C_5H_4)(fluorenyl)$ZrCl_2$ with $HB(C_6F_5)_2$ (Scheme B.3) proceeds rapidly and in high NMR yield to give the hydroborated complex Me($C_4H_8B(C_6F_5)_2$)C(C_5H_4)(fluorenyl)$ZrCl_2$. The high solubility of the pendant borane

complex hindered isolation of the product, which appeared to be quantitatively formed by NMR. Hydroboration is accompanied by the complete disappearance of olefinic signals as well as a splitting of the diastereotopic resonances of the Cp ring (Figure B.2). ^{19}F NMR yields the typical pattern of 3 peaks seen for C_6F_5 groups with a splitting between *meta* and *para* fluorides of 14.1 ppm comparable to that of free $B(C_6F_5)_3$ (18.0 ppm) or $HB(C_6F_5)_2$ (12.7 ppm), indicative of a three coordinate borane and also with that observed for $Me(C_2H_4B(C_6F_5)_2)Si(3\text{-}^tBu\text{-}C_5H_3)(C_5H_4)ZrCl_2$ (14.5 ppm). Attempts to crystallize the pendant borate were hindered by the high solubility of the complex in aromatic solvents. Vapor diffusion of pentane into aromatic solutions of the pendant borane resulted in powders. A similar species has been reported which was formed from via the hydroboration of $Me(3\text{-butenyl})C(C_5H_4)(fluorenyl)ZrCl_2$ with 9-H-borabicyclo[3.3.1] nonane (9-BBN) and was found to polymerize ethene upon activation with MAO.[50]

Scheme B.3

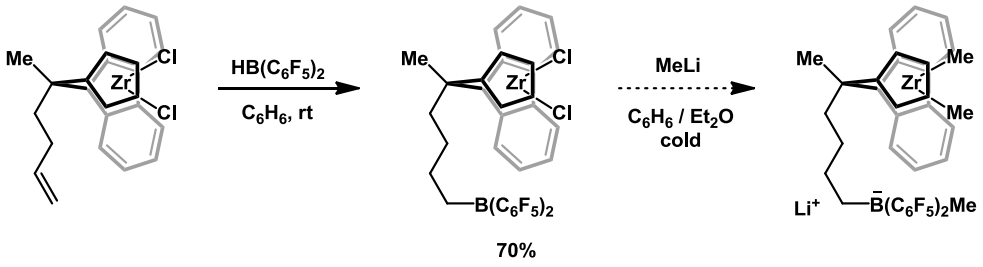

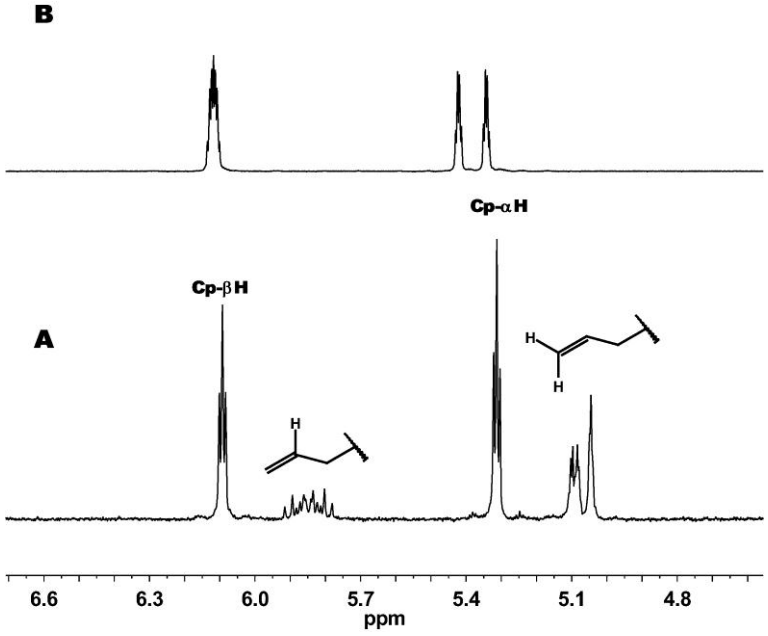

Figure B.2: ^{1}H NMR of the Cp and olefinic region of Me(3-butenyl)C(C_5H_4)(fluorenyl)ZrCl_2 and Me($C_4H_8B(C_6F_5)_2$)C(C_5H_4)(fluorenyl)ZrCl_2 in benzene-d_6.

Attempts to make a silyl-bridged analog from the commercially available Me(vinyl)SiCl_2 or Me(allyl)SiCl_2 proved impractical due to the inability to metallate the complexes. Attempts to deprotonate the complexes invariably resulted in decomposition, while attempts to metallate through the amine elimination reaction resulted in rapid coordination of the Cp ring, however decomposition occurred prior to coordination of the fluorenyl ring.

B.4 Conclusions

Synthesis of a zirconocene with a pendant borane has been achieved through hydroboration of complexes with pendant olefins. Attempts to form pendant borates of these complexes have shown limited success.

B.5 Future Directions

Future work on these complexes would entail synthesis and isolation of zirconocene dimethyl complexes with pendant borate anions which will then be reacted with cationizing reagents such as $[Ph_3C][B(C_6F_5)_4]$ or $[PhNMe_2H][B(C_6F_5)_4]$ to yield zwitterionic complexes (Scheme B.4). These complexes should be active for the polymerization of propene and analysis of the propene produced by these reactions will provide valuable insight into the effect of anions on polymerizations.

Scheme B.4

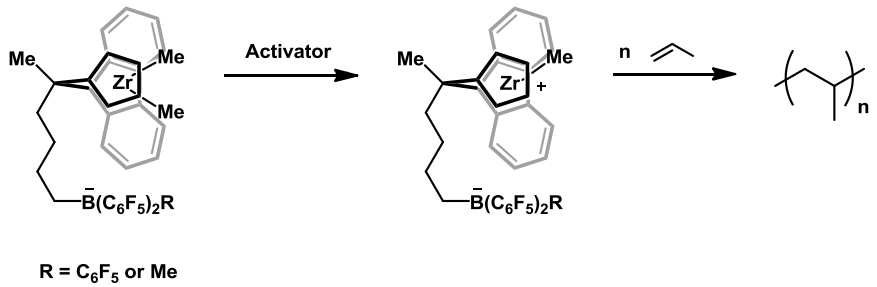

If strong anion pairing effects exist then it should be manifest as a move toward isotacticity in polypropene from the (Ewen)$ZrCl_2$-derived complex. As the anion is constrained to one side of the metallocene wedge there should be an energy difference between the two conformations of the catalyst with the polymeryl chain on opposite sides of the metallocene wedge (Scheme B.5). Site epimerization would be expected to cause the chain to swing to the side away from the anion to give the more stable complex. This site epimerization would be expected to result in more insertions from one side of the wedge yielding a more isotactic polymer. Increasing propene pressures would be expected to counteract this effect resulting in more syndiotactic polypropene.

Scheme B.5

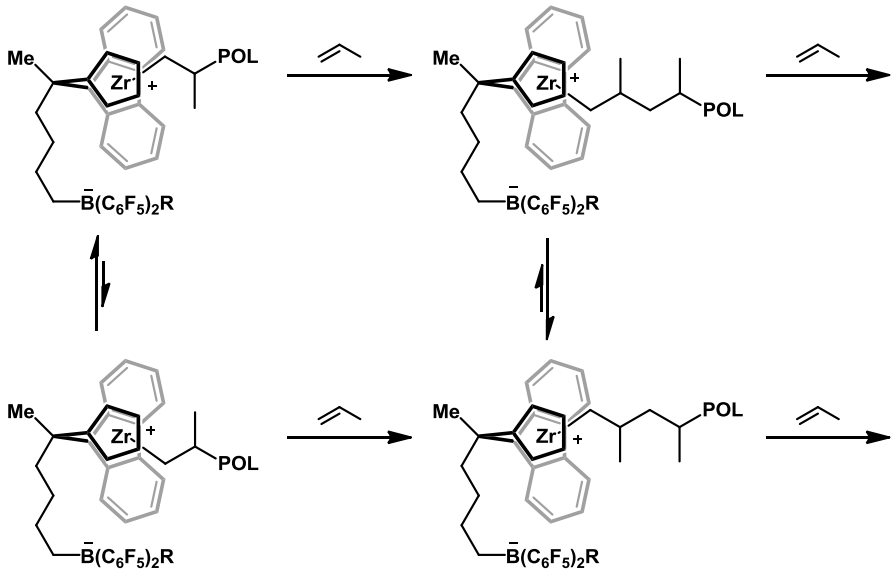

B.6 Experimental

General Considerations. All operations were carried out under a protective dinitrogen or argon atmosphere, either in a glovebox or on a vacuum manifold. Benzene-d_6 and other solvents used were dried by vacuum transfer either from sodium benzophenone. NMR spectra were obtained using Varian Inova 500 or Mercury 300 spectrometers. ^{1}H chemical shifts are referenced to residual solvents peaks (7.16 ppm) for ^{1}H benzene. ^{19}F chemical shifts were referenced to an external standard of neat $CFCl_3$ at 0.00 ppm. $HB(C_6F_5)_2$ was prepared by Alex Miller following the procedure of Piers.[51] Me(3-butenyl)C(C_5H_4)(fluorenyl)$ZrCl_2$ was prepared following literature methods.[43] $Zr(NMe_2)_4$ was prepared following literature methods.[38]

Me(vinyl)Si(3-^{t}Bu-C_5H_4)Cl. 1.7405 g (13.583 mmol) Li(^{t}BuC_5H_4) was weighed into an oven dried 250 mL round bottom flask and a 180º joint was attached. Into a second 250 mL oven dried round bottom with attached 180º joint was vacuum transferred 12.0 mL (91.9 mmol, 6.76 equiv) Me(vinyl)$SiCl_2$. ~ 75 mL of thf and Et_2O were vacuum transferred from a Na/Ph_2CO pot onto the Cp and silane respectively. The Cp solution was slowly transferred onto the silane solution at –78 ºC via cannula. The reaction was allowed to warm to room temperature with stirring. The solution was allowed to stir overnight after which time the solvent was pumped off to yield a white powder and orange liquid. The mixture was taken into the glove box, taken up in petroleum ether and filtered through celite to remove the LiCl byproduct. The petroleum ether was pumped off to yield 2.9442 g (96% yield) of Me(vinyl)Si(3-^{t}Bu-C_5H_4)Cl as an orange oil. ^{1}H NMR revealed two isomers as expected for a protonated disubstituted Cp ring. ^{1}H NMR (300 MHz, benzene-d_6) δ 6.64 (s, 2H, Cp-H), 6.47 (d, J = 18 Hz, 2H, Cp-H), 6.12 (dd, J = 11, 9 Hz, 3H, Cp-H), 5.86 (m, 8H, Cp-H, =CH-), 1.14 (s, 18H, C(CH_3)), 0.11 (s, 3H, Si-CH_3), 0.09 (s, 3H, Si-CH_3).

Me(vinyl)Si(3-^{t}Bu-C_5H_4)(C_5H_5). 2.1490 g (13.910 mmol) of $MgCp_2$ was weighed into an oven dried 100 mL round bottom. 3.1398 g (13.843 mmol) of Me(vinyl)Si(3-^{t}Bu-C_5H_4)Cl was added as a petroleum ether solution and a 180º joint was attached. The solvent was removed under vacuum and ~45 mL of thf was vacuum transferred in from a Na/Ph_2CO pot at –78 ºC. The reaction was allowed to warm to room temperature with stirring overnight. The thf was removed under vacuum to give a red oil. The oil was taken up in Et_2O and washed with saturated aqueous NH_4Cl followed by 3 washes with water. The solution was dried with $MgSO_4$ and filtered. Ether was removed via rotovap to yield 3.3491

g of a yellow oil (94 % yield) which was shown to be Me(vinyl)Si(3-^{t}Bu-C_5H_4)(C_5H_5) by GC-MS.

Me(vinyl)Si(3-^{t}Bu-C_5H_3)(C_5H_4)Zr(NMe_2)$_2$. 0.5232 g (1.956 mmol) of Zr(NMe_2)$_4$ was weighed into a 100 mL oven dried round bottom flask to which was attached a condenser and 180 º joint. To a second 100 mL oven dried round bottom flask was added 0.5010 g (1.954 mmol, 1 equiv) Me(vinyl)Si(3-^{t}Bu-C_5H_4)(C_5H_5). ~ 50 mL toluene were vacuum transferred onto the ligand from a Na/Ph_2CO pot. The ligand solution was cannula transferred into the flask containing the Zr. Heating with stirring to 50 ºC resulted in the immediate evolution of an orange color. Over the course of 1 hour the temperature was increased to 100 ºC with an Ar flow over the reaction. The reaction was kept at 100 ºC for 36 hours until the Ar flow was no longer basic (no more $HNMe_2$ evolution). The reaction was allowed to cool to room temperature and the toluene was removed under vacuum to give a gooey solid of reddish color. In the glove box the goo was taken up in petroleum ether and filtered. Removal of the petroleum ether affored 727.2 mg (86% yield) of Me(vinyl)Si(3-^{t}Bu-C_5H_3)(C_5H_4)Zr(NMe_2)$_2$ as a red solid. ^{1}H NMR revealed a 1.08(1):1 mixture of the two possible diastereomers. ^{1}H NMR (300 MHz, benzene-d_6) δ 6.55 (m, 6H, =CH-/Cp-H), 6.17 (m, 3H), 6.09 (d, *J* = 2 Hz, 1H), 5.93 (dd, *J* = 5, 2 Hz, 1H, Cp-H), 5.83 (dt, *J* = 5, 2 Hz, 2H, Cp-H), 5.77 (dd, *J* = 4.9, 3 Hz, 2H, Cp-H), 5.68 (dd, *J* = 4, 3 Hz, 1H, Cp-H), 5.63 (t, *J* = 3 Hz, 1H, Cp-H), 5.56 (t, *J* = 3 Hz, 1H, Cp-H), 2.90 (s, 6H, N(CH_3)$_2$), 2.87 (s, 6H, N(CH_3)$_2$), 2.58 (s, 6H, N(CH_3)$_2$), 2.57 (s, 6H, N(CH_3)$_2$), 1.29 (s, 9H, Cp-CMe_3), 1.28 (s, 9H, Cp-CMe_3), 0.56 (s, 3H, Si-CH_3), 0.48 (s, 3H, Si-CH_3).

Me(vinyl)Si(3-^{t}Bu-C_5H_3)(C_5H_4)$ZrCl_2$. 727.2 mg (1.676 mmol) of Me(vinyl)Si(3-^{t}Bu-C_5H_3)(C_5H_4)Zr(NMe_2)$_2$ was weighed into a 20 mL vial in the glove box and dissolved in 10 mL of benzene. 1.1 mL (8.6 mmol, 2.6 equiv) of Me_3SiCl was added dropwise and the vial was closed and allowed to stir for 5.5 hours. All volatiles were removed under vacuum to give a brown goop. The mixture was taken up in petroleum ether, filtered and pumped down to yield 645.6 mg (93 % yield) of a beige powder. ^{1}H NMR revealed a 1:1 mixture of the two diastereomers. ^{1}H NMR (300 MHz, benzene-d_6) δ 6.85 (m, 4H, Cp-H), 6.69 (m, 1H, Cp-H), 6.63 (m, 1H, Cp-H), 5.98 (m, 7H, =CH-), 5.82 (dd, *J* = 3, 2 Hz, 1H, Cp-H), 5.78 (m, 2H, Cp-H), 5.72 (m, 1H, Cp-H), 5.65 (t, *J* = 3 Hz, 1H, Cp-H), 5.58 (dd, *J* = 5, 3 Hz, 1H, Cp-H), 5.56 (t, *J* = 3 Hz, 1H, Cp-H), 5.49 (m, 1H, Cp-H), 1.45 (s, 9H, Cp-CMe_3), 1.42 (s, 9H, Cp-CMe_3), 0.29 (m, 3H, Si-CH_3), 0.16 (m, 3H, Si-CH_3).

Me($C_2H_4B(C_6F_5)_2$)Si(3-^{t}Bu-C_5H_3)(C_5H_4)$ZrCl_2$. 141.1 mg (0.3387 mmol) Me(vinyl)Si(3-^{t}Bu-C_5H_3)(C_5H_4)$ZrCl_2$ and 118.4 mg (0.3423 mmol, 1.01 equiv) were added to a 50 mL oven dried round bottom flask and a 180º joint was attached. 20 mL of benzene was vacuum transferred in at –78 ºC. The reaction was allowed to warm to room temperature with stirring to give a brown solution. After 20 minutes everything dissolved to give a yellow solution. The solution was lyophilized to yield 248.8 mg yellow powder (96% yield). ^{1}H NMR yielded a 1:1 mixture of diastereomers. ^{1}H NMR (300 MHz, benzene-d_6) δ 6.85 (m, 6H, Cp-H), 6.69 (dd, *J* = 5, 3 Hz, 2H, Cp-H), 6.61 (dd, *J* = 5, 3 Hz, 2H, Cp-H), 5.87 (dd, *J* = 5, 2 Hz, 3H, Cp-H), 5.79 (m, 2H, Cp-H), 5.64 (m, 2H, Cp-H), 5.56 (d, *J* = 3 Hz, 3H, Cp-H), 5.44 (s, 1H, Cp-H), 1.91 (t, *J* = 9 Hz, 3H, C_2H_4), 1.44 (d, 18H, Cp-CMe_3), 1.36 (dd, *J* = 9, 4 Hz, 14H, C_2H_4), 1.20 (m, 8H, , C_2H_4), 0.94 (ddd, *J* = 23, 17, 9 Hz, 10H,

C_2H_4), 0.38 (s, 3H, $SiCH_3$), 0.22 (s, 2H, $SiCH_3$). ^{19}F NMR (282 MHz, benzene-d_6) δ –130.29 (m, 4F), –145.85 (t, J = 20 Hz, 1F), –146.13 (t, J = 22 Hz, 1F), –160.54 (m, 4F).

Me($C_4H_8B(C_6F_5)_2$)C(C_5H_4)(fluorenyl)$ZrCl_2$. 53.0 mg (0.112 mmol) of Me(3-butenyl)-C(C_5H_4)(fluorenyl)$ZrCl_2$ was weighed into a 20 mL scintillation vial. 38.8 mg (0.112 mmol) of $HB(C_6F_5)_2$ was weighed into a separate 1 dram vial. 4 mL of toluene was added to the $HB(C_6F_5)_2$ to yield a colorless slurry. The $HB(C_6F_5)_2$ slurry was added to the zirconocene. Upon stirring everything dissolved to give an orange solution without much visible color change from the starting zirconocene. After stirring for 30 minutes the toluene was removed under vacuum to give an orange oil. The oil was redissolved in ~ 1 mL toluene and pentane was added to precipitate the product as a 31.4 mg (34% yield) of pale orange powder. More product could be obtained by pumping down the filtrate and lyophilizing to afford an additional 32.9 mg (70 % total yield). ^1H NMR (500 MHz, benzene-d_6) δ 7.81 (dd, $^3J_{HH}$ = 10, 9 Hz, 2H, Ar-H), 7.44 (d, $^3J_{HH}$ = 9 Hz, 1H, Ar-H), 7.33 (m, 3H, Ar-H), 7.06 (m, 2H, Ar-H), 6.11 (m, 2H, Cp-βH), 5.42 (dd, $^3J_{HH}$ = 5, 3 Hz, 1H, Cp-αH), 5.34 (dd, $^3J_{HH}$ = 5, 3 Hz, 1H, CH_2), 2.77 (m, 1H, CH_2), 1.91 (m, 5H, CH_2 & CH_3), 1.67 (m, 6H, CH_2). ^{19}F NMR (282 MHz, benzene-d_6) δ –130.76 (d, $^3J_{FF}$ = 23 Hz, 4F, p-C_6F_5), –146.93 (s, 2F, p-C_6F_5), –160.81 (td, $^3J_{FF}$ = 25, 10 Hz, 4F, p-C_6F_5).

B.7 References

1. Brintzinger, H. H.; Fischer, D.; Mulhaupt, R.; Rieger, B.; Waymouth, R. M. *Angew. Chem.-Int. Edit. Engl.*, **1995**, *34*, 1143.
2. Coates, G. W. *Chem. Rev.*, **2000**, *100*, 1223.
3. Gibson, V. C.; Spitzmesser, S. K. *Chem. Rev.*, **2003**, *103*, 283.

4. Resconi, L.; Cavallo, L.; Fait, A.; Piemontesi, F. *Chem. Rev.*, **2000**, *100*, 1253.
5. Chen, Y. X.; Metz, M. V.; Li, L. T.; Stern, C. L.; Marks, T. J. *J. Am. Chem. Soc.*, **1998**, *120*, 6287.
6. Chen, M. C.; Marks, T. J. *J. Am. Chem. Soc.*, **2001**, *123*, 11803.
7. Zhou, J. M.; Lancaster, S. J.; Walker, D. A.; Beck, S.; Thornton-Pett, M.; Bochmann, M. *J. Am. Chem. Soc.*, **2001**, *123*, 223.
8. Landis, C. R.; Rosaaen, K. A.; Uddin, J. *J. Am. Chem. Soc.*, **2002**, *124*, 12062.
9. Wilmes, G. M.; Polse, J. L.; Waymouth, R. M. *Macromolecules*, **2002**, *35*, 6766.
10. Mohammed, M.; Nele, M.; Al-Humydi, A.; Xin, S. X.; Stapleton, R. A.; Collins, S. *J. Am. Chem. Soc.*, **2003**, *125*, 7930.
11. Chen, M. C.; Roberts, J. A. S.; Marks, T. J. *J. Am. Chem. Soc.*, **2004**, *126*, 4605.
12. Rodriguez-Delgado, A.; Hannant, M. D.; Lancaster, S. J.; Bochmann, M. *Macromol. Chem. Phys.*, **2004**, *205*, 334.
13. Song, F. Q.; Hannant, M. D.; Cannon, R. D.; Bochmann, M. *Macromol. Symp.*, **2004**, *213*, 173.
14. Al-Humydi, A.; Garrison, J. C.; Youngs, W. J.; Collins, S. *Organometallics*, **2005**, *24*, 193.
15. Stahl, N. G.; Salata, M. R.; Marks, T. J. *J. Am. Chem. Soc.*, **2005**, *127*, 10898.
16. Bochmann, M.; Cannon, R. D.; Song, F. *Kinet. Catal.*, **2006**, *47*, 160.
17. Wilson, P. A.; Hannant, M. H.; Wright, J. A.; Cannon, R. D.; Bochmann, M. *Macromol. Symp.*, **2006**, *236*, 100.
18. Lanza, G.; Fragalà, I. L.; Marks, T. J. *J. Am. Chem. Soc.*, **1998**, *120*, 8257.
19. Lanza, G.; Fragalà, I. L.; Marks, T. J. *J. Am. Chem. Soc.*, **2000**, *122*, 12764.
20. Vanka, K.; Chan, M. S. W.; Pye, C. C.; Ziegler, T. *Organometallics*, **2000**, *19*, 1841.
21. Nifant'ev, I. E.; Ustynyuk, L. Y.; Laikov, D. N. *Organometallics*, **2001**, *20*, 5375.
22. Lanza, G.; Fragalà, I. L.; Marks, T. J. *Organometallics*, **2002**, *21*, 5594.
23. Xu, Z. T.; Vanka, K.; Firman, T.; Michalak, A.; Zurek, E.; Zhu, C. B.; Ziegler, T. *Organometallics*, **2002**, *21*, 2444.
24. Zurek, E.; Ziegler, T. *Faraday Discuss.*, **2003**, *124*, 93.
25. Xu, Z. T.; Vanka, K.; Ziegler, T. *Organometallics*, **2004**, *23*, 104.

26. Silanes, M.; Ugalde, J. M. *Organometallics*, **2005**, *24*, 3233.
27. Vanka, K.; Xu, Z.; Seth, M.; Ziegler, T. *Top. Catal.*, **2005**, *34*, 143.
28. Ziegler, T.; Vanka, K.; Xu, Z. T. *C. R. Chim.*, **2005**, *8*, 1552.
29. Martinez, S.; Ramos, J.; Cruz, V. L.; Martinez-Salazar, J. *Polymer*, **2006**, *47*, 883.
30. Tomasi, S.; Razavi, A.; Ziegler, T. *Organometallics*, **2007**, *26*, 2024.
31. Aldridge, S.; Bresner, C. *Coordin. Chem. Rev.*, **2003**, *244*, 71.
32. Piers, W. E. *Chem.-Eur. J.*, **1998**, *4*, 13.
33. Piers, W. E.; Sun, Y. M.; Lee, L. W. M. *Top. Catal.*, **1999**, *7*, 133.
34. Mise, T.; Miya, S.; Yamazaki, H. *Chem. Lett.*, **1989**, 1853.
35. Schofer, S. J. PhD Thesis, California Institute of Technology, Pasadena, CA, 2004.
36. Zhong, H. A. PhD Thesis, California Institute of Technology, Pasadena, CA, 2001.
37. Ewen, J. A.; Jones, R. L.; Razavi, A.; Ferrara, J. D. *J. Am. Chem. Soc.*, **1988**, *110*, 6255.
38. Diamond, G. M.; Rodewald, S.; Jordan, R. F. *Organometallics*, **1995**, *14*, 5.
39. Diamond, G. M.; Jordan, R. F.; Petersen, J. L. *J. Am. Chem. Soc.*, **1996**, *118*, 8024.
40. Diamond, G. M.; Jordan, R. F.; Petersen, J. L. *Organometallics*, **1996**, *15*, 4045.
41. Diamond, G. M.; Jordan, R. F.; Petersen, J. L. *Organometallics*, **1996**, *15*, 4030.
42. Christopher, J. N.; Diamond, G. M.; Jordan, R. F.; Petersen, J. L. *Organometallics*, **1996**, *15*, 4038.
43. Peifer, B.; Milius, W.; Alt, H. G. *J. Organomet. Chem.*, **1998**, *553*, 205.
44. Kneale, B.; Boone, J. E.; Diefenbach, S. P.; Loechelt, C. P.; Prindle, J., J. C. Patent WO0198381, 2001.
45. Kneale, B.; Boone, J. E.; Diefenbach, S. P.; Loechelt, C. P.; Prindle, J., J. C. Patent US6677265, 2004.
46. Yang, Q.; Jensen, M. D.; McDaniel, M. P. *Macromolecules*, **2010**, *43*, 8836.
47. Jensen, M. D.; Martin, J. L.; Yang, Q.; Thorn, M. G.; McDaniel, M. P.; Rolfing, D. C.; Sukhadia, A. M.; Yu, Y.; Lanier, J. T. Patent US20050288461, 2005.
48. Jensen, M. D.; Martin, J. L.; McDaniel, M. P.; Rolfing, D. C.; Yang, Q.; Thorn, M. G.; Sukhadia, A. M.; Yu, Y.; Lanier, J. T. Patent US20050288462, 2005.

49. Jensen, M. D.; Martin, J. L.; McDaniel, M. P.; Rholfing, D. C.; Yang, Q.; Thorn, M. G.; Sukhadia, A. M.; Yu, Y.; Lanier, J. T. Patent US7148298, 2006.
50. Kestel-Jakob, A.; Alt, H. G. *Z. Naturforsch., B: Chem. Sci.*, **2007**, *62*, 314.
51. Parks, D. J.; Spence, R. E. V. H.; Piers, W. E. *Angew. Chem.-Int. Edit. Engl.*, **1995**, *34*, 809.

APPENDIX C

X-ray Crystallographic Data

C.1 $[(Me_2Si)_2(C_5H_3)_2Zr(\mu\text{-}H)_3(Al^iBu_2)_2][B(C_6F_5)_4]$

Table C.1: Crystal data and structure refinement for SMB04 (CCDC 776421).

Empirical formula	$[C_{30}H_{54}Al_2Si_2ZrH_3]^+ [BC_{24}F_{20}]^-$
Formula weight	1298.17
Crystallization Solvent	Benzene
Crystal Habit	Blade
Crystal size	0.28 x 0.20 x 0.04 mm^3
Crystal color	Colorless
Data Collection	
Type of diffractometer	Bruker KAPPA APEX II
Wavelength	0.71073 Å MoKα
Data Collection Temperature	100(2) K
θ range for 9643 reflections used in lattice determination	2.30 to 24.63°
Unit cell dimensions	a = 16.2579(8) Å α= 90° b = 17.1922(7) Å β= 103.262(3)° c = 21.1975(10) Å γ = 90°
Volume	5766.9(5) $Å^3$
Z	4
Crystal system	Monoclinic
Space group	P $2_1/n$
Density (calculated)	1.495 Mg/m^3
F(000)	2640
Data collection program	Bruker APEX2 v2009.7-0
θ range for data collection	1.43 to 27.17°
Completeness to θ = 27.17°	99.1 %
Index ranges	$-20 \le h \le 20$, $-22 \le k \le 22$, $-27 \le l \le 25$
Data collection scan type	ω scans; 10 settings
Data reduction program	Bruker SAINT-Plus v7.66A
Reflections collected	75246
Independent reflections	12697 [R_{int}= 0.0580]
Absorption coefficient	0.364 mm^{-1}
Absorption correction	Semi-empirical from equivalents
Max. and min. transmission	0.7455 and 0.6208
Structure Solution and Refinement	
Structure solution program	SHELXS-97 (Sheldrick, 2008)
Primary solution method	Direct methods
Secondary solution method	Difference Fourier map
Hydrogen placement	Geometric positions
Structure refinement program	SHELXL-97 (Sheldrick, 2008)
Refinement method	Full matrix least-squares on F^2
Data / restraints / parameters	12697 / 0 / 745
Treatment of hydrogen atoms	Riding

Goodness-of-fit on F^2	1.883
Final R indices [I>2σ(I), 8862 reflections]	R1 = 0.0422, *w*R2 = 0.0681
R indices (all data)	R1 = 0.0795, *w*R2 = 0.0719
Type of weighting scheme used	Sigma
Weighting scheme used	$w=1/\sigma^2(Fo^2)$
Max shift/error	0.002
Average shift/error	0.000
Largest diff. peak and hole	0.741 and -0.489 e.Å^{-3}

Special Refinement Details

Crystals were mounted in a loop with oil, then placed on the diffractometer under a nitrogen stream at 100K.

The three hydrides, H1H, H2H and H3H were located in the difference Fourier map and refined during least-squares without any restraints.

Refinement of F^2 against ALL reflections. The weighted R-factor (*w*R) and goodness of fit (S) are based on F^2, conventional R-factors (R) are based on F, with F set to zero for negative F^2. The threshold expression of $F^2 > 2\sigma(F^2)$ is used only for calculating R-factors(gt) etc. and is not relevant to the choice of reflections for refinement. R-factors based on F^2 are statistically about twice as large as those based on F, and R-factors based on ALL data will be even larger.

All esds (except the esd in the dihedral angle between two l.s. planes) are estimated using the full covariance matrix. The cell esds are taken into account individually in the estimation of esds in distances, angles and torsion angles; correlations between esds in cell

parameters are only used when they are defined by crystal symmetry. An approximate (isotropic) treatment of cell esds is used for estimating esds involving l.s. planes.

Table C.2: Atomic coordinates (x 10^4) and equivalent isotropic displacement parameters (Å^2 x 10^3) for SMB04 (CCDC 776421). U_{eq} is defined as the trace of the orthogonalized U^{ij} tensor.

	x	y	z	U_{eq}
Zr(1)	8551(1)	3284(1)	1687(1)	17(1)
Si(1)	7285(1)	2526(1)	442(1)	20(1)
Si(2)	6798(1)	4193(1)	1234(1)	21(1)
Al(1)	10273(1)	2445(1)	2090(1)	21(1)
Al(2)	9571(1)	4053(1)	2938(1)	24(1)
C(1)	7275(2)	2540(1)	1328(1)	19(1)
C(2)	7069(2)	3230(1)	1663(1)	19(1)
C(3)	7451(2)	3127(1)	2330(1)	22(1)
C(4)	7896(2)	2421(1)	2421(1)	24(1)
C(5)	7776(2)	2057(1)	1812(1)	22(1)
C(6)	7956(2)	3436(1)	544(1)	16(1)
C(7)	7751(2)	4130(1)	872(1)	18(1)
C(8)	8524(2)	4536(1)	1096(1)	20(1)
C(9)	9195(2)	4124(1)	932(1)	19(1)
C(10)	8842(2)	3456(1)	587(1)	19(1)
C(11)	7893(2)	1670(1)	277(1)	26(1)
C(12)	6241(2)	2564(1)	-134(1)	28(1)
C(13)	5770(2)	4264(1)	642(1)	27(1)
C(14)	6928(2)	4993(1)	1841(1)	28(1)
C(15)	10371(2)	1744(1)	2830(1)	29(1)
C(16)	10118(2)	892(2)	2669(1)	37(1)
C(17)	10242(2)	401(2)	3280(1)	45(1)
C(18)	10590(2)	550(2)	2198(2)	52(1)
C(19)	11065(2)	2813(1)	1596(1)	22(1)
C(20)	11872(2)	2333(1)	1626(1)	23(1)
C(21)	12468(2)	2390(2)	2284(1)	37(1)
C(22)	12322(2)	2576(1)	1100(1)	31(1)
C(23)	9325(2)	3623(1)	3721(1)	30(1)
C(24)	9082(2)	4263(2)	4157(1)	46(1)
C(25)	9028(3)	3944(2)	4812(2)	112(2)
C(26)	8267(2)	4633(2)	3841(2)	58(1)
C(27)	10432(2)	4839(1)	2950(1)	28(1)
C(28)	11233(2)	4730(1)	3478(1)	32(1)
C(29)	11684(2)	3987(2)	3365(2)	47(1)
C(30)	11827(2)	5424(2)	3514(2)	60(1)
B(1)	9501(2)	7307(2)	1273(1)	19(1)
F(1)	10546(1)	8346(1)	2173(1)	26(1)
F(2)	10794(1)	8379(1)	3458(1)	40(1)
F(3)	10030(1)	7318(1)	4083(1)	49(1)

F(4)	8972(1)	6245(1)	3380(1)	42(1)
F(5)	8629(1)	6251(1)	2100(1)	30(1)
F(6)	11124(1)	8056(1)	1000(1)	24(1)
F(7)	12556(1)	7302(1)	1046(1)	25(1)
F(8)	12711(1)	5771(1)	1330(1)	28(1)
F(9)	11359(1)	4976(1)	1586(1)	29(1)
F(10)	9915(1)	5716(1)	1546(1)	23(1)
F(11)	9738(1)	7680(1)	3(1)	24(1)
F(12)	9461(1)	9019(1)	-635(1)	32(1)
F(13)	8910(1)	10285(1)	-85(1)	36(1)
F(14)	8660(1)	10176(1)	1149(1)	34(1)
F(15)	8891(1)	8846(1)	1782(1)	25(1)
F(16)	9438(1)	6058(1)	213(1)	26(1)
F(17)	8070(1)	5352(1)	-430(1)	36(1)
F(18)	6520(1)	5699(1)	-220(1)	41(1)
F(19)	6396(1)	6800(1)	683(1)	40(1)
F(20)	7769(1)	7533(1)	1339(1)	29(1)
C(41)	9549(2)	7321(1)	2054(1)	19(1)
C(42)	10112(2)	7826(1)	2453(1)	22(1)
C(43)	10266(2)	7849(2)	3112(1)	27(1)
C(44)	9874(2)	7316(2)	3429(1)	32(1)
C(45)	9338(2)	6783(2)	3076(1)	29(1)
C(46)	9183(2)	6799(1)	2409(1)	23(1)
C(47)	10414(2)	6919(1)	1244(1)	15(1)
C(48)	11129(2)	7282(1)	1133(1)	17(1)
C(49)	11881(2)	6911(1)	1153(1)	18(1)
C(50)	11970(2)	6124(1)	1300(1)	19(1)
C(51)	11295(2)	5745(1)	1430(1)	19(1)
C(52)	10556(2)	6137(1)	1408(1)	18(1)
C(53)	9353(2)	8185(1)	932(1)	17(1)
C(54)	9466(2)	8290(1)	314(1)	19(1)
C(55)	9323(2)	8968(1)	-37(1)	24(1)
C(56)	9050(2)	9609(1)	247(1)	25(1)
C(57)	8920(2)	9546(1)	857(1)	24(1)
C(58)	9066(2)	8844(1)	1186(1)	20(1)
C(59)	8689(2)	6818(1)	841(1)	18(1)
C(60)	8706(2)	6266(1)	363(1)	20(1)
C(61)	7996(2)	5892(1)	15(1)	24(1)
C(62)	7216(2)	6062(2)	115(1)	28(1)
C(63)	7153(2)	6620(2)	568(1)	27(1)
C(64)	7879(2)	6978(1)	906(1)	24(1)

Table C.3: Bond lengths [Å] and angles [°] for SMB04 (CCDC 776421).

Zr(1)-H(3H)	1.950(18)	C(28)-C(30)	1.526(4)
Zr(1)-H(1H)	1.979(19)	B(1)-C(41)	1.640(4)
Zr(1)-H(2H)	2.09(2)	B(1)-C(47)	1.641(4)
Zr(1)-C(2)	2.401(2)	B(1)-C(59)	1.653(4)
Zr(1)-C(7)	2.402(2)	B(1)-C(53)	1.666(3)
Zr(1)-C(1)	2.407(2)	F(1)-C(42)	1.358(3)
Zr(1)-C(6)	2.410(2)	F(2)-C(43)	1.348(3)
Zr(1)-C(8)	2.487(2)	F(3)-C(44)	1.349(3)
Zr(1)-C(3)	2.499(2)	F(4)-C(45)	1.342(3)
Zr(1)-C(10)	2.502(2)	F(5)-C(46)	1.362(3)
Zr(1)-C(5)	2.502(2)	F(6)-C(48)	1.359(2)
Zr(1)-C(4)	2.552(2)	F(7)-C(49)	1.349(3)
Zr(1)-C(9)	2.553(2)	F(8)-C(50)	1.336(3)
Zr(1)-Al(2)	3.0831(8)	F(9)-C(51)	1.361(2)
Zr(1)-Al(1)	3.0893(8)	F(10)-C(52)	1.356(3)
Si(1)-C(12)	1.851(2)	F(11)-C(54)	1.365(2)
Si(1)-C(11)	1.852(2)	F(12)-C(55)	1.340(3)
Si(1)-C(1)	1.882(2)	F(13)-C(56)	1.350(3)
Si(1)-C(6)	1.891(2)	F(14)-C(57)	1.362(3)
Si(2)-C(13)	1.849(2)	F(15)-C(58)	1.356(3)
Si(2)-C(14)	1.863(2)	F(16)-C(60)	1.348(3)
Si(2)-C(7)	1.883(3)	F(17)-C(61)	1.347(3)
Si(2)-C(2)	1.891(2)	F(18)-C(62)	1.345(3)
Al(1)-C(19)	1.942(3)	F(19)-C(63)	1.344(3)
Al(1)-C(15)	1.956(2)	F(20)-C(64)	1.363(3)
Al(2)-C(23)	1.940(3)	C(41)-C(46)	1.391(3)
Al(2)-C(27)	1.942(3)	C(41)-C(42)	1.397(3)
C(1)-C(5)	1.422(3)	C(42)-C(43)	1.362(3)
C(1)-C(2)	1.462(3)	C(43)-C(44)	1.378(4)
C(2)-C(3)	1.418(3)	C(44)-C(45)	1.364(4)
C(3)-C(4)	1.403(3)	C(45)-C(46)	1.378(3)
C(4)-C(5)	1.408(3)	C(47)-C(48)	1.387(3)
C(6)-C(10)	1.422(3)	C(47)-C(52)	1.394(3)
C(6)-C(7)	1.457(3)	C(48)-C(49)	1.372(3)
C(7)-C(8)	1.422(3)	C(49)-C(50)	1.389(3)
C(8)-C(9)	1.408(3)	C(50)-C(51)	1.358(3)
C(9)-C(10)	1.410(3)	C(51)-C(52)	1.368(3)
C(15)-C(16)	1.537(3)	C(53)-C(54)	1.374(3)
C(16)-C(18)	1.510(4)	C(53)-C(58)	1.381(3)
C(16)-C(17)	1.521(3)	C(54)-C(55)	1.375(3)
C(19)-C(20)	1.539(3)	C(55)-C(56)	1.377(3)
C(20)-C(21)	1.507(3)	C(56)-C(57)	1.361(3)
C(20)-C(22)	1.525(3)	C(57)-C(58)	1.386(3)
C(23)-C(24)	1.546(4)	C(59)-C(64)	1.383(3)
C(24)-C(26)	1.483(4)	C(59)-C(60)	1.394(3)
C(24)-C(25)	1.515(4)	C(60)-C(61)	1.378(3)
C(27)-C(28)	1.521(3)	C(61)-C(62)	1.366(4)
C(28)-C(29)	1.518(4)	C(62)-C(63)	1.377(4)

C(63)-C(64)	1.378(3)
H(3H)-Zr(1)-H(1H)	128.6(8)
H(3H)-Zr(1)-H(2H)	63.8(8)
H(1H)-Zr(1)-H(2H)	64.8(8)
C(2)-Zr(1)-C(7)	68.43(8)
C(2)-Zr(1)-C(1)	35.39(7)
C(7)-Zr(1)-C(1)	78.97(8)
C(2)-Zr(1)-C(6)	79.24(8)
C(7)-Zr(1)-C(6)	35.26(7)
C(1)-Zr(1)-C(6)	67.76(8)
C(2)-Zr(1)-C(8)	96.94(8)
C(7)-Zr(1)-C(8)	33.75(8)
C(1)-Zr(1)-C(8)	112.72(8)
C(6)-Zr(1)-C(8)	56.08(8)
C(2)-Zr(1)-C(3)	33.58(7)
C(7)-Zr(1)-C(3)	96.92(8)
C(1)-Zr(1)-C(3)	56.10(8)
C(6)-Zr(1)-C(3)	112.81(8)
C(8)-Zr(1)-C(3)	115.87(8)
C(2)-Zr(1)-C(10)	112.82(8)
C(7)-Zr(1)-C(10)	56.19(8)
C(1)-Zr(1)-C(10)	95.82(8)
C(6)-Zr(1)-C(10)	33.59(8)
C(8)-Zr(1)-C(10)	54.00(8)
C(3)-Zr(1)-C(10)	146.38(8)
C(2)-Zr(1)-C(5)	56.12(8)
C(7)-Zr(1)-C(5)	112.57(8)
C(1)-Zr(1)-C(5)	33.60(7)
C(6)-Zr(1)-C(5)	95.86(8)
C(8)-Zr(1)-C(5)	146.31(8)
C(3)-Zr(1)-C(5)	53.89(8)
C(10)-Zr(1)-C(5)	113.94(8)
C(2)-Zr(1)-C(4)	55.49(8)
C(7)-Zr(1)-C(4)	123.91(8)
C(1)-Zr(1)-C(4)	55.53(8)
C(6)-Zr(1)-C(4)	123.29(8)
C(8)-Zr(1)-C(4)	148.09(8)
C(3)-Zr(1)-C(4)	32.23(7)
C(10)-Zr(1)-C(4)	146.27(8)
C(5)-Zr(1)-C(4)	32.33(7)
C(2)-Zr(1)-C(9)	124.19(8)
C(7)-Zr(1)-C(9)	55.76(8)
C(1)-Zr(1)-C(9)	123.34(8)
C(6)-Zr(1)-C(9)	55.58(8)
C(8)-Zr(1)-C(9)	32.41(7)
C(3)-Zr(1)-C(9)	148.27(7)
C(10)-Zr(1)-C(9)	32.38(7)
C(5)-Zr(1)-C(9)	146.33(8)
C(4)-Zr(1)-C(9)	178.65(8)
C(2)-Zr(1)-Al(2)	111.95(6)

C(7)-Zr(1)-Al(2)	117.05(6)
C(1)-Zr(1)-Al(2)	138.95(6)
C(6)-Zr(1)-Al(2)	146.19(5)
C(8)-Zr(1)-Al(2)	90.34(6)
C(3)-Zr(1)-Al(2)	83.61(6)
C(10)-Zr(1)-Al(2)	124.85(6)
C(5)-Zr(1)-Al(2)	117.09(6)
C(4)-Zr(1)-Al(2)	86.72(6)
C(9)-Zr(1)-Al(2)	94.58(6)
C(2)-Zr(1)-Al(1)	146.06(6)
C(7)-Zr(1)-Al(1)	142.03(6)
C(1)-Zr(1)-Al(1)	120.00(6)
C(6)-Zr(1)-Al(1)	117.24(6)
C(8)-Zr(1)-Al(1)	116.95(6)
C(3)-Zr(1)-Al(1)	121.04(6)
C(10)-Zr(1)-Al(1)	87.71(6)
C(5)-Zr(1)-Al(1)	91.37(6)
C(4)-Zr(1)-Al(1)	92.24(6)
C(9)-Zr(1)-Al(1)	87.81(6)
Al(2)-Zr(1)-Al(1)	71.85(2)
C(12)-Si(1)-C(11)	110.61(11)
C(12)-Si(1)-C(1)	116.15(12)
C(11)-Si(1)-C(1)	109.02(11)
C(12)-Si(1)-C(6)	117.66(11)
C(11)-Si(1)-C(6)	111.12(11)
C(1)-Si(1)-C(6)	90.75(10)
C(12)-Si(1)-Zr(1)	147.35(8)
C(11)-Si(1)-Zr(1)	101.99(8)
C(1)-Si(1)-Zr(1)	47.81(7)
C(6)-Si(1)-Zr(1)	47.92(7)
C(13)-Si(2)-C(14)	111.18(11)
C(13)-Si(2)-C(7)	115.32(11)
C(14)-Si(2)-C(7)	110.56(11)
C(13)-Si(2)-C(2)	117.26(11)
C(14)-Si(2)-C(2)	109.65(11)
C(7)-Si(2)-C(2)	91.38(10)
C(13)-Si(2)-Zr(1)	147.19(8)
C(14)-Si(2)-Zr(1)	101.62(8)
C(7)-Si(2)-Zr(1)	48.32(7)
C(2)-Si(2)-Zr(1)	48.33(7)
C(19)-Al(1)-C(15)	133.69(11)
C(19)-Al(1)-Zr(1)	111.71(7)
C(15)-Al(1)-Zr(1)	114.28(9)
C(23)-Al(2)-C(27)	122.86(12)
C(23)-Al(2)-Zr(1)	113.37(8)
C(27)-Al(2)-Zr(1)	123.63(9)
C(5)-C(1)-C(2)	106.3(2)
C(5)-C(1)-Si(1)	125.30(18)
C(2)-C(1)-Si(1)	123.40(17)
C(5)-C(1)-Zr(1)	76.86(14)
C(2)-C(1)-Zr(1)	72.06(13)

Si(1)-C(1)-Zr(1)	96.78(10)
C(3)-C(2)-C(1)	106.6(2)
C(3)-C(2)-Si(2)	126.16(17)
C(1)-C(2)-Si(2)	122.05(18)
C(3)-C(2)-Zr(1)	77.00(14)
C(1)-C(2)-Zr(1)	72.55(13)
Si(2)-C(2)-Zr(1)	95.64(9)
C(4)-C(3)-C(2)	109.9(2)
C(4)-C(3)-Zr(1)	75.98(14)
C(2)-C(3)-Zr(1)	69.42(13)
C(3)-C(4)-C(5)	107.4(2)
C(3)-C(4)-Zr(1)	71.79(13)
C(5)-C(4)-Zr(1)	71.88(14)
C(4)-C(5)-C(1)	109.7(2)
C(4)-C(5)-Zr(1)	75.79(14)
C(1)-C(5)-Zr(1)	69.54(13)
C(10)-C(6)-C(7)	106.8(2)
C(10)-C(6)-Si(1)	125.23(17)
C(7)-C(6)-Si(1)	122.83(18)
C(10)-C(6)-Zr(1)	76.74(14)
C(7)-C(6)-Zr(1)	72.05(13)
Si(1)-C(6)-Zr(1)	96.46(9)
C(8)-C(7)-C(6)	106.3(2)
C(8)-C(7)-Si(2)	125.65(18)
C(6)-C(7)-Si(2)	122.77(17)
C(8)-C(7)-Zr(1)	76.44(13)
C(6)-C(7)-Zr(1)	72.69(12)
Si(2)-C(7)-Zr(1)	95.84(10)
C(9)-C(8)-C(7)	110.2(2)
C(9)-C(8)-Zr(1)	76.35(13)
C(7)-C(8)-Zr(1)	69.81(12)
C(8)-C(9)-C(10)	107.0(2)
C(8)-C(9)-Zr(1)	71.23(13)
C(10)-C(9)-Zr(1)	71.81(13)
C(9)-C(10)-C(6)	109.8(2)
C(9)-C(10)-Zr(1)	75.81(14)
C(6)-C(10)-Zr(1)	69.67(13)
C(16)-C(15)-Al(1)	116.14(17)
C(18)-C(16)-C(17)	111.0(2)
C(18)-C(16)-C(15)	111.5(2)
C(17)-C(16)-C(15)	111.3(2)
C(20)-C(19)-Al(1)	117.87(16)
C(21)-C(20)-C(22)	110.1(2)
C(21)-C(20)-C(19)	111.3(2)
C(22)-C(20)-C(19)	111.8(2)
C(24)-C(23)-Al(2)	111.77(18)
C(26)-C(24)-C(25)	109.5(3)
C(26)-C(24)-C(23)	111.1(3)
C(25)-C(24)-C(23)	111.5(2)
C(28)-C(27)-Al(2)	114.67(17)
C(29)-C(28)-C(27)	110.5(2)
C(29)-C(28)-C(30)	110.1(2)
C(27)-C(28)-C(30)	111.5(2)
C(41)-B(1)-C(47)	102.07(19)
C(41)-B(1)-C(59)	114.4(2)
C(47)-B(1)-C(59)	112.73(19)
C(41)-B(1)-C(53)	113.15(19)
C(47)-B(1)-C(53)	113.2(2)
C(59)-B(1)-C(53)	101.75(19)
C(46)-C(41)-C(42)	112.1(2)
C(46)-C(41)-B(1)	127.6(2)
C(42)-C(41)-B(1)	119.6(2)
F(1)-C(42)-C(43)	115.9(2)
F(1)-C(42)-C(41)	118.6(2)
C(43)-C(42)-C(41)	125.5(2)
F(2)-C(43)-C(42)	121.6(2)
F(2)-C(43)-C(44)	119.4(2)
C(42)-C(43)-C(44)	119.0(3)
F(3)-C(44)-C(45)	120.7(3)
F(3)-C(44)-C(43)	120.1(3)
C(45)-C(44)-C(43)	119.2(3)
F(4)-C(45)-C(44)	119.8(3)
F(4)-C(45)-C(46)	120.6(3)
C(44)-C(45)-C(46)	119.6(2)
F(5)-C(46)-C(45)	115.1(2)
F(5)-C(46)-C(41)	120.3(2)
C(45)-C(46)-C(41)	124.6(2)
C(48)-C(47)-C(52)	112.2(2)
C(48)-C(47)-B(1)	128.54(19)
C(52)-C(47)-B(1)	118.9(2)
F(6)-C(48)-C(49)	115.1(2)
F(6)-C(48)-C(47)	120.7(2)
C(49)-C(48)-C(47)	124.2(2)
F(7)-C(49)-C(48)	121.0(2)
F(7)-C(49)-C(50)	118.5(2)
C(48)-C(49)-C(50)	120.4(2)
F(8)-C(50)-C(51)	122.3(2)
F(8)-C(50)-C(49)	119.9(2)
C(51)-C(50)-C(49)	117.7(2)
C(50)-C(51)-F(9)	119.6(2)
C(50)-C(51)-C(52)	120.1(2)
F(9)-C(51)-C(52)	120.3(2)
F(10)-C(52)-C(51)	116.3(2)
F(10)-C(52)-C(47)	118.4(2)
C(51)-C(52)-C(47)	125.3(2)
C(54)-C(53)-C(58)	113.3(2)
C(54)-C(53)-B(1)	119.6(2)
C(58)-C(53)-B(1)	127.0(2)
F(11)-C(54)-C(53)	119.2(2)
F(11)-C(54)-C(55)	115.0(2)
C(53)-C(54)-C(55)	125.7(2)
F(12)-C(55)-C(54)	121.5(2)

F(12)-C(55)-C(56)	120.2(2)
C(54)-C(55)-C(56)	118.2(2)
F(13)-C(56)-C(57)	121.3(2)
F(13)-C(56)-C(55)	119.5(2)
C(57)-C(56)-C(55)	119.2(2)
C(56)-C(57)-F(14)	120.0(2)
C(56)-C(57)-C(58)	120.1(2)
F(14)-C(57)-C(58)	119.9(2)
F(15)-C(58)-C(53)	121.8(2)
F(15)-C(58)-C(57)	114.7(2)
C(53)-C(58)-C(57)	123.5(2)
C(64)-C(59)-C(60)	112.7(2)
C(64)-C(59)-B(1)	120.1(2)
C(60)-C(59)-B(1)	127.1(2)
F(16)-C(60)-C(61)	115.2(2)
F(16)-C(60)-C(59)	121.2(2)
C(61)-C(60)-C(59)	123.6(2)
F(17)-C(61)-C(62)	119.5(2)
F(17)-C(61)-C(60)	119.9(2)
C(62)-C(61)-C(60)	120.6(2)
F(18)-C(62)-C(61)	121.1(2)
F(18)-C(62)-C(63)	120.3(3)
C(61)-C(62)-C(63)	118.6(2)
F(19)-C(63)-C(62)	120.3(2)
F(19)-C(63)-C(64)	120.9(2)
C(62)-C(63)-C(64)	118.8(3)
F(20)-C(64)-C(63)	115.7(2)
F(20)-C(64)-C(59)	118.7(2)
C(63)-C(64)-C(59)	125.6(2)

Table C.4: Anisotropic displacement parameters ($Å^2$ x 10^4) for SMB04 (CCDC 776421). The anisotropic displacement factor exponent takes the form: $-2\pi^2[h^2a^{*2}U^{11} + \ldots + 2\ h\ k\ a^*b^*U^{12}]$

	U^{11}	U^{22}	U^{33}	U^{23}	U^{13}	U^{12}
Zr(1)	180(1)	176(1)	169(1)	13(1)	73(1)	9(1)
Si(1)	226(4)	192(4)	197(4)	0(3)	84(3)	-17(3)
Si(2)	188(4)	220(4)	227(4)	1(3)	84(3)	21(3)
Al(1)	218(4)	203(4)	207(5)	14(3)	63(4)	31(3)
Al(2)	246(5)	253(4)	223(5)	-31(4)	55(4)	37(4)
C(1)	189(14)	201(13)	213(16)	11(11)	94(12)	-21(11)
C(2)	161(13)	233(13)	192(15)	3(11)	88(11)	-32(11)
C(3)	220(15)	254(14)	232(16)	-6(11)	151(12)	-17(12)
C(4)	220(15)	308(15)	212(16)	82(12)	86(12)	-14(12)
C(5)	236(15)	201(13)	246(16)	31(12)	121(13)	-30(12)
C(6)	191(14)	187(13)	131(14)	36(10)	64(11)	24(11)
C(7)	204(14)	144(12)	202(15)	58(11)	54(12)	29(11)
C(8)	253(15)	152(12)	218(16)	51(11)	87(12)	15(11)
C(9)	194(14)	199(13)	184(15)	43(11)	72(12)	-29(11)
C(10)	228(14)	195(13)	173(15)	36(11)	113(12)	7(11)
C(11)	352(16)	198(13)	255(17)	26(12)	97(13)	-11(13)
C(12)	265(16)	321(15)	253(17)	-50(12)	83(13)	-36(13)
C(13)	253(16)	288(15)	286(17)	-7(12)	95(13)	48(13)
C(14)	252(16)	275(15)	318(18)	-4(13)	91(13)	52(13)
C(15)	285(16)	330(15)	251(17)	46(13)	76(13)	36(14)
C(16)	308(17)	404(17)	380(20)	180(15)	51(15)	-49(14)
C(17)	364(19)	453(19)	540(20)	273(16)	104(17)	-43(15)
C(18)	800(30)	250(16)	520(20)	11(15)	210(20)	-110(17)
C(19)	227(15)	232(13)	179(16)	12(11)	33(12)	31(12)
C(20)	239(15)	224(14)	235(17)	22(11)	82(13)	17(12)
C(21)	305(17)	534(19)	300(19)	83(14)	107(15)	85(15)
C(22)	272(16)	365(16)	303(18)	70(13)	110(14)	35(13)
C(23)	307(17)	323(15)	242(17)	-44(12)	32(13)	41(13)
C(24)	550(20)	540(20)	330(20)	28(15)	200(17)	131(18)
C(25)	2090(60)	1070(30)	370(30)	220(20)	630(30)	840(40)
C(26)	580(20)	580(20)	640(30)	-101(18)	310(20)	87(19)
C(27)	320(17)	193(14)	339(18)	11(12)	81(14)	58(12)
C(28)	342(18)	326(16)	289(18)	-53(13)	57(14)	-69(14)
C(29)	347(19)	408(18)	610(20)	116(16)	-6(17)	88(15)
C(30)	550(20)	410(19)	790(30)	-112(18)	70(20)	-191(18)
B(1)	231(17)	165(14)	198(18)	-1(12)	115(14)	3(13)
F(1)	308(9)	216(7)	252(9)	-43(6)	72(7)	-26(7)
F(2)	422(10)	456(10)	259(10)	-134(8)	-20(8)	105(8)
F(3)	629(12)	681(11)	178(10)	67(8)	146(9)	300(10)
F(4)	515(11)	441(9)	405(11)	237(8)	316(9)	192(8)
F(5)	348(9)	261(8)	351(10)	66(7)	189(8)	-18(7)
F(6)	279(9)	153(7)	308(9)	31(6)	121(7)	-24(6)
F(7)	217(8)	259(8)	313(10)	9(6)	118(7)	-38(7)

F(8)	205(8)	255(8)	389(10)	-55(7)	95(7)	37(7)
F(9)	317(9)	146(7)	419(10)	32(7)	129(8)	42(7)
F(10)	245(8)	165(7)	321(9)	42(6)	133(7)	-5(6)
F(11)	362(9)	198(7)	201(9)	-33(6)	128(7)	23(7)
F(12)	488(10)	308(8)	201(9)	51(7)	144(8)	9(8)
F(13)	517(11)	216(8)	391(10)	127(7)	181(8)	84(7)
F(14)	500(10)	200(8)	375(10)	37(7)	205(8)	139(8)
F(15)	363(9)	229(7)	211(9)	28(6)	168(7)	86(7)
F(16)	291(9)	246(8)	265(9)	-76(6)	109(7)	3(7)
F(17)	485(11)	278(8)	309(10)	-110(7)	61(8)	-72(8)
F(18)	339(10)	456(10)	392(11)	0(8)	-3(8)	-164(8)
F(19)	213(9)	555(10)	467(11)	-10(8)	124(8)	-26(8)
F(20)	276(9)	346(8)	299(10)	-54(7)	156(7)	30(7)
C(41)	219(14)	175(13)	207(16)	24(11)	103(12)	83(11)
C(42)	258(15)	203(13)	210(17)	15(12)	99(13)	66(12)
C(43)	309(17)	285(15)	215(17)	-47(13)	50(14)	124(13)
C(44)	386(18)	436(18)	147(17)	42(14)	93(14)	250(15)
C(45)	345(17)	317(15)	275(18)	140(14)	207(14)	165(14)
C(46)	256(15)	211(14)	261(17)	2(12)	116(13)	62(13)
C(47)	217(14)	138(12)	121(14)	-22(10)	67(11)	-7(11)
C(48)	235(15)	137(12)	151(15)	-2(10)	53(12)	1(11)
C(49)	178(14)	237(14)	166(15)	-36(11)	95(11)	-63(11)
C(50)	163(14)	214(13)	210(16)	-56(11)	58(12)	26(11)
C(51)	239(15)	132(12)	210(16)	-32(11)	53(12)	4(11)
C(52)	166(14)	200(13)	200(15)	-30(11)	78(12)	-42(11)
C(53)	187(14)	159(13)	184(15)	-34(11)	59(11)	-6(11)
C(54)	219(14)	163(12)	213(15)	-40(12)	83(12)	7(12)
C(55)	306(16)	269(15)	152(16)	40(12)	102(13)	-9(12)
C(56)	328(17)	160(14)	266(17)	69(12)	73(14)	21(12)
C(57)	300(16)	161(13)	282(17)	-5(12)	130(13)	65(12)
C(58)	221(15)	230(14)	185(16)	18(11)	104(12)	2(12)
C(59)	227(14)	158(13)	162(15)	38(11)	78(11)	-9(11)
C(60)	227(15)	178(13)	208(16)	30(11)	87(12)	7(12)
C(61)	369(18)	184(14)	172(16)	-7(11)	57(13)	-40(13)
C(62)	277(17)	311(15)	222(17)	43(13)	-8(13)	-113(13)
C(63)	225(16)	316(16)	291(18)	58(13)	89(13)	-10(13)
C(64)	296(16)	238(14)	199(16)	-3(12)	108(13)	2(12)

Table C.5: Hydrogen coordinates (x 10^4) and isotropic displacement parameters (Å^2 x 10^3) for SMB04 (CCDC 776421).

	x	y	z	U_{iso}
H(1H)	9319(13)	2412(10)	1615(10)	16(6)
H(2H)	9698(14)	3282(11)	2373(10)	24(6)
H(3H)	8716(12)	4120(10)	2325(9)	12(6)

C.2 [(SBI)Zr(μ-H)$_3$(Al^{i}Bu$_2$)$_2$][B(C$_6$F$_5$)$_4$]·½(toluene)

Table C.6: Crystal data and structure refinement for SMB10 (CCDC 778255).

Empirical formula	$[C_{36}H_{57}Al_2SiZr]^+ [BC_{24}BF_{20}]^- \bullet ½ (C_7H_8)$
Formula weight	1388.20
Crystallization Solvent	Toluene
Crystal Habit	Block
Crystal size	0.27 x 0.22 x 0.09 mm^3
Crystal color	Yellow
Data Collection	
Type of diffractometer	Bruker KAPPA APEX II
Wavelength	0.71073 Å MoKα
Data Collection Temperature	100(2) K
θ range for 9981 reflections used in lattice determination	2.36 to 20.95°
Unit cell dimensions	a = 17.3916(7) Å α = 90° b = 26.6355(12) Å β = 90° c = 27.3497(12) Å γ = 90°
Volume	12669.3(9) Å^3
Z	8
Crystal system	Orthorhombic
Space group	P $2_12_12_1$
Density (calculated)	1.456 Mg/m^3
F(000)	5656
Data collection program	Bruker APEX2 v2009.7-0
θ range for data collection	1.39 to 26.97°
Completeness to θ = 26.97°	89.9 %
Index ranges	$-18 \le h \le 21$, $-32 \le k \le 33$, $-33 \le l \le 34$
Data collection scan type	ω scans; 6 settings
Data reduction program	Bruker SAINT-Plus v7.66A
Reflections collected	115139
Independent reflections	23731 [R_{int}= 0.0698]
Absorption coefficient	0.318 mm^{-1}
Absorption correction	None
Max. and min. transmission	0.9719 and 0.9189
Structure solution and Refinement	
Structure solution program	SHELXS-97 (Sheldrick, 2008)
Primary solution method	Direct methods
Secondary solution method	Difference Fourier map
Hydrogen placement	Geometric positions

Structure refinement program	SHELXL-97 (Sheldrick, 2008)
Refinement method	Full matrix least-squares on F^2
Data / restraints / parameters	23731 / 8713 / 1456
Treatment of hydrogen atoms	Riding
Goodness-of-fit on F^2	1.804
Final R indices [I>2σ(I), 13557 reflections]	R1 = 0.0623, *w*R2 = 0.0749
R indices (all data)	R1 = 0.1201, *w*R2 = 0.0779
Type of weighting scheme used	Sigma
Weighting scheme used	$w=1/\sigma^2(Fo^2)$
Max shift/error	0.001
Average shift/error	0.000
Absolute structure determination	Anomalous differences
Absolute structure parameter	-0.02(2)
Largest diff. peak and hole	0.703 and -0.470 e.Å^{-3}

Special Refinement Details

The following commands were used during least-squares refinement. Additionally, all six member rings were constrained to be regular hexagons.

```
DFIX 1.54 0.001 C71A C77A
DFIX 2.54 0.001 C77A C72A C77A C76A
FLAT 0.001 C71A > C77A
ISOR 0.01 C71A > C77A

SAME_ISOB 0.001 0.001 C21 > C24
ISOR_ISOB
```

The toluene solvent was restrained to be flat and the ADP's to simulate isotropic behavior.

The eight isobutyl groups coordinated to Al were organized as residues (RESI) numbered 1-8 with atom names C21-C24 then restrained to have the same geometry (SAME_ISOB) without introducing target values for the 1-2 and 1-3 distances. Their ADP's were restrained to simulate isotropic behavior. Some of these atoms have extremely large ADP’s and no restraints were placed on size.

The difference Fourier map revealed the hydride positions as the six largest peaks near Zr. The positions of the six hydrides (H1H-H6H) were refined during least-squares with the temperature factors restrained to be 1.2 times the U_{eq} of the corresponding metal atom.

Crystals were mounted on a glass fiber using Paratone oil, then placed on the diffractometer under a nitrogen stream at 100K.

Table C.7: Atomic coordinates (x 10^4) and equivalent isotropic displacement parameters ($Å^2$ x 10^3) for SMB10 (CCDC 778255). U_{eq} is defined as the trace of the orthogonalized U^{ij} tensor.

	x	y	z	U_{eq}
Zr(1)	7730(1)	879(1)	9694(1)	41(1)
Si(1)	7600(1)	-348(1)	9923(1)	56(1)
Al(1)	7603(1)	1643(1)	8806(1)	69(1)
Al(2)	8000(1)	1959(1)	10072(1)	72(1)
C(1A)	8408(3)	75(2)	9726(2)	49(2)
C(2A)	8501(3)	259(2)	9248(2)	43(2)
C(3A)	8963(3)	686(2)	9248(2)	53(2)
C(4A)	9204(2)	759(2)	9739(1)	48(2)
C(5A)	8841(2)	412(1)	10039(2)	42(2)
C(6A)	8981(2)	414(1)	10540(2)	55(2)
C(7A)	9485(2)	764(2)	10739(1)	74(2)
C(8A)	9848(2)	1111(1)	10438(2)	81(2)
C(9A)	9708(2)	1109(1)	9938(2)	67(2)
C(10A)	6910(3)	184(2)	9968(2)	46(2)
C(11A)	6898(3)	553(2)	10332(2)	48(2)
C(12A)	6525(3)	971(2)	10187(2)	53(2)
C(13A)	6244(2)	876(2)	9707(1)	58(2)
C(14A)	6502(2)	409(2)	9553(2)	49(2)
C(15A)	6299(2)	229(1)	9094(2)	55(2)
C(16A)	5838(2)	518(2)	8788(1)	81(2)
C(17A)	5579(2)	985(2)	8942(2)	87(2)
C(18A)	5782(2)	1165(1)	9402(2)	86(2)
C(19A)	7413(3)	-819(2)	9443(2)	76(2)
C(20A)	7716(3)	-665(2)	10509(2)	78(2)
C211	8538(3)	1652(2)	8418(2)	95(3)
C221	8754(3)	2002(2)	8059(2)	195(5)
C231	9404(4)	1847(3)	7760(3)	256(7)
C241	8836(4)	2516(2)	8204(3)	201(5)
C212	6835(3)	2152(2)	8868(2)	88(2)
C222	6292(3)	2373(2)	8555(2)	142(4)

C232	6596(3)	2529(2)	8084(2)	82(2)
C242	5802(3)	2755(2)	8754(2)	110(3)
C213	8995(3)	2295(2)	10044(2)	109(3)
C223	9120(3)	2816(2)	10015(2)	171(5)
C233	8973(6)	3032(3)	9537(2)	299(8)
C243	8800(4)	3124(2)	10393(3)	209(5)
C214	6998(3)	2326(2)	10219(2)	98(2)
C224	6813(3)	2494(2)	10692(2)	203(6)
C234	7067(5)	2163(3)	11083(2)	273(7)
C244	6042(4)	2661(3)	10779(2)	264(7)
Zr(2)	7271(1)	5638(1)	8926(1)	44(1)
Si(2)	7383(1)	4399(1)	9037(1)	65(1)
Al(3)	7020(1)	6683(1)	9402(1)	80(1)
Al(4)	7424(1)	6469(1)	8090(1)	64(1)
C(1B)	6592(3)	4844(2)	8904(2)	47(2)
C(2B)	6495(3)	5062(2)	8441(2)	53(2)
C(3B)	6027(3)	5500(2)	8464(2)	50(2)
C(4B)	5786(2)	5535(2)	8963(1)	51(2)
C(5B)	6143(2)	5150(1)	9221(2)	45(2)
C(6B)	5993(2)	5086(2)	9716(2)	70(2)
C(7B)	5486(3)	5408(2)	9954(1)	107(3)
C(8B)	5129(2)	5792(2)	9697(2)	98(3)
C(9B)	5279(2)	5856(1)	9201(2)	71(2)
C(10B)	8087(3)	4909(2)	9136(2)	53(2)
C(11B)	8080(3)	5234(2)	9538(2)	58(2)
C(12B)	8477(3)	5689(3)	9427(2)	74(2)
C(13B)	8769(3)	5637(2)	8961(1)	59(2)
C(14B)	8521(2)	5185(2)	8762(2)	58(2)
C(15B)	8747(3)	5048(1)	8293(2)	77(2)
C(16B)	9222(3)	5364(2)	8023(1)	98(3)
C(17B)	9471(2)	5816(2)	8222(2)	104(3)
C(18B)	9244(2)	5953(1)	8691(2)	91(3)
C(19B)	7258(3)	4033(2)	9605(2)	95(2)
C(20B)	7593(3)	3974(2)	8525(2)	102(2)
C215	8203(3)	6950(2)	8187(2)	99(3)
C225	8442(3)	7397(2)	7960(2)	271(7)
C235	9202(3)	7569(2)	8105(3)	149(4)
C245	8344(5)	7439(3)	7442(2)	241(6)
C216	6473(3)	6505(2)	7699(2)	69(2)
C226	6280(3)	6855(2)	7334(2)	121(3)
C236	6723(3)	6804(3)	6885(2)	176(4)
C246	5480(3)	6921(3)	7224(3)	192(5)
C217	8041(4)	6968(2)	9623(3)	147(4)
C227	8163(4)	7485(2)	9696(2)	233(6)
C237	8965(5)	7638(3)	9671(4)	363(10)
C247	7790(6)	7716(3)	10105(4)	337(9)
C218	6032(3)	7040(2)	9399(2)	143(4)
C228	5722(3)	7417(2)	9098(2)	890(30)
C238	6252(4)	7612(3)	8734(3)	288(7)
C248	4981(4)	7329(3)	8886(3)	333(8)

B(1)	6967(4)	4642(2)	6468(2)	46(2)
F(1A)	8044(2)	4386(1)	7251(1)	83(1)
F(2A)	9222(2)	3754(2)	7209(2)	132(2)
F(3A)	9541(2)	3252(2)	6351(2)	148(2)
F(4A)	8655(2)	3425(1)	5542(2)	118(2)
F(5A)	7458(2)	4012(1)	5588(1)	78(1)
F(6A)	6770(2)	3762(1)	7209(1)	82(1)
F(7A)	5729(2)	3758(2)	7936(1)	103(1)
F(8A)	4728(2)	4537(1)	8055(1)	94(1)
F(9A)	4830(2)	5341(1)	7463(1)	82(1)
F(10A)	5902(2)	5387(1)	6760(1)	58(1)
F(11A)	6117(2)	3764(1)	6214(1)	79(1)
F(12A)	5009(2)	3686(2)	5545(1)	104(1)
F(13A)	4604(2)	4460(1)	4989(1)	93(1)
F(14A)	5350(2)	5364(1)	5092(1)	79(1)
F(15A)	6426(2)	5481(1)	5761(1)	62(1)
F(16A)	7280(2)	5343(1)	7355(1)	61(1)
F(17A)	8241(2)	6106(1)	7356(1)	71(1)
F(18A)	9001(2)	6364(1)	6546(1)	101(1)
F(19A)	8818(2)	5837(1)	5702(1)	94(1)
F(20A)	7882(2)	5045(1)	5682(1)	66(1)
C(41A)	7674(2)	4215(1)	6432(2)	51(2)
C(42A)	8138(3)	4151(2)	6841(1)	70(2)
C(43A)	8768(3)	3831(2)	6820(2)	88(3)
C(44A)	8934(2)	3575(2)	6390(2)	98(3)
C(45A)	8469(3)	3639(2)	5981(2)	84(2)
C(46A)	7839(3)	3959(2)	6002(1)	64(2)
C(47A)	6377(2)	4588(2)	6961(1)	40(2)
C(48A)	6337(2)	4168(1)	7262(2)	57(2)
C(49A)	5786(3)	4143(2)	7629(1)	63(2)
C(50A)	5274(2)	4538(2)	7696(1)	69(2)
C(51A)	5314(2)	4958(2)	7395(2)	57(2)
C(52A)	5865(2)	4983(1)	7028(1)	48(2)
C(53A)	6340(2)	4622(2)	6008(1)	46(2)
C(54A)	5962(3)	4166(2)	5950(1)	55(2)
C(55A)	5374(2)	4121(2)	5609(2)	60(2)
C(56A)	5163(2)	4531(2)	5325(1)	64(2)
C(57A)	5541(3)	4987(2)	5383(1)	57(2)
C(58A)	6129(2)	5033(1)	5724(2)	50(2)
C(59A)	7511(2)	5170(1)	6507(2)	38(2)
C(60A)	7609(2)	5442(2)	6936(1)	51(2)
C(61A)	8114(2)	5847(2)	6947(1)	52(2)
C(62A)	8520(2)	5979(1)	6529(2)	59(2)
C(63A)	8422(2)	5707(2)	6100(1)	62(2)
C(64A)	7918(2)	5302(1)	6088(1)	47(2)
B(2)	7925(3)	9595(2)	7401(2)	40(2)
F(1B)	8172(2)	8833(1)	8260(2)	107(2)
F(2B)	9284(3)	8936(2)	8932(2)	177(2)
F(3B)	10315(2)	9687(2)	8889(2)	166(2)

F(4B)	10161(2)	10395(2)	8207(1)	132(2)
F(5B)	9077(2)	10342(1)	7559(1)	78(1)
F(6B)	7749(2)	10456(1)	8145(1)	60(1)
F(7B)	6854(2)	11240(1)	8036(1)	85(1)
F(8B)	6010(2)	11356(1)	7208(1)	102(1)
F(9B)	6077(2)	10651(2)	6498(1)	92(1)
F(10B)	6988(2)	9847(1)	6585(1)	66(1)
F(11B)	8472(2)	10285(1)	6561(1)	64(1)
F(12B)	9545(2)	10074(1)	5916(1)	92(1)
F(13B)	10264(2)	9172(2)	5935(1)	110(2)
F(14B)	9875(2)	8472(1)	6606(2)	120(2)
F(15B)	8770(2)	8674(1)	7260(1)	89(1)
F(16B)	6918(2)	9511(1)	8220(1)	79(1)
F(17B)	5735(2)	8892(2)	8330(2)	111(2)
F(18B)	5387(2)	8206(2)	7627(2)	123(2)
F(19B)	6224(2)	8191(2)	6803(2)	123(2)
F(20B)	7401(2)	8795(1)	6664(1)	94(1)
C(41B)	8556(2)	9590(2)	7869(1)	50(2)
C(42B)	8600(3)	9213(2)	8220(2)	90(3)
C(43B)	9178(4)	9225(2)	8570(2)	107(4)
C(44B)	9712(3)	9613(3)	8571(2)	109(4)
C(45B)	9668(2)	9990(2)	8221(2)	84(3)
C(46B)	9090(3)	9979(2)	7870(2)	65(2)
C(47B)	7437(2)	10123(1)	7358(2)	39(2)
C(48B)	7397(2)	10482(2)	7726(1)	47(2)
C(49B)	6922(2)	10898(1)	7671(1)	56(2)
C(50B)	6487(2)	10955(1)	7248(2)	61(2)
C(51B)	6527(2)	10595(2)	6880(1)	56(2)
C(52B)	7002(2)	10180(2)	6936(1)	46(2)
C(53B)	8553(2)	9484(2)	6929(1)	43(2)
C(54B)	8761(2)	9842(1)	6582(2)	49(2)
C(55B)	9342(3)	9738(2)	6248(1)	62(2)
C(56B)	9716(2)	9277(2)	6261(2)	70(2)
C(57B)	9509(2)	8920(2)	6608(2)	72(2)
C(58B)	8928(3)	9024(2)	6941(2)	58(2)
C(59B)	7231(2)	9175(1)	7445(2)	52(2)
C(60B)	6796(3)	9190(2)	7871(1)	58(2)
C(61B)	6176(2)	8865(2)	7929(2)	78(2)
C(62B)	5992(2)	8526(2)	7561(2)	83(2)
C(63B)	6428(3)	8511(2)	7135(2)	75(2)
C(64B)	7047(3)	8835(2)	7077(1)	75(2)
C(71A)	7784(3)	2227(2)	6522(2)	245(5)
C(72A)	8274(4)	2351(2)	6140(2)	507(13)
C(73A)	8786(3)	1996(3)	5959(2)	399(9)
C(74A)	8808(3)	1517(3)	6160(3)	248(6)
C(75A)	8318(4)	1393(2)	6543(3)	428(11)
C(76A)	7806(4)	1748(2)	6724(2)	245(5)
C(77A)	7216(4)	2620(3)	6724(3)	254(5)

Table C.8: Bond lengths [Å] and angles [°] for SMB10 (CCDC 778255).

Zr(1)-H(1H)	1.92(4)	C223-C243	1.432(4)
Zr(1)-H(3H)	1.99(4)	C223-C233	1.453(4)
Zr(1)-H(2H)	1.88(3)	C214-C224	1.407(3)
Zr(1)-C(11A)	2.427(5)	C224-C244	1.432(4)
Zr(1)-C(2A)	2.451(5)	C224-C234	1.454(4)
Zr(1)-C(1A)	2.445(5)	Zr(2)-H(6H)	1.94(4)
Zr(1)-C(10A)	2.453(5)	Zr(2)-H(4H)	1.99(4)
Zr(1)-C(5A)	2.483(4)	Zr(2)-H(5H)	1.92(3)
Zr(1)-C(12A)	2.504(5)	Zr(2)-C(1B)	2.425(5)
Zr(1)-C(14A)	2.506(4)	Zr(2)-C(11B)	2.438(5)
Zr(1)-C(3A)	2.519(5)	Zr(2)-C(2B)	2.437(5)
Zr(1)-C(13A)	2.586(4)	Zr(2)-C(10B)	2.475(5)
Zr(1)-C(4A)	2.586(4)	Zr(2)-C(5B)	2.489(4)
Zr(1)-Al(1)	3.1778(18)	Zr(2)-C(12B)	2.510(5)
Zr(1)-Al(2)	3.0944(19)	Zr(2)-C(14B)	2.526(4)
Si(1)-C(20A)	1.822(4)	Zr(2)-C(3B)	2.533(5)
Si(1)-C(19A)	1.843(5)	Zr(2)-C(4B)	2.600(4)
Si(1)-C(10A)	1.862(5)	Zr(2)-C(13B)	2.608(4)
Si(1)-C(1A)	1.881(5)	Zr(2)-Al(3)	3.1016(21)
Al(1)-C212	1.911(4)	Zr(2)-Al(4)	3.1917(18)
Al(1)-C211	1.940(5)	Si(2)-C(20B)	1.837(5)
Al(2)-C213	1.949(5)	Si(2)-C(10B)	1.848(6)
Al(2)-C214	2.038(5)	Si(2)-C(19B)	1.844(5)
C(1A)-C(2A)	1.406(6)	Si(2)-C(1B)	1.852(5)
C(1A)-C(5A)	1.450(6)	Al(3)-C218	1.964(5)
C(2A)-C(3A)	1.392(6)	Al(3)-C217	2.024(6)
C(3A)-C(4A)	1.419(6)	Al(4)-C215	1.883(5)
C(4A)-C(5A)	1.3900	Al(4)-C216	1.971(4)
C(4A)-C(9A)	1.3900	C(1B)-C(2B)	1.403(6)
C(5A)-C(6A)	1.3900	C(1B)-C(5B)	1.424(6)
C(6A)-C(7A)	1.3900	C(2B)-C(3B)	1.425(6)
C(7A)-C(8A)	1.3900	C(3B)-C(4B)	1.432(6)
C(8A)-C(9A)	1.3900	C(4B)-C(5B)	1.3900
C(10A)-C(11A)	1.399(7)	C(4B)-C(9B)	1.3900
C(10A)-C(14A)	1.465(6)	C(5B)-C(6B)	1.3900
C(11A)-C(12A)	1.349(6)	C(6B)-C(7B)	1.3900
C(12A)-C(13A)	1.423(6)	C(7B)-C(8B)	1.3900
C(13A)-C(14A)	1.3900	C(8B)-C(9B)	1.3900
C(13A)-C(18A)	1.3900	C(10B)-C(11B)	1.400(7)
C(14A)-C(15A)	1.3900	C(10B)-C(14B)	1.468(6)
C(15A)-C(16A)	1.3900	C(11B)-C(12B)	1.426(7)
C(16A)-C(17A)	1.3900	C(12B)-C(13B)	1.380(7)
C(17A)-C(18A)	1.3900	C(13B)-C(14B)	1.3900
C211-C221	1.406(3)	C(13B)-C(18B)	1.3900
C221-C241	1.432(4)	C(14B)-C(15B)	1.3900
C221-C231	1.454(4)	C(15B)-C(16B)	1.3900
C212-C222	1.406(3)	C(16B)-C(17B)	1.3900
C222-C242	1.432(4)	C(17B)-C(18B)	1.3900
C222-C232	1.454(4)	C215-C225	1.405(3)
C213-C223	1.407(3)	C225-C245	1.431(4)

C225-C235	1.454(4)
C216-C226	1.408(3)
C226-C246	1.433(4)
C226-C236	1.455(4)
C217-C227	1.407(3)
C227-C247	1.432(4)
C227-C237	1.454(4)
C218-C228	1.407(3)
C228-C248	1.432(4)
C228-C238	1.454(4)
B(1)-C(53A)	1.666(6)
B(1)-C(47A)	1.702(6)
B(1)-C(41A)	1.676(6)
B(1)-C(59A)	1.698(6)
F(1A)-C(42A)	1.294(4)
F(2A)-C(43A)	1.341(4)
F(3A)-C(44A)	1.366(4)
F(4A)-C(45A)	1.369(5)
F(5A)-C(46A)	1.320(4)
F(6A)-C(48A)	1.325(4)
F(7A)-C(49A)	1.329(4)
F(8A)-C(50A)	1.367(4)
F(9A)-C(51A)	1.336(4)
F(10A)-C(52A)	1.305(4)
F(11A)-C(54A)	1.320(4)
F(12A)-C(55A)	1.332(4)
F(13A)-C(56A)	1.352(4)
F(14A)-C(57A)	1.324(4)
F(15A)-C(58A)	1.305(4)
F(16A)-C(60A)	1.308(3)
F(17A)-C(61A)	1.334(4)
F(18A)-C(62A)	1.325(4)
F(19A)-C(63A)	1.332(4)
F(20A)-C(64A)	1.307(4)
C(41A)-C(42A)	1.3900
C(41A)-C(46A)	1.3900
C(42A)-C(43A)	1.3900
C(43A)-C(44A)	1.3900
C(44A)-C(45A)	1.3900
C(45A)-C(46A)	1.3900
C(47A)-C(48A)	1.3900
C(47A)-C(52A)	1.3900
C(48A)-C(49A)	1.3900
C(49A)-C(50A)	1.3900
C(50A)-C(51A)	1.3900
C(51A)-C(52A)	1.3900
C(53A)-C(54A)	1.3900
C(53A)-C(58A)	1.3900
C(54A)-C(55A)	1.3900
C(55A)-C(56A)	1.3900
C(56A)-C(57A)	1.3900
C(57A)-C(58A)	1.3900
C(59A)-C(60A)	1.3900
C(59A)-C(64A)	1.3900
C(60A)-C(61A)	1.3900
C(61A)-C(62A)	1.3900
C(62A)-C(63A)	1.3900
C(63A)-C(64A)	1.3900
B(2)-C(59B)	1.650(6)
B(2)-C(47B)	1.648(6)
B(2)-C(41B)	1.686(6)
B(2)-C(53B)	1.718(6)
F(1B)-C(42B)	1.262(5)
F(2B)-C(43B)	1.267(5)
F(3B)-C(44B)	1.378(5)
F(4B)-C(45B)	1.379(5)
F(5B)-C(46B)	1.289(5)
F(6B)-C(48B)	1.301(3)
F(7B)-C(49B)	1.358(4)
F(8B)-C(50B)	1.358(4)
F(9B)-C(51B)	1.314(4)
F(10B)-C(52B)	1.306(4)
F(11B)-C(54B)	1.286(4)
F(12B)-C(55B)	1.323(4)
F(13B)-C(56B)	1.334(4)
F(14B)-C(57B)	1.351(4)
F(15B)-C(58B)	1.304(4)
F(16B)-C(60B)	1.300(4)
F(17B)-C(61B)	1.341(4)
F(18B)-C(62B)	1.366(4)
F(19B)-C(63B)	1.294(5)
F(20B)-C(64B)	1.292(4)
C(41B)-C(42B)	1.3900
C(41B)-C(46B)	1.3900
C(42B)-C(43B)	1.3900
C(43B)-C(44B)	1.3900
C(44B)-C(45B)	1.3900
C(45B)-C(46B)	1.3900
C(47B)-C(48B)	1.3900
C(47B)-C(52B)	1.3900
C(48B)-C(49B)	1.3900
C(49B)-C(50B)	1.3900
C(50B)-C(51B)	1.3900
C(51B)-C(52B)	1.3900
C(53B)-C(54B)	1.3900
C(53B)-C(58B)	1.3900
C(54B)-C(55B)	1.3900
C(55B)-C(56B)	1.3900
C(56B)-C(57B)	1.3900
C(57B)-C(58B)	1.3900
C(59B)-C(60B)	1.3900
C(59B)-C(64B)	1.3900

C(60B)-C(61B)	1.3900
C(61B)-C(62B)	1.3900
C(62B)-C(63B)	1.3900
C(63B)-C(64B)	1.3900
C(71A)-C(72A)	1.3900
C(71A)-C(76A)	1.3900
C(71A)-C(77A)	1.5406
C(72A)-C(73A)	1.3900
C(73A)-C(74A)	1.3900
C(74A)-C(75A)	1.3900
C(75A)-C(76A)	1.3900
H(1H)-Zr(1)-H(3H)	123.1(14)
H(1H)-Zr(1)-H(2H)	56.7(13)
H(3H)-Zr(1)-H(2H)	66.4(14)
H(1H)-Zr(1)-C(11A)	129.6(10)
H(3H)-Zr(1)-C(11A)	83.5(10)
H(2H)-Zr(1)-C(11A)	125.2(11)
H(1H)-Zr(1)-C(2A)	83.5(10)
H(3H)-Zr(1)-C(2A)	126.5(10)
H(2H)-Zr(1)-C(2A)	118.4(11)
C(11A)-Zr(1)-C(2A)	116.30(19)
H(1H)-Zr(1)-C(1A)	115.2(10)
H(3H)-Zr(1)-C(1A)	110.5(10)
H(2H)-Zr(1)-C(1A)	145.2(11)
C(11A)-Zr(1)-C(1A)	87.06(19)
C(2A)-Zr(1)-C(1A)	33.37(15)
H(1H)-Zr(1)-C(10A)	112.8(10)
H(3H)-Zr(1)-C(10A)	115.1(11)
H(2H)-Zr(1)-C(10A)	147.3(11)
C(11A)-Zr(1)-C(10A)	33.32(15)
C(2A)-Zr(1)-C(10A)	87.83(18)
C(1A)-Zr(1)-C(10A)	67.02(17)
H(1H)-Zr(1)-C(5A)	133.7(10)
H(3H)-Zr(1)-C(5A)	77.1(10)
H(2H)-Zr(1)-C(5A)	122.6(11)
C(11A)-Zr(1)-C(5A)	90.66(16)
C(2A)-Zr(1)-C(5A)	55.03(15)
C(1A)-Zr(1)-C(5A)	34.23(13)
C(10A)-Zr(1)-C(5A)	87.66(15)
H(1H)-Zr(1)-C(12A)	105.6(10)
H(3H)-Zr(1)-C(12A)	79.6(10)
H(2H)-Zr(1)-C(12A)	96.0(11)
C(11A)-Zr(1)-C(12A)	31.69(15)
C(2A)-Zr(1)-C(12A)	142.34(19)
C(1A)-Zr(1)-C(12A)	118.0(2)
C(10A)-Zr(1)-C(12A)	54.75(18)
C(5A)-Zr(1)-C(12A)	119.71(18)
H(1H)-Zr(1)-C(14A)	79.8(10)
H(3H)-Zr(1)-C(14A)	133.6(10)
H(2H)-Zr(1)-C(14A)	119.2(11)

C(11A)-Zr(1)-C(14A)	54.80(15)
C(2A)-Zr(1)-C(14A)	93.06(17)
C(1A)-Zr(1)-C(14A)	88.82(16)
C(10A)-Zr(1)-C(14A)	34.34(13)
C(5A)-Zr(1)-C(14A)	118.13(11)
C(12A)-Zr(1)-C(14A)	54.42(16)
H(1H)-Zr(1)-C(3A)	79.5(10)
H(3H)-Zr(1)-C(3A)	101.6(10)
H(2H)-Zr(1)-C(3A)	90.6(11)
C(11A)-Zr(1)-C(3A)	141.52(19)
C(2A)-Zr(1)-C(3A)	32.50(15)
C(1A)-Zr(1)-C(3A)	55.18(17)
C(10A)-Zr(1)-C(3A)	119.29(18)
C(5A)-Zr(1)-C(3A)	54.60(16)
C(12A)-Zr(1)-C(3A)	173.2(2)
C(14A)-Zr(1)-C(3A)	123.30(17)
H(1H)-Zr(1)-C(13A)	77.4(9)
H(3H)-Zr(1)-C(13A)	108.3(10)
H(2H)-Zr(1)-C(13A)	93.7(11)
C(11A)-Zr(1)-C(13A)	52.63(15)
C(2A)-Zr(1)-C(13A)	123.52(15)
C(1A)-Zr(1)-C(13A)	118.67(17)
C(10A)-Zr(1)-C(13A)	54.01(16)
C(5A)-Zr(1)-C(13A)	140.47(15)
C(12A)-Zr(1)-C(13A)	32.41(13)
C(14A)-Zr(1)-C(13A)	31.6
C(3A)-Zr(1)-C(13A)	148.97(15)
C(20A)-Si(1)-C(19A)	109.4(2)
C(20A)-Si(1)-C(10A)	111.5(2)
C(19A)-Si(1)-C(10A)	116.8(2)
C(20A)-Si(1)-C(1A)	116.5(3)
C(19A)-Si(1)-C(1A)	109.6(2)
C(10A)-Si(1)-C(1A)	92.5(2)
C212-Al(1)-C211	128.7(2)
C212-Al(1)-Zr(1)	115.73(16)
C211-Al(1)-Zr(1)	111.56(18)
C213-Al(2)-C214	123.2(2)
C213-Al(2)-Zr(1)	123.19(17)
C214-Al(2)-Zr(1)	112.48(17)
C(2A)-C(1A)-C(5A)	105.9(5)
C(2A)-C(1A)-Si(1)	124.1(4)
C(5A)-C(1A)-Si(1)	126.1(4)
C(2A)-C(1A)-Zr(1)	73.5(3)
C(5A)-C(1A)-Zr(1)	74.3(3)
Si(1)-C(1A)-Zr(1)	100.1(2)
C(1A)-C(2A)-C(3A)	110.6(5)
C(1A)-C(2A)-Zr(1)	73.1(3)
C(3A)-C(2A)-Zr(1)	76.4(3)
C(2A)-C(3A)-C(4A)	106.4(5)
C(2A)-C(3A)-Zr(1)	71.1(3)
C(4A)-C(3A)-Zr(1)	76.5(3)

C(5A)-C(4A)-C(9A)	120.0
C(5A)-C(4A)-C(3A)	109.5(4)
C(9A)-C(4A)-C(3A)	130.5(4)
C(5A)-C(4A)-Zr(1)	70.03(18)
C(9A)-C(4A)-Zr(1)	124.12(16)
C(3A)-C(4A)-Zr(1)	71.3(3)
C(6A)-C(5A)-C(4A)	120.0
C(6A)-C(5A)-C(1A)	132.4(4)
C(4A)-C(5A)-C(1A)	107.3(4)
C(6A)-C(5A)-Zr(1)	120.57(17)
C(4A)-C(5A)-Zr(1)	78.22(19)
C(1A)-C(5A)-Zr(1)	71.5(2)
C(5A)-C(6A)-C(7A)	120.0
C(6A)-C(7A)-C(8A)	120.0
C(9A)-C(8A)-C(7A)	120.0
C(8A)-C(9A)-C(4A)	120.0
C(11A)-C(10A)-C(14A)	104.9(5)
C(11A)-C(10A)-Si(1)	126.2(4)
C(14A)-C(10A)-Si(1)	124.9(4)
C(11A)-C(10A)-Zr(1)	72.3(3)
C(14A)-C(10A)-Zr(1)	74.8(3)
Si(1)-C(10A)-Zr(1)	100.4(2)
C(12A)-C(11A)-C(10A)	112.1(5)
C(12A)-C(11A)-Zr(1)	77.3(3)
C(10A)-C(11A)-Zr(1)	74.4(3)
C(11A)-C(12A)-C(13A)	106.9(5)
C(11A)-C(12A)-Zr(1)	71.0(3)
C(13A)-C(12A)-Zr(1)	77.0(3)
C(14A)-C(13A)-C(18A)	120.0
C(14A)-C(13A)-C(12A)	109.1(5)
C(18A)-C(13A)-C(12A)	130.9(5)
C(14A)-C(13A)-Zr(1)	71.00(19)
C(18A)-C(13A)-Zr(1)	124.60(16)
C(12A)-C(13A)-Zr(1)	70.6(3)
C(13A)-C(14A)-C(15A)	120.0
C(13A)-C(14A)-C(10A)	106.7(4)
C(15A)-C(14A)-C(10A)	133.0(4)
C(13A)-C(14A)-Zr(1)	77.4(2)
C(15A)-C(14A)-Zr(1)	121.82(17)
C(10A)-C(14A)-Zr(1)	70.8(3)
C(16A)-C(15A)-C(14A)	120.0
C(15A)-C(16A)-C(17A)	120.0
C(18A)-C(17A)-C(16A)	120.0
C(17A)-C(18A)-C(13A)	120.0
C221-C211-Al(1)	127.9(4)
C211-C221-C241	117.7(3)
C211-C221-C231	114.4(3)
C241-C221-C231	110.5(3)
C222-C212-Al(1)	135.5(3)
C212-C222-C242	117.8(3)
C212-C222-C232	114.5(3)
C242-C222-C232	110.6(3)
C223-C213-Al(2)	126.3(4)
C213-C223-C243	117.7(3)
C213-C223-C233	114.5(3)
C243-C223-C233	110.7(3)
C224-C214-Al(2)	122.0(3)
C214-C224-C244	117.7(3)
C214-C224-C234	114.4(3)
C244-C224-C234	110.5(3)
H(6H)-Zr(2)-H(4H)	129.4(14)
H(6H)-Zr(2)-H(5H)	65.0(14)
H(4H)-Zr(2)-H(5H)	64.9(14)
H(6H)-Zr(2)-C(1B)	111.1(10)
H(4H)-Zr(2)-C(1B)	115.6(10)
H(5H)-Zr(2)-C(1B)	150.6(10)
H(6H)-Zr(2)-C(11B)	81.1(10)
H(4H)-Zr(2)-C(11B)	120.4(10)
H(5H)-Zr(2)-C(11B)	121.2(11)
C(1B)-Zr(2)-C(11B)	84.96(18)
H(6H)-Zr(2)-C(2B)	128.8(10)
H(4H)-Zr(2)-C(2B)	86.2(10)
H(5H)-Zr(2)-C(2B)	124.2(11)
C(1B)-Zr(2)-C(2B)	33.55(16)
C(11B)-Zr(2)-C(2B)	114.5(2)
H(6H)-Zr(2)-C(10B)	113.1(10)
H(4H)-Zr(2)-C(10B)	102.5(10)
H(5H)-Zr(2)-C(10B)	143.0(10)
C(1B)-Zr(2)-C(10B)	66.37(18)
C(11B)-Zr(2)-C(10B)	33.11(16)
C(2B)-Zr(2)-C(10B)	87.05(19)
H(6H)-Zr(2)-C(5B)	79.2(10)
H(4H)-Zr(2)-C(5B)	138.4(10)
H(5H)-Zr(2)-C(5B)	125.2(10)
C(1B)-Zr(2)-C(5B)	33.67(14)
C(11B)-Zr(2)-C(5B)	90.08(18)
C(2B)-Zr(2)-C(5B)	53.88(16)
C(10B)-Zr(2)-C(5B)	88.07(16)
H(6H)-Zr(2)-C(12B)	76.0(10)
H(4H)-Zr(2)-C(12B)	97.7(10)
H(5H)-Zr(2)-C(12B)	90.2(11)
C(1B)-Zr(2)-C(12B)	117.8(2)
C(11B)-Zr(2)-C(12B)	33.47(16)
C(2B)-Zr(2)-C(12B)	142.5(2)
C(10B)-Zr(2)-C(12B)	55.65(19)
C(5B)-Zr(2)-C(12B)	120.6(2)
H(6H)-Zr(2)-C(14B)	129.0(10)
H(4H)-Zr(2)-C(14B)	69.9(10)
H(5H)-Zr(2)-C(14B)	115.7(10)
C(1B)-Zr(2)-C(14B)	89.86(16)
C(11B)-Zr(2)-C(14B)	54.11(17)
C(2B)-Zr(2)-C(14B)	94.52(18)

C(10B)-Zr(2)-C(14B)	34.13(13)
C(5B)-Zr(2)-C(14B)	119.09(12)
C(12B)-Zr(2)-C(14B)	53.35(19)
H(6H)-Zr(2)-C(3B)	104.4(10)
H(4H)-Zr(2)-C(3B)	86.7(10)
H(5H)-Zr(2)-C(3B)	95.4(11)
C(1B)-Zr(2)-C(3B)	56.25(17)
C(11B)-Zr(2)-C(3B)	140.46(19)
C(2B)-Zr(2)-C(3B)	33.25(15)
C(10B)-Zr(2)-C(3B)	119.42(19)
C(5B)-Zr(2)-C(3B)	53.97(16)
C(12B)-Zr(2)-C(3B)	173.9(2)
C(14B)-Zr(2)-C(3B)	125.27(18)
H(6H)-Zr(2)-C(4B)	76.1(10)
H(4H)-Zr(2)-C(4B)	117.0(10)
H(5H)-Zr(2)-C(4B)	97.4(10)
C(1B)-Zr(2)-C(4B)	54.86(16)
C(11B)-Zr(2)-C(4B)	119.96(16)
C(2B)-Zr(2)-C(4B)	53.46(16)
C(10B)-Zr(2)-C(4B)	118.51(17)
C(5B)-Zr(2)-C(4B)	31.6
C(12B)-Zr(2)-C(4B)	144.53(18)
C(14B)-Zr(2)-C(4B)	144.22(15)
C(3B)-Zr(2)-C(4B)	32.36(13)
C(20B)-Si(2)-C(10B)	115.6(3)
C(20B)-Si(2)-C(19B)	109.8(3)
C(10B)-Si(2)-C(19B)	110.1(3)
C(20B)-Si(2)-C(1B)	113.1(3)
C(10B)-Si(2)-C(1B)	92.9(2)
C(19B)-Si(2)-C(1B)	114.6(3)
C218-Al(3)-C217	125.9(3)
C218-Al(3)-Zr(2)	123.8(2)
C217-Al(3)-Zr(2)	109.76(19)
C215-Al(4)-C216	130.3(2)
C215-Al(4)-Zr(2)	115.54(16)
C216-Al(4)-Zr(2)	110.57(15)
C(2B)-C(1B)-C(5B)	104.2(5)
C(2B)-C(1B)-Si(2)	122.1(5)
C(5B)-C(1B)-Si(2)	130.9(4)
C(2B)-C(1B)-Zr(2)	73.7(3)
C(5B)-C(1B)-Zr(2)	75.6(3)
Si(2)-C(1B)-Zr(2)	101.1(2)
C(1B)-C(2B)-C(3B)	111.6(5)
C(1B)-C(2B)-Zr(2)	72.8(3)
C(3B)-C(2B)-Zr(2)	77.1(3)
C(4B)-C(3B)-C(2B)	105.3(5)
C(4B)-C(3B)-Zr(2)	76.4(3)
C(2B)-C(3B)-Zr(2)	69.7(3)
C(5B)-C(4B)-C(9B)	120.0
C(5B)-C(4B)-C(3B)	107.7(4)
C(9B)-C(4B)-C(3B)	132.2(4)

C(5B)-C(4B)-Zr(2)	69.78(19)
C(9B)-C(4B)-Zr(2)	125.69(17)
C(3B)-C(4B)-Zr(2)	71.2(3)
C(6B)-C(5B)-C(4B)	120.0
C(6B)-C(5B)-C(1B)	128.8(4)
C(4B)-C(5B)-C(1B)	111.1(4)
C(6B)-C(5B)-Zr(2)	121.85(18)
C(4B)-C(5B)-Zr(2)	78.6(2)
C(1B)-C(5B)-Zr(2)	70.7(3)
C(5B)-C(6B)-C(7B)	120.0
C(6B)-C(7B)-C(8B)	120.0
C(9B)-C(8B)-C(7B)	120.0
C(8B)-C(9B)-C(4B)	120.0
C(11B)-C(10B)-C(14B)	103.9(5)
C(11B)-C(10B)-Si(2)	124.3(5)
C(14B)-C(10B)-Si(2)	127.5(4)
C(11B)-C(10B)-Zr(2)	72.0(3)
C(14B)-C(10B)-Zr(2)	74.9(3)
Si(2)-C(10B)-Zr(2)	99.4(2)
C(10B)-C(11B)-C(12B)	110.8(6)
C(10B)-C(11B)-Zr(2)	74.9(3)
C(12B)-C(11B)-Zr(2)	76.0(3)
C(13B)-C(12B)-C(11B)	106.9(6)
C(13B)-C(12B)-Zr(2)	78.3(3)
C(11B)-C(12B)-Zr(2)	70.5(3)
C(14B)-C(13B)-C(18B)	120.0
C(14B)-C(13B)-C(12B)	109.4(5)
C(18B)-C(13B)-C(12B)	130.6(5)
C(14B)-C(13B)-Zr(2)	71.1(2)
C(18B)-C(13B)-Zr(2)	124.99(18)
C(12B)-C(13B)-Zr(2)	70.5(3)
C(15B)-C(14B)-C(13B)	120.0
C(15B)-C(14B)-C(10B)	131.0(5)
C(13B)-C(14B)-C(10B)	108.8(5)
C(15B)-C(14B)-Zr(2)	122.17(19)
C(13B)-C(14B)-Zr(2)	77.5(2)
C(10B)-C(14B)-Zr(2)	71.0(3)
C(14B)-C(15B)-C(16B)	120.0
C(15B)-C(16B)-C(17B)	120.0
C(18B)-C(17B)-C(16B)	120.0
C(17B)-C(18B)-C(13B)	120.0
C225-C215-Al(4)	136.7(3)
C215-C225-C245	117.9(3)
C215-C225-C235	114.6(3)
C245-C225-C235	110.6(3)
C226-C216-Al(4)	128.1(4)
C216-C226-C246	117.6(3)
C216-C226-C236	114.3(3)
C246-C226-C236	110.4(3)
C227-C217-Al(3)	122.9(4)
C217-C227-C247	117.7(3)

C217-C227-C237	114.4(3)
C247-C227-C237	110.5(3)
C228-C218-Al(3)	133.1(4)
C218-C228-C248	117.7(3)
C218-C228-C238	114.4(3)
C248-C228-C238	110.5(3)
C(53A)-B(1)-C(47A)	101.6(4)
C(53A)-B(1)-C(41A)	114.5(4)
C(47A)-B(1)-C(41A)	115.5(4)
C(53A)-B(1)-C(59A)	116.0(4)
C(47A)-B(1)-C(59A)	110.9(4)
C(41A)-B(1)-C(59A)	99.0(4)
C(42A)-C(41A)-C(46A)	120.0
C(42A)-C(41A)-B(1)	117.6(4)
C(46A)-C(41A)-B(1)	122.2(4)
F(1A)-C(42A)-C(43A)	115.7(5)
F(1A)-C(42A)-C(41A)	124.3(4)
C(43A)-C(42A)-C(41A)	120.0
F(2A)-C(43A)-C(44A)	118.4(5)
F(2A)-C(43A)-C(42A)	121.6(5)
C(44A)-C(43A)-C(42A)	120.0
F(3A)-C(44A)-C(43A)	122.3(5)
F(3A)-C(44A)-C(45A)	117.7(5)
C(43A)-C(44A)-C(45A)	120.0
F(4A)-C(45A)-C(46A)	118.6(4)
F(4A)-C(45A)-C(44A)	121.2(4)
C(46A)-C(45A)-C(44A)	120.0
F(5A)-C(46A)-C(45A)	115.2(4)
F(5A)-C(46A)-C(41A)	124.7(4)
C(45A)-C(46A)-C(41A)	120.0
C(48A)-C(47A)-C(52A)	120.0
C(48A)-C(47A)-B(1)	124.5(4)
C(52A)-C(47A)-B(1)	115.2(4)
F(6A)-C(48A)-C(47A)	124.4(4)
F(6A)-C(48A)-C(49A)	115.5(4)
C(47A)-C(48A)-C(49A)	120.0
F(7A)-C(49A)-C(50A)	116.9(4)
F(7A)-C(49A)-C(48A)	123.1(4)
C(50A)-C(49A)-C(48A)	120.0
F(8A)-C(50A)-C(49A)	122.5(4)
F(8A)-C(50A)-C(51A)	117.5(4)
C(49A)-C(50A)-C(51A)	120.0
F(9A)-C(51A)-C(50A)	120.1(4)
F(9A)-C(51A)-C(52A)	119.8(4)
C(50A)-C(51A)-C(52A)	120.0
F(10A)-C(52A)-C(51A)	118.7(4)
F(10A)-C(52A)-C(47A)	121.3(4)
C(51A)-C(52A)-C(47A)	120.0
C(54A)-C(53A)-C(58A)	120.0
C(54A)-C(53A)-B(1)	115.0(4)
C(58A)-C(53A)-B(1)	124.7(4)

F(11A)-C(54A)-C(53A)	123.5(4)
F(11A)-C(54A)-C(55A)	116.5(4)
C(53A)-C(54A)-C(55A)	120.0
F(12A)-C(55A)-C(56A)	119.0(4)
F(12A)-C(55A)-C(54A)	121.0(4)
C(56A)-C(55A)-C(54A)	120.0
F(13A)-C(56A)-C(57A)	122.6(5)
F(13A)-C(56A)-C(55A)	117.4(5)
C(57A)-C(56A)-C(55A)	120.0
F(14A)-C(57A)-C(56A)	118.5(4)
F(14A)-C(57A)-C(58A)	121.5(4)
C(56A)-C(57A)-C(58A)	120.0
F(15A)-C(58A)-C(57A)	115.1(4)
F(15A)-C(58A)-C(53A)	124.8(4)
C(57A)-C(58A)-C(53A)	120.0
C(60A)-C(59A)-C(64A)	120.0
C(60A)-C(59A)-B(1)	123.6(4)
C(64A)-C(59A)-B(1)	116.2(4)
F(16A)-C(60A)-C(59A)	125.5(4)
F(16A)-C(60A)-C(61A)	114.5(4)
C(59A)-C(60A)-C(61A)	120.0
F(17A)-C(61A)-C(62A)	118.3(4)
F(17A)-C(61A)-C(60A)	121.6(4)
C(62A)-C(61A)-C(60A)	120.0
F(18A)-C(62A)-C(63A)	120.8(4)
F(18A)-C(62A)-C(61A)	119.2(4)
C(63A)-C(62A)-C(61A)	120.0
F(19A)-C(63A)-C(62A)	119.3(4)
F(19A)-C(63A)-C(64A)	120.7(4)
C(62A)-C(63A)-C(64A)	120.0
F(20A)-C(64A)-C(63A)	117.1(3)
F(20A)-C(64A)-C(59A)	122.8(3)
C(63A)-C(64A)-C(59A)	120.0
C(59B)-B(2)-C(47B)	102.0(4)
C(59B)-B(2)-C(41B)	114.6(4)
C(47B)-B(2)-C(41B)	113.3(4)
C(59B)-B(2)-C(53B)	113.9(4)
C(47B)-B(2)-C(53B)	114.8(4)
C(41B)-B(2)-C(53B)	99.0(3)
C(42B)-C(41B)-C(46B)	120.0
C(42B)-C(41B)-B(2)	124.3(4)
C(46B)-C(41B)-B(2)	115.5(4)
F(1B)-C(42B)-C(43B)	112.5(5)
F(1B)-C(42B)-C(41B)	127.4(5)
C(43B)-C(42B)-C(41B)	120.0
F(2B)-C(43B)-C(42B)	129.2(6)
F(2B)-C(43B)-C(44B)	110.7(6)
C(42B)-C(43B)-C(44B)	120.0
F(3B)-C(44B)-C(45B)	112.0(6)
F(3B)-C(44B)-C(43B)	128.0(6)
C(45B)-C(44B)-C(43B)	120.0

C(44B)-C(45B)-C(46B)	120.0
C(44B)-C(45B)-F(4B)	123.3(5)
C(46B)-C(45B)-F(4B)	116.6(5)
F(5B)-C(46B)-C(45B)	116.8(5)
F(5B)-C(46B)-C(41B)	123.2(5)
C(45B)-C(46B)-C(41B)	120.0
C(48B)-C(47B)-C(52B)	120.0
C(48B)-C(47B)-B(2)	124.2(3)
C(52B)-C(47B)-B(2)	115.6(3)
F(6B)-C(48B)-C(47B)	125.2(4)
F(6B)-C(48B)-C(49B)	114.7(4)
C(47B)-C(48B)-C(49B)	120.0
F(7B)-C(49B)-C(50B)	119.5(4)
F(7B)-C(49B)-C(48B)	120.4(4)
C(50B)-C(49B)-C(48B)	120.0
F(8B)-C(50B)-C(49B)	119.1(4)
F(8B)-C(50B)-C(51B)	120.9(4)
C(49B)-C(50B)-C(51B)	120.0
F(9B)-C(51B)-C(50B)	117.9(4)
F(9B)-C(51B)-C(52B)	122.0(4)
C(50B)-C(51B)-C(52B)	120.0
F(10B)-C(52B)-C(51B)	116.7(4)
F(10B)-C(52B)-C(47B)	123.2(4)
C(51B)-C(52B)-C(47B)	120.0
C(54B)-C(53B)-C(58B)	120.0
C(54B)-C(53B)-B(2)	124.1(4)
C(58B)-C(53B)-B(2)	115.4(4)
F(11B)-C(54B)-C(53B)	123.9(4)
F(11B)-C(54B)-C(55B)	116.0(4)
C(53B)-C(54B)-C(55B)	120.0
F(12B)-C(55B)-C(54B)	120.7(4)
F(12B)-C(55B)-C(56B)	119.3(4)
C(54B)-C(55B)-C(56B)	120.0
F(13B)-C(56B)-C(57B)	119.8(5)
F(13B)-C(56B)-C(55B)	120.2(5)
C(57B)-C(56B)-C(55B)	120.0
F(14B)-C(57B)-C(58B)	121.4(4)
F(14B)-C(57B)-C(56B)	118.6(4)
C(58B)-C(57B)-C(56B)	120.0
F(15B)-C(58B)-C(57B)	116.7(4)
F(15B)-C(58B)-C(53B)	123.3(4)
C(57B)-C(58B)-C(53B)	120.0
C(60B)-C(59B)-C(64B)	120.0
C(60B)-C(59B)-B(2)	116.1(4)
C(64B)-C(59B)-B(2)	123.8(4)
F(16B)-C(60B)-C(61B)	116.9(4)
F(16B)-C(60B)-C(59B)	123.1(4)
C(61B)-C(60B)-C(59B)	120.0
F(17B)-C(61B)-C(60B)	120.3(5)
F(17B)-C(61B)-C(62B)	119.6(5)
C(60B)-C(61B)-C(62B)	120.0
F(18B)-C(62B)-C(63B)	120.8(5)
F(18B)-C(62B)-C(61B)	119.2(5)
C(63B)-C(62B)-C(61B)	120.0
F(19B)-C(63B)-C(62B)	117.2(5)
F(19B)-C(63B)-C(64B)	122.8(5)
C(62B)-C(63B)-C(64B)	120.0
F(20B)-C(64B)-C(63B)	114.7(4)
F(20B)-C(64B)-C(59B)	125.3(4)
C(63B)-C(64B)-C(59B)	120.0
C(72A)-C(71A)-C(76A)	120.0
C(72A)-C(71A)-C(77A)	120.05(5)
C(76A)-C(71A)-C(77A)	119.95(5)
C(73A)-C(72A)-C(71A)	120.0
C(74A)-C(73A)-C(72A)	120.0
C(73A)-C(74A)-C(75A)	120.0
C(74A)-C(75A)-C(76A)	120.0
C(75A)-C(76A)-C(71A)	120.0

Table C.9: Anisotropic displacement parameters ($Å^2$ x 10^4) for SMB10 (CCDC 778255). The anisotropic displacement factor exponent takes the form: $-2\pi^2[h^2a^{*2}U^{11} + ... + 2 h k a^* b^* U^{12}]$

	U^{11}	U^{22}	U^{33}	U^{23}	U^{13}	U^{12}
Zr(1)	385(3)	511(4)	340(3)	-12(3)	36(3)	29(3)
Si(1)	688(13)	547(11)	433(11)	6(9)	5(10)	-37(11)
Al(1)	842(16)	593(13)	647(14)	188(11)	19(12)	87(12)
Al(2)	721(15)	612(14)	819(16)	-214(12)	38(12)	38(12)
C(1A)	540(40)	500(40)	420(40)	0(40)	10(30)	160(30)
C(2A)	450(40)	430(40)	400(40)	-20(30)	40(30)	90(30)
C(3A)	550(40)	600(50)	440(40)	40(40)	130(30)	140(40)
C(4A)	230(40)	610(50)	600(50)	-120(40)	10(30)	80(30)
C(5A)	290(40)	620(50)	340(40)	130(40)	50(30)	-10(30)
C(6A)	470(40)	710(50)	470(40)	30(40)	-20(30)	90(40)
C(7A)	700(50)	990(60)	550(50)	-120(50)	-320(40)	180(40)
C(8A)	460(40)	780(60)	1180(70)	-350(50)	200(50)	-180(40)
C(9A)	550(50)	800(50)	670(50)	40(40)	200(40)	260(40)
C(10A)	420(40)	550(40)	400(40)	20(30)	30(30)	50(30)
C(11A)	420(40)	710(50)	300(30)	100(40)	30(30)	-40(40)
C(12A)	330(40)	720(50)	540(40)	-170(40)	200(30)	-180(40)
C(13A)	170(40)	680(50)	880(60)	-110(50)	110(40)	130(30)
C(14A)	330(40)	530(40)	630(50)	-60(40)	60(40)	-60(30)
C(15A)	390(40)	880(50)	390(40)	70(40)	40(30)	-70(40)
C(16A)	430(50)	1430(70)	560(50)	-20(50)	-100(40)	-240(50)
C(17A)	440(40)	1150(70)	1010(70)	0(60)	-250(50)	-40(50)
C(18A)	390(50)	910(60)	1260(70)	-100(60)	180(50)	150(40)
C(19A)	820(50)	570(40)	900(50)	-240(40)	-30(40)	-90(40)
C(20A)	1060(50)	740(40)	550(40)	300(40)	60(40)	-180(40)
C211	1400(70)	750(50)	710(50)	230(40)	330(50)	110(50)
C221	1180(80)	1590(100)	3100(140)	470(100)	1360(90)	230(80)
C231	1120(70)	2870(130)	3690(160)	2190(120)	1070(90)	390(80)
C241	1040(70)	1070(80)	3910(160)	300(100)	-710(90)	-180(60)
C212	1080(60)	780(50)	780(50)	20(40)	120(50)	340(40)
C222	1290(70)	2320(100)	640(50)	620(60)	580(50)	1350(70)
C232	870(50)	690(50)	890(60)	20(40)	-190(40)	190(40)
C242	1000(60)	1430(70)	870(60)	360(50)	290(50)	790(50)
C213	850(50)	740(50)	1690(80)	-710(60)	-60(50)	-160(50)
C223	2750(120)	720(70)	1660(100)	-400(70)	-940(90)	430(80)
C233	3210(140)	1910(110)	3850(180)	990(120)	720(130)	1650(100)
C243	1410(80)	970(70)	3900(170)	-330(100)	330(100)	-190(60)
C214	720(50)	900(50)	1340(70)	-410(50)	120(50)	-220(40)
C224	1520(90)	3550(160)	1020(80)	-1200(100)	360(70)	250(90)
C234	4690(170)	2260(110)	1250(90)	-60(90)	500(120)	1420(120)
C244	1510(80)	4590(160)	1830(100)	-1910(110)	-120(70)	1560(100)
Zr(2)	435(3)	553(4)	339(3)	77(3)	-90(3)	-48(3)
Si(2)	717(13)	587(11)	651(12)	110(11)	-7(11)	50(12)
Al(3)	1170(20)	658(14)	557(14)	-43(12)	-156(13)	-62(14)
Al(4)	712(15)	633(13)	591(13)	206(10)	-112(11)	-58(11)
C(1B)	540(40)	540(40)	330(40)	190(30)	-40(30)	-50(30)

C(2B)	560(40)	620(50)	400(40)	-160(40)	-90(30)	-70(40)
C(3B)	420(40)	610(50)	480(40)	60(40)	-140(30)	-160(30)
C(4B)	380(40)	740(50)	420(40)	-20(40)	90(40)	20(40)
C(5B)	460(40)	570(50)	320(40)	130(30)	-10(30)	-50(30)
C(6B)	540(40)	1070(60)	470(40)	200(50)	-60(40)	-260(40)
C(7B)	920(70)	1730(90)	550(50)	-80(60)	180(50)	-40(60)
C(8B)	690(50)	1560(80)	690(50)	-330(60)	300(50)	-270(50)
C(9B)	580(50)	630(50)	920(60)	-50(50)	-260(40)	40(40)
C(10B)	480(40)	800(50)	320(40)	160(40)	-120(30)	120(40)
C(11B)	560(40)	660(50)	520(40)	260(40)	-250(40)	40(40)
C(12B)	680(50)	920(60)	620(50)	-70(50)	-460(40)	-40(40)
C(13B)	430(40)	770(50)	570(50)	170(50)	-80(40)	-90(40)
C(14B)	450(40)	890(60)	390(40)	140(40)	-180(40)	-10(40)
C(15B)	650(50)	920(60)	730(60)	270(50)	-40(40)	380(50)
C(16B)	570(50)	1410(80)	950(60)	510(60)	240(50)	290(50)
C(17B)	450(50)	1280(80)	1390(80)	820(70)	-60(50)	-50(50)
C(18B)	450(50)	1040(60)	1250(70)	520(60)	-280(50)	-110(50)
C(19B)	880(40)	770(50)	1180(60)	570(40)	-110(50)	-110(40)
C(20B)	1000(60)	810(50)	1240(60)	-330(50)	20(50)	250(50)
C215	1320(60)	620(50)	1030(60)	0(40)	-710(50)	-220(50)
C225	2710(130)	3070(140)	2360(140)	-390(120)	-740(110)	-2560(110)
C235	1400(70)	1180(70)	1880(100)	10(70)	-40(70)	-600(60)
C245	2350(110)	2720(130)	2160(120)	-1000(100)	-150(90)	-1500(100)
C216	600(40)	880(50)	590(40)	370(40)	-120(40)	-60(40)
C226	680(60)	2270(100)	680(60)	540(70)	30(50)	140(60)
C236	1880(90)	1090(70)	2310(110)	990(80)	-400(80)	-50(70)
C246	620(50)	2220(100)	2920(130)	1400(90)	-730(70)	-110(60)
C217	1790(80)	1080(70)	1530(80)	-310(60)	-910(70)	-410(60)
C227	2460(130)	960(80)	3580(170)	-710(100)	-20(120)	-700(90)
C237	4590(190)	2780(140)	3540(190)	740(130)	-860(160)	-2550(140)
C247	4480(190)	2360(130)	3280(170)	-1300(120)	420(150)	390(140)
C218	1080(60)	930(60)	2280(100)	-700(70)	720(60)	160(50)
C228	9200(300)	8800(400)	8800(400)	1600(300)	700(300)	0(300)
C238	2870(130)	3730(160)	2060(120)	410(120)	-90(100)	2370(120)
C248	6900(200)	2340(120)	760(80)	220(90)	0(130)	220(150)
B(1)	510(50)	480(40)	390(40)	110(40)	-20(40)	20(40)
F(1A)	780(30)	1130(30)	590(20)	110(20)	-190(20)	50(20)
F(2A)	820(30)	1740(50)	1410(40)	580(40)	-400(30)	430(30)
F(3A)	760(30)	1170(40)	2500(60)	440(40)	310(30)	440(30)
F(4A)	1220(30)	750(30)	1560(40)	-50(30)	490(30)	270(30)
F(5A)	730(30)	950(30)	640(20)	-50(20)	70(19)	170(20)
F(6A)	870(30)	650(30)	950(30)	330(20)	140(20)	20(20)
F(7A)	940(30)	1320(40)	840(30)	520(30)	0(20)	-380(30)
F(8A)	650(20)	1720(40)	460(20)	140(30)	230(20)	-270(30)
F(9A)	410(20)	1350(40)	680(30)	30(30)	33(19)	140(20)
F(10A)	560(20)	770(30)	410(20)	80(20)	-30(17)	160(20)
F(11A)	760(30)	770(30)	840(30)	90(20)	-90(20)	-50(20)
F(12A)	840(30)	1380(40)	910(30)	30(30)	-230(20)	-370(30)
F(13A)	610(20)	1510(40)	660(30)	-50(30)	-280(20)	160(20)
F(14A)	750(20)	1110(30)	510(20)	200(20)	-26(19)	410(20)

F(15A)	760(20)	570(20)	510(20)	190(20)	-48(18)	80(20)
F(16A)	650(20)	840(20)	332(18)	86(17)	15(19)	-120(20)
F(17A)	760(20)	820(30)	540(20)	-70(20)	-136(19)	-120(20)
F(18A)	1240(30)	1020(30)	780(30)	120(30)	-150(20)	-460(30)
F(19A)	850(30)	1270(30)	690(30)	260(30)	200(20)	-420(20)
F(20A)	630(20)	910(20)	440(20)	-100(20)	234(19)	-20(20)
C(41A)	600(40)	480(40)	460(40)	150(30)	160(40)	-60(40)
C(42A)	460(50)	690(50)	940(60)	420(50)	-120(50)	70(40)
C(43A)	960(70)	950(70)	740(60)	40(50)	200(50)	-40(50)
C(44A)	320(50)	790(60)	1810(100)	480(60)	-360(60)	150(40)
C(45A)	980(60)	470(50)	1070(70)	110(50)	480(60)	180(40)
C(46A)	470(50)	530(40)	940(60)	80(40)	0(40)	160(40)
C(47A)	380(40)	410(40)	410(40)	80(30)	-90(30)	-120(30)
C(48A)	610(50)	690(50)	410(40)	100(40)	-10(40)	10(40)
C(49A)	570(50)	900(60)	440(40)	250(40)	-80(40)	-190(40)
C(50A)	400(40)	1290(70)	380(40)	60(50)	30(40)	-320(50)
C(51A)	370(40)	790(50)	560(50)	150(40)	-60(40)	20(40)
C(52A)	410(40)	700(50)	310(40)	50(40)	20(30)	40(40)
C(53A)	430(40)	480(40)	470(40)	120(40)	220(30)	100(30)
C(54A)	600(50)	730(50)	330(40)	60(40)	120(30)	80(40)
C(55A)	400(40)	860(60)	540(50)	-60(50)	90(40)	-30(40)
C(56A)	420(40)	1090(60)	400(40)	-70(50)	80(40)	340(50)
C(57A)	490(50)	860(60)	360(40)	-40(40)	120(40)	100(40)
C(58A)	440(40)	660(50)	400(40)	40(40)	130(30)	170(40)
C(59A)	270(40)	570(40)	310(30)	180(30)	50(30)	130(30)
C(60A)	530(40)	600(40)	420(40)	90(30)	30(40)	60(40)
C(61A)	510(40)	610(50)	440(40)	30(40)	100(30)	-40(40)
C(62A)	430(40)	490(50)	840(50)	90(40)	-170(40)	-200(40)
C(63A)	430(40)	960(60)	470(40)	80(40)	50(40)	-190(40)
C(64A)	330(40)	620(40)	450(40)	170(40)	50(40)	0(30)
B(2)	420(40)	520(40)	260(40)	-50(30)	50(30)	10(40)
F(1B)	1390(40)	830(30)	990(30)	530(30)	240(30)	520(30)
F(2B)	1860(50)	2730(60)	720(30)	470(40)	-120(30)	1460(40)
F(3B)	860(30)	3430(70)	690(30)	-430(40)	-400(30)	660(40)
F(4B)	610(30)	2660(60)	700(30)	-720(40)	-140(20)	-10(30)
F(5B)	590(20)	1170(30)	570(30)	-140(20)	-10(20)	-240(20)
F(6B)	690(20)	710(20)	414(19)	-91(17)	-80(20)	20(20)
F(7B)	980(30)	690(30)	880(30)	-110(20)	200(20)	240(20)
F(8B)	1030(30)	870(30)	1140(30)	220(30)	310(30)	460(30)
F(9B)	650(20)	1500(40)	620(30)	160(30)	-210(20)	330(20)
F(10B)	620(20)	940(30)	420(20)	-180(20)	-73(18)	60(20)
F(11B)	630(20)	700(30)	580(20)	40(20)	-20(19)	-30(20)
F(12B)	740(30)	1390(40)	640(30)	50(30)	290(20)	-350(30)
F(13B)	750(30)	1560(40)	990(30)	-580(30)	430(20)	-100(30)
F(14B)	1290(40)	970(30)	1350(40)	-140(30)	350(30)	370(30)
F(15B)	1000(30)	780(30)	890(30)	-20(30)	130(20)	290(20)
F(16B)	920(30)	960(30)	490(20)	10(20)	140(20)	170(20)
F(17B)	820(30)	1350(40)	1170(40)	340(30)	350(30)	70(30)
F(18B)	840(30)	1110(40)	1750(50)	450(30)	-120(30)	-330(30)
F(19B)	1020(30)	940(30)	1740(50)	-350(30)	-170(30)	-340(30)

F(20B)	1010(30)	1020(30)	790(30)	-310(20)	260(20)	-160(20)
C(41B)	470(40)	620(50)	420(40)	20(40)	60(30)	100(40)
C(42B)	1160(70)	1210(80)	340(40)	-50(50)	50(50)	730(60)
C(43B)	820(60)	1870(100)	510(50)	-160(60)	-230(50)	670(60)
C(44B)	890(70)	2000(100)	390(50)	-280(60)	-390(50)	1010(70)
C(45B)	310(50)	1440(80)	780(60)	-480(60)	30(40)	90(50)
C(46B)	370(40)	1140(70)	440(50)	-120(50)	-10(40)	50(50)
C(47B)	320(40)	600(40)	250(30)	0(30)	-10(30)	-190(30)
C(48B)	540(40)	500(40)	370(40)	50(30)	-130(30)	10(30)
C(49B)	600(50)	720(50)	360(40)	40(40)	150(30)	-30(40)
C(50B)	440(40)	540(50)	850(50)	260(40)	220(40)	260(40)
C(51B)	400(40)	820(50)	470(40)	40(40)	110(40)	-20(40)
C(52B)	240(40)	720(50)	420(40)	30(40)	120(30)	-60(30)
C(53B)	440(40)	500(40)	330(40)	-50(30)	-230(30)	50(30)
C(54B)	470(50)	640(50)	350(40)	-50(40)	-70(30)	-30(40)
C(55B)	430(50)	910(60)	510(50)	-210(50)	-20(40)	-50(40)
C(56B)	490(50)	1130(70)	490(40)	-330(50)	170(40)	-70(50)
C(57B)	860(60)	640(50)	650(50)	-190(50)	-40(40)	-40(50)
C(58B)	600(50)	480(50)	660(50)	-150(40)	140(40)	30(40)
C(59B)	640(40)	480(40)	450(40)	-170(30)	10(40)	90(40)
C(60B)	530(40)	490(50)	700(50)	140(40)	250(40)	-20(40)
C(61B)	860(60)	800(60)	670(50)	170(50)	320(50)	180(50)
C(62B)	720(60)	590(50)	1170(70)	70(50)	-30(50)	-220(50)
C(63B)	550(50)	730(60)	980(60)	-360(50)	80(50)	-20(40)
C(64B)	780(60)	720(50)	760(50)	-120(50)	150(50)	130(40)
C(71A)	2770(80)	2470(80)	2110(80)	770(70)	610(70)	540(70)
C(72A)	4940(140)	4890(140)	5370(150)	-220(80)	-20(80)	360(80)
C(73A)	4230(110)	3380(110)	4360(120)	400(80)	-860(80)	-400(80)
C(74A)	2260(80)	2270(80)	2890(90)	80(70)	-640(70)	-70(70)
C(75A)	4410(130)	4440(130)	3970(130)	-110(80)	290(80)	10(80)
C(76A)	2990(80)	2010(80)	2360(80)	340(70)	800(70)	-290(70)
C(77A)	3080(80)	2680(80)	1860(70)	110(70)	910(70)	610(70)

Table C.10: Hydrogen coordinates (x 10^4) and isotropic displacement paramters (Å^2 x 10^3) for SMB10 (CCDC 778255).

	x	**y**	**z**	$\mathbf{U_{iso}}$
H(1H)	7474(18)	1111(13)	9048(13)	49
H(2H)	7790(20)	1555(12)	9505(13)	49
H(3H)	8099(19)	1332(13)	10223(14)	49
H(4H)	7720(20)	5865(13)	8292(13)	53
H(5H)	7290(20)	6354(13)	8832(13)	53
H(6H)	6972(19)	6032(13)	9492(13)	53